université de BORDEAUX

THESIS PRESENTED TO OBTAIN THE DEGREE OF

DOCTOR OF THE UNIVERSITY OF BORDEAUX

ÉCOLE DOCTORALE DES SCIENCES DE LA VIE ET DE LA SANTÉ

SPECIALIZATION: NEUROSCIENCES

Presented in public on December 13th, 2019

at the Neurocentre Magendie, INSERM U1215, Université de Bordeaux, France

By Vincent SIMON

Characterization of different subpopulations of hypothalamic POMC neurons in the regulation of energy balance

Directed by: Daniela Cota, MD, HDR

Members of the jury:

Mme Agnès NADJAR, Professor, UMR INRA 1286 – Laboratoire NutriNeurO, Université de Bordeaux, France. Chairwoman and examiner *(Présidente du jury et examinatrice)*

Mme Carole ROVERE, Research Director, UMR CNRS 7275 – Institut de Pharmacologie Moléculaire et Cellulaire (IPMC), Université Côte d'Azur, Nice, France. Referee *(Rapporteure)*

M. Marc CLARET, Associate professor, Group leader – Institut d'Investigacions Biomèdiques August Pi i Sunyer (IDIBAPS), Barcelona, Spain. Referee *(Rapporteur)*

M. Philippe CIOFI, Researcher, INSERM U1215 – Neurocentre Magendie, Université de Bordeaux, France. Examiner *(Examinateur)*

Mme. Daniela COTA, Research Director, INSERM U1215 – Neurocentre Magendie, Université de Bordeaux, France. Thesis director, invited member *(Directrice de thèse, membre invitée)*

RESEARCH UNIT

Team “Energy Balance and Obesity”

Led by Daniela Cota, MD, HDR

INSERM U1215, Université de Bordeaux

Neurocentre Magendie

146 rue Léo Saignat

33077 Bordeaux

France

https://neurocentre-magendie.fr

« Là où il y a une volonté, il y a un chemin »

Vladimir Ilitch Oulianov, dit Lénine (apocryphe)

Remerciements

Tout d'abord, je tiens à remercier très chaleureusement Mme Carole ROVERE et M. Marc CLARET pour avoir accepté d'évaluer ce manuscrit. Je suis conscient que je ne vous ai laissé que très peu de temps pour effectuer ce travail vu le (grand) retard que j'ai pris lors de la rédaction et vous prie une nouvelle fois de m'excuser pour cela.

Je remercie également M. Philippe CIOFI pour sa présence lors de ma soutenance, en qualité d'examinateur. Enfin, merci également à Mme Agnès NADJAR d'avoir accepté la présidence de mon jury de thèse. J'ai hâte de pouvoir discuter avec vous tous des résultats présentés ici.

Daniela…par où commencer…En 2015 je suis arrivé dans ton équipe sans trop savoir si je voulais poursuivre mon parcours dans la recherche. Tu m'as encouragé à continuer, et la qualité scientifique et humaine de l'équipe que j'ai découverte lors de mon stage de M2 m'a définitivement convaincu de réaliser cette thèse. Ces quatre années ont été particulièrement riches en rebondissements, en particulier avec cette agréable mise au point de cette merveilleuse technique qu'est la FISH/IHC ! Je n'oublie pas que c'était ton idée, à la base (merci…) et que j'étais fort sceptique quant à son succès (pour changer). Il aura fallu 2 ans et demi de frustrations et faux espoirs pour réussir, mais on y est finalement arrivés ! Pour cela, je te remercie vraiment de m'avoir laissé le temps d'aller jusqu'au bout pour résoudre tous les problèmes qui semblaient pourtant s'enchaîner sans fin (allez, encore un dernier test, c'est le dernier, promis !). À plusieurs moments j'ai failli perdre espoir, mais cette fois-ci, la persévérance a été récompensée. Plus généralement, merci pour la qualité de ton encadrement et ton soutien au quotidien, surtout durant ces dernières semaines de rédaction particulièrement éprouvantes. J'ai beaucoup appris en travaillant dans ton équipe et suis ravi de pouvoir en faire partie pendant quelques temps encore !

À l'équipe Cota. C'est un véritable de plaisir de travailler à vos côtés tous les jours (c'est réciproque n'est-ce pas ?.....N'EST-CE PAS ???). **Lady James**, « main droite » de Daniela, il n'y a que toi pour arriver à me supporter lorsque les manips ne marchent pas. I don't know how you manage that, but apparently, **it is possible**. Tu n'imagines pas le bonheur que c'est de savoir qu'on peut toujours compter sur toi, que ce soit pour des manips ou tout autre chose. Ta touffe blonde est un vrai rayon de soleil, capable d'illuminer les journées les plus obscures ! J'espère en tout cas qu'on ne va jamais « se divorcer » ! ;) Passons désormais à **Monsieur ZIZ**, le MacGyver de l'équipe. Tes connaissances scientifiques et techniques ainsi que ton esprit pratique sont tout bonnement impressionnants. Ça a été très enrichissant pour moi de pouvoir me reposer sur ton expérience, en particulier pour tout ce qui concerne l'expérimentation animale. Tu es toujours disponible pour donner un coup de main et j'espère encore continuer à apprendre à tes côtés. À l'inverse, je compte encore bien t'influencer pour ton vote de 2022 ! ;) En parlant de vote, je souhaite remercier **Wahiba** pour les longues conversations politiques que nous avons pu avoir et que j'attendais souvent comme une bouffée d'oxygène lorsque rien ne marchait au labo. Discuter avec toi a toujours été un réel plaisir (tout autant que tes pâtisseries !). **Nathalie**, heureusement que tu es là pour t'occuper de la logistique et de tout un tas de choses qui me donnent mal à la tête rien que d'y penser ! Merci de t'être occupée de mes souris, en particulier durant ces dernières semaines de rédaction. J'attends une démo de danse africaine pour après la soutenance ! **Valérie**, ton empathie, ta compassion et tes encouragements ont été salutaires dans les moments difficiles. J'ai beaucoup apprécié tous les moments passés ensemble à essayer de percer les mystères de la FISH ! Ça m'a vraiment fait du bien de ne pas être le seul à galérer avec tout ça…**Ashley**, euh non, Dr Castellanos, pardonnez-moi ! Je ne sais pas comment tu fais pour être toujours aussi rayonnante dans toutes les circonstances, mais je me dis qu'au final, avec nous deux, un équilibre se créée ! Le nombre de choses que tu es capable de gérer en parallèle (MT180, Symposium, manips, thèse etc.) force l'admiration. Ce fut un réel plaisir de partager ces années avec une collègue thésarde aussi sympathique que vous, très chère, et j'espère passer une soutenance aussi réussie que la vôtre ! ;) **Camille**, merci de venir renforcer la diaspora limougeaude au sein de l'équipe ! Ton sens de la rigueur est sans commune mesure et

c'est certainement un atout majeur de travailler avec quelqu'un comme toi…mais bon des fois…j'avoue que tu me fais un peu peur quand tu reproches à tes stagiaires de ne pas être suffisamment précis dans leur cahier de labo alors que je suis juste à côté avec mon protocole gribouillé sur un sopalin ! J'essaierai de m'améliorer pour l'année prochaine (#bonnesrésolutions). **Carmelo**, je suis ravi de voir que la FIHC/IHC n'aura pas servi que pour un seul projet, et c'est grâce à toi ! J'ai fortement apprécié toutes les discussions que j'ai pu avoir avec toi et j'espère pouvoir continuer à bosser à tes côtés (au moins jusqu'à ce que tu sois complètement bilingue ! ;)). **Stéphane**...mon pauvre Stéphane…dans quoi t'es-tu donc embarqué pour faire une thèse avec de la FISH ! En général je suis assez avare en compliments (sauf ici évidemment), mais je dois t'avouer que la rapidité avec laquelle tu t'es adapté au projet et habitué à cette technique est assez admirable (voilà, c'est dit, je ne le redirai pas !). J'imagine qu'à 2 sur cette technique, lorsque j'aurai retrouvé le chemin de la paillasse, on devrait pouvoir faire de bien jolies choses…(ou pas, c'est de la FISH après tout !).

Quelques mots désormais pour les anciens de l'équipe, dont la plupart étaient présents à mon arrivée au laboratoire en stage de M1. À mon ancien encadrant, **Nicolas**, merci à toi qui m'a tout appris, des gestes basiques en expérimentation animale, jusqu'à la chirurgie, immunos, stats, etc. Je n'oublierai jamais que lorsque j'étais totalement bloqué pour le concours de l'école doctorale, c'est ton aide qui m'a permis de passer le cap. On peut dire que j'ai suivi tes pas, 4ème année avec la FRM et soutenance en décembre, j'espère seulement que la fin en sera digne ! **Wilfrid**, l'origine du projet POMC-GABA/Glut c'est toi. J'espère en avoir correctement pris la suite, même sans électrophy ! Je garde toujours un très bon souvenir de nos échanges et j'espère qu'on se recroisera dans le labo pour de futures collaborations ! ;) **Caroline**, c'est toi qui a réalisé les toutes premières manips de FISH, lorsque tout restait à faire. Merci pour tout le travail que tu as effectué et qui m'a fait gagner un temps précieux. À cette époque-là, on ne se doutait pas que ça prendrait autant de temps, ni que ça pourrait aussi bien marcher ! **Omar**, félicitations pour ton poste au Mexique, même si c'est dommage de ne plus t'avoir au labo…C'était toujours agréable de pouvoir discuter de science ou de politique avec toi, j'espère que tu passeras nous voir bientôt ! (Et Vive AMLO !). **Dominika**, ma chère stagiaire, tu es vraiment quelqu'un d'atypique (dans le bon sens du terme) !

Ton esprit est vif, tu comprends tout très vite et tes remarques étaient souvent pertinentes (pas toujours hein, faut pas exagérer). J'ai eu de la chance de tomber sur une stagiaire aussi matinale que moi (hum hum…) et qui ne se prend pas au sérieux. Je pourrais terminer par quelques mots en slovaque, mais je ne connais que ceux que tu m'as appris…et qui ne sont donc pas totalement appropriés en cette circonstance ! J'ai une pensée également pour **Magalie** et **Amandine** (châtoooon) qui ont assisté à mes débuts dans l'équipe. Notre bureau a vraiment perdu en vitalité sans vous, les filles. Sachez que votre présence reste parmi les meilleurs souvenirs de mon stage ! Je remercie également tous les stagiaires qui ont passé quelques temps parmi nous dans l'équipe : **Pauline**, **Audrey**, **Sarah**, **Martin**, **Maëlig** (bon courage pour ta thèse !). **Jeflie** et **Selma**, on se revoit bientôt pour votre stage ! Quant à **Alexia**, la reine autoproclamée des stagiaires, tu sais pertinemment ce que tu mérites ! Je te souhaite en tout cas bon courage pour ta thèse, en espérant pouvoir t'appeler « Reine des docteurs » lorsque ce sera fini !

À l'équipe Marsicano. Merci à nos voisins de couloir qui apportent une touche de chaos sans laquelle notre existence serait bien monotone ! Merci **Astrid** pour ton soutien moral et technique ! Je n'ose même pas imaginer la quantité de sondes que tu as faites pour moi. **Imane**, nos discussions sur motivation vs plaisir m'ont été bien utiles ! Les pauses boulangerie/éclairs en ta présence sont toujours des plus exquises. Et ne t'inquiète pas, peut-être que toi aussi un jour, tu verras du cFos ! ;) **Luigi**, ton expertise des virus est un atout précieux, j'ai quelques idées en tête et je risque d'avoir une fois de plus besoin de toi ! **Yamuna**, ne t'en fais pas, ça va aller, on finit toujours par s'en sortir (^^). **Toto**, tu resteras à jamais mon (ex)-voisin préféré (pour les 3 fois où on s'est accidentellement croisés…ce fut court, mais tellement intense…). **Bibi**, je risque d'être moins souvent présent les week-ends désormais...donc j'imagine qu'on ne se verra plus. Voilà. Au revoir. **Fran**, j'imagine que tu viens de copier/coller cette phrase dans deepL, car tu n'as pas fait tes devoirs de français ! Attention, petit Dino te surveille…

Merci également à la formidable équipe Oliet ! **Shakira** et son rire discret, **Aurélie** et ses spams hebdomadaires (oui, sortie des déchets, on sait…), **Aymeric** (t'aurais dû travailler pour moi, ça m'aurait fait gagner un temps précieux !), **Dorian** et

ses phrases sorties de nulle part, **Dylan** (bon ben j'aurais rendu ma thèse au même point que toi, heureusement que t'es passé avant, je me sens moins seul ! ^^), **Philippe**, merci pour toute ton expertise technique et nos discussions sur les marquages IHC dans l'hypothal (entre autres), **Claire** et **Stéphanie**, avec qui j'avais passé un excellent stage de M1 riche en émotions lui aussi (je me souviendrai toujours des manips en aveugle qui ont failli le rester à jamais !). En repensant à ce stage de M1, j'ai une pensée particulière pour **Aude**, qui m'a libéré d'une pièce de son labo un soir alors qu'on m'avait enfermé à clé, la veille d'un pont de 4 jours…Ma « carrière » dans la recherche aurait alors pu prendre fin prématurément !

Mention spéciale désormais pour la FISH TEAM : **la Marj** et le **ptit Juju** ! La FISH nous a réunis, et désormais rien ne peut nous arrêter ! J'ai été ravi d'avoir partagé tous ces moments avec vous, entre les doutes, le désespoir et la joie ultime quand quelque chose fonctionnait enfin ! Clairement, sans nos échanges constants, vos remarques et suggestions, ce protocole n'aurait jamais vu le jour. En espérant pouvoir tous se retrouver ailleurs, dans un labo ou une entreprise, pourquoi pas dans l'équipe de la Marj, notre incompétente préférée !

De manière générale, merci à toutes celles et ceux qui ont contribué à faire de ces 4 années d'agréables souvenirs. **Christel**, pour les longues discussions que nous avons pu avoir concernant les séries, la politique, la religion. Tu es une des seules personnes avec lesquelles on peut rigoler énormément et à la fois être avoir des discussions profondes sur des sujets sérieux, ce qui est particulièrement agréable. **Maïté**, merci pour ta disponibilité quand on a eu besoin de renseignements pour le RNAscope et pour ta gentillesse toutes les fois où j'ai eu besoin de tester un anticorps ou avoir des conseils techniques. **Giovanni**, vu tes talents d'orateur, je ne me fais pas de soucis pour toi, ta soutenance, quand elle aura lieu, promet d'être un beau spectacle. **Nadia**, ne commence pas à stresser dès maintenant, tu auras tout le temps pour ça ! Et ne t'en fais pas, ça va aller car dans tous les cas, il te restera toujours de belles images de FISH à montrer ! **Agnès**, merci pour ta bonne humeur et ton énergie communicative, je me suis toujours senti « énergisé » après t'avoir parlé !

Un immense merci désormais aux plateformes techniques du Neurocentre Magendie. Tout le travail que vous réalisez pour nous au quotidien représente une charge immense dont nous n'avons pas à nous occuper. Merci en particulier à **Delphine** et toute la plateforme de génotypage. Delphine, même si ma thèse est finie, il se peut que je vienne encore faire des visites vers 17h30-18h comme d'habitude, avec tout plein de questions ! Merci à **Elizabeth** pour la gestion des lignées et à **Fiona** qui s'occupe de l'élevage. C'est particulièrement agréable de pouvoir se reposer sur des personnes comme vous. Merci également aux animaliers, en particulier **JB** et **Ruby** pour le R+2 pour leur professionnalisme et le soin qu'ils apportent à nos animaux. Merci à **Sara** et **Julie** pour la gestion des animaleries et à **Nathalie**, notre super véto avec qui j'ai de longues discussions de type drogues & bien-être (il faudra toujours que tu me montres comment préparer ton espèce de gelée à la fraise là…).

Enfin, merci également au Bordeaux Imaging Center et en particulier à **Fabrice**, pour les dizaines (centaines ?) d'heures passées à préparer des macros. J'espère que je t'ai moins traumatisé que Valérie malgré tout !

À tous mes camarades des Master, bordelais, canadiens ou autres qui sont encore en thèse, je vous souhaite beaucoup de courage pour la fin, et à ceux qui ont déjà fini, beaucoup de réussite pour la suite (quelle qu'elle soit !). **Olivier**, j'espère qu'on se croisera pour que tu reçoives ta dose annuelle de communisme. **Benoît**, avec un peu de chance et si l'avenir le permet, recréons notre binôme de M1 qui fut particulièrement fructueux (en tout sauf en science, ceci dit…) ! **Clémence**, c'est un plaisir de voir que tu t'épanouis dans la recherche, je te souhaite sincèrement de garder cette envie le plus longtemps possible ! **Kim**, bon courage pour la fin de ta thèse, et dans tous les cas, on se retrouve bientôt pour une raclette bien méritée !

Pour terminer, je souhaite remercier ma famille pour le soutien indéfectible qu'elle me porte, en particulier mes parents **Catherine** et **Didier**. À mon frère, **Romain**, courage pour ta thèse, au pire viens l'écrire ici, l'air bordelais m'a particulièrement inspiré pour la mienne (→ ha ha ^^'). À mes amis, **Benoît**, **Mathilde**, **Camille**, je sais que je n'ai pas toujours été présent ces dernières années et je vous remercie pour votre indulgence à mon égard ! =) **Clément**, j'espère pouvoir bientôt retourner boire une bière

à Limoges avec toi pour refaire le monde une fois de plus (d'ailleurs, j'ai vu la dernière saison du Bureau des Légendes). **Fulya**, j'admire ta volonté et ton ambition. Ton parcours ces dernières années est impressionnant, j'espère sincèrement que tu te plairas dans ta nouvelle vie. Tu es et seras à jamais ma binôme de cœur…(t'as vu, tmtc bb).

Ça y est, c'est fini…ou presque. Il me reste une personne à remercier. Et non des moindres. Je l'imagine déjà trépignant en train de lire ces lignes en se demandant comme j'ai pu faire pour l'oublier. Je ne vous ai point oubliée **Mme TOUBZ**, **petite belette ferroviaire**, **Colette Ducul** ou quel que soit le nom que vous portez réellement et qui n'a que peu d'importance. Je me souviendrai toujours de cette fraîche matinée de janvier 2015 où vous êtes entrée dans notre burz en posant lourdement votre sac de militante LR et allumant sauvagement votre ordi comme si vous viviez là depuis 15 ans. J'ai cru avoir à faire à Nadine Morano ce jour-là…j'étais loin d'imaginer ce qu'il en était réellement. Vous êtes la personne qui a le plus animé mes journées durant ces folles années Magendiennes. Les Pitayas sur la terrasse, #GP, concorde, entonnoir, pièce sombre aux rideaux rouges et autres délires sont trop nombreux et indécents pour être évoqués ici (tout comme notre historique de conversation FB). Sachez seulement que votre présence me manque, et en particulier vos sièges chauffant à 60°C pour les soirées où le fond de l'air est frais. J'espère ainsi rapidement vous revoir pour que nous puissions engloutir de nouveau les délicieux éclairs de la boulange. En attendant, je serai toujours là pour suivre à distance les nouveaux drames que votre présence démoniaque ne manquera pas de déclencher.

Voilà, cette fois-ci c'est vraiment fini.

Bonne lecture !

Abstract

Résumé

Résumé étendu

Abstract

Title: **Characterization of different subpopulations of hypothalamic POMC neurons in the regulation of the energy balance**

Introduction: Obesity is a chronic multifactorial disease, characterized by a health-threatening accumulation of body fat and whose prevalence has been increasing worldwide since the 1980s. Obesity is a risk factor for type II diabetes, cardiovascular disease and various forms of cancer and is now a major public health issue. Unfortunately, available pharmacological treatments are rare and not very effective. Thus, the study of the biological mechanisms underlying body weight regulation could lead to the discovery of new therapeutic targets and prove useful in the fight against this modern curse.

The brain plays a key role in controlling food intake and metabolism. In particular, some hypothalamic neurons called POMC neurons are classically described as being responsible for satiety. To date, most studies on these neurons have focused on their neuropeptide production, but recent discoveries have uncovered the existence of subpopulations, characterized by their ability to secrete different neurotransmitters (glutamate, GABA or both). The functional consequences of this heterogeneity are largely unknown to this day.

Objectives: The general objective of this thesis is to study the specific roles of different sub-populations of POMC neurons, depending on the neurotransmitter they release: we will then distinguish between POMC-Glut (pure glutamatergic), POMC-GABA (pure GABAergic) and POMC-Glut/GABA (mixed) neurons. Three objectives have been defined:

- To develop a new neuroanatomical technical approach to identify subpopulations of activated POMC neurons on mouse brain slices.

- To determine the impact of a hypercaloric diet on POMC subpopulations.

- To determine the role of the POMC Glutamatergic population in energy balance by using a novel genetic model.

Results: First, we developed a new technique for the simultaneous detection of mRNAs of GAD65/67, vglut2 and POMC combined with an immunostaining of the cFos protein (a marker of cellular activity), in order to identify the subpopulations of activated POMC neurons under various experimental conditions. Then, we applied this technique in a context of an acute exposure to a high-calorie diet (HFD, for "high-fat-diet"). We then discovered that POMC-GABA neurons were the main sub-population to be activated by HFD, unlike POMC-Glut which were less likely to respond to the diet. Of note this preferential activation of POMC-GABA happens in a context of HFD-driven hyperphagia. Finally, we created a new genetically modified mouse line that allows the deletion of the vglut2 protein from POMC neurons in an inducible way, thus preventing the release of glutamate from POMC neurons. After carrying out the necessary controls, we conducted a metabolic characterization of this mouse line. Inducible POMC-vglut2-KO mice, in which POMC glutamatergic transmission is suppressed, have an exaggerated hyperphagic response following a 24-hour fast. In addition, when placed on a HFD, these mice eat more and have an increased energy expenditure.

Conclusions: This work led to the development of a new neuroanatomical technique whose versatility is a major asset in the study of neurons controlling energy balance, but which can also be used in many other projects. Our data suggest that there is a functional dichotomy between POMC-Glut and POMC-GABA neurons, the former playing mainly the expected role of satietogenic POMC neurons, while activity of the latter is associated with an increase in HFD consumption. Future studies will be necessary to manipulate these different sub-populations and identify their specific sites of action, in the hope to further clarify their role in the regulation of energy balance.

Keywords: **FISH, POMC, glutamate, GABA, hypothalamus, energy balance**

Résumé

Titre **: Caractérisation de différentes sous-populations de neurones à POMC hypothalamiques dans la régulation de la balance énergétique**

Introduction : L'obésité est une maladie chronique d'origine multifactorielle, caractérisée par une accumulation excessive de graisse corporelle néfaste pour la santé et dont la prévalence n'a cessé de croître au niveau mondial depuis les années 1980. Représentant un facteur de risque pour le diabète de type II, les maladies cardiovasculaires et différentes formes de cancer, l'obésité est aujourd'hui un enjeu majeur de santé publique. Malheureusement, les traitements pharmacologiques disponibles sont rares et peu efficaces. Ainsi, l'étude des mécanismes biologiques qui sous-tendent la régulation du poids corporel pourrait permettre de découvrir de nouvelles cibles thérapeutiques et se révéler utile dans la lutte contre ce fléau moderne.

Le cerveau joue un rôle clé dans le contrôle de la prise alimentaire et du métabolisme. En particulier, certains neurones hypothalamiques, appelés neurones à POMC, sont classiquement décrits comme étant responsables de la satiété. Jusqu'alors, la plupart des études menées sur ces neurones se sont concentrées sur leur production de neuropeptides, mais de récentes découvertes ont mis à jour l'existence de sous-populations, caractérisées par leur capacité à sécréter différents neurotransmetteurs (glutamate, GABA ou les deux). Les conséquences fonctionnelles de cette hétérogénéité, jusqu'à alors largement insoupçonnée, sont à ce jour inconnues.

Objectifs : L'objectif général de cette thèse est d'étudier le rôle spécifique de différentes sous-populations de neurones à POMC, en fonction du neurotransmetteur qu'ils libèrent : on distinguera alors les neurones à POMC-Glut (glutamatergiques purs), POMC-GABA (GABAergiques purs) et POMC-Glut/GABA (mixtes). Trois objectifs ont été définis :

- Développer une nouvelle technique de neuro-anatomie afin de détecter les différentes sous-populations de neurones à POMC activés, dans des coupes flottantes de cerveau de souris.
- Déterminer l'impact d'un régime hypercalorique sur les sous-populations de neurones à POMC.

- Déterminer le rôle des POMC-Glut dans la régulation de la balance énergétique à partir d'un nouveau modèle de souris génétiquement modifiées.

Résultats : Tout d'abord, nous avons mis au point une nouvelle technique de détection simultanée des ARNm de GAD65/67, vglut2 et POMC combinée à un marquage de la protéine cFos (un marqueur d'activité cellulaire), afin d'identifier les différentes sous-populations de neurones à POMC activées dans diverses conditions expérimentales. Puis, nous avons mis en pratique cette technique lors d'une exposition aiguë à un régime hypercalorique (nommé HFD, pour « high-fat-diet »). Nous avons alors découvert que les neurones à POMC-GABA étaient la principale sous-population à être activée par le HFD, contrairement aux neurones à POMC-Glut qui étaient moins nombreux à y répondre. Cette activation préférentielle des POMC-GABA s'effectue de plus dans un contexte d'hyperphagie pour le HFD. Pour finir, nous avons créé une nouvelle lignée de souris génétiquement modifiées permettant la délétion inductible de la protéine vglut2 des neurones à POMC, empêchant ainsi la libération de glutamate des neurones à POMC. Après avoir effectué les contrôles nécessaires, nous avons entrepris une caractérisation métabolique de cette lignée. Les souris POMC-vglut2-KO inductibles, dont la transmission POMC glutamatergique est supprimée, ont une réponse hyperphagique exagérée suite à un jeûne de 24h. De plus, lorsqu'elles sont placées sous HFD, ces souris mangent davantage et ont une dépense énergétique augmentée.

Conclusions : Ce travail aura permis la mise une point d'une nouvelle technique neuro-anatomique dont la versatilité représente un atout majeur dans l'étude des neurones qui contrôlent la balance énergétique, mais qui pourra être également employée dans bien d'autres projets. Nos données suggèrent qu'il existe une dichotomie fonctionnelle entre les neurones à POMC-Glut et POMC-GABA, les premiers jouant principalement le rôle satiétogène « classique » des neurones à POMC alors que l'activité des autres serait au contraire associée à une stimulation de la consommation de HFD. De futures études permettant de manipuler ces différentes sous-populations et identifier leurs sites d'actions cérébraux spécifiques seront nécessaires afin d'éclaircir davantage leur rôle dans la régulation de la balance énergétique.

Mots-clés : **FISH, POMC, glutamate, GABA, hypothalamus, balance énergétique**

Résumé étendu

***Titre* : Caractérisation de différentes sous-populations de neurones à POMC hypothalamiques dans la régulation de la balance énergétique**

Introduction

Chapitre 1 : L'obésité est une pathologie chronique caractérisée par une accumulation de graisse corporelle néfaste pour la santé dont la prévalence mondiale ne fait qu'augmenter depuis 50 ans, à tel point qu'on parle actuellement de pandémie. En tant que facteur de risque de nombreuses autres maladies (diabète, maladies cardiovasculaires, cancers…), l'obésité se traduit par une diminution de 5 à 20 ans de l'espérance de vie. Malheureusement, à l'heure actuelle, aucun régime alimentaire spécifique ou traitement pharmacologique efficace n'a été trouvé pour lutter contre cette pathologie. Seule la chirurgie bariatrique est efficace, mais elle s'accompagne de nombreux effets secondaires, et son caractère invasif, souvent irréversible, en fait un choix de dernier recours pour les cas les plus graves. De nouvelles stratégies thérapeutiques doivent donc être trouvées pour aider la majorité des patients. Pour cela, il est nécessaire d'en apprendre plus sur les causes de l'obésité. Cette maladie est d'origine multifactorielle, résultant d'une combinaison de facteurs environnementaux (alimentation hypercalorique, sédentarisation) et biologiques (génétique, épigénétique, maladies métaboliques, médicaments, microbiote intestinal, virus) qui concourent à une plus ou moins forte accumulation de graisse corporelle. Une connaissance plus approfondie des déterminants biologiques qui sous-tendent la régulation du poids est donc nécessaire, dans l'espoir d'endiguer ce fléau moderne.

Chapitre 2 : Plusieurs cadres théoriques existent pour tenter d'expliquer les variations de poids corporel chez les individus. Tout d'abord, la « théorie du point de référence » (ou « set point theory ») part de l'idée que le poids corporel est régulé comme la température le serait avec un thermostat. Il y aurait un point de référence (« set point ») génétiquement déterminé qui fixerait le poids au-dessus et en-dessous duquel des mécanismes physiologiques s'enclenchent pour lutter contre toute variation. Ce modèle permet d'expliquer pourquoi les individus ont généralement tendance à

garder un poids stable sur le long terme, malgré des fluctuations constantes d'apport et dépense énergétiques. Cependant, il ne permet pas d'expliquer l'épidémie d'obésité observée à l'heure actuelle : si notre poids est génétiquement fixé, pourquoi certaines personnes échappent au contrôle et deviennent obèses ? Une autre théorie prend le contre-pied de celle-ci et propose qu'il n'y a pas de régulation active du poids corporel, mais seulement un équilibre qui se crée passivement entre l'apport et les dépenses caloriques : c'est la « théorie du point d'équilibre » (ou « settling point theory »). Dans ce modèle, un excès de calories se traduit par un remplissage des réserves (i.e. de graisse corporelle) jusqu'à ce que la dépense énergétique augmente suffisamment pour compenser l'apport et qu'un point d'équilibre ne soit atteint. Cette théorie offre ainsi une explication à l'épidémie d'obésité, mais se heurte à des contradictions. En effet, les patients obèses ont une très forte tendance à reprendre le poids qu'ils ont perdu après une période de restriction calorique, ce qui explique pourquoi les interventions alimentaires se soldent presque toujours par des échecs à long terme. Si le poids n'était pas activement régulé, il serait aussi facile de perdre du poids que d'en gagner, ce qui n'est pas le cas. Ainsi, une troisième théorie prétend réconcilier les deux précédentes au sein d'un seul modèle : le modèle à double point d'intervention (« dual intervention point model »). Ce modèle propose l'existence de deux limites génétiquement déterminées qui encadrent une gamme de poids corporel. Au-dessus de la limite supérieure et en-dessous de la limite inférieure, des mécanismes biologiques s'activent pour contrer la variation de poids, tout comme dans la théorie du point de référence. Cependant, entre ces deux limites, le poids ne subirait pas de régulation active, tout comme dans la théorie du point d'équilibre. Le niveau des limites supérieures et inférieures aurait été façonné par l'évolution, la limite inférieure ne pouvant pas descendre trop bas par pression évolutive des maladies, qui tuent prioritairement les plus maigres. À l'inverse, la limite haute n'a pas pu monter trop haut à cause d'un risque accru de prédation envers les plus gros. Cependant, depuis *Homo erectus*, la maîtrise du feu et la constitution de groupes sociaux plus larges a aboli le risque de prédation pour l'espèce humaine. La limite haute aurait ainsi dérivé génétiquement, au gré des mutations aléatoires, sans être soumise à une quelconque pression évolutive. Cela expliquerait la grande variabilité de poids corporel dans les

sociétés modernes, où différents individus plongés dans le même environnement obésogène ne deviendront pas tous obèses, la limite supérieure des individus résistants à l'obésité devant être beaucoup plus basse que pour les autres. Quant aux systèmes biologiques qui sous-tendent les régulations biologiques aux différentes limites, ils sont pour l'heure inconnus, même si des hypothèses ont été émises. Une chose semble certaine cependant : s'il y a un organe central dans la régulation du poids, c'est le cerveau, car la majorité des variations génétiques associées au poids corporel concernent des gènes impliqués dans le fonctionnement du système nerveux. L'étude du cerveau dans la régulation du poids corporel apparaît ainsi comme primordiale.

Chapitre 3 : Dans le cerveau, différentes régions sont impliquées dans la régulation de la « balance énergétique », à savoir l'équilibre entre l'apport et la dépense calorique. L'hypothalamus et le tronc cérébral sont des structures centrales, car elles rassemblent de nombreux neurones qui contrôlent la régulation endostatique (= homéostatique) du poids corporel. D'autres régions sont quant à elles impliquées dans la régulation exostatique de la balance énergétique, à savoir la motivation et le plaisir de manger. Parmi ces structures, on trouve le noyau accumbens et l'aire tegmentale ventrale pour la motivation ainsi que le pallidum ventral et le noyau parabrachial pour le plaisir. Leur action conduit généralement à une stimulation de la prise alimentaire. Cependant, il serait inapproprié de considérer ces deux systèmes de régulation comme séparés l'un de l'autre. En effet, certains neurones hypothalamiques participent à la fois aux circuits endostatiques et exostatiques de la régulation du poids corporel. C'est le cas notamment des neurones à POMC du noyau arqué de l'hypothalamus, qui sont connus pour stimuler la satiété en libérant des neuropeptides anorexigènes.

Chapitre 4 : Les neurones à POMC sont nécessaires à la régulation de la balance énergétique. Leur fonction peut cependant être altérée en situation d'obésité ou à cause d'une alimentation riche en gras (HFD, pour « high-fat-diet »), ce qui contribue au développement de l'obésité. Parmi ces altérations, on trouve notamment : une résistance à la leptine, des altérations de la dynamique mitochondriale, des défauts d'homéostasie protéique, etc. Cependant, la plupart des études menées sur les neurones à POMC

considèrent cette population comme un ensemble homogène, mais de récentes données mettent l'accent sur leur hétérogénéité bien trop souvent négligée.

Chapitre 5 : Plusieurs éléments mettent en lumière l'hétérogénéité des neurones à POMC hypothalamiques. Tout d'abord, suivant leur localisation rostro-caudale dans le noyau arqué, ils ne projettent pas sur les mêmes régions cérébrales. De plus, il existe une ségrégation spatiale et fonctionnelle entre les neurones à POMC qui sont sensibles à l'insuline, la leptine ou la sérotonine. Enfin, on distingue également 3 sous-populations de neurones suivant le neurotransmetteur qu'ils libèrent : POMC-Glut (glutamatergiques purs), POMC-GABA (GABAergiques purs) et POMC-Glut/GABA (mixtes). Des données précédentes de notre équipe ont par ailleurs montré que ces sous-populations répondaient de manière opposée à un traitement à la rapamycine (RAPA), une molécule inhibitrice de la voie de signalisation mTORC1 qui est impliquée dans la régulation hypothalamique de la balance énergétique. En effet, la RAPA active les POMC-GABA et inhibe les POMC-Glut, suggérant une dichotomie fonctionnelle de ces deux sous-populations. Enfin, des analyses d'ARNm de neurones à POMC en cellule unique ont confirmé leur grande hétérogénéité, bien que les conséquences fonctionnelles de cette diversité moléculaire soient encore largement inconnues.

Objectifs

L'objectif général de cette thèse est d'étudier le rôle spécifique des différentes sous-populations de neurones à POMC : POMC-GABA, POMC-Glut et POMC-Glut/GABA. Trois objectifs ont été définis :

- Développer une nouvelle technique de neuro-anatomie afin de détecter les différentes sous-populations de neurones à POMC activés, dans des coupes flottantes de cerveau de souris.
- Déterminer l'impact d'un régime hypercalorique sur les sous-populations de neurones à POMC.
- Déterminer le rôle des POMC-Glut dans la régulation de la balance énergétique à partir d'un nouveau modèle de souris génétiquement modifiées.

Résultats

<u>Chapitre 1</u> : Nous avons tout d'abord mis au point une nouvelle technique de détection simultanée des ARNm de GAD65/67 (marqueurs des neurones GABAergiques), vglut2 (marqueur des neurones glutamatergiques) et POMC en FISH (hybridation *in situ* en fluorescence) combinée à un immunomarquage (IHC) de la protéine cFos (un marqueur d'activité cellulaire), afin d'identifier les différentes sous-populations de neurones à POMC activées dans diverses conditions expérimentales. Le premier défi était d'adapter le protocole de FISH dont nous disposions à l'origine, qui était optimisé pour des coupes fraîches sur lames. Disposant uniquement de coupes flottantes perfusées, nous avons dû modifier dans un premier temps ce protocole, afin de préserver au mieux le tissu, qui se retrouve dans un état de fragilité extrême après les incubations à forte température nécessaires au marquage FISH. Nous avons ainsi enlevé l'étape d'incubation à la protéinase K et adapté et limité notre manipulation des coupes au maximum. Ensuite, nous avons entrepris de combiner un simple marquage FISH avec l'IHC pour cFos. Il nous a fallu tester 3 anticorps différents ainsi que plusieurs protocoles pour réussir. Ici, l'IHC doit être réalisée avant la FISH, avec une révélation basée sur la déposition de biotine, qui est fixée par une nouvelle incubation au formaldéhyde et finalement révélée à la fin du protocole par un système de complexe Avidine-Biotine couplé à une amplification du signal par tyramide. Pour le simple marquage FISH de POMC, la sensibilité de l'anticorps secondaire dirigé contre la sonde était tellement faible qu'il a fallu que nous fabriquions nous-même un réactif d'amplification du signal qui soit suffisamment concentré pour permettre une détection du marquage. Une autre difficulté a été la mise au point du marquage FISH de vglut2 : 4 sondes différentes ont été testées avant d'obtenir un marquage satisfaisant. La combinaison des marquages de GAD65/67 et vglut2 a également posé problème. Nous avons testé 7 recettes de mix d'hybridation (solution dans laquelle les sondes pour FISH sont diluées) et en avons trouvé une seule pour laquelle le co-marquage GAD/vglut2 fonctionnait. Après toutes ces péripéties, nous avons enfin mis au point un protocole pour le co-marquage de GAD65/67, vglut2 et POMC en FISH combiné au marquage IHC de cFos.

Chapitre 2 : Nous avons voulu étudier quelles sous-populations de neurones à POMC étaient activées lors d'une exposition à un régime hypercalorique et palatable (HFD). Tout d'abord, nous avons mené une expérience de choix, où des souris avaient la possibilité de manger du HFD ou une nourriture standard (CD, pour « chow diet ») pendant 2h, durant la phase diurne (moment de la journée où les souris sont généralement inactives). Nous avons vu que les souris consommaient une grande quantité de HFD. Dans une autre expérience nous avons exposé les souris à du HFD pendant 24h et les avons comparées à des souris qui étaient uniquement sous CD. Nous avons observé une hyperphagie à 1h, 2h et 24h pour les souris ayant accès au HFD. Cela s'accompagnait également d'une prise de poids corporel. Le jour d'après, lorsque les souris ayant eu le HFD sont mises de nouveau sous une alimentation standard, un effet rebond a été observé, avec une forte hypophagie et une diminution du poids corporel à 24h. Nous avons alors voulu savoir si les neurones à POMC étaient impliqués dans ces réponses au HFD et si oui, quelles sous-populations en particulier. Le co-marquage IHC de POMC et cFos a révélé qu'une courte exposition (2h) au HFD pendant la phase diurne activait environ 1/3 des neurones à POMC. Le co-marquage vglut2/GAD/POMC/cFos développé précédemment a permis de montrer que c'était principalement la population de POMC-GABA qui était recrutée dans cette situation. Dans l'autre situation expérimentale, où les souris qui avaient accès au HFD reviennent à leur ancien régime, nous avons également observé qu'1/3 des neurones à POMC était activés. Cependant, un problème technique dans le marquage FISH/IHC a rendu impossible la quantification des images et nous n'avons donc pas de réponse quant aux sous-populations de neurones qui sont activés dans ces conditions.

Chapitre 3 : Afin d'étudier les conséquences fonctionnelles de la transmission glutamatergique des neurones à POMC, nous avons généré un nouveau modèle de souris génétiquement modifiées, permettant la délétion inductible de la protéine vglut2 des neurones à POMC (avec un traitement au tamoxifène), empêchant ainsi la libération de glutamate des neurones à POMC. Nous avons tout d'abord confirmé que cette délétion avait bien lieu dans l'hypothalamus par PCR. La spécificité de la recombinaison a été vérifiée grâce à un autre modèle de souris pour lesquelles une molécule fluorescente s'exprime dans les cellules dans lesquelles la recombinaison a eu lieu. Nous avons ainsi confirmé que ce

sont bien les neurones à POMC qui sont devenus fluorescents après le traitement au tamoxifène. Nous avons alors entrepris une caractérisation métabolique de cette nouvelle lignée. Nous avons observé que les souris POMC-vglut2-KO inductibles, dont la transmission POMC glutamatergique est supprimée, ont une réponse hyperphagique exagérée suite à un jeûne de 24h. De plus, lorsqu'elles sont placées sous HFD, ces souris mangent plus et ont une dépense énergétique augmentée qui vient compenser l'augmentation des apports caloriques, d'où une absence de variation du poids corporel. À noter que l'hyperphagie induite par le HFD n'a pas été retrouvée dans un lot de souris indépendant qui était placé dans des cages calorimétriques pour étudier finement leur dépense énergétique, mais l'augmentation de la dépense énergétique sous HFD a elle, bien été reproduite.

Discussion

Mise au point de la combinaison FISH/IHC :

Ce travail aura tout d'abord permis la mise au point d'une nouvelle technique neuro-anatomique permettant la détection simultanée de trois ARNm et une protéine en fluorescence, sur des coupes flottantes de cerveau n'ayant pas été récupérées en conditions « RNAse-free ». Les deux ans et demi qui ont été nécessaires pour mettre au point ce protocole nous ont permis d'identifier les facteurs critiques qui peuvent déterminer la réussite ou l'échec de ce type de marquage (température d'hybridation, concentration des anticorps, ordre des différentes étapes, méthodes d'amplification du signal, etc.). Loin d'avoir mis au point un protocole « universel » qui s'appliquerait à toutes les conditions, nous disposons néanmoins de trois grands modèles permettant de combiner FISH et IHC, selon que l'IHC soit réalisée avant la FISH, après celle-ci, ou même entremêlée. Nous avons été en mesure de combiner 4 marquages simultanément, mais pensons que de futures améliorations permettront de dépasser cette limite, en particulier grâce à l'utilisation d'une gamme de fluorophores (Opal, PerkinElmer), dont les spectres d'excitation/émission sont suffisamment éloignés pour permettre la détection de 6 marqueurs simultanément (7 en rajoutant un fluorophore bleu).

Indentification des sous-populations de neurones à POMC activés :

Ce nouveau marquage a été immédiatement mis en application afin d'étudier le phénotype des neurones à POMC activés lors d'une exposition aiguë à un régime hypercalorique. Notons tout d'abord que nous avons observé les 3 sous-populations attendues : POMC-Glut, POMC-GABA et POMC-Glut/GABA. Un quatrième groupe a également été identifié, pour lequel aucun marqueur glutamatergique ou GABAergique n'a pu être détecté (appelé « POMC-only »). Les proportions de POMC-GABA et POMC-Glut/GABA sont par ailleurs comparables à celles obtenues dans une étude de PCR sur cellule unique, confirmant la robustesse de la technique de FISH dans l'étude de ces sous-populations. La proportion de POMC-Glut semble être cependant sous-estimée par la FISH, comparée à la PCR, sauf si l'on rassemble les POMC-only et POMC-Glut au sein du même groupe. En effet, aucune cellule POMC-only n'a été décrite en PCR, laissant penser que ces neurones soient en réalité glutamatergiques, mais dont l'expression de vglut2 est insuffisante pour être détectée par FISH. De plus, le marquage cFos obtenu lors de la combinaison FISH/IHC est similaire à celui obtenu lors d'une IHC classique, confirmant le fait que le protocole FISH/IHC n'a pas altéré l'antigénicité de cFos et permet donc une quantification optimale des neurones activés. Enfin, notre méthode de quantification a consisté en un comptage visuel des cellules POMC qui étaient positives pour les trois autres marqueurs (GAD65/67, vglut2 et /ou cFos). Pour approfondir les résultats obtenus, nous pourrions à l'avenir étudier la localisation spatiale des neurones activés, en fonction du niveau rostro-caudal et de la latéralité par rapport au troisième ventricule. Une quantification de l'intensité des marquages apporterait également une information supplémentaire, car nous avons remarqué une grande variabilité dans l'intensité des marquages vglut2 et GAD65/67, notamment dans les neurones mixtes POMC-Glut/GABA.

POMC-GABA et HFD : des neurones hyperphagiques ?

Les résultats de la quantification précédente ont montré une activation préférentielle des POMC-GABA (environ 40%) après une exposition de 2h à du HFD au cours de la phase diurne, chez des souris ayant déjà été exposées à cette nourriture hypercalorique et palatable. Cette exposition s'accompagnant d'une hyperphagie, il est tentant d'imaginer que les POMC-GABA y participent, bien que nos données ne permettent d'établir aucune relation de causalité en ce sens. Cependant, si tel était le cas, nous pourrions imaginer que

cet effet passe par une libération de γ-MSH dans l'aire tegmentale ventrale, où l'activation des récepteurs MC3R est connue pour promouvoir la motivation pour manger, ou encore une libération de β-endorphine dans les régions hédoniques du cerveau qui augmenterait le plaisir lié à la prise alimentaire. En effet, la γ-MSH et la β-endorphine sont deux neuropeptides produits par le clivage de POMC, ce qui souligne la pertinence de l'étude des sécrétions neuropeptidergiques des différentes sous-populations de neurones à POMC que nous devrions être amenés à réaliser dans le futur. Il est à noter cependant que dans cette condition, environ 60% des POMC-GABA ne répondent pas au HFD et 20% des POMC-Glut y répondent, ce qui suggère qu'au sein même des populations glutamatergiques et GABAergiques, des différences fonctionnelles existent, complexifiant encore plus le rôle de ces neurones. Enfin, qu'en est-il de l'énigmatique population mixte POMC-Glut/GABA ? À l'heure actuelle, nous ne savons pas si ces neurones sont capables de co-libérer du glutamate et du GABA, que ce soit au sein des mêmes vésicules ou sur différentes synapses. Il est possible également qu'ils servent de neurones de réserve dont le phénotype s'adapterait en fonction des conditions physiologiques. Nos données montrent que ces neurones répondent au HFD d'une manière similaire aux POMC-GABA, avec environ 1/3 de neurones activés, suggérant que leur phénotype fonctionnel se rapproche plus de celui des POMC-GABA. Comme évoqué précédemment, une analyse plus précise de l'intensité relative du marquage GAD65/67 et vglut2 au sein de ces neurones permettrait de clarifier ce point.

L'effet rebond lors du retour à une alimentation standard :

Nous avons observé un effet rebond (hypophagie et perte de poids) lorsque les souris retournaient à une alimentation standard après 24h d'exposition au HFD. Malheureusement, des problèmes techniques lors du marquage FISH/IHC n'ont pas rendu possible l'identification des sous-populations de neurones à POMC activés dans cette condition. Nous pouvons cependant supposer que, contrairement à la situation précédente, les POMC-Glut seraient ici plus nombreux à être recrutés, participant à l'effet satiétogène classiquement décrit pour les neurones à POMC. Il est à noter que lors du double-marquage POMC/cFos en IHC, l'intensité du marquage cFos était beaucoup plus variable que lors de l'exposition à 2h de HFD. Le sacrifice ayant été réalisé au début de la phase nocturne, correspondant à la phase active des souris, il est ainsi plus difficile d'interpréter le marquage

cFos : certaines cellules peuvent être positives, non pas parce qu'elles ont répondu au changement de nourriture *per se*, mais parce que les souris ont commencé à manger à des temps différents après le changement, induisant une accumulation plus ou moins forte de cFos au sein des neurones à POMC. Le marquage cFos dans cette condition ne reflète donc pas forcément la réponse neuronale au changement de nourriture. Pour surmonter ce problème, il pourrait être intéressant de s'intéresser à d'autres marqueurs d'activité cellulaire plus précoces, tels que ERK, dont la phosphorylation (pERK) peut survenir dans les minutes qui suivent un stimulus. Ainsi, l'effet du changement de nourriture pourrait être étudié plus directement, sans les facteurs de confusion induits par la prise alimentaire « normale » durant la phase nocturne.

Caractérisation du modèle POMC-vglut2-KO :

Nous avons créé une nouvelle lignée de souris transgéniques où la délétion de vglut2 est réalisée spécifiquement dans les neurones à POMC après un traitement au tamoxifène. Le contrôle de la délétion a été effectué par PCR sur hypothalamus total et la spécificité de la recombinaison a été vérifiée grâce à une lignée rapportrice. Pour autant, la délétion de vglut2 n'a pas été directement observée dans les neurones à POMC, ce que nous ferons par FISH lorsque nous disposerons d'une sonde permettant de détecter uniquement l'exon 2 du gène *Slc17a6* (codant pour vglut2), qui est excisé dans notre modèle. De même, il serait important de vérifier que cette délétion entraîne bien une suppression de la transmission glutamatergique des neurones à POMC, par électrophysiologie. Les données obtenues sur ce modèle montrent que la délétion de vglut2 entraîne une hyperphagie lors d'une réalimentation suite à un jeûne de 24h (également appelé « refeeding »), sous une alimentation standard. Il est intéressant de noter que ce phénotype correspond également à ce que notre laboratoire a observé dans de précédentes expériences, lorsque de la rapamycine est administrée dans le ventricule latéral. Cette molécule, un inhibiteur de la voie de signalisation mTORC1, provoque également une hyperphagie en situation de refeeding, et inhibe les neurones à POMC glutamatergiques. De ce fait, la suppression génétique de vglut2 récapitule le phénotype observé lors de l'inhibition pharmacologique des neurones POMC-Glut par la rapamycine. Les souris POMC-vglut2-KO présentent également une légère augmentation de la prise alimentaire sous HFD, qui s'accompagne d'une augmentation de la dépense énergétique, si bien que leur poids reste constant. Toutes

ces données placent la transmission glutamatergique des neurones à POMC comme un signal anorexigène, caractéristique du rôle classique des neurones à POMC. Cependant, plusieurs limitations sont à prendre en considération dans cette étude. Tout d'abord, le traitement au tamoxifène utilisé pour provoquer la délétion induit lui-même des modifications métaboliques à long terme, notamment en réponse au HFD, en agissant sur les neurones à POMC. Cela souligne l'importance d'utiliser des contrôles qui auront eux-mêmes reçus ce traitement, comme dans notre étude. Ensuite, la délétion touche l'ensemble des neurones à POMC, à savoir ceux situés dans le noyau arqué de l'hypothalamus de même que ceux situés dans le noyau du faisceau solitaire, que nous n'avons pas étudié ici. Pour ces derniers, le phénotype glutamatergique/GABAergique n'a pour l'instant jamais été étudié. Les neurones mixtes POMC-Glut/GABA sont également affectés par cette délétion, qui transforme leur phénotype en neurones à POMC GABAergiques purs. Enfin, l'hyperphagie observée lorsque les souris sont soumises à une alimentation HFD n'a été observée que dans une cohorte sur les deux étudiées ici. Dans la deuxième cohorte cependant, le HFD a été donné dans des cages métaboliques, et lorsque les souris étaient plus jeunes, suggérant un rôle de l'âge dans la survenue de cette hyperphagie. De futures expériences sont prévues, où le HFD sera donné à différents âges afin d'en étudier l'impact. Nous comptons également étudier le métabolisme glucidique et effectuer des tests de préférence entre nourriture standard et nourriture HFD chez ces souris. À plus long terme, la délétion de GAD65/67 des neurones à POMC est également prévue, par la création d'une lignée similaire à celle-ci, en croisant des souris POMC-creER^{T2} avec des souris Gad1/Gad2-flox.

Conclusion générale et perspectives :

L'ensemble de ce travail tend à montrer qu'il existe une dichotomie fonctionnelle entre les neurones à POMC GABAergiques et glutamatergiques. Les POMC-GABA sont préférentiellement activés par une courte exposition à un régime hypercalorique et palatable et nous pouvons émettre l'hypothèse qu'ils jouent un rôle orexigène en agissant sur la régulation exostatique de la prise alimentaire (stimulation de la motivation/plaisir pour la nourriture). À l'inverse, les POMC-Glut auraient un rôle anorexigène, plus en lien avec la régulation endostatique de la balance énergétique. Ces données préliminaires devront être néanmoins confirmées et approfondies par de nouvelles études, en gardant à l'esprit qu'il

est plus que probable qu'au sein même de ces sous-populations, il existe également des différences fonctionnelles. Ainsi, pour aller plus loin, il serait primordial de pouvoir manipuler sélectivement les POMC-Glut, POMC-GABA et POMC-Glut/GABA afin de les activer ou inhiber de manière inductible et en étudier les conséquences sur le métabolisme. Cela serait possible grâce à une approche originale, combinant souris transgéniques et vecteurs viraux pour une modulation pharmaco- ou optogénétique de ces sous-populations. Des souris Gad2-Cre et vglut2-Flip pourraient être croisées pour créer une nouvelle lignée de souris dans lesquelles les neurones GABAergiques expriment la Cre-recombinase et les neurones glutamatergiques expriment la Flippase. L'injection d'AAV dont l'expression nécessite la présence (-on) ou l'absence (-off) de la Cre et la Flip (système INTERSECT) permettrait alors de cibler sélectivement les neurones glutamatergiques, GABAergiques et mixtes. L'expression spécifique dans les neurones à POMC serait quant à elle possible si le transgène porté par le virus (molécule fluorescente, DREADD, opsine, etc.) est sous la dépendance du promoteur de POMC. Ainsi, nous pourrions cibler spécifiquement les POMC-Glut (Cre-off/Flip-on), POMC-GABA (Cre-on/Flip-off) ou POMC-Glut/GABA (Cre-on/Flip-on) pour étudier les sites de projection spécifiques de ces sous-populations ou encore les conséquences directes de leur activation/inhibition sur le comportement alimentaire et le métabolisme.

Mots-clés : **FISH, POMC, glutamate, GABA, hypothalamus, balance énergétique**

Scientific production

List of abbreviations

Table of contents

Scientific production

Published articles:

1. **Simon V,** Cota, D. (2017). "MECHANISMS IN ENDOCRINOLOGY: Endocannabinoids and metabolism: past, present and future." Eur J Endocrinol **176**(6): R309-r324.

2. Haissaguerre M., Ferrière A, **Simon V**, Saucisse N, Dupuy N, André C, Clark S, Guzman-Quevedo O, Tabarin A, Cota D. (2018). "mTORC1-dependent increase in oxidative metabolism in POMC neurons regulates food intake and action of leptin." Mol Metab **12**: 98-106.

3. Mazier W, Saucisse N, **Simon V**, Cannich A, Marsicano G, Massa F, Cota D. (2019). "mTORC1 and CB1 receptor signaling regulate excitatory glutamatergic inputs onto the hypothalamic paraventricular nucleus in response to energy availability." Mol Metab **28**: 151-159.

Article in submission:

Saucisse N#, Mazier W#, **Simon V#,** Binder E, Catania C, Bellocchio L., Romanov RA, Matias I, Zizzari P, Léon S, Quarta C, Cannich A, Meece K, Gonzales D, Clark S, Becker J, Yeo GSH, Merkle F, Wardlaw SL, Harkany T, Massa F, Marsicano G, Cota D. “mTORC1 signaling orchestrates bidirectional control of food intake by hypothalamic POMC neurons.”

Submitted to Cell Metabolism. #Share first co-authorship.

Articles in preparation:

1. **Simon V**, Cannich A, Clark S, Marsicano G, Cota D. A new methodological approach to assess the recruitment of POMC neurons subtypes in response to energy availability.
2. **Simon V**, Zizzari P, Dupuy N, Gonzalez D, Cota D. POMC glutamatergic neurons inhibit feeding.

Individual fellowships:

1. Individual PhD fellowship from the French Ministry of Higher Education, Research and Innovation. 2015-2018
2. PhD Extension Grant from the Fondation pour la Recherche Médicale (FRM ; FDT201805005371). 2018-2019.

Oral communication:

Saucisse N, **Simon V**, Clark S, Cota D. Unraveling the role of p62 in the hypothalamic regulation of energy balance. (study conducted during my Master 2)

Presented at: Neuroscience in Bordeaux Association Symposium, 2015, Bordeaux.

Prize: **Outstanding speaker award.**

Posters:

1. Saucisse N, **Simon V**, Clark S, Cota D. Unraveling the role of p62 in the hypothalamic regulation of energy balance.
   Presented at: Neurocentre Magendie Symposium, 2015, Bordeaux.

2. Saucisse N, Mazier W, Binder E, Catania C, Bellocchio L, Romanov RA, Matias I, Cannich A, Meece K, **Simon V**, Gonzales D, Clark S, Wardlaw SL, Harkany T, Massa F, Marsicano G, Cota D**.** mTORC1 signaling orchestrates bidirectional control of food intake by hypothalamic POMC neurons.

Presented at: Keystone Symposium "Neuronal Control of Appetite, Metabolism and Weight", 2017, Copenhagen.

3. **Simon V**, Andre C, Cannich A, Clark S, Fénelon V, Varilh M, Marsicano G, Cota D. Combining FISH and IHC techniques in thick free-floating brain sections
   Presented at: Neurocentre Magendie Symposium, 2018, Bordeaux
   Prize: **Best poster award**

4. **Simon V**, Zizzari P, Cota D. mTORC1 in hypothalamic SF1 neurons regulates metabolic adaptation to caloric overload: preliminary evidence.
   Presented at: TOR de France Symposium, 2018, Nice

5. Léon S, **Simon V**, Fisette A, Yi CX, Tschöp M, Garcia-Caceres C, Cota D, Quarta C. Identity plasticity in hypothalamic neurons in response to metabolic stress.
   Presented at: Metabolism in action-Copenhagen Bioscience Conference, 2019, Copenhagen

Participation to national/international scientific meetings:

1. Keystone Symposium "Neuronal Control of Appetite, Metabolism and Weight", Copenhagen, 2017.
2. NeuroFrance, Bordeaux, 2018
3. TOR de France, Nice, 2018

List of abbreviations

4-OHT: 4-hydroxy tamoxifen

AGB: adjustable gastric banding

AgRP: agouti-related peptide

AMA: American Medical Association

AMCA: aminomethylcoumarin acetate

α-MSH: alpha-melanocyte-stimulating hormone

ARC: arcuate nucleus of the hypothalamus

BBB: blood-brain barrier

BMI: body mass index

BPD-DS: biliopancreatic diversion with a duodenal switch

CART: cocaine- and amphetamine-regulated transcript

CCK: cholecystokinin

CD: chow diet

CRH: corticotrophin releasing hormone

Cy3: cyanine 3

Cy5: cyanine 5

CYP2D6: cytochrome P2D6

CYP3A: cytochrome P3A

DA neurons: dopaminergic neurons

DIG: digoxigenin

DIO: diet-induced obesity

DMH: dorsomedial nucleus of the hypothalamus

DMSO: dimethylsulfoxide

DNP: 2,4-dinitrophenol

DS: dextran sulfate

DTT: 1,4-dithiothreitol

DVC: dorsal vagal complex

ER: estrogen receptor

EWL: excessive weight loss

FITC: fluorescein isothiocyanate

FISH: fluorescent in situ hybridization

FFM: fat-free mass

FM: fat mass

GAD65: glutamic acid decarboxylase, 65kDa

GAD67: glutamic acid decarboxylase, 67kDa

GHSR: growth hormone secretagogue receptor (= ghrelin receptor)

GI tract: gastrointestinal tract

GLP-1: glucagon-like peptide 1

γ-MSH: gamma-melanocyte-stimulating hormone

HCl: hydrochloric acid

HRP: horseradish peroxidase

IEG: immediate early gene

IHC: immunohistochemistry

InsR: insulin receptor

KO: knockout

LepR: leptin receptor

LHA: lateral hypothalamic area

MAPK: mitogen-activated protein kinases

mCPP: meta-Chlorophenylpiperazine

MRI: magnetic resonance imaging

mTORC1: mechanistic target of rapamycin, complex 1

NAc: nucleus accumbens

NAcc: core of the nucleus accumbens

NAcSH: shell of the nucleus accumbens

NBF: neutral buffered formalin

NPY: neuropeptide tyrosine

NTS: nucleus tractus solitarii

PBS: phosphate buffered saline

PCR: polymerase chain reaction

POMC: proopiomelanocortin

POMC-GABA: gabaergic proopiomelanocortin neurons

POMC-Glut: glutamatergic proopiomelanocortin neurons

PVH: paraventricular nucleus of the hypothalamus

PYY: peptide tyrosine tyrosine

RAPA: rapamycin

RYGB: roux-en-Y gastric bypass

SEM: standard error of the mean

sEPSC: spontaneous excitatory post-synaptic current

SF1: steroidogenic factor 1

SG: sleeve gastrectomy

SSC: saline-sodium citrate buffer

TRH: thyrotropin-releasing hormone

TSA: tyramide signal amplification

UTP: uridine triphosphate

vGat: vesicular GABA transporter

vglut2: vesicular glutamate transporter 1

vglut2: vesicular glutamate transporter 2

VMH: ventromedial nucleus of the hypothalamus

VTA: ventral tegmental area

WHO: World Health Organization

WT: wild type

Table of contents

Introduction

Chapter 1

Globesity
A worldwide epidemic

This chapter will present the latest epidemiological data on worldwide obesity and its human and economic consequences. The treatments and main aetiological factors identified to date will also be discussed.

❖ Definition

Obesity is a pathological condition defined by an accumulation of fat that presents a risk to health. According to the World Health Organization (WHO), an individual is obese at a Body Mass Index ($BMI = \frac{weight}{height^2}$) of at least 30kg/m² (Whitlock, Lewington *et al.* 2009, Rahman and Berenson 2010). The BMI is frequently used to estimate an individual's health risks relative to his weight, defining different categories, presented in Figure 1.

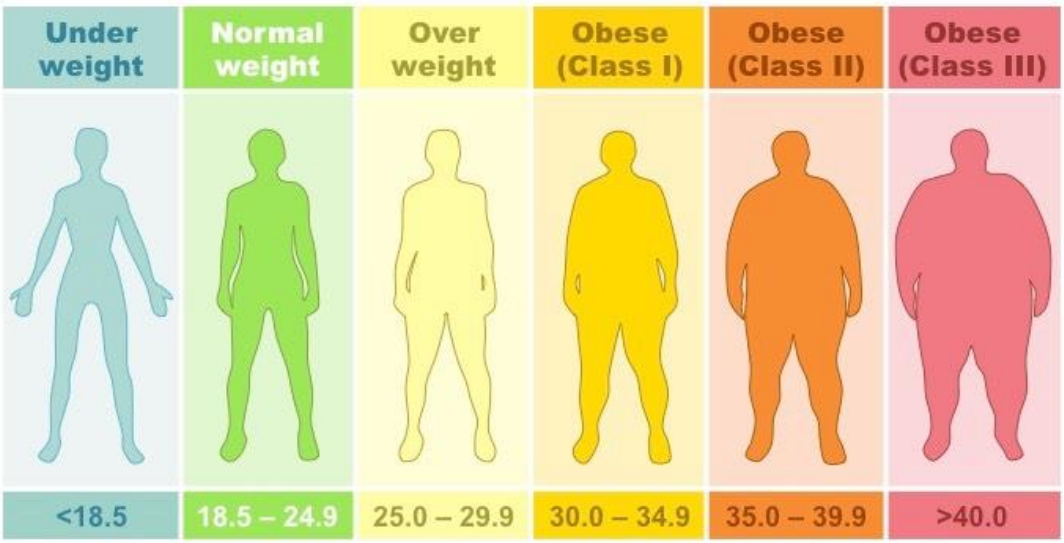

Figure 1: **World Health Organization adult Body Mass Index classification**

Figure taken from https://wikplus.blogspot.com/2019/03/obesity-and-overweight.html

However, many authors criticize the simplistic nature of this index, which takes into account an individual's total mass, without differentiating the fat mass from the fat-free mass (muscle mass + bone mass) (Hebert, Allison *et al.* 2013). This distinction matters, since a top-level athlete who has developed a high muscle mass may be wrongly classified as obese, although he or she does not have any excessive accumulation of fat

(Kraemer, Torine *et al.* 2005). Other anthropometric measurements can be made, such as waist circumference and waist-to-hip ratio. The WHO consider them as better indicators than the BMI, because they give a more accurate representation of abdominal fat (which is thought to have the most negative impact on health), with a more precise classification, depending on age and gender. Of note, different methods exist to better quantify the amount of adipose tissue: hydrostatic weighing, dual x-ray absorptiometry, computed tomography and magnetic resonance imaging (MRI), but these techniques are more expensive and impractical for routine clinical examinations (Purnell 2018).

Hence, despite their imprecision, the anthropometric indicators meet an imperative of practicality and remain the reference used to define obesity in clinical and epidemiological studies.

❖ Is obesity a disease?

Describing obesity as a disease or not is a long-standing debate in the medical field, the difficulty coming from the fact that there is no universal definition of a disease (Kyle, Dhurandhar *et al.* 2016). In Hippocrates' time, overweight was already considered as a risk factor of increased mortality (Rosen 2014), an assertion that has not been denied since. However, for most of the 20th century, obese people were held personally responsible for their condition, which was considered to be the reflection of their poor lifestyle and uncontrolled gluttony. In this view, an obese person is not a patient suffering from a pathology, but an individual whose moral weaknesses and lack of control have led to a state that could only be reverted by his own will.

This stigmatizing view of obesity has since been challenged by recent discoveries in the identification of the real causes of obesity, including multiple biological factors (genetic and hormonal) that influence fat accumulation. This new knowledge has gradually led various organizations to change their definition of obesity and recognize it as a real disease. In 1998, the US National Institutes of Health (NIH) recognized obesity for the first time as a "complex chronic multifactorial disease". Several organizations did the same in the following years, but it was in 2013 that a decisive step

was reached, with the recognition by the American Medical Association (AMA) of obesity as a "chronic progressive disease", and not just a mere risk factor for other pathologies (Rosen 2014). This decision is emblematic because the AMA is the largest medical association in the United States.

Although still controversial to date, the qualification of obesity as a chronic disease serves a more utilitarian than scientific purpose, in order to change the negative view of the general public (and some doctors) towards obese people, encourage research in its endeavour and a allow people to have medical coverage/insurance related to obesity (Kyle, Dhurandhar *et al.* 2016).

❖ Worldwide prevalence of obesity

Since 1975, the prevalence of overweight and obesity has almost tripled, reaching about one-third of the world's population, including 1.9 billion adults (over 18 years of age) and 381 million children/adolescents (under 19 years of age) in 2016, according to the WHO. Overall, the obesity rate is higher among women than men (Figure 2A) regardless of socio-economic background, and it increases with age, with a maximum gender difference between 50 and 60 years of age (Chooi, Ding *et al.* 2019). However, there is a fairly large regional disparity in the prevalence of obesity, with rich countries being the most severely affected, with the notable exception of some South-East Asian countries such as Japan and South Korea, where the obesity rate is below 5% despite very high industrialization (Figure 2B). It should also be noted that obesity differently affects social classes: in rich countries, obesity mainly affects the underprivileged, while in poor countries, it preferentially affects the urban upper class (Swinburn, Sacks *et al.* 2011).

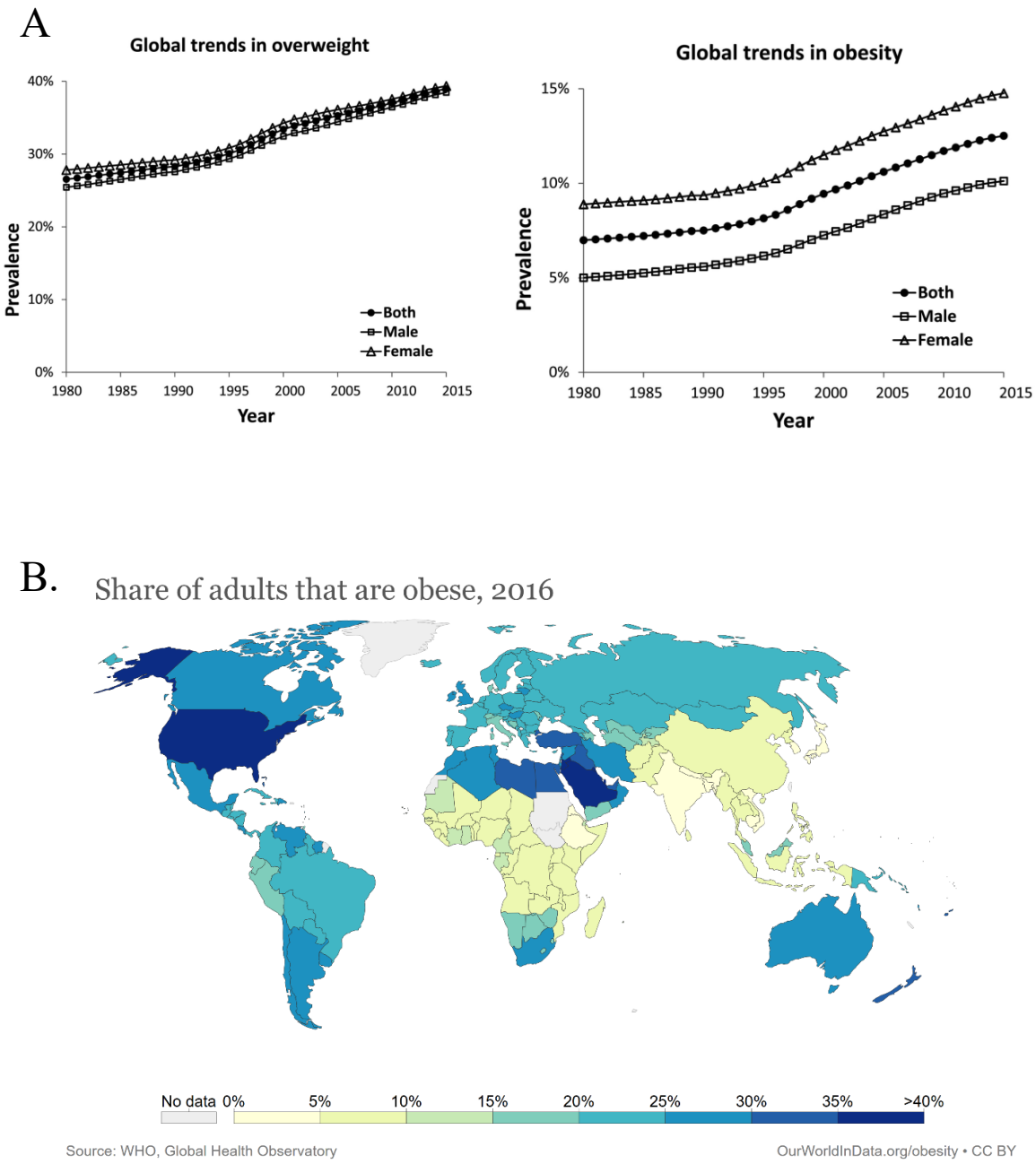

<u>Figure 2</u>: Prevalence of obesity

A: Age-standardized global prevalence of overweight (left) and obesity (right) in men and women >20 years old by year, from 1980 to 2015. *Taken from (Chooi, Ding et al. 2019).*
B: Percentage of obese adults within each country, worldwide. *Source: WHO*

Thus, while the obesity rate seems to have stabilized in some rich countries over the past 10 years, such as in the United States where it remained at around 30-34% between 2005 and 2015, the overall prevalence has increased worldwide, with a general trend towards acceleration (Chooi, Ding *et al.* 2019). If this trend does not change, 57.8% of the world's population could be overweight or obese by 2030 (Kelly, Yang *et al.* 2008). However, this prediction might be still below reality, as all these studies use the BMI and associated thresholds to define overweight and obesity. As explained above, this index is not necessarily the most precise, because a given BMI value can underlie an almost twofold inter-individual variation in the percentage of body fat, depending on age, sex and ethnicity (Gallagher, Visser *et al.* 1996, Gallagher, Heymsfield *et al.* 2000). For example, Asian populations have a higher adiposity than European ones for a similar BMI, which led some Asian countries to lower the threshold above which an individual is considered obese. For instance, in China, the Working Group on Obesity has lowered this threshold from 30kg/m² to 28kg/m² (Zhou 2002). As a result, the number of people whose health is threatened by an excess amount of body fat could be even greater than in the current estimates, which are already particularly alarming.

❖ Aetiology

In the last decades, the production and distribution of food has changed dramatically, together with lifestyle modifications, especially in the most industrialized countries. Since the 1970s, there has been an overproduction of high-calorie processed food and sweetened beverages to feed an increasingly urbanized population, leading to an overall increase in calorie intake (Kadouh and Acosta 2017). This was accompanied by an increased sedentarization (e.g. time spent watching television) that promotes weight gain (Hu 2003) and an overall decrease in physical activity, which in turn, increases the risk of cardiovascular diseases and diabetes, among other things (Fox and Hillsdon 2007). Other factors such as sleep deprivation are correlated with an increase in obesity, although to date, no causal relationship is clearly established (Cappuccio, Taggart *et al.* 2008). Taken together, these results show that the huge increase in the prevalence of

obesity occurred in a period characterized by a profound environmental transformation, in favour of caloric overload and physical inactivity (Piazza, Cota *et al.* 2017).

However, not all individuals living in this new “obesogenic” environment become obese. This apparent discrepancy is not necessarily due to a difference in lifestyle choice, but can be explained by the biological factors underlying body weight regulation. Among these, the genetic factors are certainly the most important ones. Indeed, studies of twins and adoptees suggest that up to 70% of the inter-individual variation in fat mass has a genetic aetiology (Farooqi and O'Rahilly 2008). Some forms of obesity are caused by the mutation of a single gene (e.g. POMC, leptin, leptin receptor, melanocortin receptor 4...) or chromosome abnormalities (e.g. Prader-Willi syndrome) but this is rare. Most of the time, multiple genetic variants contribute together to the determination of the BMI (Kadouh and Acosta 2017), which is a highly hereditable trait. Of note, gene expression is itself subjected to variations due to chromatin modifications (acetylation, methylation) which take place particularly in pre- and peri-natal periods. These "epigenetic" (from the Greek: “on top of genetics”) changes are often considered to reflect the environment at the genetic level and could therefore be a link between environmental changes and the development of obesity (Lopomo, Burgio *et al.* 2016). In addition to these (epi)genetic determinants, other factors can promote the development of obesity, such as physiological changes (e.g. pregnancy, menopause), various endocrine diseases (e.g. Cushing's syndrome, hypothyroidism) or drugs’ side effects. Finally, the composition of the gut microbiota and some adenoviruses (namely Ad36 and Ad37) are also known to play an aetiological role that is being studied with growing interest.

Thus, the current obesity pandemic is likely caused by an interaction between environmental and biological factors (Figure 3). However, the debate about what is the main cause of obesity, i.e. environment (Wilding 2012) or genetics, (Frayling 2012) still rages on.

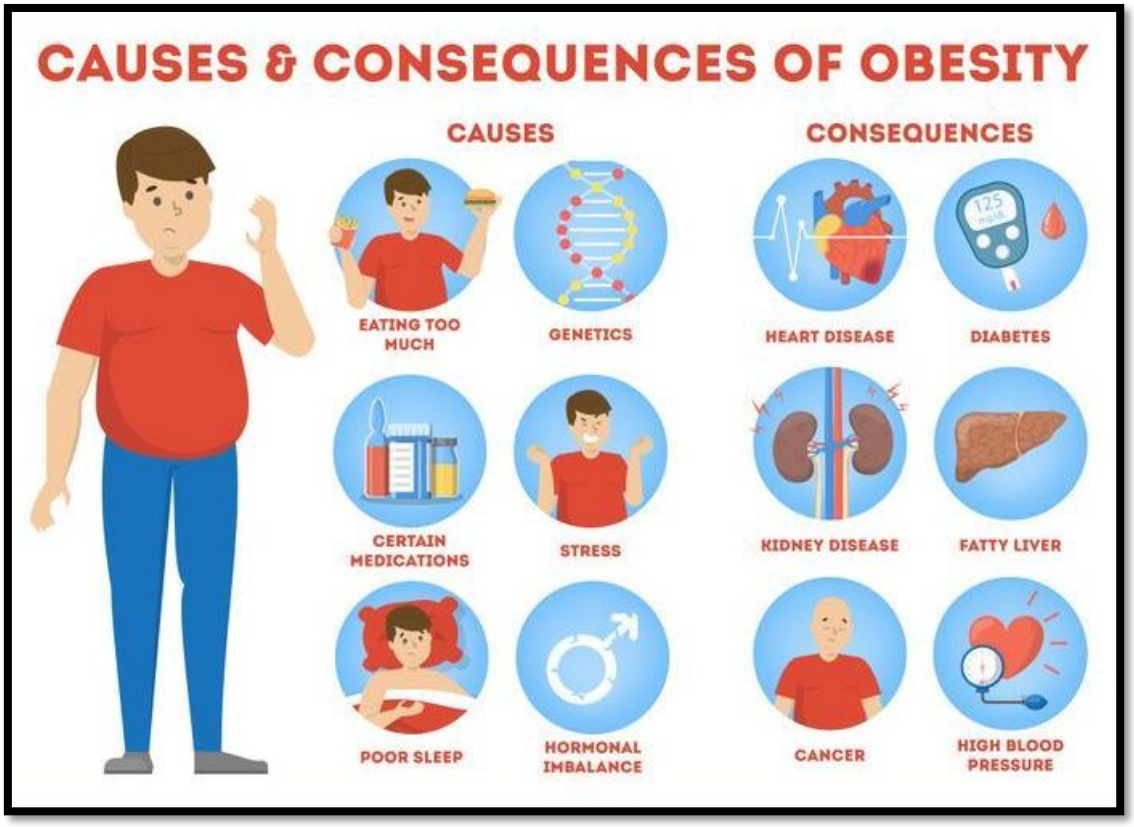

<u>Figure 3</u>: Principal causes and consequences of obesity

Figure taken from https://www.pinterest.fr/obesitybild/

❖ Consequences

Such an obesity pandemic has consequences, in terms of quality of life for obese patients as well as socio-economic burden for the most affected countries. Globally, overweight and obesity are estimated to be responsible for 5% of deaths, making them the 5th leading cause of death. Obesity is associated with a decrease in life expectancy from 5 to 20 years, depending on the severity of the associated co-morbidities (Hruby, Manson *et al.* 2016). Indeed, obesity is a major risk factor for a large number of non-communicable diseases (Figure 3). For example, oxidative stress and chronic inflammation are common features of obesity and are among main causes of insulin resistance, which can lead to the development of type 2 diabetes (Salmon 2016). Thus, it is estimated that 85% of patients with type 2 diabetes are overweight or obese (Bhupathiraju and Hu 2016).

Many other health problems can result from obesity and diabetes, such as hypertension, dyslipidaemia, fatty liver, vascular and renal impairment, retinal vascular disease, peripheral neuropathy, peripheral vascular disease (Meldrum, Morris *et al.* 2017). Depending on how well patients are treated, these diseases can have serious consequences such as amputations, blindness or senility, dramatically degrading their quality of life. In general, obesity increases the risk of cardiovascular diseases such as arrhythmias, heart attacks (Plourde, Sarrazin *et al.* 2014) or strokes (Rexrode, Hennekens *et al.* 1997).

Obesity is also a risk factor for many cancers: colon, rectum, breast, uterus, ovaries, oesophagus, pancreas, kidney, gallbladder, brain, lymphoma (Hruby, Manson *et al.* 2016, Meldrum, Morris *et al.* 2017). Overall, high BMI and its increase are associated with an enhanced risk of cancer and overweight contributes to 20% of all cancer-related deaths, according to the American Cancer Association.

Moreover, obese patients have a 2-fold increase in the incidence of osteoarthritis compared to thin subjects (Blagojevic, Jinks *et al.* 2010). Other physical (thrombophlebitis, gallstones, urinary incontinence, easy fatigability) or mental health problems (sexual dysfunction, depression, low self-esteem, motivational disorders, eating disorders, impaired body image, interpersonal communication problems) and neurodegenerative diseases like Alzheimer's disease, occur more frequently in obese people, but we will not discuss them further for the sake of space (Djalalinia, Qorbani *et al.* 2015, Meldrum, Morris *et al.* 2017).

Economically, it is difficult to quantify the exact cost of obesity, since not all studies include the same co-morbidities, often omitting the mental health problems (Tremmel, Gerdtham *et al.* 2017). However, the McKinsey Global Institute estimated that in 2012, obesity-related spending reached US$2,000 billion worldwide (i.e. 2.8% of GDP). Obesity is thus an economic burden, both at the individual and national level, through an increase in healthcare spending, but also in the number of people with disabilities or unable to work (Runge 2007). Unfortunately, the increasing prevalence of worldwide obesity is likely to weigh even more heavily on the economies of developed countries.

❖ Current treatments

Different strategies have been elaborated to fight against the global obesity epidemic, although to date, no single country has succeeded in reverting the phenomenon (Roberto, Swinburn *et al.* 2015). There are three main categories of treatments: lifestyle interventions, pharmacological treatments and bariatric surgery.

First, the lifestyle interventions consist of changing patients' lifestyles in order to achieve weight loss. In fact, the goal is to limit their caloric intake while promoting physical activity, to place them in a state of "negative energy balance". The energy balance represents the balance between energy intake and expenditure and, by extension, body weight gain or loss. Thus, dietary interventions are combined with behavioural therapies in order to achieve weight loss. Different types of diets can be used for this purpose, most of which vary in macronutrient composition (fat/protein/carbohydrates) and/or in overall amount of calories (Ruban, Stoenchev *et al.* 2019) :

- **Low fat diets**: in these diets, lipids provide less than 30% of the total energy. As these are the macronutrients with the highest calorie density (9 kcal/g), their drastic reduction in the diet results in weight loss.
- **Very low/Low carbohydrate diet**: in these diets, the more or less significant reduction in carbohydrates leads to an inversion of the energy balance. Initial weight loss is faster than for low fat diets, probably due to the mobilization of glycogen stocks and dehydration (Bray 2003).
- **High protein diet**: in these diets, more than 30% of the energy is provided by proteins, because proteins are the most satietogenic nutrients. As a consequence, their consumption in large quantities is expected to extend satiety, but the effects on body weight are small (Santesso, Akl *et al.* 2012).
- **Very low/Low calorie diet**: unlike previous diets which varied in one specific macronutrient, these diets are nutritionally balanced, but their total energy density is reduced, to achieve a negative energy balance.

Overall, none of the aforementioned diets are successful in fighting against obesity in the long term. It seems that caloric restriction, regardless of macronutrients, is the most

effective way to lose weight, but the longstanding results of such dietary intervention are very disappointing because of systematic weight regain. At best, the net benefit is a long-term (3-year) weight reduction of 5% (Ruban, Stoenchev *et al.* 2019). The weight regain can be explained by metabolic adaptations (i.e. reduction of energy expenditure) to weight loss but also by patients' lack of compliance with overly restrictive diets. An alternative is the "Mediterranean diet", which is less restrictive, characterized by a high consumption of fruit, fish and vegetables with less meat and fat. This diet can lead to weight loss and reduced risk of cardiovascular problems (Huo, Du *et al.* 2015).

Alone, lifestyles interventions are not very effective, but complementary pharmacological treatments can potentiate their effects, particularly on weight loss maintenance, although in some cases, their anti-obesity mechanisms are not known. The main treatments approved by the US Food and Drug Administration are the following (Ruban, Stoenchev *et al.* 2019) :

- **Orlistat**: this pancreatic lipase inhibitor prevents the absorption of about 30% of the ingested lipids, which are then excreted in the feces. It causes modest weight loss (generally less than 5%) and a reduction in cardiovascular risk and type 2 diabetes (Torgerson, Hauptman *et al.* 2004). The main side effects include oily stools and incontinence.
- **Saxenda®**: its active substance, Liraglutide, is Glucacon-like peptide 1 (GLP-1) receptor agonist. GLP-1 is a satiety hormone produced by the gastrointestinal tract (GI tract). It allows a dose-dependent weight reduction of up to 6% at 1 year (Davies, Bergenstal *et al.* 2015). Side effects include gastrointestinal disorders and acute pancreatitis.
- **Mysimba®**: this drug combines naltrexone, an opioid antagonist used in alcohol and opioid addiction and bupropion, a dopamine and norepinephrine recapture inhibitor, used as an antidepressant and for smoking cessation. Together, these two molecules act as an appetite suppressant, resulting in a weight reduction of about 6% (Greenway, Fujioka *et al.* 2010). Side effects include nausea, headache and constipation.

- **Belviq®**: its active substance, Lorcaserin, is a serotonin 5-HT2c receptor agonist that increases serotonin reuptake, leading to a weight reduction of about 5%, without causing heart problems, which are usually caused by other 5-HT2c agonists such as fenfluramine (Bohula, Wiviott *et al.* 2018).
- **Qsymia®**: this new drug combines phentermine (an amphetamine derivative that acts as an appetite moderator) and topiramate (an anti-convulsant that induces moderate weight loss through an unknown mechanism). Together, they allow a weight loss of about 13% over 2 years (Yanovski and Yanovski 2014).

Thus, all the treatments mentioned above have a modest efficacy and their use is limited by the many associated side effects. Of note, in France, only Orlistat is available as an anti-obesity drug.

When all dietary and/or drug interventions have failed, and for the most severe cases of obesity, bariatric surgery is an interesting alternative because its effectiveness on weight loss and associated comorbidities is much greater than other treatments (Colquitt, Pickett *et al.* 2014). There are four types of bariatric surgery (Figure 4):

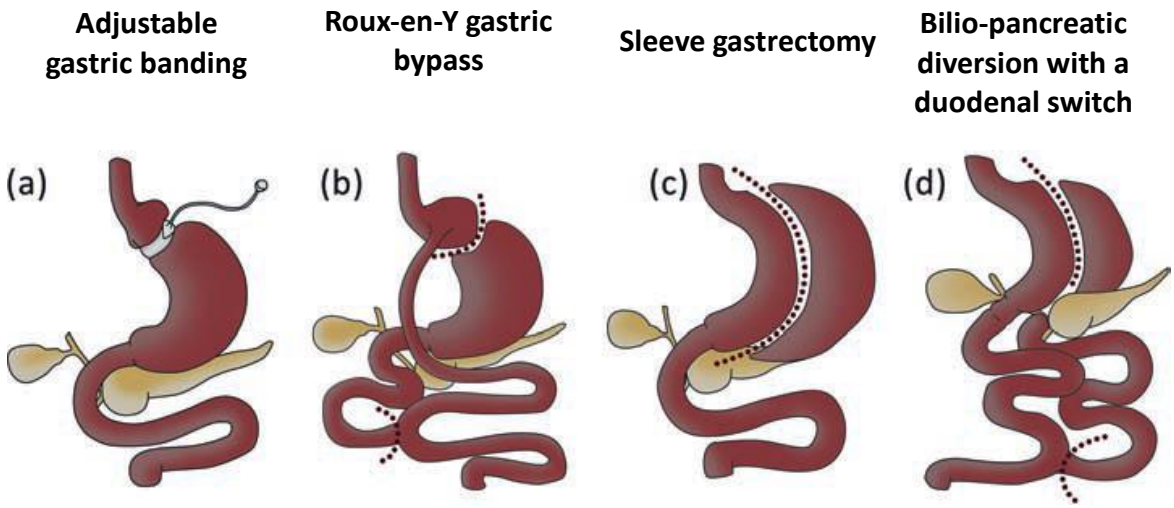

<u>Figure 4</u>: Different bariatric surgeries

Figure modified from (Ruban, Stoenchev et al. 2019).

- **Adjustable gastric banding (AGB)**: this operation consists of placing a silicone band around the upper part of the stomach in order to limit the amount of food ingested (Figure 4A). This allows an excessive weight loss (EWL) of 55% within 2 years of the procedure, as well as the remission of many associated comorbidities (Chang, Stoll *et al.* 2014). Of note, the %EWL is the percentage of weight lost with respect to the theoretical weight that a patient has to lose in order to reach a BMI of 25. Side effects include gastroesophageal reflux and band slippage.
- **Sleeve gastrectomy (SG)**: this operation consists of excising 80% of the stomach (Figure 4C), thereby reducing the volume of food ingested. Unlike the previous technique, this one is obviously irreversible but is more effective, with a %EWL of 70% at one year, as well as the remission of many comorbidities (Chang, Stoll *et al.* 2014). As with gastric banding, gastroesophageal reflux is one of the side effects encountered. More serious complications, such as anastomotic leakage, are also possible.
- **Roux-en-Y gastric bypass (RYGB)**: this operation consists of separating an upper pouch of the stomach, which is then connected to the distal part of the intestine (Figure 4B). The food ingested avoids most of the stomach and the proximal part of the intestine. This technique achieves a %EWL of 72% at 1 year, a significant remission of comorbidities and a good long-term weight loss maintenance (Chang, Stoll *et al.* 2014). However, some severe surgical complications can lead to bowel obstruction and perforation.
- **Biliopancreatic diversion with a duodenal switch (BPD-DS)**: this operation consists first of a SG. Then, the distal part of the intestine (ileum) is connected to the proximal part (duodenum), thus shunting most of the intestine (Figure 4D). This operation achieves a %EWL of 73% with weight loss maintained up to 8 years, and decreased comorbidities (Buchwald, Estok *et al.* 2009). As BPD-DS is a rather complex procedure, it also combines the complications observed in SG and RYGB, including anastomotic leaks and bowel obstruction.

Bariatric surgery techniques are the most effective for long-term weight loss. However, the risks associated with the surgery, the side effects and the irreversible nature of these procedures (except for AGB) mean that they are generally reserved for the most severe cases of obesity (BMI $\geq$ 40kg/m² or BMI $\geq$ 30kg/m² with co-morbidities) for which everything else have failed. In addition to the surgical complications, patients frequently suffer from dumping syndrome and nutritional deficiencies (lipophilic vitamins, minerals…) after bariatric surgeries, and need aesthetic type of surgery to remove the excess of skin. Finally, they are more likely to develop behavioural disorders, often because the underlying behavioural alterations related to food intake were not appropriately addressed (Ruban, Stoenchev *et al.* 2019). Thus, if bariatric surgery can surely save lives, it is far from an ideal solution for the majority of obese patients.

Therefore, a better understanding of the biological mechanisms at work in body weight regulation is needed in the hope of developing new therapeutic strategies.

Chapter 2

Theoretical framework(s) of body weight regulation

This chapter will present the main models developed to explain whether and how body weight is regulated. The advantages and disadvantages of the different models will be discussed, as well as their possible biological correlates.

❖ Set point model

In the 1950s, studies made in rats laid the foundation for the first major theoretical model of body weight regulation: the lipostatic model. Based on the observation that rats were able to maintain stable fat stores according to different physiological situations with highly variable energy demands, Kennedy hypothesized that the adipose tissue was responsible for a feedback loop, in order to match energy intake with energy demands (Kennedy 1953). This mechanism, called "lipostat", is disrupted after hypothalamic lesions in rats, suggesting that the hypothalamus is the brain region able to detect signals from the adipose tissue (Figure 5A). These data were subsequently supported by other experiments in which rats were subjected to a high-calorie diet or caloric restriction to gain or lose weight, respectively (situations illustrated in Figure 5B and Figure 5C). When the overload or caloric restriction stopped, the rats regained a body weight similar to that of control-fed rats (Mitchel and Keesey 1977, Rothwell and Stock 1979). These data therefore support the existence of a set point for body weight, whose role is to maintain body weight constant in the long term despite temporary variations in energy intake. In accordance with the high heritability (65-70%) of BMI discussed in the previous chapter, this set point would likely be genetically determined.

The discovery of the leptin gene, which codes for an anorectic hormone produced by adipocytes, subsequently provided a biological basis for the lipostatic theory (Zhang, Proenca *et al.* 1994). The circulating levels of leptin are in proportion to the amount of adipose tissue, making it an adiposity signal that is detected in many brain regions involved in the control of energy balance, including the hypothalamus (Schwartz and Zeltser 2013). The importance of leptin is further highlighted by the fact that humans whose leptin gene or receptor is mutated are hyperphagic and develop morbid obesity (Montague, Farooqi *et al.* 1997, Clement, Vaisse *et al.* 1998).

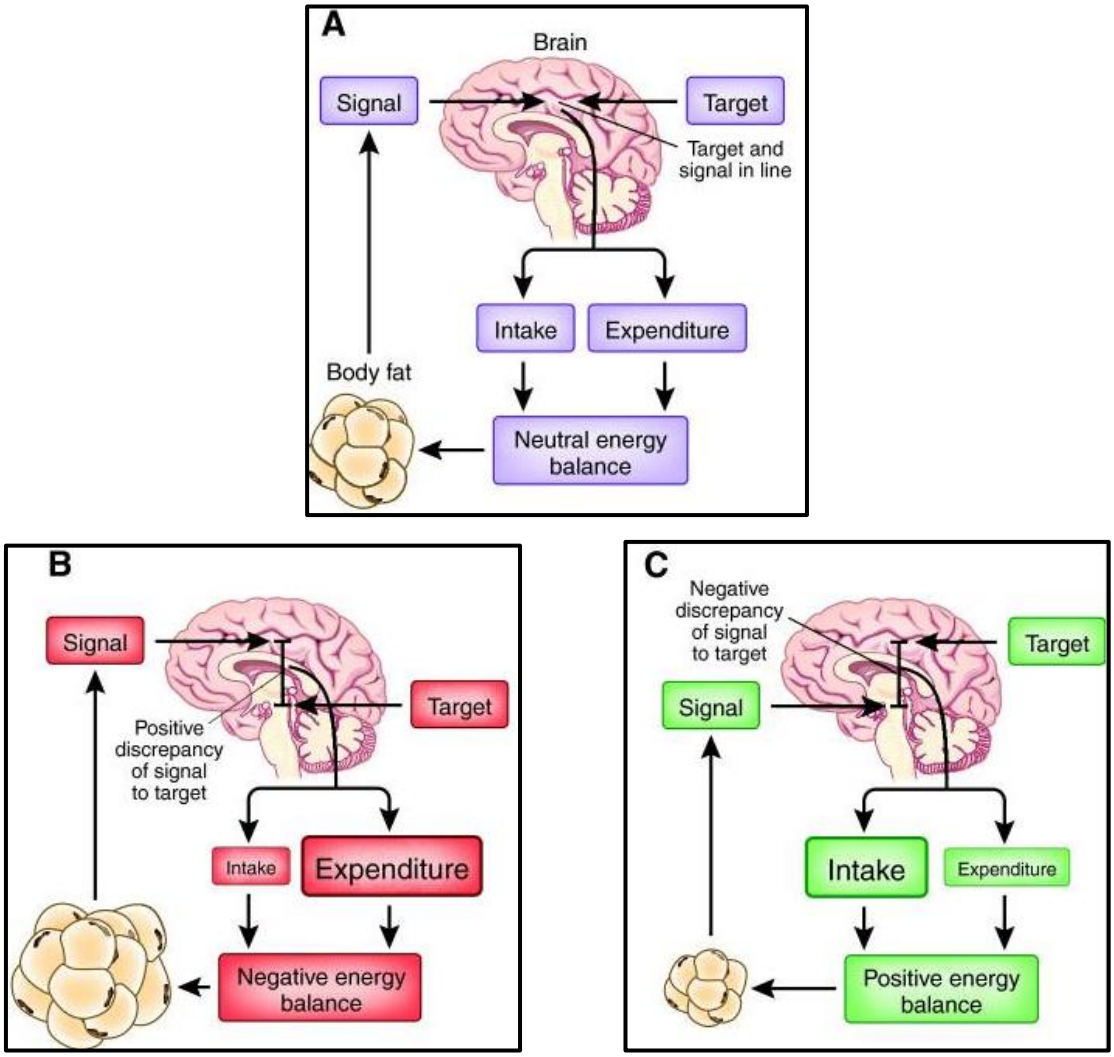

<u>Figure 5</u>: **The lipostatic model of body fat regulation.**

In this model, fat tissue produces a signal (generally presumed to include leptin) that is passed to the brain, where it is compared with a target (the set point of the system)
A: Discrepancies between the level of the signal and the target are translated into effects on energy expenditure and energy intake to equalize the discrepancy and maintain homeostasis.
B: When body fatness is above the target level, expenditure is increased and intake decreased until fatness falls and the signal and target are brought back in line.
C: When the individual is too thin as determined by the set point, intake is increased and expenditure is reduced to drive the subject into a positive energy balance, resulting in an increase in fatness and bringing the target and signal back in line.

Figure and legend modified from (Speakman, Levitsky et al. 2011).

The set point model explains, among other things, why it is so difficult for obese people to maintain their lost weight, as their bodies try to restore the fat levels corresponding to the pre-established set point. However, this theory hardly explains why an individual would become obese in the first place, if their "lean" initial body weight was defended against any variation. In addition, most obese people have very high endogenous leptin levels, consistent with their large volume of adipose tissue, and attempts to treat obesity by adding exogenous leptin were unsuccessful (except when done in leptin-deficient people) (Speakman 2018). This apparent contradiction has given rise to the concept of "leptin resistance", to describe the fact that leptin no longer seems to produce a negative feedback on weight in obese people. In this context, the significant increase in body weight would be due to a defect in the lipostatic regulation system. Other authors support the idea of a variable set point, based on mathematical modelling. This set point would remain stable as long as environmental conditions remain the same, but could vary depending on food availability and/or risk of predation (Higginson, McNamara *et al.* 2016).

Despite this, other problems exist in this model. For example, caloric restriction induces a decrease in circulating leptin before there is even a decrease in body fat and most of the signals involved in the negative feedback loops (insulin, nutrients, hormones) respond to short-term variations in energy intake. Conversely, body weight regulation in this system is carried out over much longer periods. As a consequence, there is a discrepancy between the time period over which the regulatory signals (leptin, insulin, nutrients, hormones) are responsive to energy imbalance (hours and days) and the time period over which regulation seems to occur (weeks and months) (Speakman, Levitsky *et al.* 2011).

In summary, the set point model explains the apparent long-term stability of body weight in animal models when exposed to high variations in energy intake, similar to what is observed in humans (Speakman 2018). The set point is characterized by peripheral signals informing the brain of the body's energy stores. In response, the brain adjusts the energy balance to maintain the body weight at a genetically pre-defined level (Figure 5), but which may (or may not) vary depending on the environment.

However, this homeostatic body weight regulation model struggles to explain the explosion in obesity rates over the past 50 years and only takes into account intrinsic physiological mechanisms, denying a role for socioeconomic and environmental factors in the aetiology of obesity (Speakman, Levitsky *et al.* 2011). If we consider that the set point is variable due to environmental pressures, such variations on a genetically-determined set point could not occur within a few generations. This model therefore does not explain the rapid change in the distribution of BMI worldwide, which is increasingly skewed towards high BMIs.

❖ Settling point model

This model takes the opposite approach to the previous model because it considers that there is no active regulation of body weight. Fat stores would behave like water inside a reservoir, or a lake (Figure 6A), subject to passive regulation based on inflow and outflow, which would naturally reach a balance (Speakman, Levitsky *et al.* 2011). When the inflow increases, it temporarily surpasses the outflow, thus filling the reservoir, until a new settling point is reached by the progressive increase of the outflow (Figure 6B). Conversely, when the inflow decreases, the difference with the outflow will empty the tank until the outflow adjusts again to a lower settling point (Figure 6C). By applying this model to body weight regulation, our fat stores then only reflect our energy intake (independent of the current volume of fat) and a passive adaptation of energy expenditure (related to the current volume of fat).

The settling point model thus interprets the increasing prevalence of obesity as a consequence of the modern obesogenic environment: increasing energy intake would naturally lead to an accumulation of fat until a new equilibrium point is reached, when energy expenditure again matches the intake (Speakman 2018). The regained weight after a caloric restriction then corresponds to a rebalancing of the reserves compared to normal caloric intakes, giving the illusion of a pre-determined, fixed set point. Unlike the set point model, here, the main factors involved in body weight change are the environment and lifestyle rather than genetics and physiology.

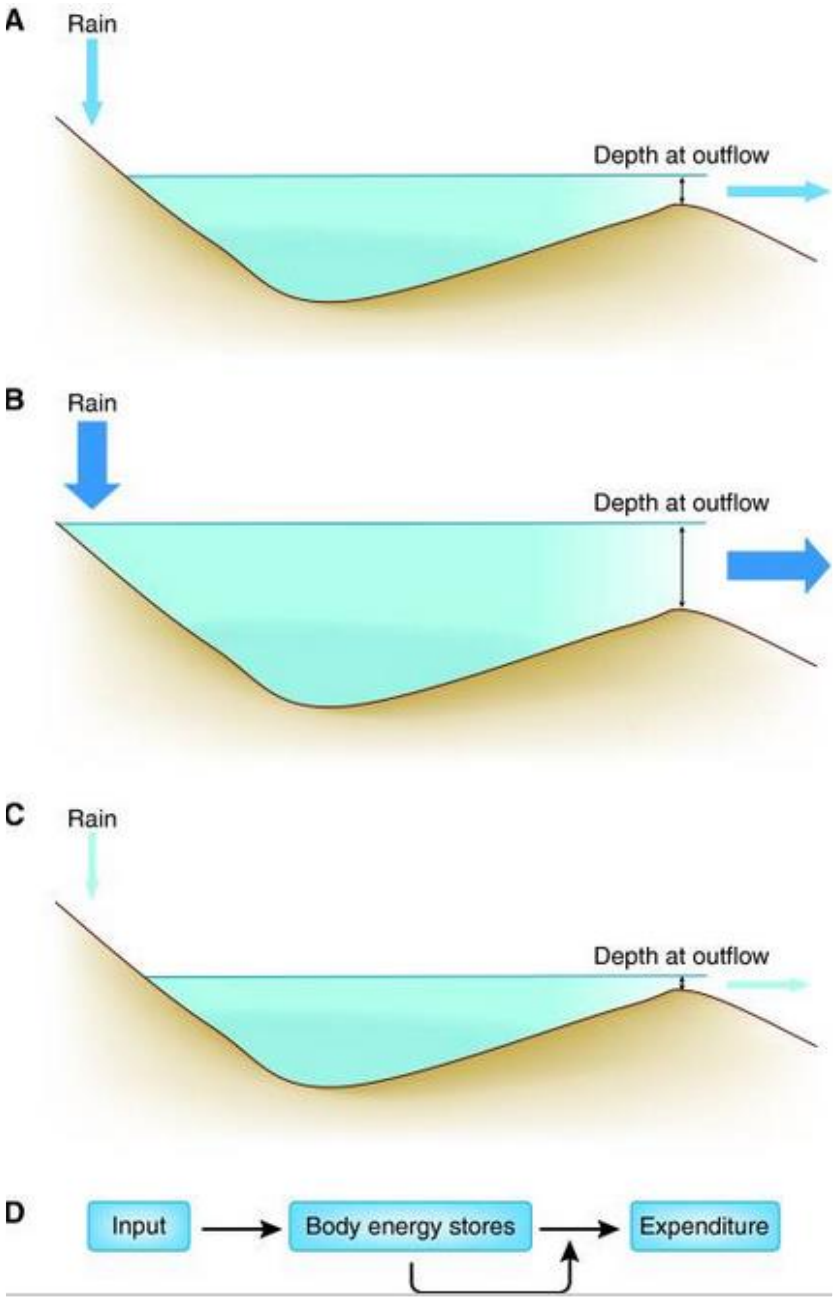

Figure 6: **An example of a settling point system: levels of water in a lake.**

A: In this schematic, the input to the lake is rain falling in the hills. The output of water from the lake is directly related to the depth of water at the outflow. The depth of the water in the lake reaches a settling point at which the outflow is equal to the inflow (indicated by the sizes of the arrows).
B: If the amount of rainfall increases (denoted by the larger arrow), the level of water in the lake increases until a new settling point is reached, at which the outflow is equal to the inflow.
C: If the amount of rainfall decreases, the water level in the lake falls until a new settling point is reached, again where the outflow matches inflow.

Figure and legend taken from (Speakman, Levitsky et al. 2011).

Of note, this model requires that one of the variables (inflow or outflow) be independent of the reserve level while the other depends on it. In the case of body weight regulation, it is tempting to imagine that it is the energy expenditure that varies according to the level of the reserve, because each variation in body weight corresponds to a variation in fat mass (FM) and fat-free-mass (FFM), the latter being an energy consumer (Speakman, Levitsky *et al.* 2011). Thus, variations in energy intake would lead to a variation in FFM in the same direction, causing an increase in energy expenditure, until a settling point is reached.

However, this model is in contradiction with numerous data. First, in a passive regulation model, it would be very easy for an obese person to lose weight and maintain it in the long term: a caloric restriction would be enough to re-establish a lower settling point without any biological mechanism to fight against it. However, physiological adaptations to caloric restriction are real and do not match the predictions of the settling point model: the decrease in energy expenditure is higher than expected and there is a difficulty for obese patients to maintain such a calorie-restricted diet over time because of increased hunger sensation. Finally, when the calorie-restriction is lifted, hyperphagia occur and weight re-gain is much faster than expected with a passive regulation model (Speakman 2018). Thus, feeding studies in humans are more consistent with the set-point rather than the settling point model (Hall and Guo 2017).

In summary, the settling point model provides a better explanation than the set point model for the current obesity epidemic, considering that energy intake and energy expenditure passively reach a state of equilibrium, allowing fat stores to be quite large if the intake is also large (Figure 6B). On the other hand, this model is in contradiction with all observations of active physiological processes that fight against weight loss. Thus, unlike the set point model, which neglects environmental aspects, the settling point model only takes into account environmental modifications and denies the existence of all the biological mechanisms at work in the regulation of body weight.

❖ Dual intervention point model

Faced with the inconsistencies of the two models described above, an alternative model was proposed: the dual intervention point model. It is actually a combination of the set point and settling point models. Here, there is not one, but two genetically determined set points that represent an upper and lower limits (called "intervention points") above and below which body weight is actively regulated by distinct physiological mechanisms. However, between these, there is a range of body weights for which no active regulation takes place (Speakman, Levitsky *et al.* 2011). Thus, just as in the set point model, predefined limits determine the activation of biological mechanisms to counteract weight gain/loss, and just as in the settling point model, the environment alone influences body weight between these limits (Figure 7).

While the set point model is based only on genetics and physiology and the settling point model only takes into account the environment, the dual intervention point model has the advantage of modelling gene-by-environment interactions (Speakman 2018). Here, the compensatory mechanisms that occur after a caloric restriction or an overfeeding period are due to the crossing of one of the limits. Moreover, the reason why some individuals gain much more weight than others in the same environment is related to the difference between these two limits: if we consider that body weight is not actively regulated in this range, two people placed in an obesogenic environment are likely to reach their upper limit, but the latter may be higher or lower depending on the genes that determine it. But then, why is such a variation in the upper intervention point possible?

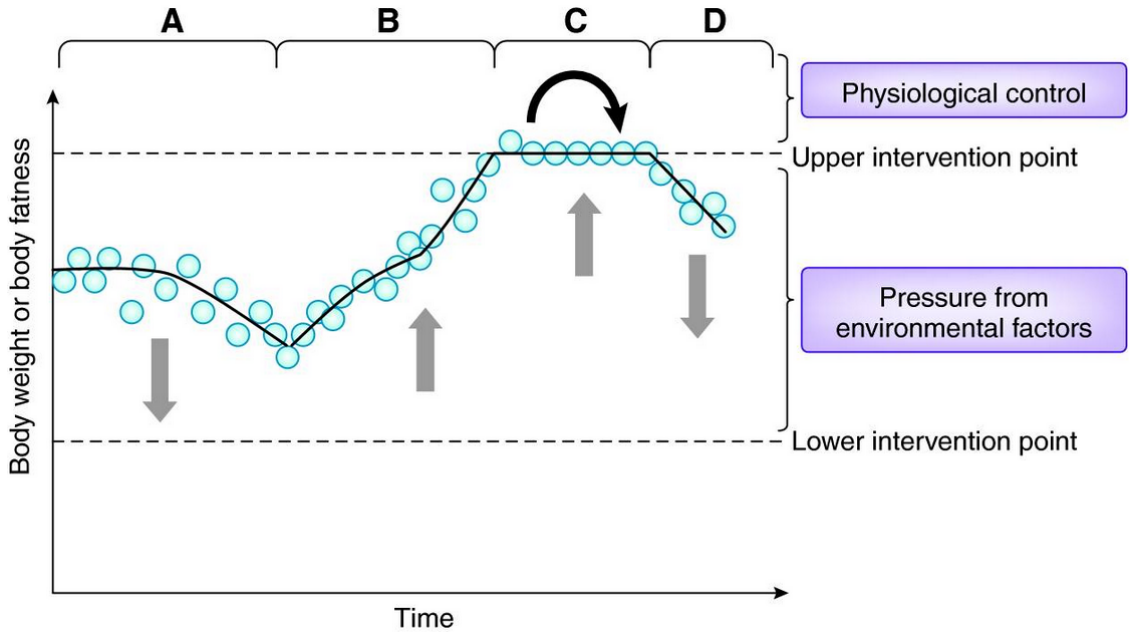

Figure 7: **The dual intervention point model.**

This model is illustrated here by changes in body weight over time. The body weight varies depending on the prevailing direction of the environmental pressures.
A: These pressures largely favour weight loss, and the body weight or adiposity declines.
B: These factors largely favour weight gain and body mass increases. At these times weight is largely dictated by environmental factors.
C: Here, the pressure to gain weight has resulted in weight increasing to the upper intervention point. Further weight gain is resisted by physiological (genetic) factors (depicted by black arrow). The weight therefore remains in balance: declines are prevented by the upward environmental pressures, and increases are prevented by physiological factors.
D: Weight only starts to decline again when the environmental pressure to increase weight is reversed (or an intervention is started).
In any situation in which there is a constant environmental pressure favouring weight gain, individuals will increase to their upper intervention points, which vary among individuals and are hypothesized to be genetically determined. (Similarly, weight loss becomes resisted at the lower intervention point by other physiological mechanisms: not illustrated here.) This model also combines the ideas of settling points and uncompensated factors, which dominate between the intervention points, and physiological feedback controls that operate when the intervention points are reached.

Figure and legend taken from (Speakman, Levitsky et al. 2011).

One explanation provided by Speakman is that we need to consider the evolutionary pressures that have shaped the levels of these intervention points over time. Classically, the starvation-predation trade-off is invoked in the set point model to explain why some individuals have a higher set point than others: during evolution, genes have been selected to promote fat storage (allowing survival in case of starvation, also referred as the "thrifty gene hypothesis") but without excessive accumulation (beyond which the risk of predation increases). In the set point model, these two evolutionary pressures oppose each other, to determine a single set point. In contrast, in the dual intervention point model, Speakman proposes that each limit was independently influenced by distinct evolutionary pressures. For instance, the lower limit was initially considered to be linked to the risk of starvation, which prevented it from decreasing too much. (Speakman, Levitsky *et al.* 2011). Speakman recently revised this model, suggesting that diseases, instead of famines, have actually set the level of the lower limit, high enough to protect individuals from pathogenic-induced anorexia (Speakman 2018). On the other hand, the upper limit is determined primarily by the risk of predation, which was abolished in the history of humanity as soon as our ancestors *Homo erectus* began to use tools, control fire and gather in large social groups. Thus, this evolutionary pressure that prevented the upper limit from rising too high disappeared, allowing mutations to accumulate and this upper limit to drift over time: this conjecture is known as the "drifty gene hypothesis" (Speakman 2018).

This drifty gene hypothesis is an interesting alternative to thrifty gene hypothesis because it better reflects the wide distribution of BMIs in Western populations. Indeed, if genetic variations have been selected under evolutionary pressure to promote body fat accumulation, people living in an obesogenic environment should be much more uniformly obese. But if we consider that this variability is in fact due to a random genetic drift that is not under evolutionary pressure, it is easier to understand why so many individuals in industrialized countries are not obese (Speakman 2018). It should be noted that a dual intervention point model, combining high pressure on the lower limit and no pressure on the upper limit, predicts a distribution of BMIs that is similar to that actually observed in humans (Speakman 2007). The model also predicts

a stabilization in the number of obese people, which is already being observed in some countries (Chooi, Ding *et al.* 2019).

However, this model is not perfect. Higginson et al criticize in particular the lack of active regulation of body weight between the two limits, which would be illogical from an evolutionary point. In their opinion, there must be an evolutionary advantage of such an absence of regulation, which this model fails to provide (Higginson, McNamara *et al.* 2016). In addition, the genetic determinants and physiological processes behind the high and low limits are still largely unknown, even if some hypotheses have been proposed. For instance, in this model, leptin would act as a signal of famine, since low levels of circulating leptin cause physiological adaptations that counteract weight loss, in accordance with what is expected when the lower limit is reached. In this view, the phenomenon of leptin resistance observed in obese people is rather irrelevant, considering that leptin would be only effective in defending the body against excessive weight loss and not weight gain (Ohlsson, Hagg *et al.* 2018, Speakman 2018). Furthermore, a new system has even been proposed as a potential biological basis for the upper limit, called "gravitostat". It consists of a homeostatic mechanism based on the detection of body mass (whether biological or inert), likely dependent on osteocytes and independent of leptin. This physiological weight-sensing mechanism could then reduce body weight in response to an increased weight load (Jansson, Palsdottir *et al.* 2018).

In summary, the dual intervention point model provides a theoretical framework that explain a large number of observations. In this model, the weight is passively regulated according to environmental pressures between two genetically determined limits, beyond which physiological mechanisms (still largely unknown) are engaged to counteract this variation. During evolution, the lower limit was influenced by the need to prevent pathogenic induced anorexia while the upper limit was limited by the risk of predation. The latter has ceased to weigh on the human species since *Homo erectus*, allowing the upper limit to drift without undergoing selective pressure. Consequently, this upper limit can now have widely varying levels in the contemporary human population. This high variability is fully apparent in Western countries, in which

people are likely to reach this limit due to the obesogenic environment, and explains the wide distribution of BMI. However, further studies are needed to determine if this model is correct, and unravel the genetic determinants and physiological mechanisms underlying its upper and lower boundaries.

❖ What's next?

To date, there is no consensual model to explain how body weight is regulated. In most models however, the brain plays a central role at integrating intrinsic (hormones, nutrients) and extrinsic (food-related cues) signals and at regulating a large number of physiological processes underlying the maintenance of energy balance. Of note, results of a genome-wide association study recently identified 97 BMI-associated loci, within which genes are enriched for expression in the brain and central nervous system (Locke, Kahali *et al.* 2015) (Figure 8). Thus, one can suggest that obesity is primarily a brain disease, which is why the study of brain circuits involved in body weight regulation holds great promise in the hope of discovering new therapeutic target

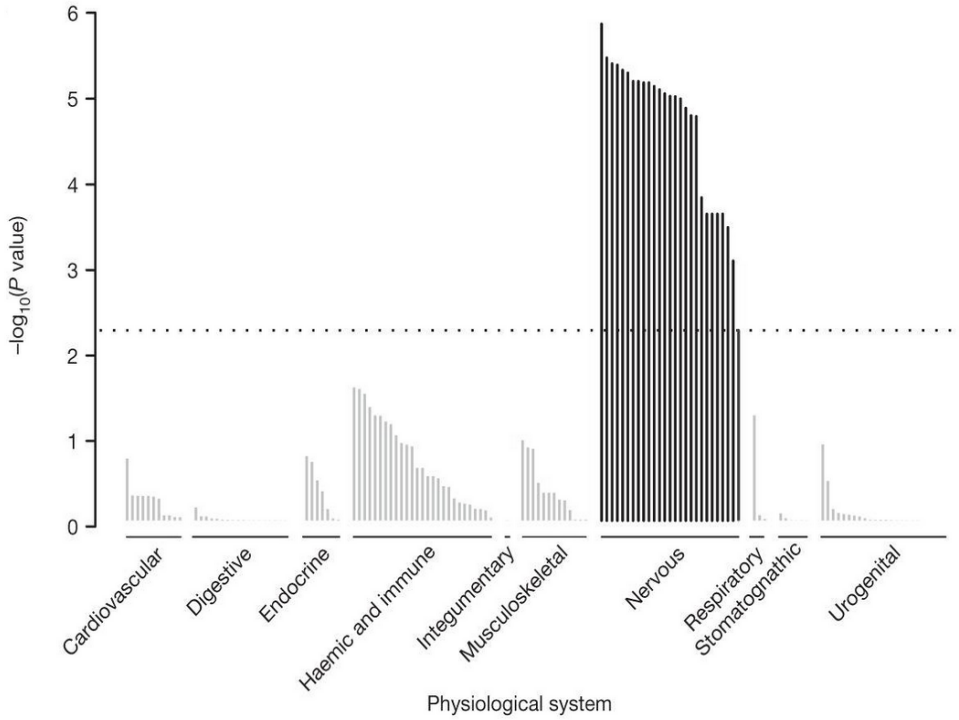

Figure 8: **Tissues significantly enriched for genes within BMI-associated loci**

Genes within BMI-associated loci ($P < 5 \times 10^{-4}$) are enriched for expression in the brain and central nervous system. Tissues are sorted by physiological system and significantly enriched tissues are in black; the dotted line represents statistically significant enrichment.

Figure and legend taken from (Locke, Kahali et al. 2015).

Chapter 3

Central regulation of energy balance
~ focus on the melanocortin system ~

This chapter will broadly present how the brain controls energy balance, with a closer look at the hypothalamic melanocortin system.

❖ General overview of the central regulation of energy balance

Our brain is constantly exposed to intrinsic and extrinsic signals related to our nutritional status and food-related cues (Piazza, Cota *et al.* 2017). Multiple neural circuits then integrate these signals and communicate with downstream brain regions in order to adapt the activity of various physiological mechanisms involved in the regulation of energy balance (food search and intake, fat storage and energy expenditure…). We will briefly introduce the different actors of this complex network (Figure 9). For more detailed reviews, please see (Schneeberger, Gomis *et al.* 2014, Waterson and Horvath 2015, Timper and Brüning 2017).

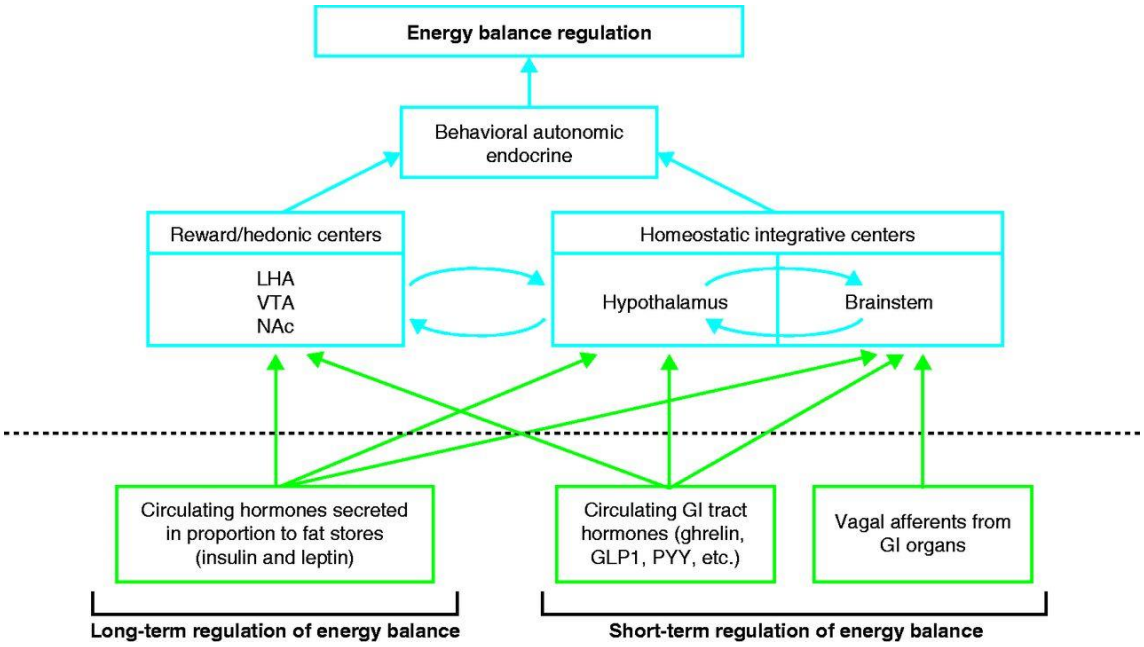

<u>Figure 9</u>: Schematic integration of the different levels of food intake and energy balance regulation.

<u>Figure 9</u>: **Schematic integration of the different levels of food intake and energy balance regulation.**

Food intake and energy balance are coordinately regulated by homeostatic and non-homeostatic neural mechanisms. Circulating hormones and vagus stimuli inform the CNS about whole-body nutritional and energy status. Leptin and insulin are believed to be involved in the long-term regulation of energy balance, while GI hormones and vagal afferents represent a short-term regulatory mechanism. These hormones act in concert to engage specific neuronal circuits in homeostatic and hedonic centers, establishing dynamic and complex interactions between these different brain regions to elaborate coordinated endocrine, autonomic, and behavioural responses to regulate energy balance. Sensory, emotional, and social cues also influence ingestive behaviours probably through non-homeostatic and higher brain structures.

LHA, lateral hypothalamic area; VTA, ventral tegmental area; NAc, nucleus accumbens.

Figure and legend taken from (Schneeberger, Gomis et al. 2014).

<u>Peripheral signals</u>: among them, the hormones leptin and insulin are classically regarded as adiposity signals. As already mentioned in Chapter 2, **leptin** is produced by the adipocytes, so that its circulating level is in proportion to the fat mass (Considine, Sinha *et al.* 1996). Leptin is able to reach the brain, where it binds to its receptor, LepR, highly expressed in hypothalamic nuclei and other brain regions involved in the regulation of energy balance (Elmquist, Bjorbaek *et al.* 1998). **Insulin** is produced by pancreatic beta-cells and regulates glucose homeostasis by acting on glucose uptake by peripheral organs (Bagdade, Bierman *et al.* 1967). Insulin receptors (InsR) are also expressed in the mediobasal hypothalamus, and especially in the arcuate nucleus (ARC), a key region for the control of energy balance (Plum, Schubert *et al.* 2005). Overall, leptin and insulin actions in the hypothalamus lead to a decrease in food intake and increase in energy expenditure, while also influencing glucose homeostasis, and these hormones are considered critical for long-term regulation of energy balance (Schneeberger, Gomis *et al.* 2014). Of note, leptin and insulin can also modulate the reward aspects of feeding by acting in the ventral tegmental area (VTA), a brain region containing dopaminergic neurons, which play a key role in motivation (Fulton, Pissios *et al.* 2006, Hommel, Trinko *et al.* 2006, Liu and Borgland 2019).

Apart from these adiposity signals, various hormones are produced by the gastrointestinal tract and act as short-term signals related to the nutritional status. Among them, ghrelin stands out, as it is the only known orexigenic hormone. **Ghrelin** is secreted by the stomach and is responsible for hunger and initiation of the meal (Yoshihara, Kojima *et al.* 2002). Its circulating levels rise just before meals and drops back shortly thereafter (Cummings, Purnell *et al.* 2001). Ghrelin acts by binding its receptor GHSR (for Growth Hormone Secretagogue receptor), which is highly expressed in the ARC (Horvath, Diano *et al.* 2001). Other gut hormones (called incretins) are produced by the intestinal epithelium, such as **PYY** (for peptide tyrosine tyrosine), **GLP-1** (for glucagon-like peptide 1) and **CCK** (cholecystokinin). Contrary to ghrelin, their circulating levels rise after a meal and exert an anorectic effect by acting centrally through their specific receptors (Schneeberger, Gomis *et al.* 2014).

Finally, the brain is able to sense many nutrients, which can participate as well in the central regulation of energy balance (Cota, Proulx *et al.* 2007). These nutrients, such as **amino acids** (Heeley and Blouet 2016), **fatty acids** (Le Foll 2019) and **glucose** (Lopez-Gambero, Martinez *et al.* 2019), have an anorectic effect.

Homeostatic (Endostatic) regulation of energy balance: the **hypothalamus** is the core region for this regulation. It is composed of many nuclei, which host different neuronal populations that integrates peripheral signals to regulate energy balance:

- **ARC** (arcuate nucleus): located in the mediobasal hypothalamus, close to the third ventricle and above the median eminence. It is home for two antagonistic populations of neurones: the anorectic POMC/CART neurons (for proopiomelanocortin / Cocaine- and amphetamine-regulated transcript) and orexigenic AgRP/NPY neurons (for agouti-related peptide / neuropeptide tyrosine) (Coupe and Bouret 2013). Of note, the proximity of the median eminence, which lacks a blood-brain barrier (BBB), allows ARC neurons to be exposed to blood-borne signals such as nutrients and hormones.
- **PVH** (paraventricular nucleus): located in the anterior hypothalamus, on top of the third ventricle. This nucleus receives a dense innervation from POMC and AgRP neurons and mediates their action on food intake (Woods 2005). It is home

to several neuronal populations involved in the regulation of energy balance, such as MC3R and MC4R neurons (for melancortin receptor 3 and 4, which are the targets of neuropeptides produced by POMC and AgRP neurons), TRH (thyrotropin-releasing hormone), CRH (corticotrophin releasing hormone) and oxytocin neurons (Schneeberger, Gomis *et al.* 2014). POMC, AgRP, MC3R and MC4R neurons are part of a neuronal system called "melanocortin system", which will be further described below.

- **VMH** (ventromedial nucleus): located above the ARC. It is a satiety centre and plays a role in glucose homeostasis (Fioramonti, Song *et al.* 2011) and adaptive thermogenesis (Yang and Ruan 2015). The main neuronal population of the VMH is SF-1 neurons (for steroidogenic factor 1), which play a significant role in the regulation of energy balance (Cardinal, André *et al.* 2014).
- **DMH** (dorsomedial nucleus): located above the VMH. This nucleus participates in the orexigenic effect of NPY (Bi, Kim *et al.* 2012) and the control of glucose homeostasis (Zhu, Yan *et al.* 2012). It is also involved in thermoregulation, stress and circadian rhythms (Schneeberger, Gomis *et al.* 2014).
- **SCN** (suprachiasmatic nucleus): located in the anterior hypothalamus, above the optic chiasm. This nucleus regulates circadian rhythms by integrating environmental and endogenous signals and induce the expression of "clock genes" which will influence the release of neuropeptides involved in the regulation of energy balance (Albrecht 2012).
- **LHA** (lateral hypothalamic area): this region is considered mainly as a hunger center, as well as a reward hot spot. It is at the interface between homeostatic and non-homeostatic (or exostatic) control of energy balance. This nucleus hosts orexin neurons and MCH neurons (for melanin-concentrating hormone), which increase the seeking and consumption of food by interacting with the nucleus accumbens and ventral tegmental area, which are part of the "reward system" of the brain. Especially, it seems that orexin neurons enhance the seeking of food, while MCH neurons integrate taste, olfactory and gut signals to increase the reward value and promote the consumption of calorically-dense type of food. (Cassidy and Tong 2017).

Besides the hypothalamus, the **brainstem** is also an important region for the control of energy homeostasis, in particular through a region called the **dorsal vagal complex (DVC)**, which is composed of the dorsal motor of the vagus, the nucleus of the tractus solitarii (NTS) and the area postrema. Importantly, the latter has an incomplete BBB, so that the neurons located here are readily exposed to peripheral signals (just as in the ARC). In addition, similarly to the hypothalamus, neurons within the brainstem can express various appetite-modulatory neuropeptides such as POMC, CART or NPY, among others. However, contrary to the hypothalamus, they also receive vagal inputs, which brings additional information related to the feeding status (e.g. stomach distension) (Schneeberger, Gomis *et al.* 2014).

In summary, peripheral signals (hormones, nutrients, vagal inputs) are detected by subsets of neurons located in the brainstem and the hypothalamus, which communicate with one another (Figure 10) in order to appropriately adapt the feeding behaviour and physiological responses to the nutritional status (Figure 9). A review of intra- and extra-hypothalamic connections involving these different brain nuclei can be found here (Waterson and Horvath 2015).

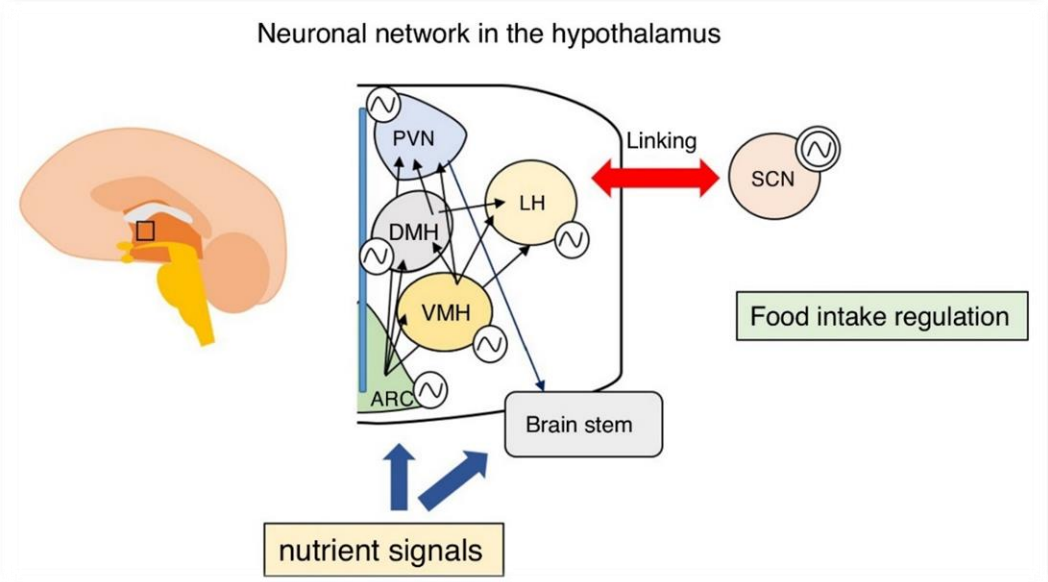

<u>Figure 10</u>: Hypothalamic networks for the regulation of energy homeostasis

The nucleus network in the hypothalamus is essential to determine the hunger signal. The neural circuit around ARC and brainstem trigger food intake behaviour modulation and reward system. In the hypothalamus, first order neurons in ARC regulate appetite by NPY/AgRP pathway and satiation by the POMC/CART pathway. The neurons interact with second order neurons in VMH, DMH, PVH, and LH, projecting further to higher brain areas and to the brainstem. The central SCN clock and peripheral clocks coordinate rhythmic gene expression and integrate nutrient signals to maintain energy homeostasis.

ARC: arcuate nucleus. VMH: ventromedian nucleus. DMH: dorsomedial nucleus. PVH: paraventricular nucleus. LH: lateral hypothalamic area. SCN: suprachiasmatic nucleus

Figure and legend taken from (Hirayama, Mure et al. 2018).

<u>Motivational and hedonic (Exostatic) regulation of energy balance:</u> contrary to the circuits involved in the homeostatic regulation of energy balance, whose functions are to match internal energy needs and food consumption, others mainly favours energy intake, by mediating reward aspects of feeding. Likely, these rewarding mechanisms have evolved to guarantee the recognition of food high in calories and hence favour its consumption and associated survival of the individual and of the species (Piazza, Cota *et al.* 2017). When talking about reward, a distinction must be made between the motivational and hedonic aspects of feeding behaviour. The motivation ("wanting")

encompasses the efforts made by an individual to obtain the food ("approach phase") as well as the amount of food eaten when obtained ("consummatory phase"). The hedonic responses ("liking") correspond to the pleasure provided by food consumption. Both "wanting" and "liking" are necessary to get a full reward, and although they often go hand in hand, their underlying circuits are quite distinct (Berridge 2009):

- **Motivation for food**: the major circuit responsible for the motivation for food is the mesolimbic dopaminergic pathway, in which dopaminergic (DA) neurons of the VTA (a brain region located near the base of the midbrain) projects to the NAc (nucleus accumbens, a basal forebrain region that is part of the ventral striatum). The NAc is divided into a medial shell (NAcSh) and lateral core (NAcc). Interestingly, the NAcSh is also connected with hypothalamic feeding-realted nuclei, and is more responsive to signals arising from the hunger system than the NAcc. In particular, and as previously mentioned, the LHA is in close relationship with this pathway (Cassidy and Tong 2017).
- **Liking of food**: some major hedonic hotspots have been identified in the forebrain and brain stem. While the entire NAc is linked with "wanting" (as previously mentioned), a hedonic hotspot can be found within it, which responds mainly to opioids and endocannabinoids in order to increase "liking". This hotspot represents around 10% of the NAc surface. Another forebrain hotspot is located in the posterior part of the ventral pallidum, onto which the NAc heavily projects. The ventral pallidum also participates in mesolimbic-thalamocortical loops to influence cognition and action. Finally, the parabrachial nucleus (PBN) within the caudal brainstem also increases "liking" responses when inhibited with benzodiazepines, and is a major relay of the taste information (Berridge and Kringelbach 2015).

As a result, motivational and hedonic circuits contribute to the regulation of food intake, by linking limbic forebrain areas with brainstem and higher cortical regions (Figure 11).

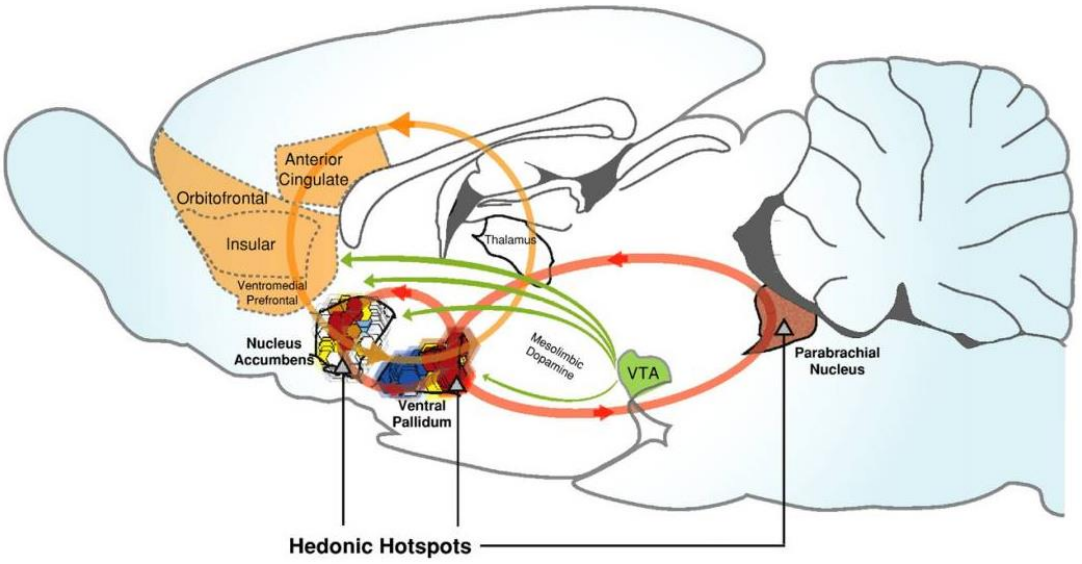

<u>Figure 11</u>: Motivational and hedonic circuits

Hedonic hotspots are shown in nucleus accumbens, ventral pallidum, and brainstem parabrachial nucleus where opioid or other signals cause amplification (in red) or diminution (in blue) of "liking" reactions. Hedonic circuits are shown in light red. Mesolimbic-thalamocortical loop is shown in light orange, in which the forebrain hedonic hotspots are connected with higher cortical areas. Mesolimbic dopaminergic pathways linked to the « wanting » circuits are shown in green.

VTA: ventral tegmental area.

Figure and legend taken from (Berridge 2009).

❖ Links between the hypothalamus and circuits of reward

Although presented in separate paragraphs in this chapter, the circuits regulating energy homeostasis and reward for food share numerous interconnections (Figure 12). We already mentioned the interaction between orexin and MCH neurons of the LHA and the mesolimbic reward system. In addition, AgRP and POMC neurons of the ARC also project onto the VTA and NAc.

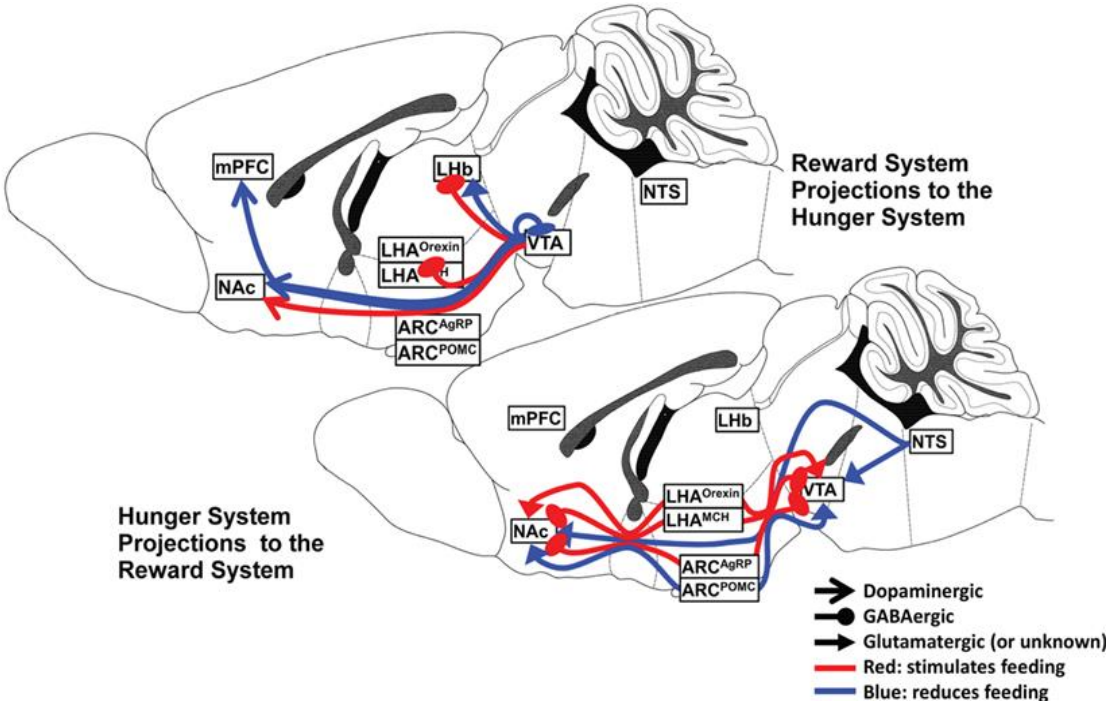

<u>Figure 12</u>: Hunger and satiety neurocircuits interface with the midbrain–basal forebrain reward pathway

ARC: arcuate nucleus. LHA: lateral hypothalamic area. VTA: ventral tegmental area. NAc: nucleus accumbens. NTS: nucleus of the tractus solitarii. LHb: lateral habenula. mPFC: medial prefrontal cortex.

Figure taken from (Cassidy and Tong 2017).

For instance, GABAergic AgRP projections to the VTA inhibits dopaminergic and glutamatergic release in the NAc (Dietrich, Bober *et al.* 2012) and yet, optogenetic stimulations of AgRP neurons enhances food-seeking ("approach") and food consuming ("consummatory") behaviours. This AgRP-induced inhibition of the reward system can be interpreted as a way to prime this system in to responding to food rather than any other stimulus (Cassidy and Tong 2017), which is confirmed by the observation that AgRP activation by hunger is able to suppress competing behaviours such as social interactions, drinking or anxiety-related behaviours when food is available (Burnett, Li *et al.* 2016). In addition, POMC projections to the VTA and NAc have been identified (Wang, He *et al.* 2015), and they might enhance sucrose consumption *via* the activation of local MC3R, although their functional relevance is still largely unknown.

❖ Close-up of the hypothalamic melanocortin system

In the ARC, the anorectic POMC and orexigenic AgRP neurons are involved primarily in the homeostatic regulation of energy balance, but are also connected with brain areas controlling the motivation for food, as we have seen previously. A number of studies suggest that they are directly activated by blood-borne hormones and nutrients leaking through the fenestrated capillaries that irrigates the nearby median eminence (Ciofi, Garret *et al.* 2009). POMC and AgRP usually respond to these signaling molecules in an opposite way. For instance, AgRP neurons are inhibited by leptin while POMC neurons are activated by it (Varela and Horvath 2012). The appetite-modulating effects of these neurons is achieved through the neuro-peptidergic innervation of target neurons. Indeed, POMC is a protein precursor which can be cleaved in (among other peptides) α-MSH, a potent appetite-suppressant neuropeptide exerting its action through the activation of G-protein coupled receptors called melanocortin receptors (MCR). AgRP, on the other hand, is an inverse agonist of the MCRs (Williams, Bing *et al.* 2001). In the central nervous system, 5 sub-types of MCRs have been identified (Abdel-Malek 2001), but only two are expressed in the hypothalamus: MC3R and MC4R (Cone, Lu *et al.* 1996). Thus, in the hypothalamus, the first-order POMC and AgRP neurons, the second-order MC3R and MC4R expressing neurons, and the MCR ligands α-MSH and AgRP together constitute what is called the "hypothalamic melanocortin system".

Among the two MCRs expressed in the hypothalamus, MC3R doesn't seem to have a critical impact on energy balance, since its deletion in mice doesn't affect food intake or body weight (although adiposity is increased) (Butler, Kesterson *et al.* 2000). On the other hand, the deletion of MC4R leads to hyperphagia, hyperinsulinemia, hyperleptinemia and obesity (Butler and Cone 2002). Accordingly, MC4R mutations are the most common form of monogenic obesity in humans and have been implicated in 1% to 6% of early-onset severe obesity (Serra-Juhé, Martos-Moreno *et al.* 2019). MC4Rs are densely expressed in the PVH, VMH, DMH and LHA, but the appetite-suppressant effects of α-MSH are mediated by the MC4R expressed by parvocellular neurons in the PVH, as assessed by a PVH-specific re-expression of this receptor in a MC4R-KO mouse, which prevented 60% of the obesity and restored a normal feeding

behaviour (Balthasar, Dalgaard *et al.* 2005). Thus, the ARC → PVH pathway is a critical circuit for the regulation of food intake within the hypothalamic melanocortin system (Figure 13A).

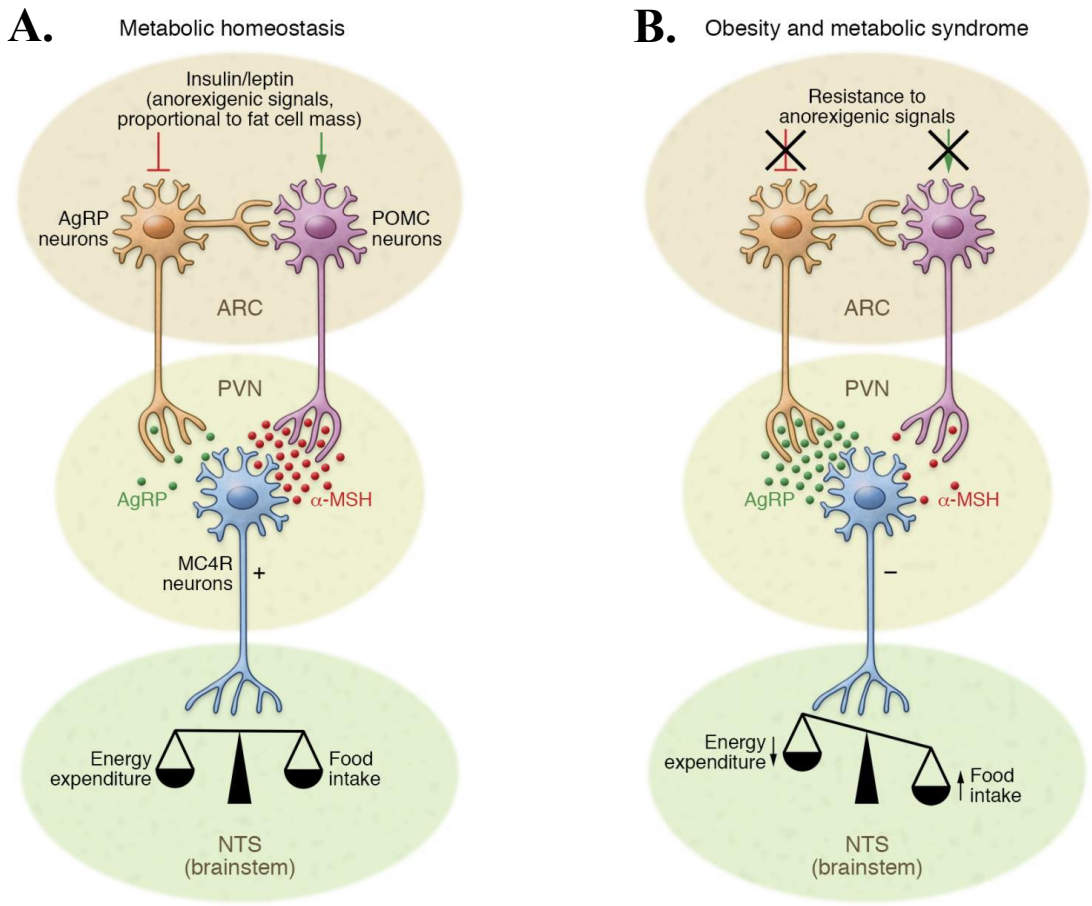

<u>Figure 13</u>: Hypothalamic melanocortin system in normal and pathological condition

A: Insulin and leptin act directly on neuronal subsets in the ARC of the hypothalamus to control energy homeostasis. Through activation of POMC neurons and inhibition of AgRP neurons, adipostatic signals activate MC4R-expressing neurons in the PVH. During fasting conditions, the expression of AgRP increases, whereas POMC expression is reduced, resulting in decreased MC4R signaling. In the fed state, AgRP levels are diminished and POMC levels increase, which triggers MC4R signaling and culminates in satiety and stimulation of energy expenditure.
B: Neuronal inflammation and the subsequent insulin and leptin resistance of ARC neurons disrupts this metabolic feedback loop, further promoting increased food intake and body weight gain.
ARC: arcuate nucleus. AgRP: agouti-related peptide. POMC: proopiomelanocortin. α-MSH: alpha-melanocyte-stimulating hormone. PVH: paraventricular nucleus. MC4R: melanocortin receptor 4. NTS: nucleus of the tractus solitarii.

Figure and legend taken from (Jais and Bruning 2017).

Optogenetic manipulation of AgRP and POMC neurons have further expanded our understanding of their specific roles. For instance, activation of AgRP neurons leads to voracious feeding as long as the photo-stimulation is maintained. Interestingly, this effect is melanocortin-independent. On the other hand, brief stimulation of POMC neurons has no impact, while prolonged stimulation leads to decreased food intake and body weight (Aponte, Atasoy *et al.* 2011). This is consistent with the results of pharmacogenetic activation of POMC neurons, which also required a long-term treatment to elicit a reduction of food intake and body weight. These results were obtained by only activating POMC neurons located in the ARC. In the same study however, acute activation of POMC neurons within the NTS was sufficient to stop food intake. Furthermore, diphtheria-toxin-induced ablation of POMC neurons in the ARC but not NTS lead to hyperphagia, decreased energy expenditure and obesity (Zhan, Zhou *et al.* 2013). Collectively, these results suggest that NTS POMC neurons may be involved in short-term feeding behaviour, such as AgRP neurons, while ARC POMC are rather critical long-term body weight regulation. To add complexity to the matter, further studies by looking at neuronal calcium dynamics in vivo by fiber photometry have shown that AgRP neurons are physiologically switched off and POMC neurons are activated as soon as food or food-associated cues are present (Chen, Lin *et al.* 2015, Brandt, Nolte *et al.* 2018).

Thus, large evidence highlight the critical role of the hypothalamic melanocortin system in the regulation of energy homeostasis. However, during obesity or when fed a high-fat-diet, multiple alterations such as leptin or insulin resistance can occur that dampens the ability of the system to accurately maintain energy balance (Figure 13B). Such alterations, particularly targeting the POMC neurons, will be discussed in the next chapter.

Chapter 4

POMC neurons alterations
in diet-induced obesity

This short chapter will present the main effects of high-fat diets on the functioning of POMC neurons and the subsequent metabolic consequences. For a detailed review on that topic, please see (Quarta, Fioramonti et al. 2019).

❖ POMC neurons dysfunction leads to obesity and metabolic disorders

The central role of POMC neurons in body weight regulation is highlighted by the fact that mutations in the POMC gene are responsible for monogenic forms of obesity (Farooqi and O'Rahilly 2005). Loss-of-POMC function studies later revealed that the action of POMC neurons extends beyond the mere regulation of fat stores. Indeed, postnatal ablation of POMC neurons leads to hyperphagia, consistent with the satiety-inducing role of POMC neurons, but also a reduction in energy expenditure *via* a lowered activity of the peripheral sympathetic nervous system and consequent reduced thermogenic activity of the adipose tissue (Greenman, Kuperman *et al.* 2013). Taken together, data obtained from ablation (Greenman, Kuperman *et al.* 2013) or pharmacogenetic inhibition (Zhan, Zhou *et al.* 2013) of POMC neurons showed that the disruption of POMC signaling leads to a broad spectrum of metabolic disorders, including glucose intolerance, insulin resistance and high cholesterol levels, all of which can be found in human obesity. Thus, POMC deficiency increases energy intake, decreases energy expenditure and causes metabolic disorders classically associated with obesity. However, is there a causal link between high-calorie diets, dysfunction in POMC neurons and diet-induced obesity?

❖ High-fat diets induce leptin resistance in POMC neurons

POMC neurons are able to detect, among other signals, different hormones such as leptin, insulin or ghrelin (Toda, Santoro *et al.* 2017). As already discussed in Chapter 3, leptin is an anorectic hormone produced by the adipocytes, thought to serve as a brain indicator of fat stores, since its circulating level is proportional to the amount of adipose tissue. Interestingly, leptin signaling (as assessed by an immunostaining of its downstream molecular target phospho-STAT3) is decreased in the ARC as early as after

6 days of high-fat-diet (HFD) in mice. This apparent leptin resistance seems specific of the ARC, since other brain regions, including intra-hypothalamic nuclei are still responsive to leptin, even after 16 weeks of HFD-feeding (Munzberg, Flier *et al.* 2004). By looking at the co-expression between AgRP, POMC and phospho-STAT3, Olofsson et al found that AgRP neurons were the first ones to show a HFD-induced leptin resistance (after 2 days of HFD only), but POMC neurons were affected as well (after at least 2 weeks of HFD) (Olofsson, Unger *et al.* 2013). Of note, these effects occur even before any change in body weight, indicating a direct effect of HFD in reducing leptin sensitivity. This early-stage defect in leptin sensitivity could in turn contribute to the development of obesity, since genetically-modified mice lacking the leptin receptor (LepR) are more susceptible to diet-induced obesity (DIO) (Bell, Harlan *et al.* 2014).

Surprisingly however, pharmacological inhibition of LepR increased feeding and body weight in lean as well as diet-induced obese mice to the same extent, suggesting that leptin still works in obese animals (Ottaway, Mahbod *et al.* 2015). These effects were associated with a decreased hypothalamic expression of the suppressor of cytokine signaling 3 (SOCS3), an inhibitor of the leptin signaling pathway. Thus, it is speculated that in DIO, the excessive fat mass leads to hyperleptinemia and subsequent constant activation of LepR, which in turn, induces an upregulation of molecular inhibitors such as SOCS3. SOCS3 accumulation would then limit the maximal amplitude of LepRb signaling in DIO mice, thereby preventing leptin to counteract diet-induced weight gain (Myers 2015). On the contrary, enhancing leptin signaling *via* a POMC-specific deletion of two other LepR signaling inhibitors (called TCPTP for T-cell protein tyrosine phosphatase and PTP1B for protein tyrosine phosphatase 1B) prevents DIO thanks to an increase in energy expenditure (Dodd, Decherf *et al.* 2015).

In summary, short-term HFD is associated with a decreased leptin sensitivity in the ARC in general, and in POMC neurons in particular, even before body weight change occurs, which could in turn exacerbate the accumulation of fat. In DIO mice, the overproduction of leptin by the adipose tissue and its failure to prevent body weight gain lead to an apparent leptin resistance state, which is likely due to an overexpression of LepR signaling inhibitors.

❖ High-fat diets alter POMC neurons *via* sustained hypothalamic inflammation

In addition to the aforementioned alteration in leptin signaling, short-term HFD also activates neuronal inflammatory pathways (Jais and Bruning 2017). Indeed, between day 1 and day 3 after HFD onset in rats, mRNA expression of pro-inflammatory cytokines are already increased in the ARC, and within the first week, markers of neuronal injury and reactive gliosis are evident (Thaler, Yi *et al.* 2012). Unlike peripheral organs, in which inflammation is considered a consequence of obesity, here inflammation precedes any change in body weight, suggesting that it may rather be a cause, especially since inflammatory processes occurring in response to hypercaloric diets can also involve hypothalamic circuits implicated in energy homeostasis (Le Thuc, Stobbe *et al.* 2017).

Moreover, in DIO mice, persistently active microglia hypersecrete pro-inflammatory cytokines such as TNFα in the hypothalamus, affecting POMC neurons (Yi, Walter *et al.* 2017). Consistent with this, our team has shown that a proliferation and recruitment of pro-inflammatory microglia occurs in the ARC of mice, after 3 weeks of HFD. Furthermore, the inhibition of such HFD-induced microglia expansion prevents diet-induced hypothalamic inflammation, and blunts diet-induced weight gain (Andre, Guzman-Quevedo *et al.* 2017). These data are in line with the emerging role of hypothalamic non-neuronal cells in metabolic control. Indeed, astrocytes and microglia are also able to detect hormones and nutrients, and can influence the melanocortin system thanks to gliotransmitter release (Garcia-Caceres, Balland *et al.* 2019). Of note, the consequences of the HFD-induced inflammation can be dramatic, since apoptotic events in the hypothalamus have been also reported (Thaler, Yi *et al.* 2012, Yi, Walter *et al.* 2017).

In summary, inflammatory-like reactions occurs in response to HFD, thanks in part to the recruitment of pro-inflammatory microglia who are able to detect nutrients and can release pro-inflammatory cytokines in the hypothalamus. This might undermine POMC neurons activity and even cause their death, thereby contributing to diet-induced obesity.

❖ High-fat diets impair mitochondria dynamics in POMC neurons

One of the consequences of HFD-induced inflammation in the hypothalamus is that TNFα is able to promote mitochondrial fusion in the neurites of POMC neurons (Yi, Walter *et al.* 2017). These fusion vs fission processes are controlled by proteins named mitofusins and are crucial for the activity of mitochondria by allowing them to connect to each other as well as to other organelles such as the endoplasmic reticulum (ER) (Schrepfer and Scorrano 2016). ER functions are essential for any cells, since this organelle is the master regulator of protein synthesis, folding and maturation.

Of note, HFD decreases the expression of mitofusin 2 in POMC neurons, leading to a reduction in mitochondria-ER contacts. Moreover, POMC-specific deletion of mitofusin 2 is associated with increased ER stress, leading to hyperphagia, decreased energy expenditure and obesity *via* altered POMC processing (Schneeberger, Dietrich *et al.* 2013). Furthermore mice lacking mitofusin 1 specifically in POMC neurons have a normal energy homeostasis, but are glucose intolerant, thanks to a defective pancreatic insulin release (Ramírez, Gómez-Valadés *et al.* 2017). On the contrary, overexpression of mitofusin 2 in the hypothalamus of DIO mice improves several metabolic defects in these animals, attenuating the obese phenotype (Schneeberger, Dietrich *et al.* 2013). Consistent with this, the deletion a mitochondrial fission protein (DRP1, for dynamin related protein 1) increases POMC neuronal activation in response to glucose and leptin and consequently improves glucose metabolism (Santoro, Campolo *et al.* 2017).

Taken together, these results suggest that POMC-specific alterations in mitochondrial dynamics (such as the ones observed after HFD feeding) lead to a reduction in mitochondria-ER connectivity, ultimately causing an increased ER stress which likely impacts energy and glucose homeostasis and participates in the aetiology of obesity.

❖ High-fat diets impair proteostasis in POMC neurons

As discussed above, a consequence of ER stress can be defective protein processing. In order to avoid the accumulation of misfolded proteins, cells can engage two distinct degradation pathways: proteasomal degradation and autophagy (Dikic 2017). Of note, these systems, that are essential for the regulation of proteostasis ("protein homeostasis") are impaired in obesity, leading to an aggregation of ubiquitinated and damaged proteins that undermines neuronal activity in the hypothalamus and negatively impacts body weight control and systemic glucose metabolism (Cavadas, Aveleira *et al.* 2016). Consistent with this, when autophagy is permanently suppressed in POMC neurons by preventing the expression of Atg7 (Autophagy-related gene 7), mice become hyperphagic and obese and display an impaired glucose tolerance and leptin response. At a cellular level, these Atg7-deficient POMC neurons display disrupted axonal projections (Coupe, Ishii *et al.* 2012). Hence, defective proteostasis might participate, at the level of POMC neurons, in the development of obesity and related metabolic disorders.

❖ But wait…are all POMC neurons equal?

It is clear that the function of POMC neurons during DIO is impaired by multiple phenomena, which contribute to exacerbating body weight gain and metabolic disorders. All the literature mentioned in this chapter has studied POMC neurons as a whole, as a homogeneous population. However, the recent discovery of the molecular heterogeneity of POMC neurons inevitably raises the question of the functional consequences of this diversity. Do all POMC neurons respond in the same way to the same signals? Are they all working towards the same goal, through different mechanisms? Or do they have as many different roles as their molecular differences?

Chapter 5

POMC neurons:
a striking heterogeneity

This last chapter will briefly expose the current knowledge about the molecular and functional heterogeneity of POMC neurons and introduce the context of our own research in that matter.

❖ Different projection sites

As previously discussed in Chapter 3, the paraventricular nucleus of the hypothalamus (PVH) is a well-described projection site of POMC neurons. However, a retrograde tracing experiment using fluorogold injection in the PVH of rats combined with the labelling of POMC mRNAs revealed that only about 8% of POMC neurons projected onto this hypothalamic region. In the same study, a difference was observed in the rostro-caudal distribution of POMC cells that projected onto the PVH, most of them being located in the mid-to-caudal part of the ARC (Baker and Herkenham 1995).

Another study investigated which hypothalamic neurons project to the thoracic spinal cord by injecting fluorogold in the intermediolateral cell column of rats. Interestingly, many retrogradely labeled cells were found in the rostro-lateral part of the ARC, some of them also expressing CART (Elias, Lee *et al.* 1998). Since in the same study, between 93-97% of CART neurons co-expressed POMC, we can speculate that these rostral CART neurons projecting to the spinal cord were also POMC positive.

Taken together, these initial findings, which are more than 20 years old, suggest that not all POMC neurons project on the same regions and even that a rostro-caudal distribution pattern related to these projections sites actually exist. These findings were among the first evidence pointing towards a possible heterogeneity of these cells.

❖ Different sensitivity to hormones and neurotransmitters

POMC neurons are responsive to numerous endogenous signals (Toda, Santoro *et al.* 2017), although they do not behave equally. For instance, there is a segregation between insulin- and leptin-responsive POMC neurons in mice: insulin-inhibited POMC neurons are located in the retro-chiasmatic area and rostral ARC, while leptin-activated POMC neurons are in the mid-to-caudal part of the ARC, especially above the median eminence, as assessed by electrophysiologic recordings (Williams, Margatho *et al.* 2010).

Furthermore, a similar study looking at serotonin- vs leptin-responsive POMC neurons demonstrated that these two molecules activated distinct population of POMC neurons. Indeed, electrophysiologic recordings showed that leptin-activated POMC neurons did not respond to mCPP (for meta-Chlorophenylpiperazine, a serotonin receptor 5-HT2c agonist) while, and vice-versa, mCPP-activated POMC neurons did not respond to leptin. These two populations were anatomically segregated, with the mCPP-responsive neurons occupying a medial position while the leptin-responsive ones being more lateral, although they were on the same rostro-caudal plane (Sohn, Xu *et al.* 2011). This segregation has been confirmed by a drop-seq analysis of adult mouse hypothalamic cells. Based on the transcripts profiles, the authors were able to distinguish 3 clusters within the POMC population with LepR transcript being restricted to one cluster and 5-HT2c transcript to another (Campbell, Macosko *et al.* 2017).

In addition, POMC neurons react differently to glucose deprivation in electrophysiologic recordings from mouse brain slices. Some POMC cells decrease their spontaneous excitatory post-synaptic currents (sEPSCs) in response to low extracellular glucose levels, while others increase their sEPSCs and a third group has a bi-phasic reaction with a first decrease followed by a progressive increase, above baseline values (Hu, Jiang *et al.* 2014). The location of these neurons was however not investigated in this study.

Thus, these data clearly show that within the POMC neuronal population, subsets of anatomically segregated neurons exist, whose molecular heterogeneity affects their biological response to different signals (Figure 14).

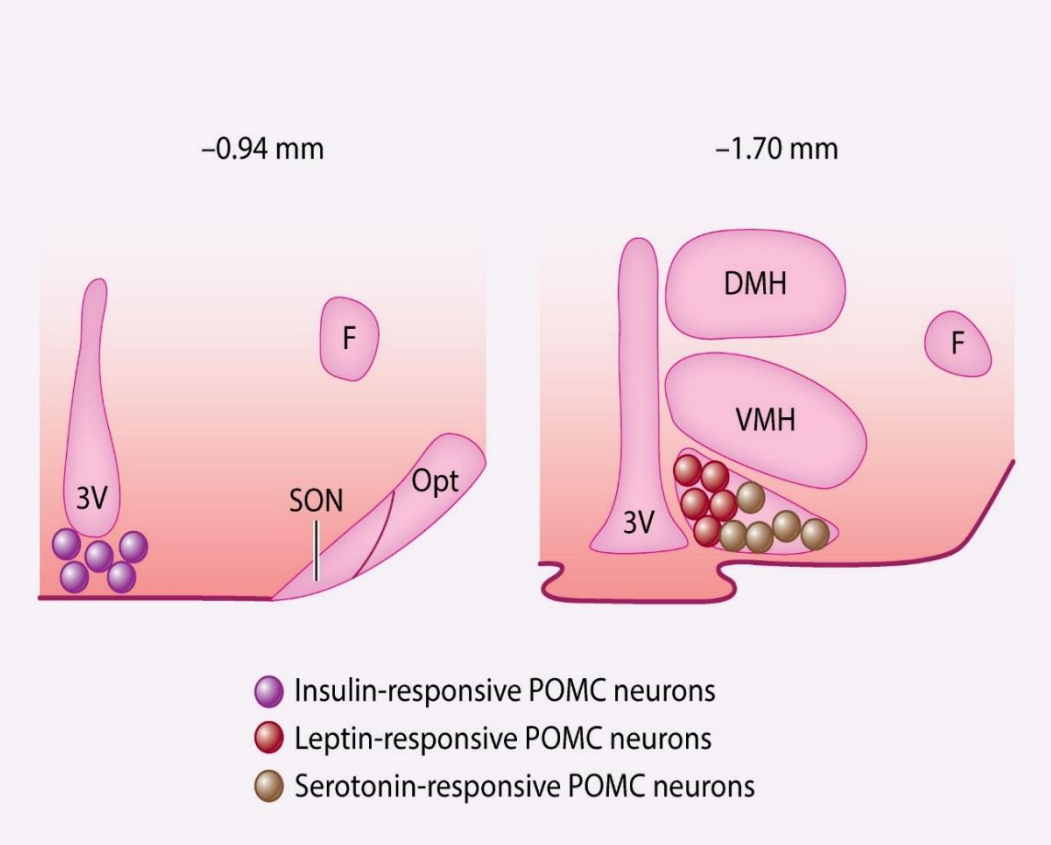

<u>Figure 14</u>: Localization of insulin-, leptin- and serotonin-responsive POMC neurons in the ARC

3V: third ventricle. F: fornix. SON: supraoptic nucleus. Opt: optic chiasma. VMH: ventromedial hypothalamus. DMH: dorsomedial hypothalamus

Figure taken from (Toda, Santoro et al. 2017).

❖ Different neurotransmitter phenotypes

Although the ability of POMC neurons to release neuropeptides is well known, they can also release classical neurotransmitters such as GABA, which is inhibitory, and glutamate, which is excitatory. Studies from Hentges *et al.* were essential in defining the different subpopulations of POMC neurons related to their neurotransmitter phenotypes. First, they used a POMC/GAD67 double fluorescent reporter mouse line (i.e. POMC cells and GAD67 cells express a distinct fluorescent marker). Of note, GAD67 (for glutamic acid decarboxylase of 67kDa) catalyzes the decarboxylation of glutamate to GABA and is thus a marker of GABAergic neurons. They found that approximately 40% of POMC neurons were also GAD67-positive (POMC-GAD67), and can release GABA when put in culture (Hentges, Otero-Corchon

et al. 2009). This was consistent with their previous report using POMC-eGFP mice, in which they had found that around 35% of POMC co-expressed Gad mRNA and released GABA (Hentges, Nishiyama *et al.* 2004). However, they also reported glutamate release from 20% of cultured POMC neurons, which were all Gad67-negative, indicating that both glutmatergic and GABAergic phenotypes could be found in POMC cells (Hentges, Otero-Corchon *et al.* 2009). This was further confirmed in intact networks by optogenetic activation of POMC neurons, which was able to elicit GABA or glutamate transmission within the ARC (Dicken, Tooker *et al.* 2012). In addition, data generated in our lab demonstrate that POMC neurons can release glutamate or GABA in the PVH, also when optogenetically activated (Figure 3 of the annexed article).

In order to study the proportion and localization of glutamatergic and GABAergic POMC neurons (POMC-Glut and POMC-GABA, respectively), mRNA staining for different glutamatergic (vglut1 and vglut2) and GABAergic (vGat, GAD65, GAD67) markers were performed in POMC-eGFP mice. No POMC neurons co-expressed vglut1 (vesicular glutamate transporter 1) or vGat (vesicular GABA transporter). However, there were around 45% of POMC-GAD65 and 38% of POMC-GAD67 neurons, confirming once again the results obtained in the previous studies mentioned above. These POMC-GABA neurons were homogeneously distributed in the rostro-caudal axis of the ARC. On the other hand, there were 7% of POMC-vglut2 (vesicular transporter 2) neurons (Jarvie and Hentges 2012), consistent with the 10% of POMC-vglut2 found in (Vong, Ye *et al.* 2011) by using a double vglut2/POMC fluorescent reporter model. Of note, there was a rostro-caudal distribution pattern for these POMC-vglut2 neurons, most of which were present in the rostral part of the arcuate nucleus. Finally, they also reported that around 5% of POMC neurons that co-expressed GAD65 and vglut2 (POMC-Glut/GABA), suggesting a co-release of both neurotransmitters by the same neurons or an identity switch in progress (Jarvie and Hentges 2012). In any case, this series of studies briefly illustrated above successfully defined 3 subpopulations of POMC neurons, based on their neurotransmitter phenotypes: POMC-Glut, POMC-GABA and POMC-Glut/GABA. They also established GAD65, GAD67 and vglut2 as key markers for the study of these different subpopulations.

Interestingly, these glutamatergic and GABAergic phenotypes are highly plastic during neurodevelopment. For instance, POMC-Glut neurons represent 40% of all POMC neurons at P1, a proportion that seems to gradually decrease to reach around 8% at 8 weeks of age. On the contrary, POMC-GABA neurons are 8% at P1 with a progressive increase until it reaches 46% at 8 weeks of age. The POMC-Glut/GABA population seems rather constant at around 7% (Dennison, King *et al.* 2016).

Besides, a recent single-cell mRNA analysis on 163 POMC neurons from adult POMC-eGFP mice was able to recapitulate these findings, although the proportions for each subpopulations were higher than expected, likely because of the greater sensitivity of this technique compared to mRNA staining by *in situ* hybridization. Indeed, they found that 70% of POMC neurons expressed GAD67, around 50% expressed vglut2 and 24% co-expressed both markers (Lam, Cimino *et al.* 2017).

Altogether, these data reveal the phenotypic heterogeneity of POMC neurons related to neurotransmission. POMC neurons can release either GABA or glutamate in the adult mouse brain, and can even co-express glutamatergic and GABAergic markers.

❖ POMC-Glut and POMC-GABA have opposite response to mTORC1 inhibition

Unpublished data from our lab further expand our knowledge of these glutamatergic and GABAergic POMC subpopulations. In the article annexed at the end of this manuscript, we studied the role of the mechanistic target of rapamycin (mTOR), which is an essential cellular energy sensor (Laplante and Sabatini 2012, Haissaguerre, Saucisse *et al.* 2014), in the regulation of POMC neurons function. In the context of these studies, we used Rapamycin (RAPA), which is a potent inhibitor of mTORC1 (mechanistic target of rapamycin complex 1), a signaling pathway that is critical for the hypothalamic regulation of food intake (Cota, Proulx *et al.* 2006). Interestingly, mTORC1 inhibition by RAPA produced different effects on POMC neurons, as assessed by electrophysiological recordings on brain slices. Some POMC cells were activated, some were inhibited and some did not respond, in equal proportion. As POMC-GABA

are smaller and have higher input resistance than POMC-Glut (Hentges, Otero-Corchon *et al.* 2009), we hypothesized the phenotype of the recorded neurons based on their electrophysiological properties. By doing so, we found that the RAPA treatment was inhibiting putative POMC-Glut neurons and activating putative POMC-GABA ones (Figure 2 of the annexed article). To go further, we tested the effect of RAPA on post-synaptic currents evoked in the PVH by optogenetic stimulation of POMC neurons. Consistent with the previous result, glutamatergic currents were decreased by RAPA, while GABAergic currents were enhanced (Figure 3 of the annexed article).

Taken together, our results suggest that mTORC1 inhibition, which mimics a fasting-like state at the level of the hypothalamus, is able to activate POMC-GABA neurons while inhibiting POMC-Glut ones (Figure 15). This differential effect is extremely interesting, since RAPA causes hyperphagia after a 24h fast in mice. Our data therefore indicate that some POMC neurons might be activated in response to an orexigenic stimulus molecularly mimicking fasting, hence challenging the classical idea of POMC neurons as exclusive drivers of satiety. Consequently, further studies, which have been the object of my thesis, have been required so to better understand the role of these different POMC subpopulations and the functional consequences of their heterogeneity in the context of body weight regulation.

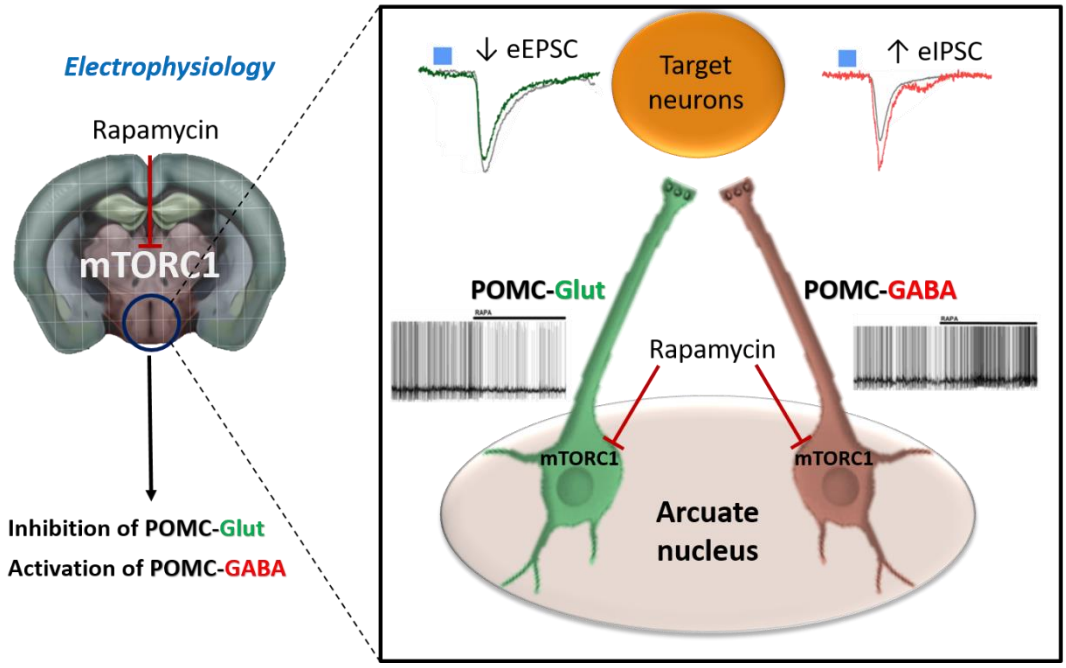

<u>Figure 15</u>: mTORC1 inhibition by RAPA activates POMC-GABA neurons and inhibits POMC-Glut neurons

Electrophysiological recordings on mouse brain slices show that RAPA, an inhibitor of mTORC1 pathway, activates POMC-Glut and inhibits POMC GABA. Consistently, RAPA enhances glutamatergic (EPSC) and reduces GABAergic (IPSC) currents evoked by optogenetic stimulation of POMC neurons in the PVH.

mTORC1: mechanistic target of rapamycin, complex 1. eEPSC: evoked excitatory post-synaptic current. eIPSC: evoked inhibitory post-synaptic current.

Figure adapted from (Mazier et al., 2019 and Saucisse et al., submitted).

Objectives of the study

Obesity is a multifactorial chronic disease whose worldwide prevalence is increasingly alarming. Since no efficient treatment is available to date, further research is needed to find suitable therapeutic strategies. Potential therapeutic targets include POMC neurons, which are a group of hypothalamic neurons known to induce satiety. For long, they have been considered as rather homogenous, but recently, several studies have highlighted their long overlooked heterogeneity. In particular, POMC neurons have been shown to be glutamatergic, GABAergic or even both, but the functional relevance of these phenotypes is still largely unknown. The overarching goal of my thesis has been to develop new tools in order to study these different subpopulations and further characterize their impact in the context of food intake and body weight regulation. The specific objectives were as follows:

1) **To develop a new neuroanatomical technical approach to identify subpopulations of activated POMC neurons on brain slices**

In order to characterize the activity of different POMC neurons subpopulations under different physiological conditions (fasting, refeeding, exposure to HFD, effects of specific hormones, etc.), and to avoid the use of several reporter mouse lines, we set up a novel fluorescent *in situ* hybridization (FISH)/immunofluorescence (IF) protocol that allows combining POMC, GAD65, GAD67 and vglut2 staining together with a marker of cellular activity such as cFos.

2) **To determine the impact of the diet on POMC subpopulations**

Given the deleterious effects of HFD that we have reviewed in Chapter 4 and knowing that POMC cells function is altered under HFD, we have used the neuroanatomical protocol we have developed to investigate the impact of an acute exposure to HFD on POMC-GABA and POMC-Glut activity.

3) To determine the role of the POMC Glutamatergic population in energy balance by using a novel genetic model

Here we wanted to understand whether inhibition of POMC glutamatergic signaling in adult animals may impact energy balance. In order to avoid any compensatory mechanism and neurodevelopmental effect that can be quite confounding when studying POMC neurons, we have generated an inducible model of deletion for vglut2 in POMC neurons. Thus, we will describe the creation of the model, provide the appropriate controls and present the data we have collected so far concerning the metabolic characterization of this new mouse line.

Materials and Methods

Animals

❖ Ethical approval and general housing conditions

All experiments were conducted in strict compliance with the European Union recommendations (2013/63/EU) and were approved by the French Ministry of Higher Education, Research and Innovation (animal experimentation authorization n°04078 and n°13232) and the local ethical committee of the University of Bordeaux (C2EA-50). Maximal efforts were made to reduce any suffering and the number of animals used. From the age of 7 weeks and after at least 3 days of acclimatization in the animal facility in collective cages, male mice were separated and housed individually in standard plastic rodent cages (332x150x130mm, #1144B, Tecniplast, Declines Charpieu, France), with poplar wood-based litter (Lignocel® Select-Fine, SAFE, Augy, France) and enriched with the following:

- cellulose squares (Lab nest, Serlab, Montataire, France) for nesting (8/cage)
- wooden stick (Aspen Bricks, S, #14155, Plexx, Elst, Netherlands) for gnawing (1/cage)
- cardboard tube for hiding/handling (Play tunnel, S, #14151, Plexx, Elst, Netherlands) (1/cage).

Animals were maintained on a 12-h light-dark cycle (lights off at 15:00 h) in a thermo-regulated facility (22°C ± 2°C) with *ad libitum* access to pelleted chow (Standard Rodent Diet, A03, 3.395kcal/g, SAFE, Augy, France) and tap water, unless otherwise specified: for some studies, mice were fasted 24h or their diet switched to a 60% high-fat-diet (HFD with 60% kcal from fat, D12492, 5.24kcal/g, Research Diets Inc., New Brunswick, NJ, USA). A radio was placed in the housing room, to decrease the sensitivity of the mice to environmental noise. All the mice were handled using their individual cardboard tube, for experiments and cage change, to reduce their stress level (Hurst and West 2010).

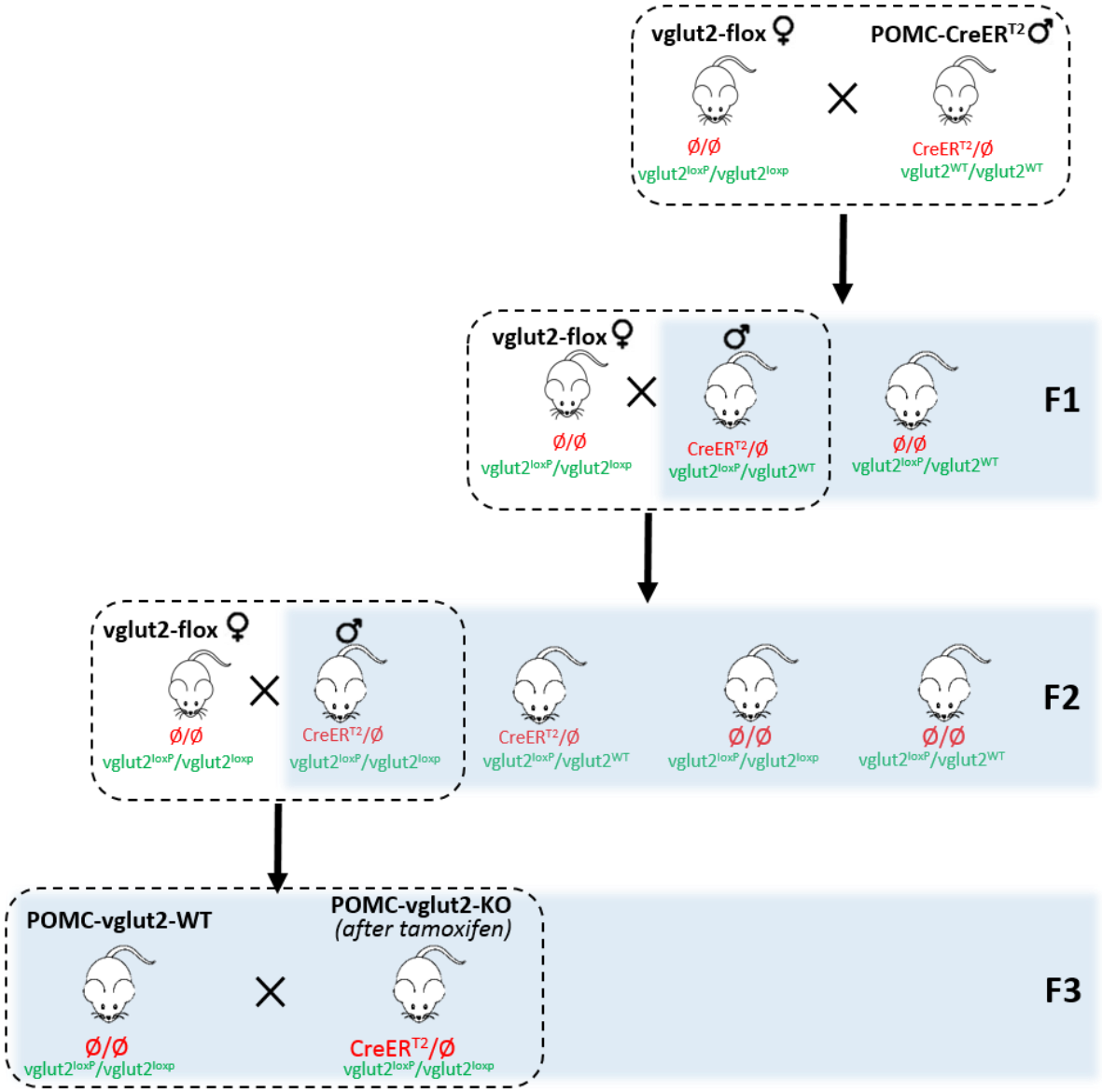

<u>Figure 16</u>: Breeding strategy for the inducible POMC-vglut2-KO mouse line.
Male POMC-CreER^{T2} (hemizygous for the CreER^{T2} gene) mice are crossed with female vglut2-flox mice (homozygous for vglut2^{loxp} allele). After the first generation (F1), male mice hemizygous for CreER^{T2} and heterozygous for vglut2^{loxp} are crossed again with female vglut2-flox mice. After the second generation (F2), male mice hemizygous for CreER^{T2} and homozygous for vglut2^{loxp} are crossed again with female vglut2-flox mice. Finally, the mice of the third generation (F3) are the "POMC-vglut2-WT" (without CreER^{T2} and homozygous for vglut2^{loxp}) and "POMC-vglut2-KO" (hemizygous for CreER^{T2} and homozygous for vglut2^{loxp}) that will be studied. Effective deletion of vglut2 in POMC-vglut2-KO mice is done after tamoxifen treatment. Male POMC-vglut2-KO are then crossed with female POMC-vglut2-WT to maintain the line. Only male POMC-vglut2-WT/KO mice were used for the experiments.

F1, F2 and F3 littermates appear on a light blue background.

❖ Mouse lines

C57BL/6J mice were bought from Janvier, Le Genest-Saint-Isle, France. Inducible POMC-vglut2-KO mice and their control littermates (POMC-vglut2-WT) were generated in the breeding facility of the Neurocentre Magendie by crossing POMC-CreER^{T2} mice [C57BL/6J-Tg(Pomc-creER^{T2}) ; (Berglund, Liu *et al.* 2013)] with vglut2-flox mice [Slc17a6^{tm1Lowl}/J ; JAX stock #012898; (Tong, Ye *et al.* 2007)] using the breeding strategy illustrated in Figure 16. Inducible POMC-Ai6-CreER^{T2}+ mice and their control littermates (POMC-Ai6-CreER^{T2}-) were generated using the same strategy, by crossing POMC-CreER^{T2} mice with Ai6 mice [B6.Cg-Gt(ROSA)26Sor$^{tm6(CAG-ZsGreen1)Hze}$/J ; JAX stock #007906; (Madisen, Zwingman *et al.* 2010)].

These new lines were generated following a three steps backcrossing method, as previously described (Bellocchio, Soria-Gomez *et al.* 2013). They were in a mixed genetic background, with a predominant C57BL/6J contribution. Effective Cre-mediated deletion of vglut2 in POMC neurons after tamoxifen treatment was evaluated by polymerase chain reaction (PCR, see below and Results, Chapter 3, Figure 27C). Effective Cre-mediated expression of Zsgreen1 in POMC neurons was assessed by immunohistochemistry (IHC, see below and Results, Chapter 3, Figure 28B). Number of animals used in the study is indicated in the figure legends.

❖ Tamoxifen treatment for the induction of Cre-mediated recombination

First, a 1g/mL suspension of tamoxifen (T5648, Sigma-Aldrich, Saint-Quentin Fallavier, France) in 100% ethanol (20821.330, VWR, Briare, France) was prepared. Then, corn oil (C8267, Sigma-Aldrich, Saint-Quentin Fallavier, France) pre-heated to 55°C was added to obtain a 50mg/mL stock solution. Enough solution was prepared for a 5-day treatment. After vortexing to ensure complete dissolution of tamoxifen, 1-day treatment aliquots were kept at -20°C.

POMC-vglut2-WT/KO or POMC-Ai6-CreER^{T2}+ mice were singly housed and handled daily for at least 7 days before starting the treatment. Then, using the stock solution previously described, they were administered with 150mg/kg of tamoxifen, daily, for 5 consecutive days by oral gavage. Each day, one aliquot was warmed up to 37°C before the drug administration. Any leftover was discarded. We used polypropylene flexible gavage needles (FTP-20, Instechlabs, Plymouth Meeting, PA, USA) to reduce trauma and decrease the risk of oesophagus perforation. Gavage volume was of 3mL/kg (i.e. 90µL for a 30g mouse).

❖ Genotyping (Cre, flox, Ai6) and excision control (vglut2)

Mice were genotyped by the genotyping facility of the Neurocentre Magendie, from genomic DNA purified from tail biopsies by PCR using specific primers for Cre, vglut2-flox and Ai6 controls. For the control of vglut2 excision in POMC-vglut2-WT/KO mice, fresh hypothalami were dissected on ice and snap frozen after cervical dislocation. Tails or hypothalami were incubated overnight at 56°C in Proteinase K buffer (100mM Tris-HCl pH8, 5mM EDTA, 0.2% SDS, 200mM NaCl, 0.2mg/mL PK). After 10min at 16300g, the supernatants were purified on silica columns, according to the manufacturer protocol (Macherey nagel kit), on a zephyr automatic station. PCR assay was carried out using a Biorad C1000 thermal cycler, with GoTaq G2 Hot Start Green Master Mix (Promega, Charbonnières-les-Bains, France), and 0.3 to 0.6µM of each primer (see Table 1) in a 25µL volume. PCR conditions were as follows: 1 cycle, 5min at 95°C; 37 cycles, 30sec at 95°C, 30sec at 58°C for, 1min at 72°C; 1 cycle, 5min at 72°C. PCR products was analyzed on a Labchip GX microfluidic electrophoresis system (Caliper) using the DNA5k kit.

Mouse line	Primer	Sequence 5'3'	Expected fragment	Length
POMC-CreER^{T2}	Cre_Forward	GCGGTCTGGCAGTAAAAACTATC	CreER^{T2}	100 bp
	Cre_Reverse	GTGAAACAGCATTGCTGTCACTT		
Ai6	Ai6_WT_Forward	AAGGGAGCTGCAGTGGAGTA	WT	300 bp
	Ai6_WT_Reverse	CCGAAAATCTGTGGGAAGTC		
	Ai6_Mutant_Forward	AACCAGAAGTGGCACCTGAC	Ai6	210 bp
	Ai6_Mutant_Reverse	GGCATTAAAGCAGCGTATCC		
vglut2-flox	vglut2_Forward	CTGAGCGAAGGTGAGCTGAA	Flox	400 bp
	vglut2_Reverse	TGGGCCAGAACACAGGATATG	WT	270 bp
	vglut2_Fwd_Excision	TCACTGCCTTGTTCCTAGTGC	Excision	700 bp

Table 1: Primers used for the genotyping.

❖ Body composition analysis by EchoMRI ™

Assessment of lean and fat mass in conscious male mice was performed using a nuclear echomagnetic resonance imaging whole-body composition analyzer (Echo MRI 900; EchoMedical Systems, Houston, TX, USA) (Kovner, Taicher *et al.* 2010). Scans were performed by placing animals into a thin-walled plastic cylinder (1.5 mm thick, 4.7 cm inner diameter) with a cylindrical plastic insert added to limit movement. While in the tube, animals were briefly subjected to a low-intensity (0.05 Tesla) electromagnetic field to measure fat mass and lean mass. For each mouse, two successive measurements of 1.5min accumulation time each were made and averaged.

❖ Indirect calorimetry – calorimetric cages

Mice were individually housed in calorimetric chambers (Labmaster, TSE Systems GmbH, Bad Homburg, Germany) in which fluid, food intake, in-cage locomotor activity, and gas exchange could be monitored. Studies were carried out at 22°C unless specified otherwise. Litter and nesting materials were provided to the animals. After 1 week of acclimatization, O_2 consumption (V_{O2}, mL/h) and CO_2 production (V_{CO2}, mL/h) were measured every 20 min to measure the gas exchange and calculate respiratory exchange ratio as well as energy expenditure. Of note, respiratory exchange ratio (RER), obtained by dividing V_{CO2} by V_{O2}, is an indicator of substrate utilization (low during lipid oxidation, and higher during carbohydrate oxidation). Simultaneously, home-cage locomotor activity was determined using a tridimensional infrared light beam system, and was defined as the sum of all X beam breaks (counts/h). For data analysis, 12 hour-light phase and 12 hour-dark phase cumulative or averaged results were obtained by summing up or averaging, respectively, data expressed as 1h-bins over the relevant period. All recordings and data analysis were done by Philippe Zizzari from our team.

❖ Food preference – polyfeeding cages

Mice were singly housed in operant polyfeeding cages (Imetronic, Pessac, France) and acclimatized to their new environment one week before the beginning of the experiment. Briefly, the cages have up to three food containers whose accessibility can be programmed. For our experiment, only the more external compartments were used. During the acclimatization phase, chow diet was placed in the two food containers to estimate mouse preference for one or the other side and the least preferred side was then paired with HFD. 2h preference for chow or HFD was evaluated during the light period (beginning 4h after the light onset), in free-fed conditions.

Immunohistochemistry and Fluorescent In situ Hyrbidization

For the exact references and suppliers of reagents, kits, and antibodies, please see Table 3, Table 4 and Table 5 respectively, at the end of this chapter. All washes last 5min each and all incubations are done at room temperature, unless otherwise specified.

❖ Perfusion and brain processing

Mice were deeply anesthetized using pentobarbital sodium (Ceva Santé Animale, Libourne, France) given intraperitoneally (IP, 300mg/kg) and then perfused transcardially with ice-cold phosphate-buffered saline [PBS: $Na_2HPO_4 \bullet 2H_2O$ (14.95g/L) + NaH_2PO_4 (2.2g/L) + NaCl (9g/L) in distilled water], pH 7.4, until full discoloration of the liver (around 30sec) followed by 10% neutral buffered formalin (NBF) perfusion for at least 2min. Brains were extracted and postfixed in 10% NBF for 24h at 4°C, then cryoprotected with 30% sucrose in PBS at 4°C until saturation (assessed by their sinking to the bottom of the tube). They were then frozen by immersion in dry ice-cooled isopentane and stored at -80°C in a tightly closed container. Free-floating coronal sections (30µm) were cut with a cryostat (CM1950, Leica, Wetzlar Germany), collected in antifreeze solution (30% ethylene glycol, 20% glycerol in PBS) and stored at -20°C until further used.

❖ Single IHC for POMC

Brain sections from POMC-Ai6-CreER^{T2}+ mice were processed for the co-expression of ZsGreen1 and POMC to evaluate the functionality and specificity of Cre-mediated recombination after treatment with tamoxifen or its vehicle (see Results, Chapter 3, Figure 29). After 3 washes in PBS, sections were incubated with rabbit anti-POMC antibody (1/2000) in [PBS+0.3% Triton X-100] overnight at 4°C. The next day, sections were washed 3 times in PBS and incubated for 2h with AlexaFluor647-conjugated donkey anti-rabbit antibody (1/500) in [PBS+0.3% Triton X-100]. After 3 washes in PBS, sections were mounted using ProLong Gold medium, cover-slipped (0.13-0.17mm thickness) and stored in the dark.

❖ Double-IHC for POMC and cFos

Brain sections from C57Bl/6J mice were processed for the co-expression of POMC, and cFos, to evaluate the percentage of activated POMC neurons under different experimental conditions (see Results, Chapter 2, Figures 25 and 26). After 3 washes in PBS, sections were incubated with rabbit anti-POMC (1/2000) and goat anti-cFos antibodies (1/250) in [PBS+0.3% Triton X-100] overnight at 4°C. The next day, sections were washed 3 times in PBS and incubated for 2h with AlexaFluor647-conjugated donkey anti-rabbit (1/500) and AlexaFluor488-conjugated donkey anti-goat (1/500) antibodies in [PBS+0.3% Triton X-100]. After 3 washes in PBS, sections were mounted using ProLong Gold medium, cover-slipped (0.13-0.17mm thickness) and stored in the dark.

❖ Riboprobes synthesis

DNP-labeled riboprobe against mouse POMC (POMC-DNP), DIG-labeled probe against mouse vglut2 (vglut2-DIG), FITC-labeled riboprobe against mouse GAD65 (GAD65-FITC) and FITC-labeled riboprobe against mouse GAD67 (GAD67-FITC) were prepared as follows: from hypothalamic RNA reverse transcribed into cDNA, DNA templates for POMC, vglut2, GAD65 and GAD67 were obtained *via* PCR with the primers described in Table 2. Subsequently, these templates were sub-cloned into pBluescript vector using the restriction enzymes EcoRI and BamHI. After linearization with BamHI, the antisense riboprobes were synthesized with T3 RNA polymerase. For the generation of the sense riboprobes, EcoRI was used for the linearization and T7 RNA polymerase for the synthesis. 35% of the uridine triphosphate (UTPs) in each reaction was replaced with either DNP-11-UTP, DIG-11-UTP or FITC-12-UTP for POMC, vglut2 and GAD65/GAD67 probe production, respectively. All riboprobes were generated by Astrid Cannich, in the lab of our collaborator Giovanni Marsicano at INSERM U1215.

Riboprobes	Primers	Reference
POMC	Forward: CGACGGAAGAGAAAAGAGGT Reverse: TTGGAATGAGAAGACCCCTG	Allen Brain Atlas : Probe RP_Baylor_102974
GAD65	Forward: GTGGCAGGAGTTAAGATGAC Reverse: AGGGTGACTCTTCTGTCCTG	Gift from Beat Lutz
GAD67	Forward: TGTGCCCAAACTGGTCCT Reverse: TGGCCGATGATTCTGGTT	Allen Brain Atlas, probe #RP_040324_01_F01
vglut2	Forward: TCATTGCTGCACTCGTCCACTA Reverse: CCCTGGGATAGTTTGCAGTCCA	Gift from Dr Gilles Yeo's lab (Cambridge)
vglut2	Forward: CCAAATCTTACGGTGCTACCTC Reverse: AGCCATCTTTCCTGTTCCACT	Allen Brain Atlas, probe #RP_050921_01_E03
vglut2	Forward: TGGCTTCATTCACGAAGATG Reverse: GCTTGGTTGATATGTTTACA	Gift from Robert Edwards' Lab (UCSF)
vglut2	Forward: TCATTGCTGCACTCGTCCAC Reverse: CCCTGGGATAGTTTGCAC	Gift from Jeffrey Macklis' lab (Addgene, pasmid #45639)

Table 2: Primers used for the DNA templates.

❖ Bench-made TSA-Cy5 reagents

Bench-made TSA-Cy5 was produced to obtain a more concentrated reagent and thus achieve higher signal amplification. First, Cy5-NHS ester (the reactive form of cyanine 5, for the labeling of amino groups) was dissolved in N,N-dimethylformamide (DMF) to obtain a 10mg/mL solution. In parallel, a 10mg/mL tyramine solution was prepared by dissolving tyramine in [DMF+1% triethylamine]. These two solutions were then mixed at a 1:1 molar ratio and the mixture was incubated in the dark for 2h. Finally, an appropriate amount of 100% ethanol was added to get a final concentration

of 5mg/mL of Cy5 after which aliquots were made and stored at -20°C. In order to know how much of the tyramine solution needs to be added to the Cy5-NHS ester solution, the following formula can be used:

$$\text{Volume of tyramine solution} = \frac{(\text{Volume of Cy5-NHS ester solution}) \times 173.64 \times 1.1}{\text{Molecular weight of Cy5}}$$

Apart from this TSA-Cy5 reagent, we also prepared a bench-made amplification buffer as follows: a stock solution was prepared by dissolving 2% dextran sulfate, 0.1% Tween20 and 500µg/mL of 4-iodophenol in 0.1M borate solution and stored at 4°C. Then, just before the TSA revelation, 0.006% of H_2O_2 was added to the previous solution, to make the amplification buffer.

❖ Triple-FISH for vglut2, GAD65/67 and POMC with IHC for cFos

Brain sections from C57Bl6/J mice were processed for the co-expression of POMC, vglut2, GAD65, GAD67 and cFos, to evaluate the phenotype of activated POMC neurons under different experimental conditions (see Results, Chapter 2). We took 4 sections per animal containing POMC neurons and spaced 300µm apart, in order to have an appropriate rostro-caudal representation of the ARC. The main steps illustrating the development of this technique are further developed in Results, Chapter 1. Only the final version of the protocol is extensively described here.

Day 1: After 3 washes in PBS, endogenous peroxidases were quenched in 3% H_2O_2 in PBST (PBS+0.1% Tween20) for 30min. After 1 wash in PBS, endogenous biotins were blocked by incubated the slices in Avidin solution for 15min, washed in PBS, incubated in Biotin solution for another 15min (Avdin/Biotin blocking kit) and washed again in PBS. Rabbit anti-cFos antibody (1/1000) in [PBS+0.3% Triton X-100] was incubated overnight at 4°C.

Day 2: Sections were washed 3 times in PBS, incubated in HRP-conjugated goat anti-rabbit (1/500) in [PBS+0.3% Triton X-100] for 2h and washed 3 times again with PBS. Tyramide signal amplification (TSA) was done, using tyramine-labeled biotins (TSA-Biotin dissolved in 1X Plus Amplification buffer, 1/250, 30min). After 3 washes in PBS, HRP were blocked by a 30min-incubation in 3% H_2O_2 in PBS followed by a 20min-incubation in 0.2M HCl (with 1 wash in PBS in between). Biotins were fixed by a 10min-incubation in ice-cold 10% NBF. After 1 wash in PBS-DEPC (PBS with 0.01% diethylpyrocarbonate) and 2 washes in PBST-DEPC (PBS-DEPC+0.1% Tween20), sections were acetylated with a treatment of 0.25% acetic anhydride in 0.1M triethanolamine (pH=8.0) for 10min (0.25% acetic anhydride were added again after the first 5min, since it's quickly degraded). After 1 wash in PBST-DEPC, the hybridization solution was prepared as follows: POMC-DNP, vglut2-DIG, GAD65-FITC and GAD67-FITC probes (1/1000 for each of them) were dissolved in hybmix (50% deionized formamide, 20mM Tris at pH=8.0, 300mM NaCl, 5mM EDTA, 10% dextran sulfate, 1X Denhardt's solution, 0.5mg/mL tRNA, 0.2mg/mL acid-cleaved carrier DNA from salmon's sperm, 1M DTT dissolved in water containing 0.01% DEPC) and heated at 90°C for 5min to ensure probe linearization. Sections were then incubated in this hybmix overnight (16h-20h) at 70°C in a waterbath.

Day 3: A series of washes with increased stringency was carried out as follows:

- 5X SSC (Saline Sodium Citrate) + 0.2% Tween20 for 5min at 65°C
- 2X SSC + 0.2% Tween20 + 50% Formamide Amide for 30min at 65°C
- 1X SSC + 0.2% Tween20 + 50% Formamide Amide for 30min at 65°C
- 0.1X SSC + 0.2% Tween20 for 30min at 65°C

After the last stringent wash, sections were washed once with TNT buffer (100mM Tris at pH=7.5 + 150mM NaCl + 0.05% Tween20), incubated 30min with 3% H_2O_2 in PBS followed by a 20min-incubation in 0.2M HCl (with 1 wash in TNT in between). After a wash in TNT, sections were incubated for 1h in TNB blocking buffer (from TSA kits, prepared as per manufacturer's instructions) then overnight at 4°C in HRP-labeled anti-DIG antibody (1/1500) in TNB.

Day 4: Sections were washed 3 times in TNT, and subjected to TSA-Cy3 revelation (TSA-Cy3 dissolved in 1X Plus Amplification buffer, 1/100, 30min). After 3 washes in TNT, HRP were blocked by a 30min-incubation in 3% H_2O_2 in PBS followed by a 20min-incubation in 0.2M HCl (with 1 wash in TNT in between). After 1 wash in TNT, sections were incubated in HRP-conjugated anti-FITC antibody (1/1500) in TNB for 2h. Sections were washed 3 times in TNT, and subjected to TSA-FITC revelation (TSA-FITC dissolved in 1X Plus Amplification buffer, 1/100, 30min). After 3 washes in TNT, HRP were blocked by a 30min-incubation in 3% H_2O_2 in PBS followed by a 20min-incubation in 0.2M HCl (with 1 wash in TNT in between). After 1 wash in TNT, sections were incubated in HRP-conjugated anti-DNP antibody (1/100) in TNB overnight at 4°C.

Day 5: Sections were washed 3 times in TNT, and subjected to bench-made TSA-Cy5 revelation (bench-made TSA-Cy5 reagent dissolved in bench-made Amplification buffer, 1/200, 30min). After 3 washes in TNT, HRP were blocked by a 30min-incubation in 3% H_2O_2 in PBS followed by a 20min-incubation in 0.2M HCl (with 1 wash in TNT in between). After 1 wash in TNT, sections were incubated for 30min in Avidin-Biotin complexes (ABC) prepared as per manufacturer's instruction (1/50 of solution A and 1/50 of solution B in PBST, mixed at least 30min before the incubation). Sections were then washed 3 times in TNT, and subjected to TSA-Coumarin revelation (TSA-Coumarin dissolved in 1X Plus Amplification buffer, 1/100, 30min). After 3 washes in TNT, HRP were blocked by a 30min-incubation in 3% H_2O_2 in PBS followed by a 20min-incubation in 0.2M HCl (with 1 wash in TNT in between). After 2 washes in TNT and 1 final wash in 50mM Tris at pH=7.5, sections were mounted using ProLong Gold medium, cover-slipped (0.13-0.17mm thickness) and stored in the dark.

❖ Image acquisition and analysis

For the development of the triple-FISH with IHC technique (Results, Chapter 1) and the expression of Zsgreen1 in POMC-Ai6-cre+ mice (Results, Chapter 3), images of the arcuate nucleus of the hypothalamus (ARC) were taken using a wide field epifluorescence microscope (DM 4000B LED with a DFC365 FX camera, Leica, Wetzlar Germany). For the POMC/cFos and POMC/vglut2/GAD65-67/cFos co-expression (Results, Chapter 2), stacks of images containing each hemi-ARC (left and right) were taken using a SP8 confocal microscope (Leica, Wetzlar, Germany) available at the Bordeaux Imaging Center (BIC). Two sequences were programmed to acquire simultaneously FITC+Cy5 channels and then coumarin+Cy3 ones. The acquisition parameters were optimized on mono-stained slices to make sure that simultaneous acquisitions could be made. We only used the hybrid detectors of the SP8 microscope in photon counting mode. The voxel size was 0.284 x 0.284 x 0.7868 μm^3, with a bit depth of 8 bits per pixels.

Image analysis was performed using ImageJ. After brightness and contrast adjustment to reduce background and increase specific staining, the co-expression of our different markers were assessed by eye. For each image, we used the multi-point tool available in ImageJ to select and count POMC neurons that co-expressed (or not) cFos, vglut2 and/or GAD65/67. Only one side (left of right) was quantified for each animal.

Statistics

Statistical analyses were performed using Prism 8.3.0 (GraphPad Software, San Diego, CA, USA). All values are reported as means ± SEM (standard error of the mean). Depending on the variables and the groups evaluated, data were analyzed by unpaired Student's t-test, Mann-Whitney test or by repeated measurements ANOVAs, two-way, one-way ANOVAs or Kruskal-Wallis test followed by post-hoc analysis as appropriate. A p-value below 0.05 denotes statistical significance.

Reagents / Antibodies / Kits Tables

Product	Reference	Supplier
4-Iodophenol	I10201	Sigma-Aldrich, Saint-Quentin Fallavier, France
Acetic anhydride	A6404	Sigma-Aldrich, Saint-Quentin Fallavier, France
BamHI	R0136	New England Biolabs, Evry, France
Borate (boric acid)	B7660	Sigma-Aldrich, Saint-Quentin Fallavier, France
Cy5 NHS ester	PA15101	GE Healthcare Life Sciences, UK
Denhardt's solution (50X)	750018	Thermo Fisher Scientific, Bordeaux, France
DEPC (diethylpyrocarbonate)	159220	Sigma-Aldrich, Saint-Quentin Fallavier, France
Dextran sulfate	D8906	Sigma-Aldrich, Saint-Quentin Fallavier, France
DIG-11-UTP	11363905910	Sigma-Aldrich, Saint-Quentin Fallavier, France
DMF (N,N-dimethylformamide)	227056	Sigma-Aldrich, Saint-Quentin Fallavier, France
DNP-11-UTP	NEL555001EA	PerkinElmer, Villebon-sur-Yvette, France
EcoRI	R0101	New England Biolabs, Evry, France
EDTA	EDS	Sigma-Aldrich, Saint-Quentin Fallavier, France
Ethylene Glycol	24041.297	VWR, Briare, France
FITC-11-UTP	11427857910	Sigma-Aldrich, Saint-Quentin Fallavier, France
Formamide (deionized)	4610	Sigma-Aldrich, Saint-Quentin Fallavier, France
Formamide Amide	1117	Euromedex, Souffelweyersheim, France
Glycerol	49781	Sigma-Aldrich, Saint-Quentin Fallavier, France
HCl (37% hydrochloric acid)	30721	Sigma-Aldrich, Saint-Quentin Fallavier, France

Hydrogen peroxide solution (30%)	H1009	Sigma-Aldrich, Saint-Quentin Fallavier, France
Isopentane (2-Methylbutane)	M32631	Sigma-Aldrich, Saint-Quentin Fallavier, France
NaCl (sodium chloride)	27810.295	VWR, Briare, France
NBF (10% Neutral Buffered Formalin)	HT501128	Sigma-Aldrich, Saint-Quentin Fallavier, France
ProLong ™ Gold antifade reagent	P36930	Thermo Fisher Scientific, Bordeaux, France
Salmon's sperm	D7656	Sigma-Aldrich, Saint-Quentin Fallavier, France
Sodium phosphate dibasic dihydrate (Na2HPO4•2H2O)	28040.291	VWR, Briare, France
Sodium phosphate monobasic monohydrate (NaH2PO4•H2O)	1.06146.1000	Sigma-Aldrich, Saint-Quentin Fallavier, France
SSC (Saline Sodium Citrate)	GHYSSC00-08	Eurobio, Les Ulis, France
Sucrose	200-301-B	Euromedex, Souffelweyersheim, France
T3 RNA polymerase	11 031 163 001	Sigma-Aldrich, Saint-Quentin Fallavier, France
T7 RNA polymerase	10 881 767 001	Sigma-Aldrich, Saint-Quentin Fallavier, France
TEA (triethylamine)	T0886	Sigma-Aldrich, Saint-Quentin Fallavier, France
Triethanolamine	33729	Sigma-Aldrich, Saint-Quentin Fallavier, France
Tris (Trizma phosphate monobasic)	93348	Sigma-Aldrich, Saint-Quentin Fallavier, France
Triton X-100	X100	Sigma-Aldrich, Saint-Quentin Fallavier, France
tRNA	TRNABAK-RO	Sigma-Aldrich, Saint-Quentin Fallavier, France
Tween20	P1379	Sigma-Aldrich, Saint-Quentin Fallavier, France
Tyramine hydrochloride	T2879	Sigma-Aldrich, Saint-Quentin Fallavier, France

Table 3: List of reagents and enzymes used for FISH and IHC.

Kits	Reference	Supplier
Avidin/Biotin Blockint Kit	SP-2001	Vector Laboratories, Peterborough, UK
TSA Coumarin System	NEL703001KT	Akoya Biosciences, Marlborough, MA, USA
TSA Plus Biotin Kit	NEL749A001KT	Akoya Biosciences, Marlborough, MA, USA
TSA Plus Cyanine 3 (Cy3) System	NEL744001KT	Akoya Biosciences, Marlborough, MA, USA
TSA Plus Fluorescein (FITC) System	NEL741001KT	Akoya Biosciences, Marlborough, MA, USA
Vectastain Elite ABC HRP Kit	PK-6100	Vector Laboratories, Peterborough, UK

Table 4: List of commercial kits used for FISH and IHC

Antibody	Reference	Supplier
Primary antibodies		
cFos (goat, polyclonal)	sc-52-G	Santa Cruz Biotechnologies, Heidelberg, Germany
cFos (guinea pig, polyclonal)	226-005	Synaptic Systems GmbH, Goettingen, Germany
cFos (rabbit, monoclonal)	2250	Cell Signaling Technology, Leiden, Netherlands
POMC (rabbit polyclonal)	H-029-30	Phoenix Pharmaceuticals, Burlingame, CA, USA
Secondary antibodies		
AlexaFluor488-conjugated donkey anti-goat	705-545-003	Jackson ImmunoResearch, Ely, UK
AlexaFluor647-conjugated donkey anti-rabbit	711-605-152	Jackson ImmunoResearch, Ely, UK
HRP-conjugated goat anti-rabbit	7074	Cell Signaling Technology, Leiden, Netherlands
HRP-conjugated anti-DIG	11207733910	Sigma-Aldrich, Saint-Quentin Fallavier, France
HRP-conjugated anti-DNP	FP1129	Akoya Biosciences, Marlborough, MA, USA
HRP-conjugated anti-FITC	11426346910	Sigma-Aldrich, Saint-Quentin Fallavier, France

Table 5: List of antibodies used for FISH and IHC.

Results

Chapter 1

Simultaneous detection of POMC, GAD65, GAD67, vglut2 and cFos on free-floating brain slices

One way to study POMC glutamatergic and GABAergic neurons is to identify them on postmortem brain sections, after performing a specific stimulus, to see if one subpopulation is more responsive than another. This requires the ability to differentiate these neurons by using cell markers that are specific to these two subpopulations. The only known glutamatergic marker of POMC neurons is a protein called "vesicular glutamate transporter 2" (vglut2) (Vong, Ye *et al.* 2011, Jarvie and Hentges 2012). This protein, encoded by the *Slc17a6* gene, allows the accumulation of glutamate in secretion vesicles and is therefore essential for glutamatergic transmission. Concerning GABAergic neurons, the "vesicular GABA transporter" vGat protein fulfils the same role as vglut2, but it is absent from GABAergic POMC neurons (Vong, Ye *et al.* 2011), which is why we use the "glutamic acid decarboxylase of 65kDa" (GAD65) and the "glutamic acid decarboxylase of 67kDa" (GAD67) as markers for this subpopulation (Hentges, Nishiyama *et al.* 2004, Hentges, Otero-Corchon *et al.* 2009, Jarvie and Hentges 2012). These two enzymes, encoded respectively by the *Gad2* and *Gad1* genes, catalyze the decarboxylation of glutamate to GABA and are thus essential to GABA production.

Unfortunately, vglut2, GAD65 and GAD67 are predominantly expressed in axon terminals (Esclapez, Tillakaratne *et al.* 1994, Fremeau, Voglmaier *et al.* 2004), which makes their detection by immunohistochemistry (IHC) unsuitable to achieve our goal. Indeed, in order to know the glutamatergic and/or GABAergic phenotype of POMC neurons, the staining must be clearly visible at the level of the cell body. For this reason, instead of the proteins, we have to detect the mRNAs of these different markers, which accumulate strongly in the cytosol, using the fluorescence *in situ* hybridization (FISH) technique. POMC neurons can obviously be identified by labelling the mRNA or POMC protein. Since the protein is expressed in both the cell bodies and axonal projections, the image analysis can be challenging, as a weak cytosolic staining can be lost among the more intense axonal labelling. We have therefore chosen to stain POMC mRNA, which is only present in the cytosol and thus facilitates image quantification.

Finally, the detection of cFos on the same slices will provide a functional information. Indeed, *FOS* is an "immediate early gene", meaning that it codes for a protein - cFos - that is only very weakly expressed or not expressed at all at a basal level. As a result, the cFos protein is used as a marker of cellular activity, because its synthesis and accumulation in the nucleus of cells only takes place when these cells have responded to a stimulus (Bullitt 1990). Both mRNA or cFos protein can be detected, depending on the delay between the stimulus and the sacrifice: a peak of mRNA is usually observed about 30 minutes after the stimulus while the peak of protein occurs between 1 hour and 3 hours after, depending on the stimulus and the region of interest (Wu, Lemus *et al.* 2014, Barros, Mundim *et al.* 2015). In all the studies of the present work, mice were sacrificed 90 minutes or 2 hours after the stimulus, so it is the cFos protein that will be used to identify the "activated" neurons under our different experimental conditions.

For all these reasons mentioned above, it was necessary to develop a technique for the combined labelling of vglut2, GAD65, GAD67, POMC mRNAs and cFos protein.

❖ Adaptation of FISH protocol on slides to a FISH protocol on free-floating slices

In the past, our team has already carried out FISH staining on fresh (unfixed) 15µm brain slices on slides (Cardinal, Andre *et al.* 2014). However, under all our experimental conditions, mice were perfused with 4% formaldehyde (in PBS) and brains processed for the classical IHC staining that we routinely perform: 24 hours of post-fixation in 4% formaldehyde, cryoprotection in a 30% sucrose solution, freezing and cryostat cut-30µm free-floating sections. It was therefore necessary to adapt the previous FISH protocol to make it compatible with free-floating, fixed sections.

The principle of mRNA detection in FISH is based on the hybridization of a nucleic probe that is complementary to some part of the target mRNA. This probe can be made of DNA or RNA. However, since RNA-RNA hybrids are more stable than

DNA-DNA ones (Farrell 2010), we systematically use RNA probes. Before the hybridization, "pre-treatment" steps are used to denature endogenous peroxidases and improve permeabilization (with 0.2M hydrochloric acid), inhibit endogenous RNAses and increase the stability of RNA-RNA hybrids (with acetylation) (Figure 17A). The hybridization step is carried out at a specific temperature, estimated at about 15°C below the melting temperature (Tm_{RNA}), i.e. the temperature at which only half of the RNA probes are hybridized. For each probe, the Tm_{RNA} is calculated in °C using the following formula (J.F and Russell 2001):

$$\mathbf{Tm_{RNA}} = 79{,}8 + 18{,}5 \times \log[Na^+] + 58{,}4 \times \frac{G+C}{Length} + 11{,}8 \times \left(\frac{G+C}{Length}\right)^2 - 0{,}35 \times (\%FA) - \frac{820}{Length}$$

With:

- $[Na^+]$: concentration of Na^+ ions in the hybridization solution (hybmix), in M
- G+C : total number of guanidine and cytosine in the probe sequence
- Length : total number of nucleotides of the probe
- % FA : percentage of deionized formamide in the hybmix

This calculation, applied to the different probes used, gives different Tm, ranging from 77.5°C to 92°C, which is why we have chosen a common hybridization temperature of 70°C.

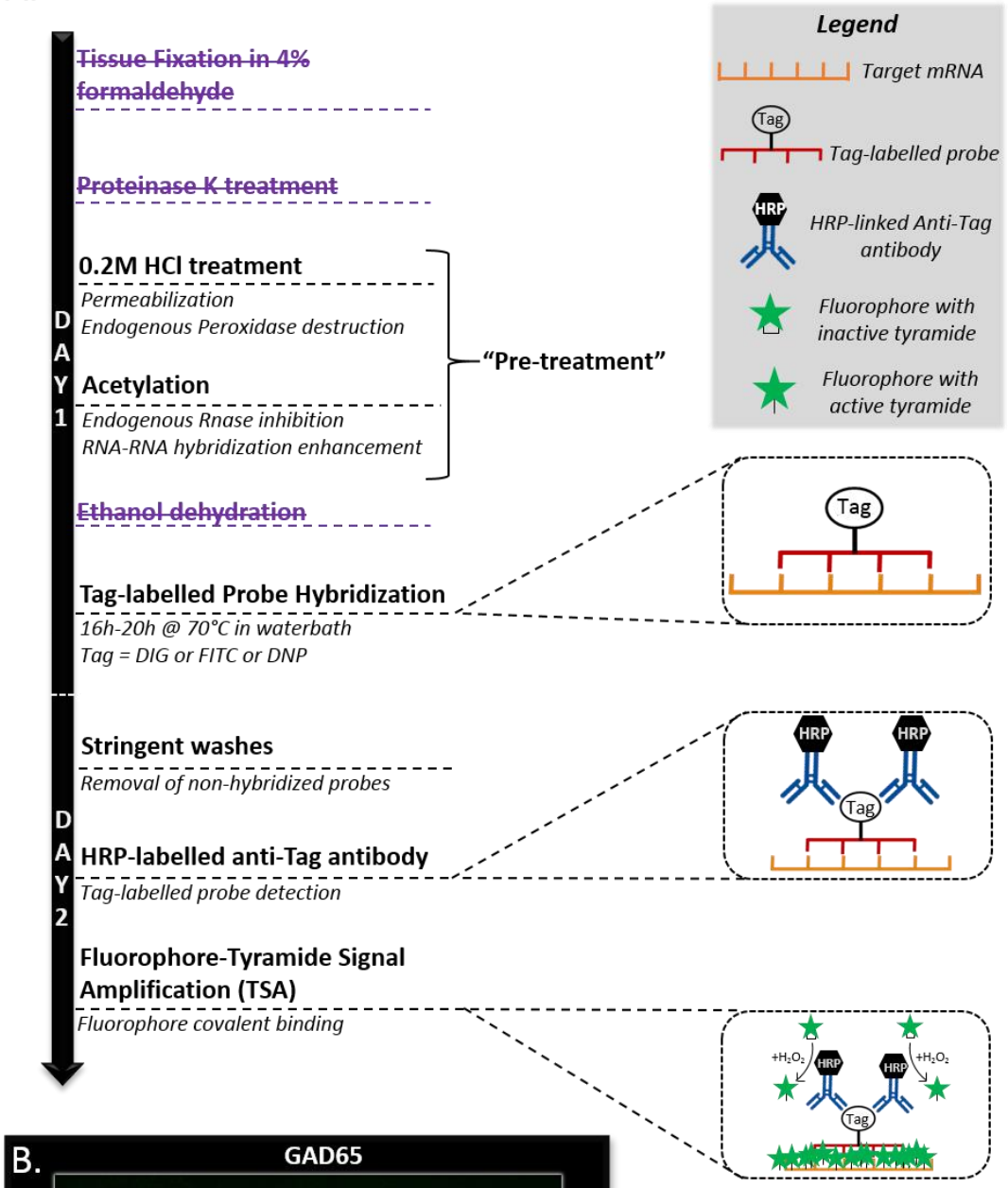

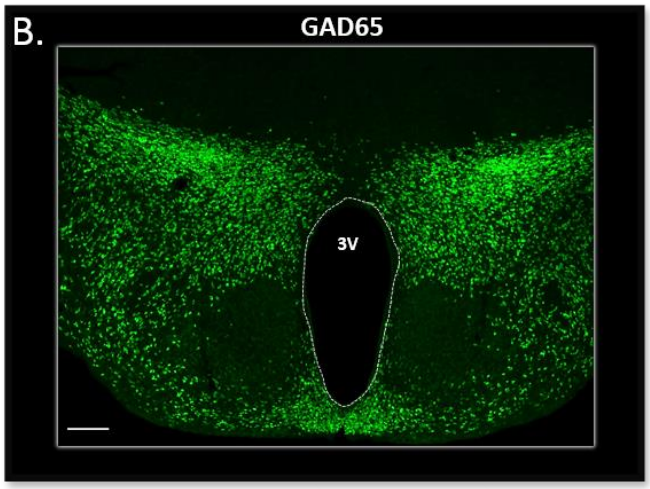

Figure 17: **Single FISH protocol**.
A: Sketched protocol of a single FISH for snap-frozen tissue sections (on slides), adapted for free-floating sections from perfused brains. Removed steps are crossed.
B: Representative image of a single FISH for GAD65 using the protocol described in A.

3V: Third ventricle. Scale bar: 200µm

After the hybridization, successive washing steps are performed at high temperature (65°C) and under increasing stringency conditions, to efficiently remove all “non-hybridized” probes. The detection of hybridized probes is possible thanks to the different "Tags" incorporated in their nucleotidic sequences. Indeed, during probe synthesis, some of the nucleotides used are labeled with a hapten or a fluorophore (hereby generally refered as "Tag", see Figure 17A): typically, some Uridines are labeled with digoxigenin (DIG), fluorescein (FITC) or 2,4-Dinitrophenol (DNP) and randomly incorporated instead of “non-labeled” Uridines. The probes are therefore detected by an anti-Tag antibody (anti-DIG, anti-FITC or anti-DNP) coupled with horseradish peroxidase (HRP). Finally, the fluorescent signal is obtained using a commercial kit relying on the tyramide signal amplification technique (TSA). This system is based on the accumulation of fluorophores (coumarin, fluorescein, cyanine 3 or cyanine 5) coupled with tyramine. Tyramine is normally inactive, but in the presence of peroxidase and H_2O_2, radicals are added to its structure, making it highly reactive and allowing its covalent binding to the nearby tyrosine moieties (Faget and Hnasko 2015). This technique allows a very strong accumulation of fluorophores in the vicinity of the HRP-linked antibody, and as such, at the probe’s location (Figure 17A).

As shown in Figure 17A, three steps of the initial protocol, intended for fresh slices on slides, have been now removed:

- Formaldehyde fixation: this step is no longer necessary, since the sections are already fixed.
- Proteinase K treatment: this step allows, through the digestion of proteins, a better accessibility of the probes. However, this treatment makes the slices so fragile that any handling is destructive for them, making slices mounting almost impossible.
- Ethanol dehydration: since the slices are not on slides, this step is unnecessary.

Figure 17B shows an example of a FISH for GAD65, using this adapted protocol. The GAD65-DIG probe was detected using an anti-DIG-HRP antibody (Sigma, #11207733910; 1/1500) followed by TSA-Cyanine 3 amplification (Akoya Biosciences, #NEL704A001KT). The quality of the signal confirms that the protocol described above allows a satisfactory detection of mRNA under our conditions.

❖ Combination of GAD65 (FISH) with cFos immunostaining

The next step was to combine FISH with cFos immunostaining. The sections on which all the following tests were performed were taken from mouse brains in a "fasting/refeeding" condition, as this paradigm allows a strong expression of cFos in the arcuate nucleus of the hypothalamus (ARC). This consists of a 24 hours fast, after which mice are given back access to food (refeeding). These mice also received an intracerebroventricular (icv) injection of 1µL of dimethylsulfoxide (DMSO) just before refeeding, causing cFos expression in tanycytes. In accordance with the temporal expression of the protein cFos, the mice were sacrificed 90 minutes after the icv injection and refeeding.

We first tried to perform the IHC after doing a FISH for GAD65, using a classic IHC protocol: incubation of the primary antibody overnight at 4°C, then the fluorophore-labeled secondary antibody (Jackson ImmunoResearch, #705-545-003 or #706-545-148; 1/500) for 2 hours the next day (Figure 18A). The first test, with a goat anti-cFos antibody (Santa Cruz, sc-52-G; 1/250) was a failure, as neither the cFos nor the GAD65 staining was visible (Figure 18B, left image). We then tried the same protocol again, using another primary antibody, made in guinea pig (Synaptic Systems, #226004; 1/1000). This time, both GAD65 and cFos signals were present (Figure 18B, central image). However, to ensure that the FISH protocol did not alter the cFos signal, we performed a simple IHC for cFos with the same antibody, but without any FISH step (Figure 18B, right image). This revealed a much larger number of positive nuclei for cFos than with the combination FISH-IHC. This suggests that the FISH protocol significantly reduces cFos labelling, probably by denaturing some of the antigens recognized by the primary antibody.

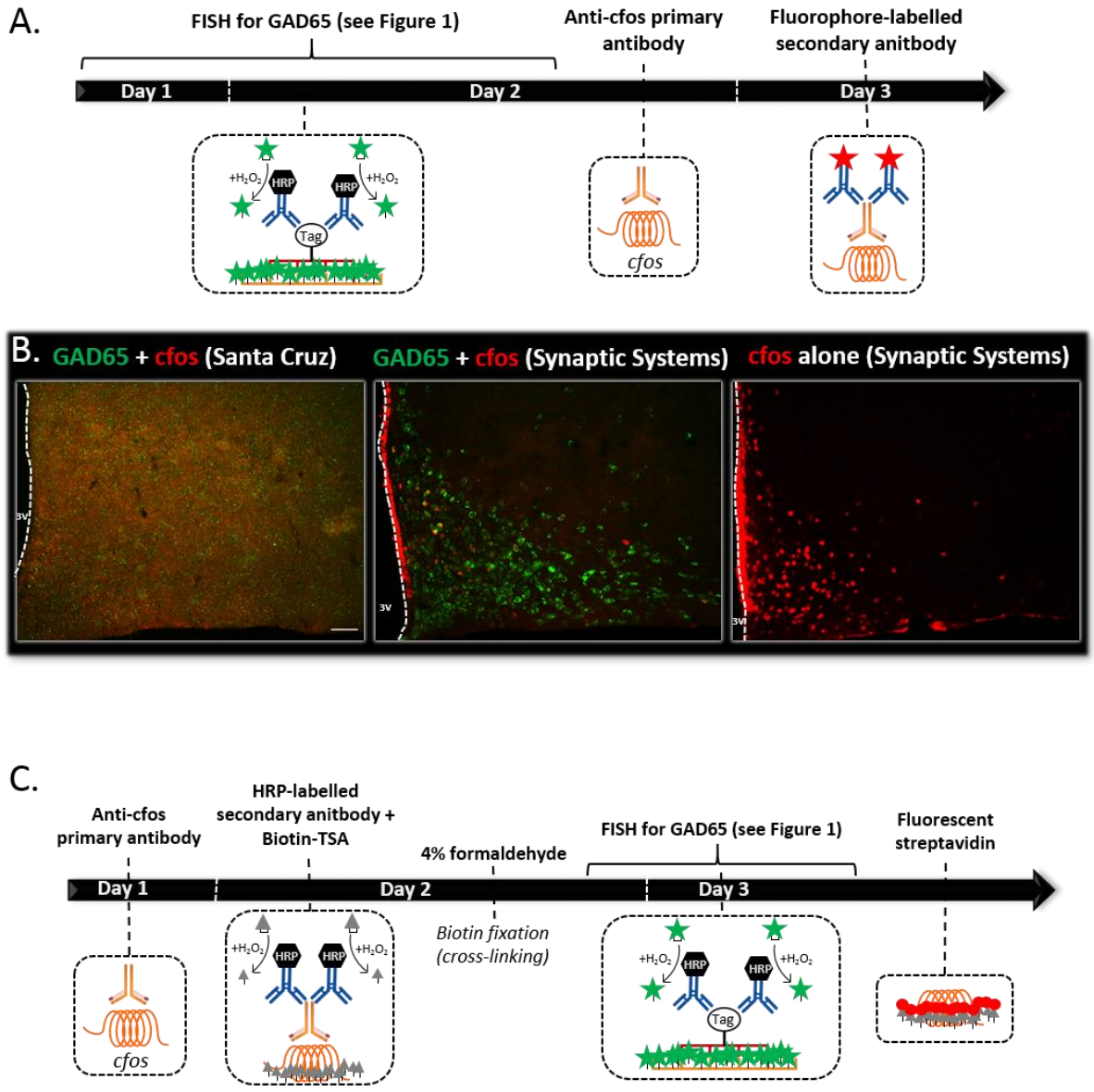

Figure 18: **Combination of FISH with cfos immunostaining**

A: Sketched protocol of a single FISH followed by cfos immunostaining (IHC).

B: Representative images of the protocol in A, using two different anti-cfos antibodies, compared with a single IHC for cfos.

C: Sketched protocol of a single FISH preceded by cfos immunostaining.

D: Representative images of the protocol in C.

3V: Third ventricle. Scale bars: 50µm

Although the previous protocol allowed the co-expression of GAD65 and cFos, the decreased cFos labeling may lead to an underestimation of the positive cell count and thus bias any quantification attempt. In order to overcome this problem, we tried to reverse the order of the FISH and IHC steps, so that the cFos staining is carried out when the antigens are still "intact" and not altered by the FISH. Several attempts (not all of which are shown here) have led to the establishment of the protocol presented in Figure 18C. A "classical" IHC staining such as in Figure 18A is not possible, because the high temperature incubations (hybridization and stringent washings) of the FISH denature fluorophores, which lose their fluorescence. The use of a tertiary antibody after the FISH, directed against the secondary antibody, was unsuccessful. After these failures, we looked for another way to strongly mark cFos before the FISH while maintaining the ability to detect the signal afterwards. As such, we opted for a staining of cFos with TSA-Biotin before the FISH (similar to the system used for probe revelation, but with biotin instead of a fluorophore), revealed with a fluorescent streptavidin after the FISH (Figure 18C). In this test, the primary antibody used is made in rabbit (Cell Signaling, #2250; 1/1000), because we only had an anti-rabbit-HRP available (Cell Signaling #7074; 1/500). TSA-Biotin allows the accumulation of biotin in the vicinity of the anti-rabbit-HRP antibody. After the FISH for GAD65, a fluorescent streptavidin (Vector Laboratories, #SA-5001; 1/500) is incubated for 30 minutes to reveal the biotin accumulated at the beginning of the protocol. The first test performed under these conditions was a failure because of a lack of cFos staining. Thinking that the biotin could have been removed by the stringent washes and high temperature, despite its covalent binding to surrounding proteins, we added a formaldehyde fixing step (4%, 10 minutes) just after the TSA-Biotin. Like this, we hoped to permanently fix the biotins allowing their detection after the FISH. The addition of this step was decisive in the success of the GAD65 and cFos co-staining (Figure 18D). Of note, under these conditions, the cFos staining is similar to the one obtained with a simple IHC, without any visible loss of signal.

❖ Optimization of single FISH for GAD65/67, POMC and vglut2

Now that we can combine FISH and IHC, we undertook to set up all the different FISH staining procedures required for our studies (GAD65, GAD67, vglut2 and POMC), one after the other in successive single FISH experiments. Since the final goal is to mix all the probes together, the "Tags" of each probe must be different, as well as the fluorophores used for their revelation. This is the list of Tags and fluorophores that we used for each probe:

- GAD65 and GAD67: Tag = FITC / Fluorophore = FITC
- POMC : Tag = DNP / Fluorophore = Cyanine 5
- vglut2 : Tag = DIG / Fluorophore = Cyanine 3

In order to simultaneously detect all GABAergic POMC neurons, we aimed at revealing GAD65 and GAD67 together, which is why the GAD65 and GAD67 probes are marked with the same Tag, namely fluorescein (FITC). The single FISH for these two enzymes give a similar result (Figure 19A, left and central images). We then incubated the two probes simultaneously, with a common revelation, using the same fluorophore, with again an excellent outcome (Figure 19A, right image). From now on, “GAD65/67” will refer to a co-staining of GAD65 and GAD67 in the same color as shown here.

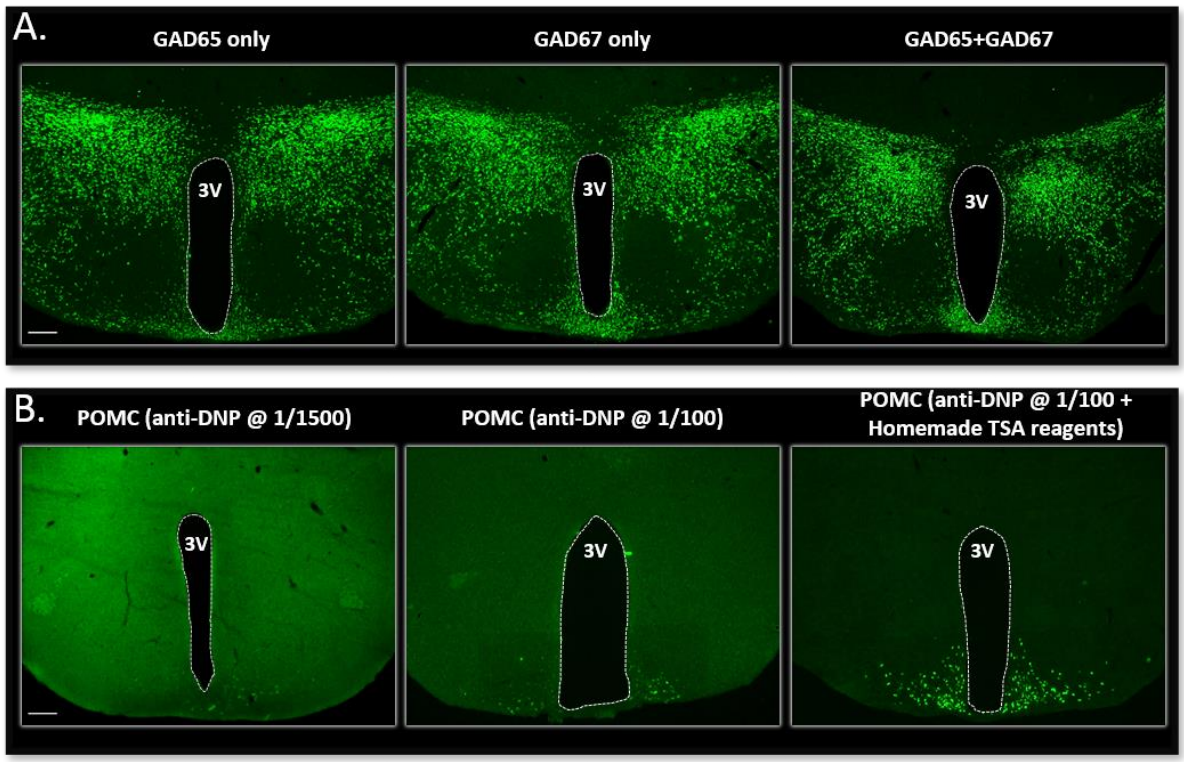

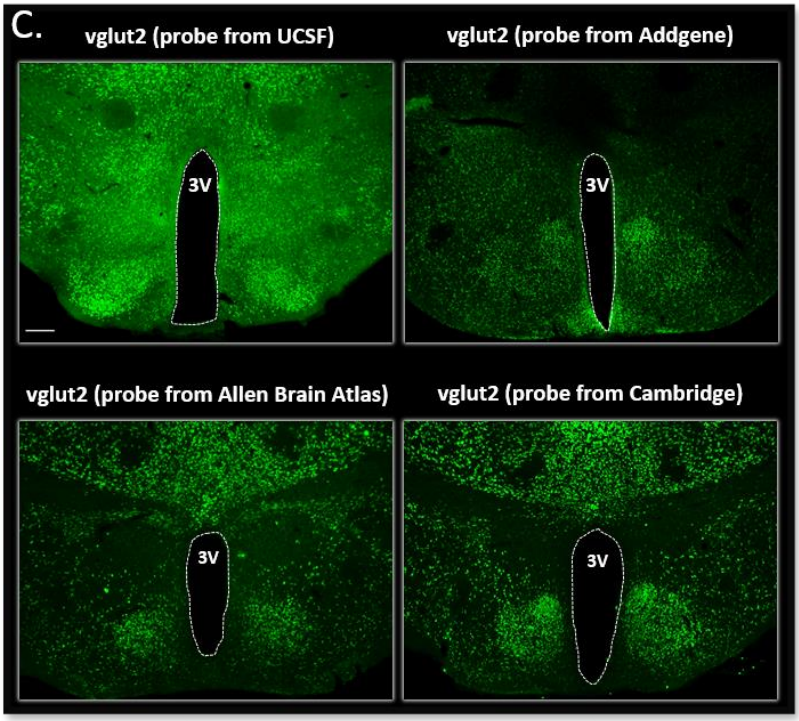

Figure 19: **Optimization of single FISH for GAD65/67, POMC and vglut2**

A: Single and double FISH for GAD65 and GAD67 using FITC-labelled probes. Both GAD65 and GAD67 are developed using the same fluorophore to detect all GABAergic neurons.

B: Optimization of the single FISH for POMC using a DNP-labelled probe, by testing two anti-DNP antibody dilutions and homemade TSA reagents.

C: Optimization of the single FISH for vglut2, using four different DIG-labelled probes.

Scale bars: 200µm

The next probe to be tested is POMC-DNP. The first try was very disappointing, as the POMC signal was barely visible (Figure 19B, left image). We tried to increase the concentration of the probe, but it did not improve the signal. We then increased the concentration of the anti-DNP-HRP antibody (Akoya Biosciences, #FP1129) from 1/1500 to 1/100, resulting in a better sensitivity (Figure 19B, central image), although many weakly stained neurons are still difficult to identify. In order to further increase the intensity of the staining, we decided to prepare the TSA-Cy5 reagents ourselves, in a much highly concentrated version than the one available in the commercial kit used until now (Akoya Biosciences, #SAT705A001EA). For these “bench-made TSA reagents”, we adapted existing protocols, often used for the "whole mount FISH" technique, where whole embryos (or pieces of tissue) undergo a FISH staining (Hopman, Ramaekers *et al.* 1998, Lauter, Söll *et al.* 2011) (see Materials and Methods for the preparation of the TSA-Cy5 and the amplification buffer). The use of these bench-made reagents combined with the high concentration of the anti-DNP-HRP antibody (1/100) significantly increased the intensity of the POMC signal and the signal-to-noise ratio (Figure 19B, right image).

The last staining to be developed was vglut2. We already had a vglut2 probe available from Robert Edwards' laboratory at the University of California, San Francisco (UCSF). Unfortunately, the resulting signal was not very clear, with an unsatisfactory signal-to-noise ratio (Figure 19C, top left image). Attempts to optimize the concentration of the probe, the anti-DIG-HRP antibody (similar to the approach used to optimize POMC staining) or the use of homemade TSA reagents were not successful in improving this signal. We then tested several probes from different sources. One of them, shared by Jeffrey Macklis' laboratory (Harvard Stem Cell Institute) on Addgene (plasmid #45639), gave an unexpected signal: the ventromedial nucleus of the hypothalamus (VMN) as well as the thalamus, although known as strong vglut2 expressing regions (Moechars, Weston *et al.* 2006) are not stained here (Figure 19C, top right image). We therefore abandoned the use of this probe. The last two probes tested came either from available ISH data from the Allen Brain Atlas (probe #RP_050921_01_E03) or from Dr. Gilles Yeo’s laboratory in Cambridge. Between these two probes, the staining obtained is very similar and of much better

quality than for previous ones: the VMN is clearly visible, cells in the thalamus are strongly stained and the signal-to-noise ratio is very satisfactory (Figure 19C, bottom images). Since the Cambridge probe gives a stronger signal than the Allen Brain Atlas probe, we chose this one for the next steps (Figure 19C, bottom right image).

❖ Combination of POMC, vglut2, GAD65/67 (FISH) and cFos (IHC)

After having developed separately all the single FISH protocols for our studies, we started to combine them, two by two. For any double- (or triple-)FISH staining, the probes are detected and revealed sequentially because the revelation is always based on a peroxidase activity. Thus, after incubation of the first anti-Tag-HRP antibody and its revelation by TSA, the sections undergo a treatment of 3% H_2O_2 (30 minutes) then 0.2M HCl (20 minutes) (Liu, Amin *et al.* 2006), in order to quench the HRPs present on the first anti-Tag-HRP so that they do not interfere with the future TSA revelation of the following probes.

The tests performed show that the double-FISH for vglut2+POMC and GAD65/67+POMC are as good as the single FISH, but the double-FISH GAD65/67+vglut2 is a failure (Figure 20A). In an attempt to solve this problem, we modified the composition of the hybridization solution (hybmix), as it has been shown that an increase in the concentration of dextran sulfate (DS) and 1,4-dithiothreitol (DTT), two of the components of the hybmix, can improve the sensitivity of radioisotopically-labeled ISH probes (Hrabovszky and Petersen 2002). Moreover, it has been reported that replacing deionized formamide with 4M urea also improves the signal-to-noise ratio in a whole-mount ISH setting, as well as being less toxic for the experimenters (Sinigaglia, Thiel *et al.* 2017). Therefore, we designed a series of different hybmix recipes, with two concentrations of DS and DTT and the replacement of deionized formamide by urea (U5378, Sigma-Aldrich, Saint-Quentin Fallavier, France) to test whether any of these recipes would be suitable for the GAD65/67+vglut2 double-FISH (Table 6):

	Deionized Formamide	Urea	Dextran Sulfate	DTT	Tris/HCl	EDTA	NaCl	Denhardt's solution	tRNA	Salmon Sperm
Original Hybmix	**50%**	**0M**	**10%**	**200mM**	**20mM**	**5mM**	**300mM**	**1X**	**0.5mg/mL**	**0.2mg/mL**
Hybmix 1	**0%**	**4M**	10%	200mM	20mM	5mM	300mM	1X	0.5mg/mL	0.2mg/mL
Hybmix 2	50%	0M	**30%**	**1M**	20mM	5mM	300mM	1X	0.5mg/mL	0.2mg/mL
Hybmix 3	**0%**	**4M**	**30%**	**1M**	20mM	5mM	300mM	1X	0.5mg/mL	0.2mg/mL
Hybmix 4	**0%**	**4M**	10%	**1M**	20mM	5mM	300mM	1X	0.5mg/mL	0.2mg/mL
Hybmix 5	50%	0M	10%	**1M**	20mM	5mM	300mM	1X	0.5mg/mL	0.2mg/mL
Hybmix 6	50%	0M	**30%**	200mM	20mM	5mM	300mM	1X	0.5mg/mL	0.2mg/mL
Hybmix 7	**0%**	**4M**	**30%**	200mM	20mM	5mM	300mM	1X	0.5mg/mL	0.2mg/mL

Table 6 : List of the different hybmix recipes tested in Figure 20B.

Of the seven hybmix recipes tested, only hybmix 5 provided a satisfactory co-staining of GAD65/67 and vglut2 (Figure 20B, central image of second line). This recipe is identical to our original hybmix recipe, but with an increased concentration of DTT, from 200mM to 1M.

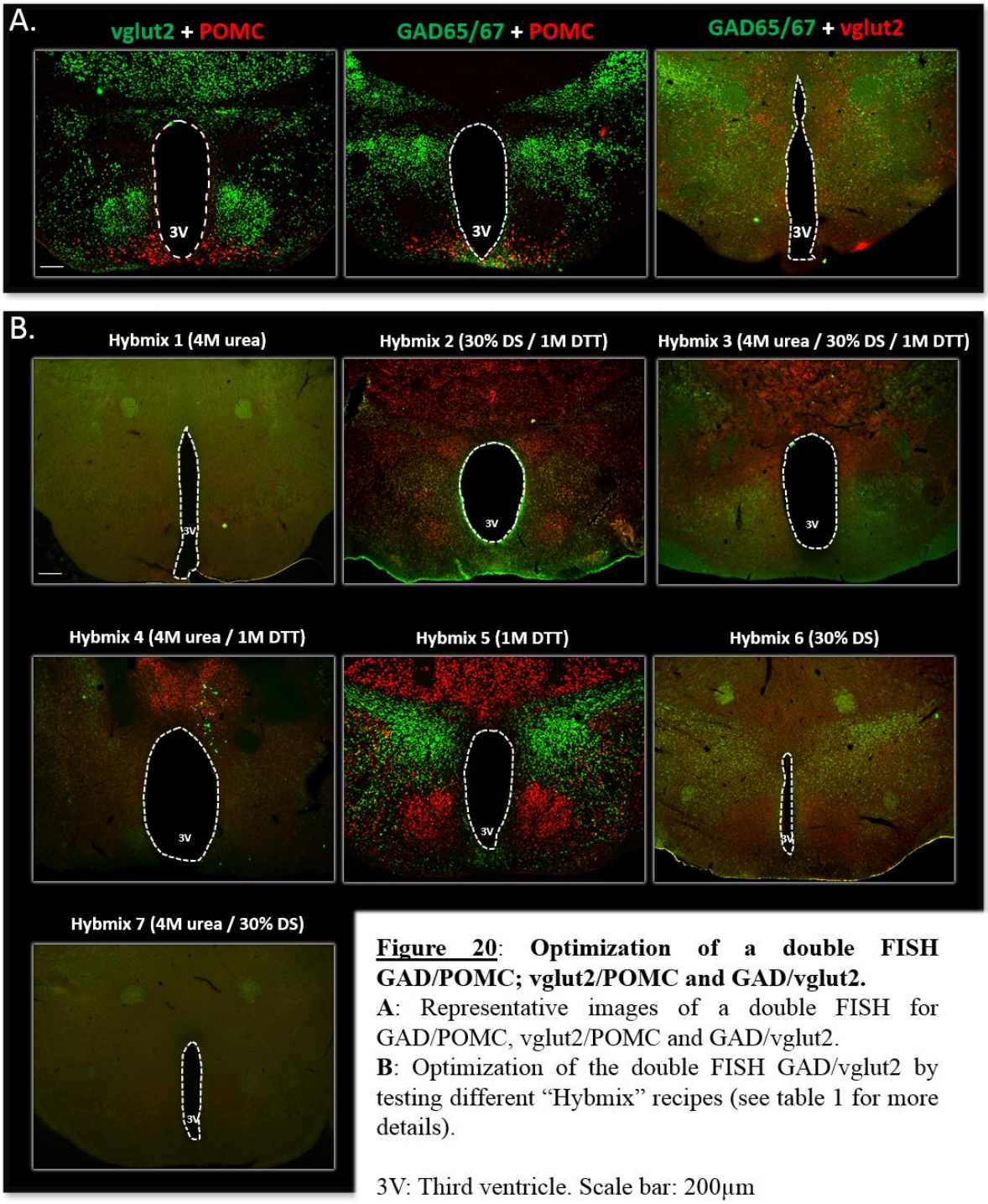

Figure 20: **Optimization of a double FISH GAD/POMC; vglut2/POMC and GAD/vglut2.**
A: Representative images of a double FISH for GAD/POMC, vglut2/POMC and GAD/vglut2.
B: Optimization of the double FISH GAD/vglut2 by testing different "Hybmix" recipes (see table 1 for more details).

3V: Third ventricle. Scale bar: 200µm

Next, the triple-FISH for GAD65/67+vglut+POMC was attempted, in combination with the cFos IHC. Since fluorophores emitting in the green, red and far red spectra are already used for GAD65/67, vglut2 and POMC respectively, the cFos staining had to be done using an AMCA-labeled streptavidin, since it's a fluorophore emitting in the blue spectrum. Unfortunately, the signal obtained for cFos under these conditions was too weak to be easily detected, probably because in this part of the light spectrum, the autofluorescence of the tissue is much higher. It was therefore necessary to find a way to further amplify the cFos staining after biotin detection. To do so, instead of using a fluorescent streptavidin, we performed an "avidine-biotin amplification", using a commercial kit (Vector laboratories, #PK-6100). This technique allows an accumulation of avidin-biotin complexes that binds to accessible biotins in the tissue (i.e. at the level of cFos in our situation). In these complexes, biotins are also coupled with HRP, so that a TSA-coumarin revelation can be performed. The amplification is such that it overcomes autofluorescence and achieves a signal-to-noise ratio sufficient to detect the cFos signal without difficulty.

Finally, all the steps described above were combined, shaping the final protocol: IHC for cFos, TSA-biotin revelation, formaldehyde fixation, pre-treatment, hybridization of vglut2-DIG, GAD65-FITC, GAD67-FITC and POMC-DNP probes at 70°C, stringent washes, detection of the different probes with anti-[DIG/FITC/DNP]-HRP antibodies, revelation with [Cy3/FITC/Homemade Cy5]-TSA, detection of biotin by avidin-biotin complexes and final revelation of cFos with TSA-coumarin (Figure 21A). The result is more than acceptable for all the markers, enabling us to identify which of the POMC subpopulations are cFos positive, on a single section (Figure 21B).

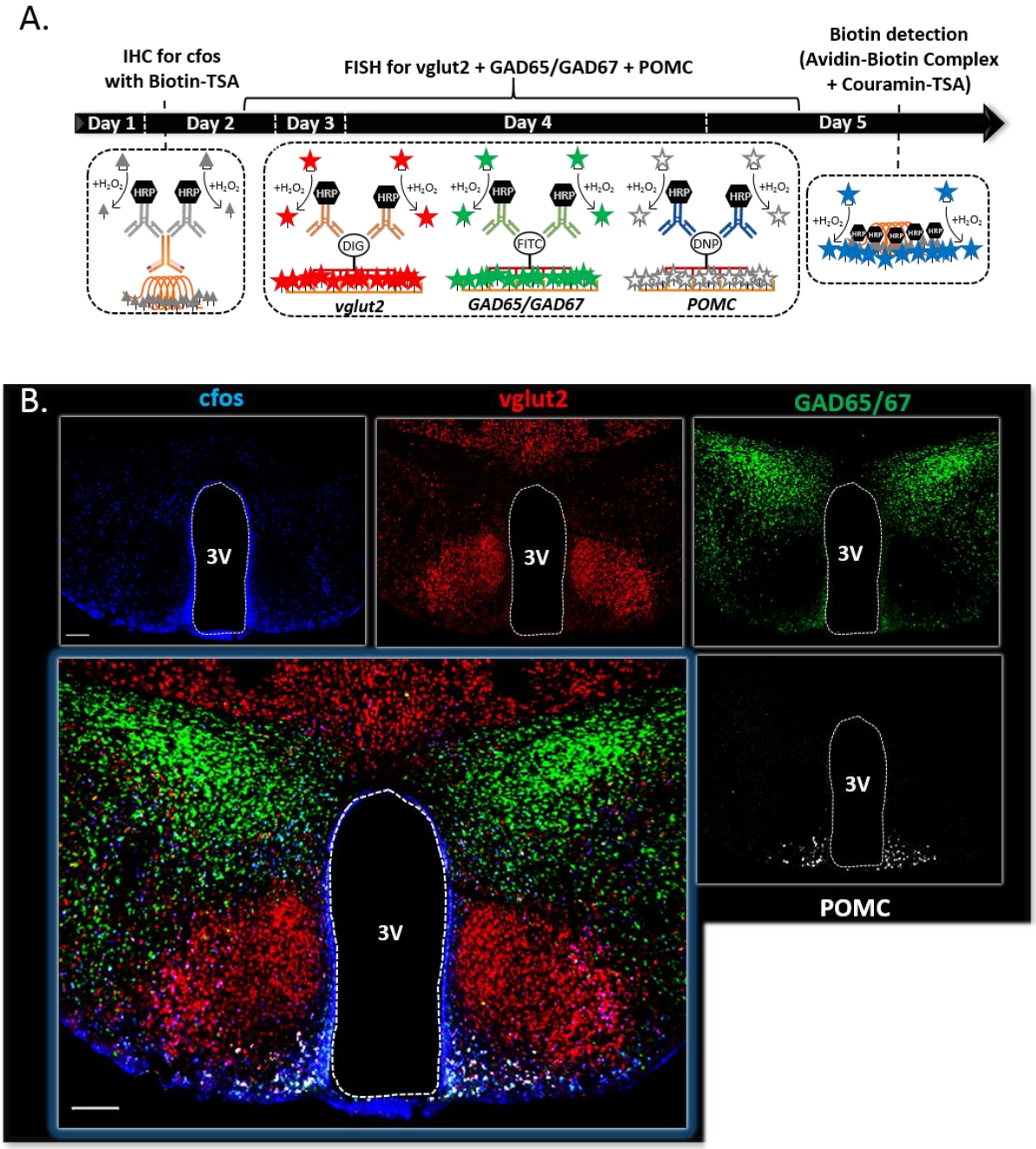

Figure 21: **Quadruple staining for POMC, GAD65/67, vglut2 (FISH) and cfos (IHC)**

A: Sketched protocol for the quadruple staining.

B: Representative images of the protocol in A.

3V: Third ventricle. Scale bar: 200µm

Chapter 2

Acute exposure to high fat diet preferentially activates POMC GABAergic neurons

In the chapter 4 of the introduction, I described the multiple alterations that POMC neurons can be subjected to, because of high-fat diet (HFD) exposure. However, the influence of the glutamatergic or GABAergic phenotypes has never been studied in this context. Taking advantage of the FISH/IHC technique that we have developed and that is described in the previous chapter, we aimed at identifying the specific subpopulations of POMC neurons that respond to HFD, if any. Results are expressed by mean ±SEM. Exact p-values and statistical analysis are reported in the figures. A p-value below 0.05 denotes statistical significance.

❖ Mice prefer high-fat diet over chow diet

First, we assessed mouse preference for HFD over chow diet (CD) by using polyfeeding cages (Imetronic, see Materials and Methods). Briefly, 8 C57Bl/6J mice aged 10 weeks were singly housed into polyfeeding cages, with two accessible food containers filled with CD and located at opposite sides of the cages. During the 1-week habituation period, mice preference for one or the other food container was recorded. Then, in the least-preferred one, CD was replaced by HFD in the middle of the light phase, for 2 hours only (Figure 22A). CD and HFD intake were measured at the end of the 2 hours. Of note, over the 2 days preceding the experiment, mice were exposed to a very small amount of HFD disposed in the cage, in order to avoid neophobia during the preference test.

A clear preference for HFD over CD was observed, with a 0.88g ±0.08g of HFD intake at 2h versus 0.08g ±0.05g of CD intake ($p<0.001$, Figure 22B). The difference was of course even more pronounced when considering the caloric intake, since HFD is more energetically dense (5.24 kcal/g) than CD (3.2 kcal/g) ($p<0.0001$, Figure 22C). Indeed, mice ate 4.6kcal ±0.22kcal of HFD, which is the equivalent of 1.4g of CD, i.e. roughly a third of their daily energy intake. This was done in the middle of the light phase, a period in which mice are inactive and usually do not engage in prolonged food seeking/intake. When looking at the data mouse per mouse, we realize that over 8 mice, 3 ate only HFD, 4 ate more than 85% of HFD and only one had a more balanced intake with approximately 60% of HFD vs 40% of CD (Figure 22D).

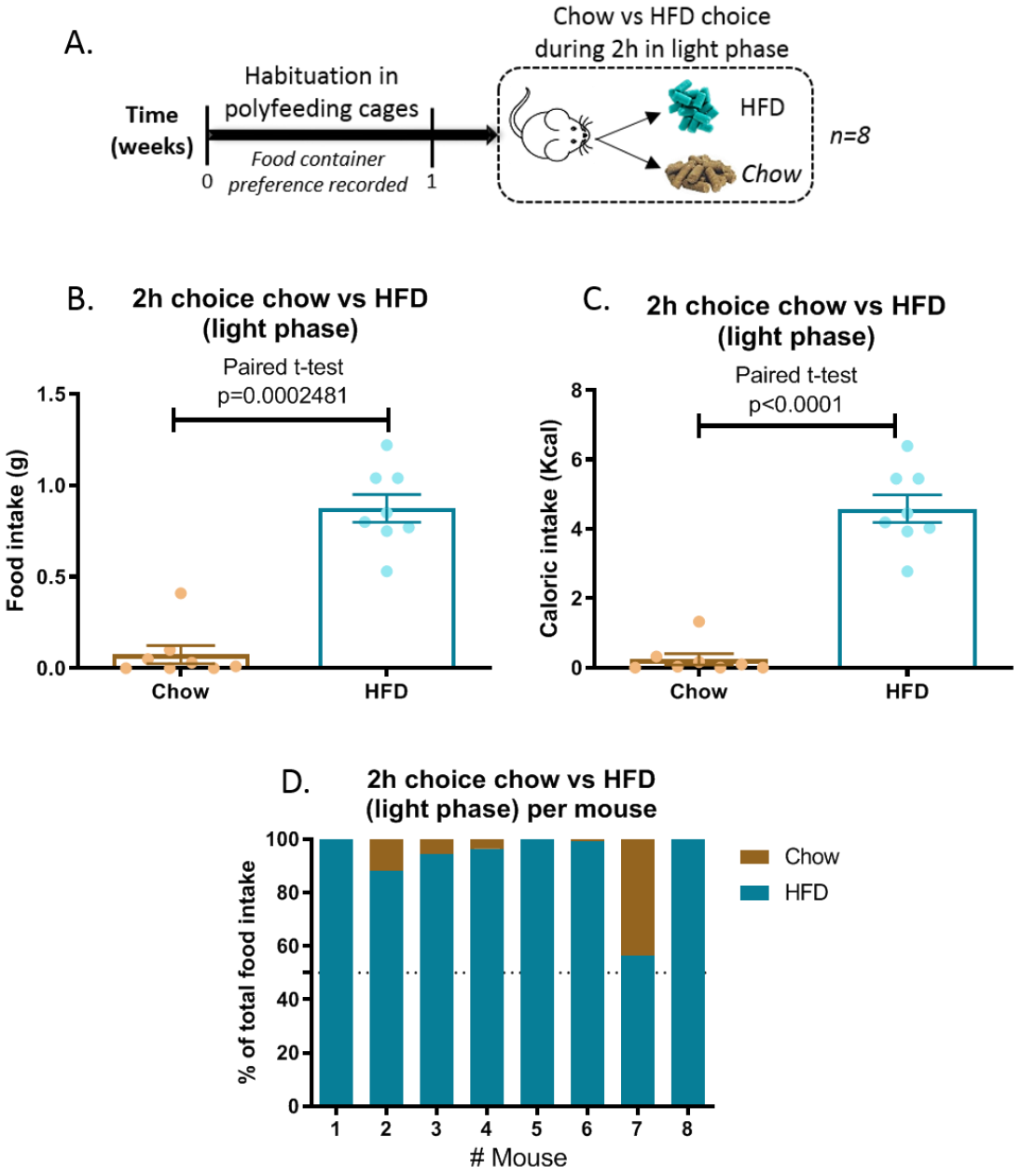

Figure 22: Mice prefer HFD over chow diet in the light phase
A: Sketched protocol for the food preference test. After 1 week of habituation in polyfeeding cages in which 8 C57Bl/6J mice are given access ad libitum to chow diet in two different food hoppers, they are given access to HFD for 2 hours in the least-explored food hopper, in the middle of the light phase.
B: Mean food intake of chow and HFD at the end of the 2 hour choice test.
C: Same as B, but with caloric intake.
D: Food preference for each mouse.

Taken together, these results show that mice prefer the HFD over CD and that the HFD strongly promotes feeding behaviour during the light phase, which is directed almost exclusively toward the consumption of this palatable diet.

❖ Acute HFD exposure during 24h causes hyperphagia and body weight gain

We then designed another experiment with a larger cohort of animals to assess body weight change and food intake after a 24h-exposure to HFD followed by a return to CD. 20 chow-fed C57Bl/6J mice aged 7 weeks were singly housed in our animal facility for 7 days before the start of the experiment and handled on a daily basis. They were then divided into two body weight-matched groups of 10 mice each: “Chow” vs “HFD”. In the HFD group, the food was switched from CD to HFD five hours before the onset of the dark phase, while the Chow group was still fed with CD. Food intake was measured at 1h, 2h and 24h after the switch. Body weights were measured before and 24h after the switch (Figure 23A). This experiment was repeated once per week during 4 consecutive weeks. The results presented below and exposed in Figure 23 and Figure 24 are the mean of these 4 experiments.

HFD-fed mice were hyperphagic at 1h (0.57g ±0.02g vs 0.05g ±0.01g, $p<0.0001$) and 2h (0.74g ±0.02g vs 0.1g ±0.01g, $p<0.0001$) compared with CD-fed mice, an effect that is still visible at 24h (5.12g ±0.2g vs 4.37g ±0.15g, $p=0.02$, Figure 23B). Consistently, their caloric intake was largely enhanced over these 24h of HFD exposure ($p<0.0001$, Figure 23C). HFD-fed mice also increased their body weight by 1.3g ±0.1g and their food efficiency (body weight change divided by caloric intake) was also much larger than in CD-fed mice, suggesting a strong recruitment of biological systems to promote body weight gain ($p<0.0001$, Figure 23D and Figure 23E, respectively).

In line with the food preference experiment, these results highlight the fact that mice fed with HFD but not CD engage in feeding behaviour during the light phase (1h and 2h food intake). Overall, they also eat a higher amount of food, corresponding to a large caloric surplus, which translates into a 24h body weight gain of more than 1g.

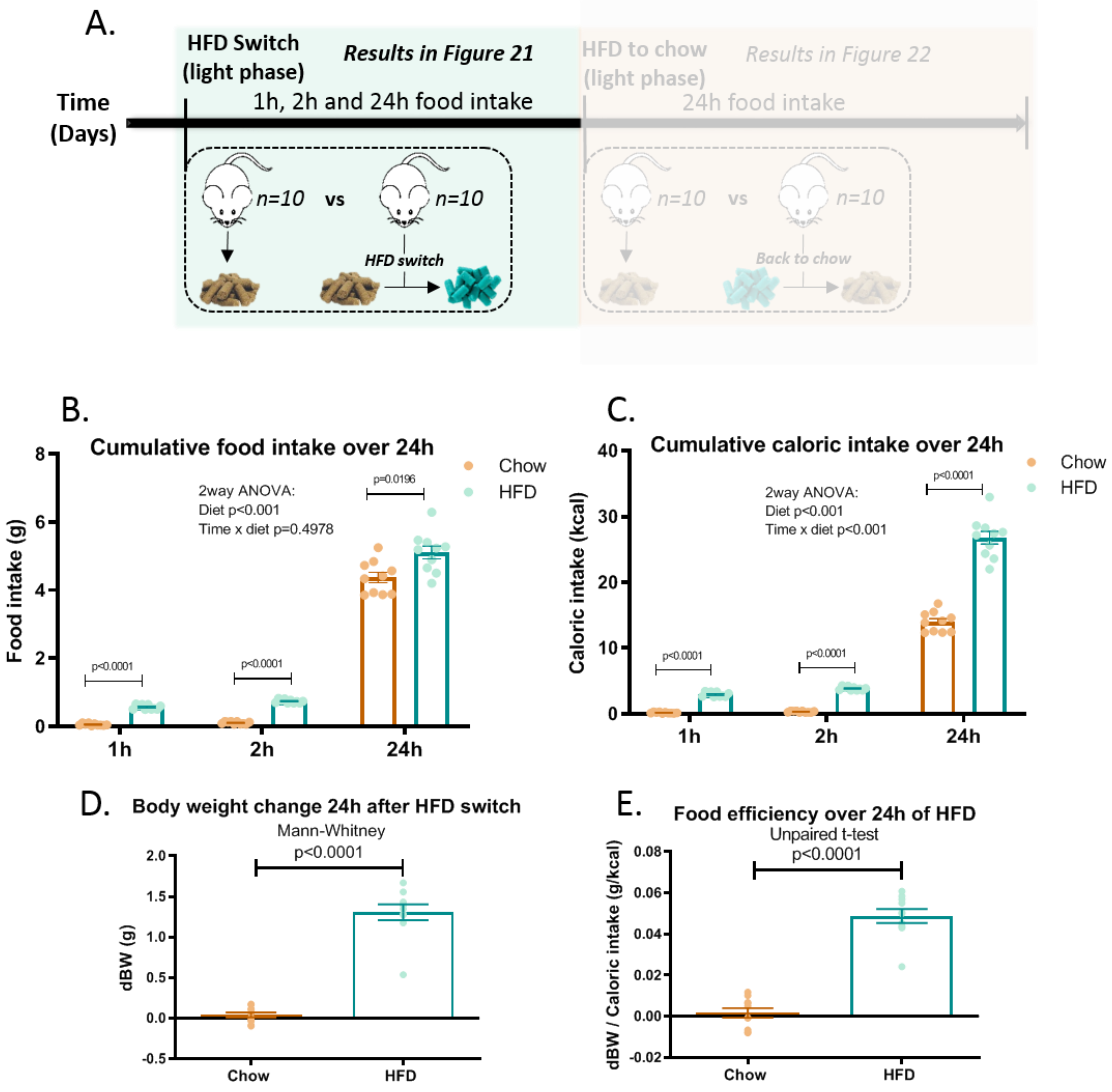

Figure 23: Mice are hyperphagic when switched to HFD during 24h.
A: Sketched protocol for the 24h HFD switch. Five hours before the onset of the dark phase, 10 C57Bl/6J mice are switched to HFD, during 24h. Their food intake is measured at 1h and 2h after the switch. Body weight and food intake are measured again the next day. They are then switched back to chow. Food intake and body weight are measured again 24h after (results shown in Figure 22). These mice are compared with 10 control chow-fed mice during the same period.
B: Mean food intake of chow and HFD 1h, 2h and 24h after the HFD switch.
C: Same as B, but with caloric intake.
D: Body weight change 24h after the HFD switch
E: Food efficiency over the 24h access to HFD

❖ The switch from HFD back to CD induces a rebound effect, with hypophagia and body weight loss

After the 24h exposure to HFD, mice in the HFD group were switched back to CD ("HFD-to-chow" group) while mice in the Chow group were still CD-fed. Body weight and food intake were again measured the next day (Figure 24A). As expected, we observed a rebound effect at 24h in food intake, body weight change and food efficiency in the HFD-to-chow mice. Indeed, they were hypophagic (1.46g ±0.15g vs 4.00g ±0.13g, $p<0.0001$, Figure 24B), resulting in a decreased 24h caloric intake ($p<0.0001$, Figure 24C). In addition, a 24h body weight loss of 1g ±0.15g was observed ($p<0.0001$, Figure 24D), as well as a strong reduction of the food efficiency ($p<0.0001$, Figure 24E), suggesting the engagement of endostatic mechanisms to drive the body weight down in response to the caloric overload of the previous day.

Altogether, these results suggest that acute exposure to HFD recruits exostatic mechanisms, which override homeostatic regulations in order to promote hyperphagia, caloric overload and subsequent body weight gain. When the CD is returned, endostatic mechanisms kick in order to restore initial body weight, by promoting hypophagia, caloric restriction and body weight loss.

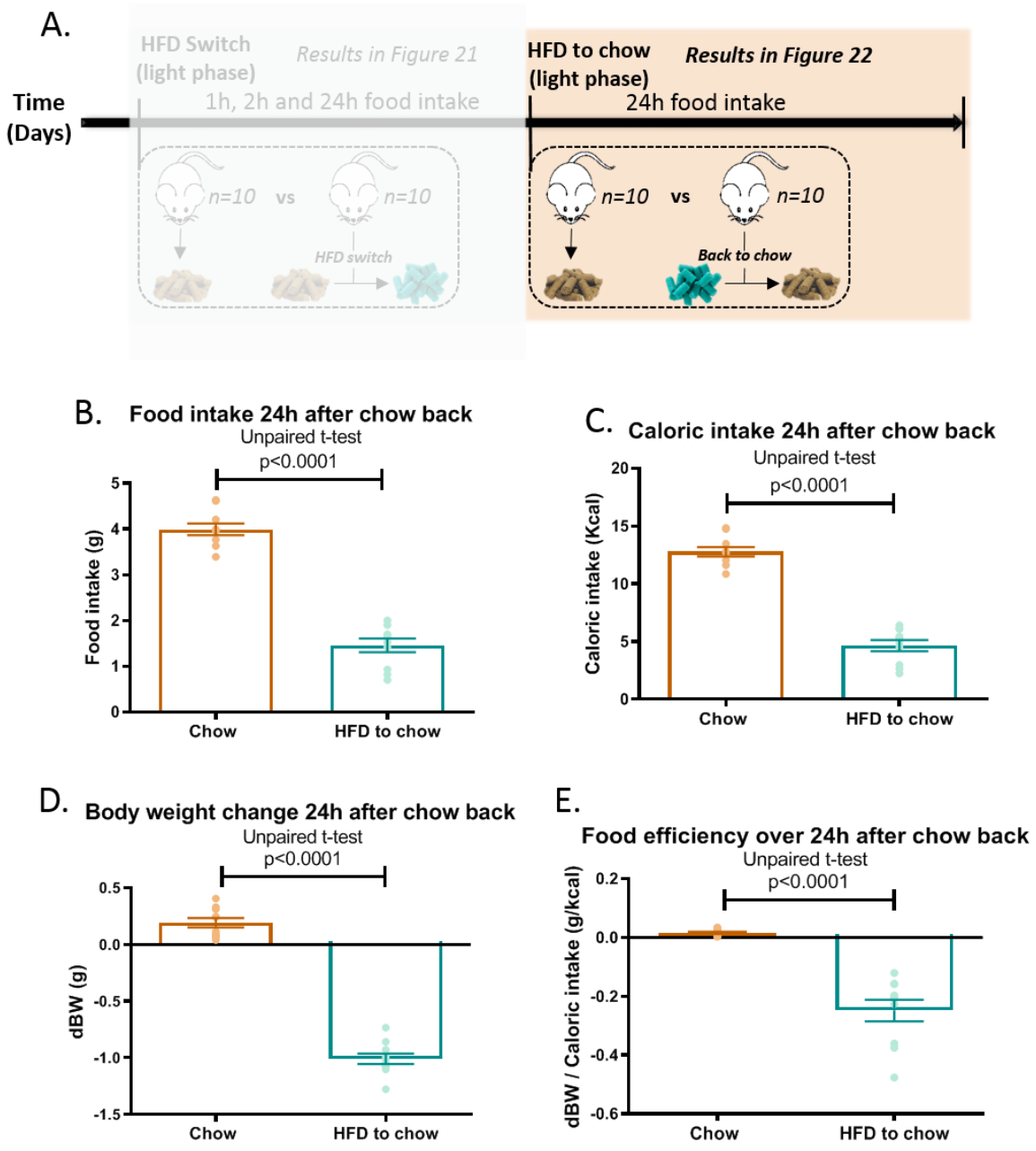

Figure 24: Rebound effect after the return to chow diet

A: The protocol is the same as in Figure 21. The results shown here are those when mice are switched from HFD back to chow diet.

B: Mean chow intake 24h after mice are switched from HFD back to chow.

C: Same as B, but with caloric intake.

D: Body weight change 24h after the HFD to chow switch.

E: Food efficiency over the 24h after the HFD to chow switch.

❖ Acute exposure to HFD in the light phase activates POMC neurons

In an attempt to unravel the biological substrates underlying these effects, we then explored the response of POMC neurons to acute HFD exposure, using the same experimental paradigm as before. Mice from the HFD group were switched to HFD 5 hours before the onset of the dark phase, while mice in the Chow group remained CD-fed. Two hours after the switch, half of each group was sacrificed by transcardial perfusion of 4% formaldehyde (Figure 25A) and their brains processed for immunohistochemical analysis (see Materials and Methods). To assess activation of POMC neurons in response to the diet, POMC/cFos co-immunostaining was performed on 3 slices per animal, containing the rostral ARC (≈ -1.06mm to Bregma), mid ARC (≈ -1.58mm to Bregma) and caudal ARC (≈ -2.06mm to Bregma). Of note, one mouse brain of each group was unusable because of a technical issue, resulting in 4 brains per group.

First, we verified that HFD-fed mice were still hyperphagic at 2h, before the sacrifice, compared to CD-fed mice (1.08g ±0.13g vs 0.10g ±0.02g, p=0.03, Figure 25B). The co-staining for POMC/cFos (Figure 25C) revealed that after HFD switch, 36% ±5% POMC neurons are activated in the HFD group, versus 6% ±1% in the Chow group (Figure 25D). To better characterize these POMC neurons, we looked at their rostro-caudal distribution in Chow and HFD groups, separately. However, there was no significant difference in the % of POMC-cFos+ cells between the rostral-, mid- and caudal ARC for either groups (Figure 25E and Figure 25F), although it seems that rostral ARCs are slightly enriched in POMC-cFos+ compared to the other ARC levels.

Thus, these results show that an acute HFD exposure in the light phase is able to recruit more than one third of POMC neurons.

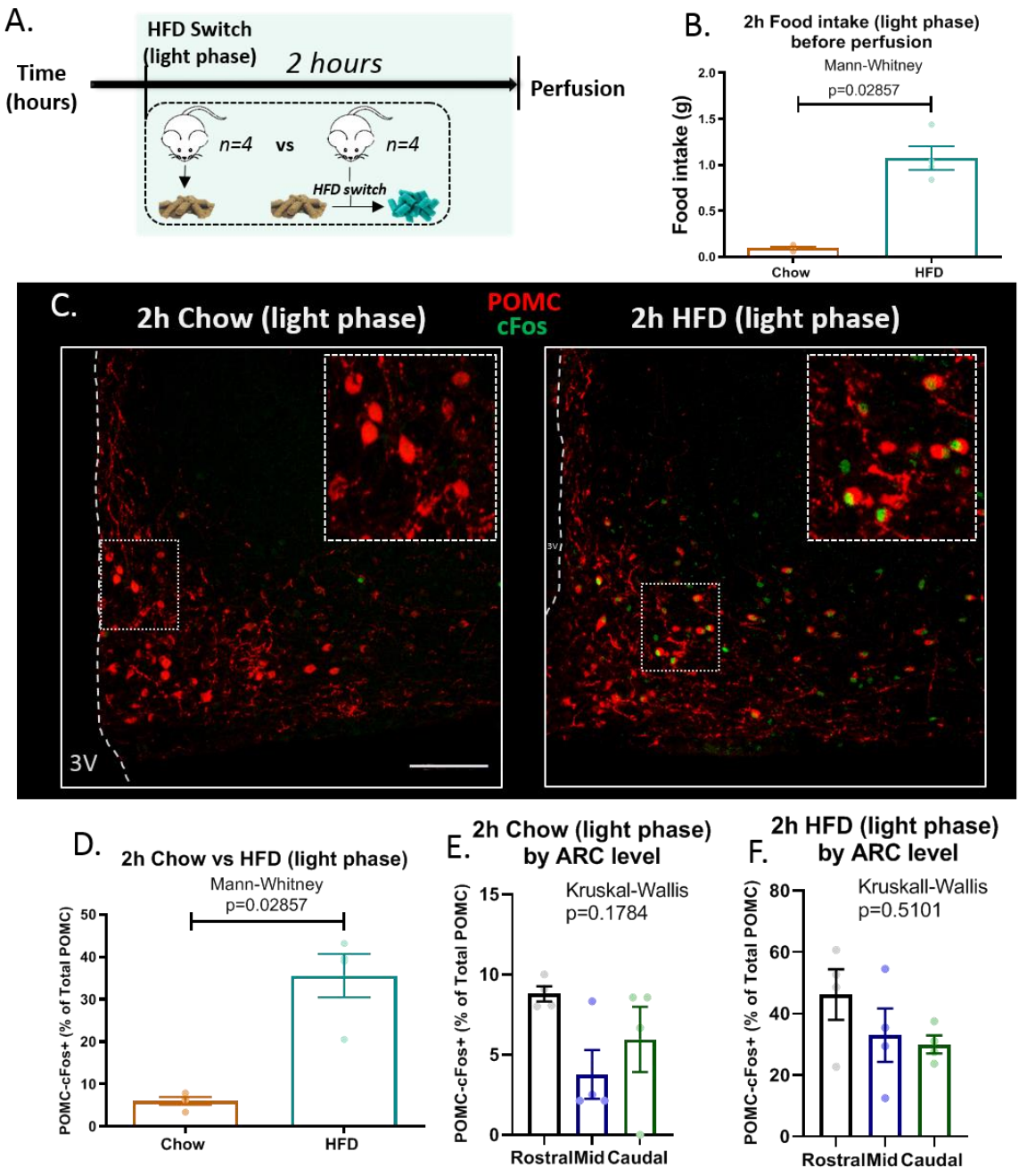

Figure 25: Acute exposition of HFD in the light phase activates POMC neurons
A: Sketched protocol: 4 mice are switched to HFD 5 hours before the onset of the dark phase, compared with 4 chow-fed mice. 2 hours after the HFD switch, they are sacrificed by transcardial perfusion.
B: Food intake 2 hours after the HFD switch, i.e. just before the mice were sacrificed.
C: Representative images POMC/cfos coexpression by IHC. 3V: third ventricle.
Scale bar = 100µm. **D:** Quantification of the POMC/cfos coexpression. **E:** Same as C, represented by the level of the ARC (rostral, mid or caudal) for the chow-fed group.
F: Same as D for the HFD group.

❖ POMC neurons are also activated after the switch from HFD back to chow

Next, we wanted to know how POMC neurons would respond to the switch from HFD back to CD. Thus, the remaining half of the HFD group was switched back to chow just before the onset of the dark phase, in order to compare them with CD-fed mice when they are physiologically engaged to eat (classically, at the beginning of the dark phase). Two hours after the diet switch (and onset of the dark phase), mice were sacrificed by transcardial perfusion and their brains processed for POMC/cFos co-immunostaining as mentioned earlier (Figure 26A).

As expected, when food intake was measured just before the sacrifice, HFD-to-chow mice were hypophagic relative to Chow mice, with a difference that was almost statistically significant (0.35g ±0.08g vs 0.65g ±0.08g, p=0.057, Figure 26B). The POMC/cFos co-staining (Figure 26C) showed an equivalent proportion of activated POMC neurons between Chow group (42% ±3%) and HFD-to-chow group (37% ±3%) (Figure 26D). However, as seen previously with the acute HFD switch, no significant difference were found in the rostro-caudal distribution of these activated POMC neurons, although the same trend towards rostral ARC enrichment was observed again (Figure 26E and Figure 26F).

Thus, the switch from HFD back to chow is also associated with POMC neurons activation, in the same proportion as chow-fed mice who engage in normal feeding behaviour. However, are these the same neurons or not?

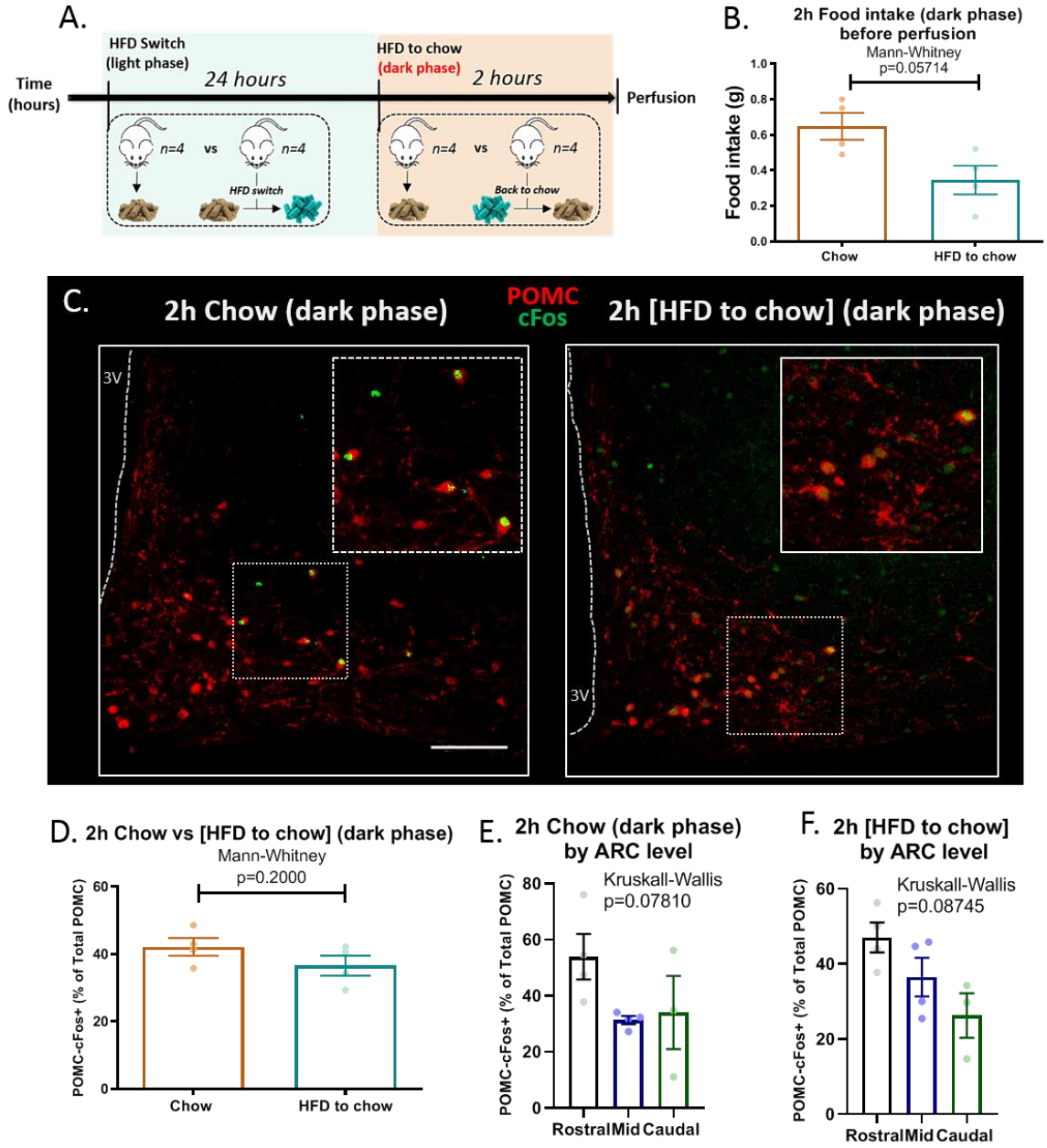

Figure 26: HFD to chow diet switch at the onset of the dark phase activates POMC neurons
A: Sketched protocol: 4 mice are switched to HFD 5 hours before the onset of the dark phase. The next day, they are switched back to chow diet at the onset of the dark phase. 2 hours later, they are sacrificed by perfusion. They are compared with 4 chow-fed mice.
B: Food intake 2 hours after the onset of the dark phase, i.e. just before the mice were sacrificed.
C: Representative images POMC/cfos coexpression by IHC. 3V: third ventricle.
Scale bar = 100µm **D:** Quantification of the POMC/cfos coexpression. **E:** Same as C, represented by the level of the ARC (rostral, mid or caudal) for the chow-fed group sacrificed in the dark phase. **F:** Same as D for the [HFD to chow] switch group.

❖ GABAergic POMC neurons are preferentially recruited by a 2h HFD switch during the light phase

So far, we demonstrated an activation of POMC neurons under different conditions (2h HFD exposure, HFD exposure followed by switch to CD or CD in dark phase). To go further, we sought to identify the GABAergic and/or glutamatergic nature of these activated POMC neurons by using the simultaneous detection of GAD65, GAD67 and vglut2 mRNAs combined with cFos immunostaining that we developed previously. Unfortunately, this experiment gave a suboptimal result for the Chow (dark phase) and HFD-to-chow groups, so that signal quantification was nearly impossible for GAD65/67 and vglut2. Therefore, we will only present here the results for the acute HFD switch during the light phase.

First, thanks to the GAD65/67, vglut2, POMC, cFos co-staining (Figure 27A), we assessed the global repartition of the different subpopulations of POMC neurons relative to their neurotransmitter phenotype. We were able to distinguish pure GABAergic (POMC-GAD+ = POMC-GABA) and pure glutamatergic (POMC-vglut2+ = POMC-Glut) POMC neurons as well as neurons that co-express both markers (POMC-GAD/vglut2+ = POMC-Glut/GABA). Of note, for some cells, we were unable to detect GAD65/67 neither vglut2 and qualified these neurons as “POMC only”. These subpopulations were unequally represented, with a higher proportion of POMC-GABA (37% ±2%) and POMC-Glut/GABA (29% ±0.7%) compared to POMC-Glut (14% ±1%) or POMC only (19% ±0.5%) (Figure 27B).

Then, we focused on activated POMC neurons by looking at the repartition of the different subpopulations within POMC-cFos+ neurons. We found that the majority of activated POMC neurons under acute exposure to HFD have GABAergic (46% ±4%) or mixed Glut/GABA (33.5% ±3%) phenotypes. Glutamatergic POMC neurons only accounted for 9.5% ±2% of activated POMC neurons, similarly as “POMC only” neurons (11% ±1.5%) (Figure 27C).

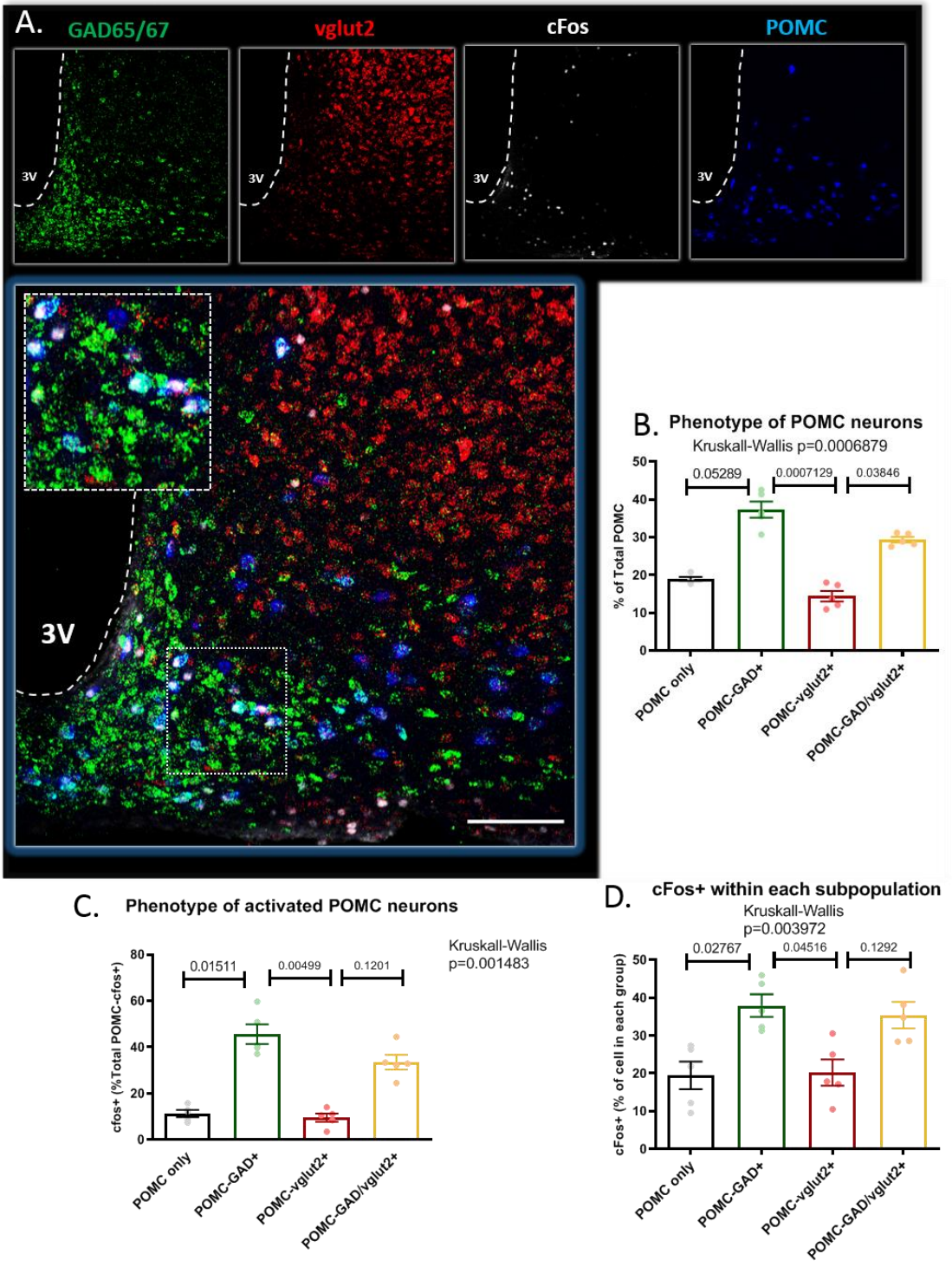

Figure 27: Acute exposure to HFD in the light phase preferentially recruits POMC-GABA over POMC-Glut.

A: Simultaneous detection of vglut2 (red), GAD65/67 (green) and POMC (blue) mRNA by FISH, combined with immunodetection of cfos (white). 3V: third ventricle. Scale bar = 100µm.

B: Representation of each subpopulation among all POMC neurons.

C: Representation of each subpopulation among all POMC-cfos+ (activated) neurons.

D: Coexpression of cfos among each subpopulation.

Finally, we expressed the number of POMC-cFos+ neurons as percentage of neurons within each POMC subpopulation. Here again, we found that the GABAergic and mixed Glut/GABA populations were the most activated ones (38% ±3% for GABA and 35.5% ±3% for Glut/GABA), while POMC-Glut and "POMC only" had only 20% ±3% and 19.5% ±3% cFos+ cells, respectively (Figure 27D).

❖ Summary

In these sets of experiments, we studied how mice react to an acute exposure to HFD and how the different subpopulations of POMC neurons respond to this calorically-dense diet. First, we observed that, when given the opportunity, mice will eat HFD over CD during the light phase, even without previous caloric restriction. When this diet is given for 24h, mice have a hyperphagic behaviour leading to an enhanced caloric intake and body weight gain, likely through exostatic mechanisms. A 2h exposure to HFD is also associated with the activation of around 36% of POMC neurons, with almost half of them being POMC-GABA (vs only 14% of POMC-Glut). This clearly highlights the fact that HFD preferentially recruits POMC-GABA neurons. Finally, when mice are switched back to CD after 24h of HFD, they are hypophagic and lose weight, likely through the activation of endostatic mechanisms. This is also associated with POMC neurons activation, but their specific phenotypes have yet to be determined.

Chapter 3

Characterization of inducible POMC-vglut2-KO mice

After studying the impact of a short exposure to HFD diet on the activation of different subpopulations of POMC neurons, and having found that the hyperphagia to HFD is associated with recruitment of the GABAergic, but not glutamatergic POMC component, which is in line with our previous study (see annexed article), our prediction was that genetic removal of the glutamatergic component would also cause hyperphagia. To test this, we generated a new transgenic mouse line for which the deletion of vglut2 is inducible in POMC neurons, after tamoxifen treatment (see Materials and Methods for details on generating this new line). In short, POMC-creER^{T2} mice (which express a cre-recombinase fused to the mutated ligand-binding domain of the human estrogen receptor ER^{T2}, specifically in POMC neurons) were crossed with vglut2-floxed mice (whose exon 2 of the vglut2 gene is flanked by two *loxP* sequences), giving rise to vglut2^{loxp}, cre-, thereafter called POMC-vglut2-WT and vglut2^{loxp}, cre+, thereafter called POMC-vglut2-KO mice.

Since ER is a nuclear receptor, it is constitutively sequestered in the cytosol until a ligand binds to it, causing its translocation to the nucleus (Jensen and Jordan 2003). The use of the fusion protein creER^{T2} allows the sequestration of cre recombinase in the cytosol, preventing any constitutive cre-dependent recombination (Feil, Valtcheva *et al.* 2009). ER^{T2} does not respond to endogenous estrogens, but it remains the target of two synthetic agonists: 4-hydroxytamoxifen (4-OHT) and 4-hydroxy-N-desmethyl tamoxifen (also called Endoxifen). These are the two main active metabolites produced by cytochrome P3A (CYP3A) and P2D6 (CYP2D6) in the liver, from tamoxifen (Felker, Nieuwenhuize *et al.* 2016). Thus, tamoxifen treatment is necessary to produce 4-OHT and endoxifen, whose binding to creER^{T2} allows its translocation to the nucleus and by extension the recombination of the floxed sequence (Figure 28A). This system is therefore particularly useful for temporally controlling the deletion, and avoiding for instance, deletion of the gene of interest during the prenatal period.

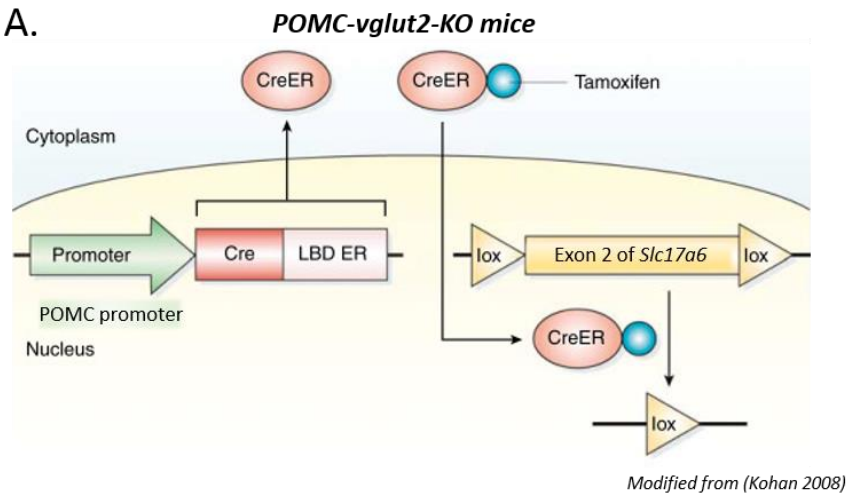

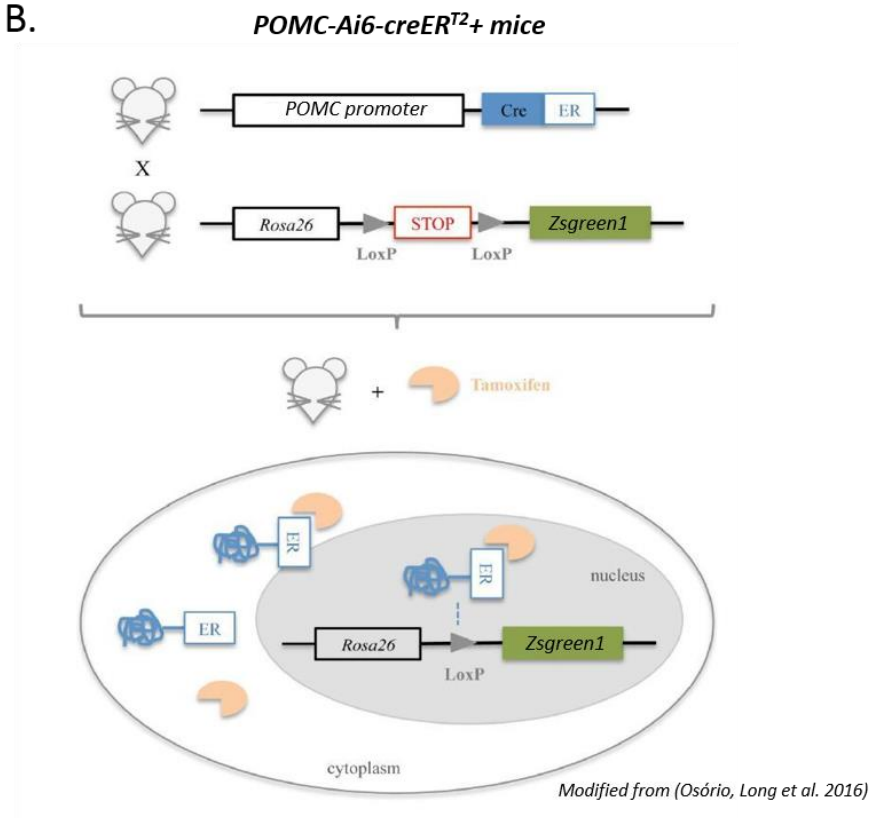

<u>Figure 28</u>: Inducible Cre-LoxP recombination systems in POMC-Ai6-creER^{T2}+ and POMC-vglut2-KO mice

A: In POMC-vglut2-KO mice, exon 2 of *Slc17a6* gene is floxed. After tamoxifen treatment, this exon excised, resulting in a *null* vglut2 allele in Cre-positive cells (i.e. POMC neurons in this model).

B: In POMC-Ai6-creER^{T2}+ mice, the expression of a reporter gene, Zsgreen1, is constitutively repressed by a floxed STOP sequence. After tamoxifen treatment, this sequence is excised, allowing the expression of Zsgreen1 in Cre-positive cells (i.e. POMC neurons in this model).

For the study of POMC neurons, temporal control of deletion is essential, as POMC is transiently expressed during development by many neurons that stop producing it in adulthood (Padilla, Reef *et al.* 2012), including some neuropeptide Y (NPY)-expressing neurons (Padilla, Carmody *et al.* 2010). A constitutive POMC-cre model would then be far from ideal because it could lead to the deletion of the gene of interest in many neurons that no longer express POMC in adulthood, inducing probable developmental effects that could bias the variables studied. Thus, our new POMC-vglut2-WT/KO model makes it possible to prevent the expression of vglut2 in POMC neurons in an inducible way, causing a probable suppression of glutamate release, while avoiding the biases associated with a constitutive deletion mentioned above. Male POMC-vglut2-KO mice are compared to their POMC-vglut2-WT littermates who also receive tamoxifen treatment, but without vglut2 deletion since they do not express creER^{T2}.

❖ Evaluation of the specificity and functionality of the model

First, we assessed the specificity and functionality of our new model. The most direct way would have been to perform a FISH for vglut2 in POMC-vglut2-WT/KO mice to verify the absence of vglut2 staining in KO mice. Unfortunately, our vglut2 probe is directed against another part of vglut2 mRNA than the one excised in this model and therefore cannot be used. While waiting for the production of a specific probe against the deleted exon 2, we used a reporter model to visualize in which cells the recombination took place. We crossed POMC-creER^{T2} mice with Ai6 mice, whose cells can express a green fluorescent protein, Zsgreen1, when the floxed STOP sequence that prevents its expression is excised in a cre-dependent manner, after tamoxifen treatment (Figure 28B). To confirm the identity of the Zsgreen1-positive neurons, 8-weeks-old male POMC-Ai6-CreER^{T2}+ mice were treated with tamoxifen (150mg/kg by gavage, daily, for 5 days, n=4) or its vehicle (5% ethanol in corn oil, n=4) after 1 week of habituation (Figure 29A). Five weeks after the end of the treatment, the mice were perfused with formaldehyde and their brains processed for POMC immunostaining (see Materials and Methods). The first observation is that in the absence of tamoxifen

(vehicle group), no Zsgreen1 expression is induced, supporting the absence of constitutive cre-dependent recombination (Figure 29B, top panel). Conversely, tamoxifen treatment induces Zsgreen1 expression, localized in POMC neurons (Figure 29B, bottom panel), validating the specificity of the POMC-CreER^{T2} model.

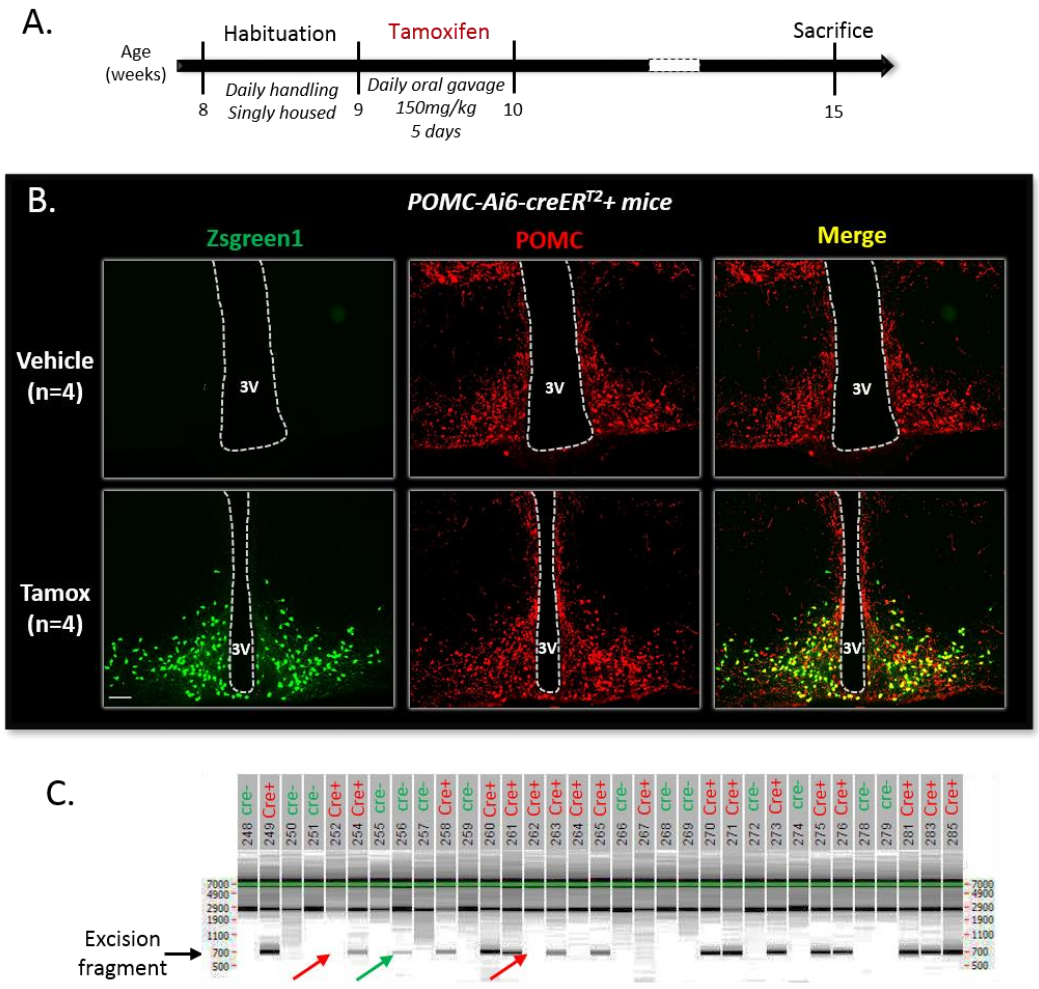

Figure 29: **Specificity and functionality of inducible Cre-recombination in POMC-CreER^{T2} mice**

A: Timeline of tamoxifen recombination in POMC-Ai6-creER^{T2}+ and POMC-vglut2-WT/KO mice

B: Representative images of the co-expression of Zsgreen1 (green) and POMC (red) in POMC-Ai6-creER^{T2}+ mice after tamoxifen treatment (n=4) or its vehicle (n=4). Zsgreen1 signal corresponds to its endogenous fluorescence, while POMC was detected by immunostaining.

C: Detection of vglut2 excision in POMC-vglut2-WT (cre-, n=14) and POMC-vglut2-KO (Cre+, n=19) mice by PCR, after tamoxifen treatment. Excision fragment is expected at 700bp. Red arrows indicate an absence of excision in POMC-vglut2-KO mice. Green arrow indicates an excision in POMC-vglut2-KO mouse.

3V: Third ventricle. Scale bar: 100µm

After confirming the location of recombination events, we wanted to check their functionality in our POMC-vglut2-WT/KO model. To do this, 33 male mice (14 POMC-vglut2-WT and 19 POMC-vglut2-KO) were treated with tamoxifen using the same protocol as before. The mice were sacrificed by cervical dislocation and their hypothalami extracted and snap-frozen to perform PCR, using specific primers to detect recombination of the floxed vglut2 allele (see Materials and Methods). We were able to detect vglut2 excision in 17 of the 19 POMC-vglut2-KO mice (Figure 29C, bands at 700bp). Surprisingly, 1 of the 14 POMC-vglut2-WT mice showed signs of recombination (Figure 29C, green arrow). These results demonstrate that our model is overall functional and can therefore be used to study the impact of vglut2 deletion in POMC neurons on metabolism and feeding behaviour.

❖ POMC-vglut2-KO mice have a normal energy balance under chow diet up to 4 weeks after the end of tamoxifen treatment

Once the model was set up, we aimed at characterizing any alterations in energy balance in POMC-vglut2-KO mice in a new cohort of animals. 15 POMC-vglut2-WT and 8 POMC-vglut2-KO mice aged 10 weeks were singly housed and handled daily for 1 week. Then, all of them received tamoxifen treatment as previously described. At the end of the treatment, a 4 weeks recovery period allowed the recombination to occur in all POMC neurons. Nonetheless, we followed the mice during this period, in which body weight and food intake were measured on a daily basis, to detect a possible differences between genotypes (Figure 30A).

During these 4 weeks, we found no significant difference between WT and KO mice in food intake although KO mice seemed to eat overall slightly more than their WT littermates at week 2 and week 3 (Figure 30B). Consistently, the cumulative food intake over these 4 weeks was slightly higher for KO mice ($p=0.2049$, Figure30C). In addition, no difference was found in body weight or food efficiency (Figure 30D, Figure 30E and Figure 30F).

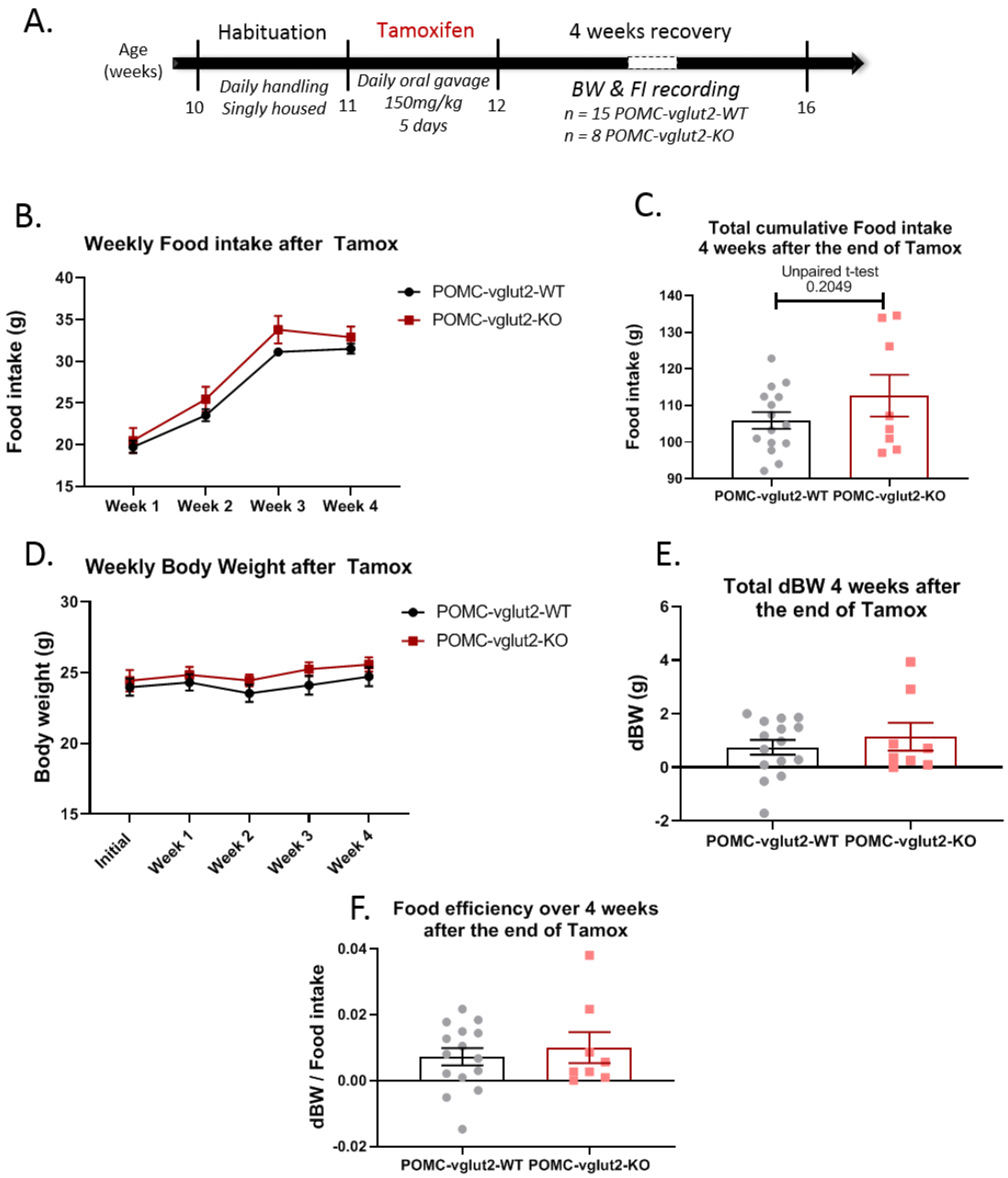

Figure 30: **Chow-fed POMC-vglut2-KO have a normal energy balance after tamoxifen treatment**

A: Sketched protocol: 15 POMC-vglut2-WT and 8 POMC-vglut2-KO received tamoxifen treatment at 11 weeks of age, after 1 week of habituation. Their body weights and food intake were recorded during a 4 weeks recovery period post-treatment.

B: Weekly food intake. **C**: Cumulative food intake over 4 weeks post-treatment.

D: Weekly body weight. **E**: Total body weight change over 4 weeks post-treatment.

F: Food efficiency over 4 weeks post-treatment

❖ POMC-vglut2-KO mice have an impaired reaction to refeeding after a 24h fast

Since we did not observe any behavioural or metabolic difference between WT and KO mice in basal condition, we challenged the mice with a fasting/refeeding experiment, in which mice are fasted for 24h, then refed in the light phase, to evaluate their adaptation to a strongly negative energy balance. First, we found a tendency towards increased body weight loss after 24h fasting in KO mice (-1.61g ±0.24g vs -1.21g ±0.13g, p=0.1272, Figure 31A). One hour after food was returned, KO mice were hyperphagic compared to their WT littermates (0.81g ±0.05 vs 0.62g ±0.04g, p=0.009, Figure 31B). Of note, one WT mouse was excluded from this data set because it wasted the food so much that is was impossible to accurately measure its actual food intake. The next day, KO mice had regained more weight (2.1g ±0.18g vs 1.5g ±0.11g, p=0.011, Figure 31C) and had a higher feed efficiency than WT controls (p=0.033, Figure 31D).

Taken together, these results highlight an exaggerated response of KO mice to refeeding, with a 1h hyperphagia and an enhanced 24h food efficiency and body weight gain.

❖ POMC-vglut2-KO mice are hyperphagic under chronic HFD exposure

In the same cohort of animals, we tested the effect of a chronic HFD exposure, up to 12 weeks. During this period, we found that overall, KO mice were hyperphagic (p=0.0102, Figure 32A), although post-hoc analysis revealed that food intake was different only during the first 3 weeks of HFD exposure (Figure 32A). Consistently, cumulative food intake was higher in KO mice compared to WT controls, at 1 week and 12 weeks of HFD exposure (Figure 32B and Figure 32C, respectively). However, despite an increased energy intake, body weights did not differ between genotypes (Figure 32D and Figure 32E), neither did the food efficiency (Figure 32F).

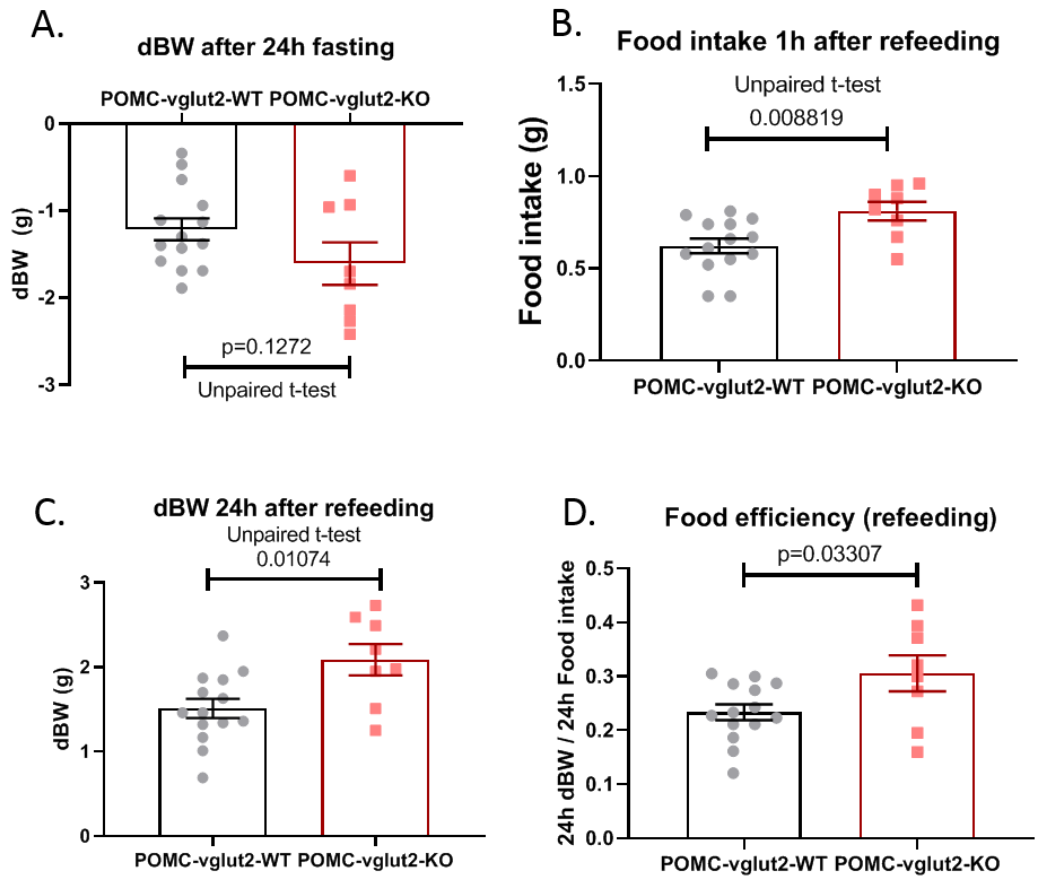

<u>Figure 31</u>: POMC-vglut2-KO mice have an impaired reaction to fasting/refeeding
14 POMC-vglut2-WT and 8 POMC-vglut2-KO chow-fed mice were fasted for 24h. The next day, the were refed 5 hours before the onset of the dark phase. Mice were 17 weeks old.
A: Body weight change after 24h of fasting.
B: Food intake after 1h of redeefing.
C: Body weight change and
D: Food efficiency 24h after refeeding.

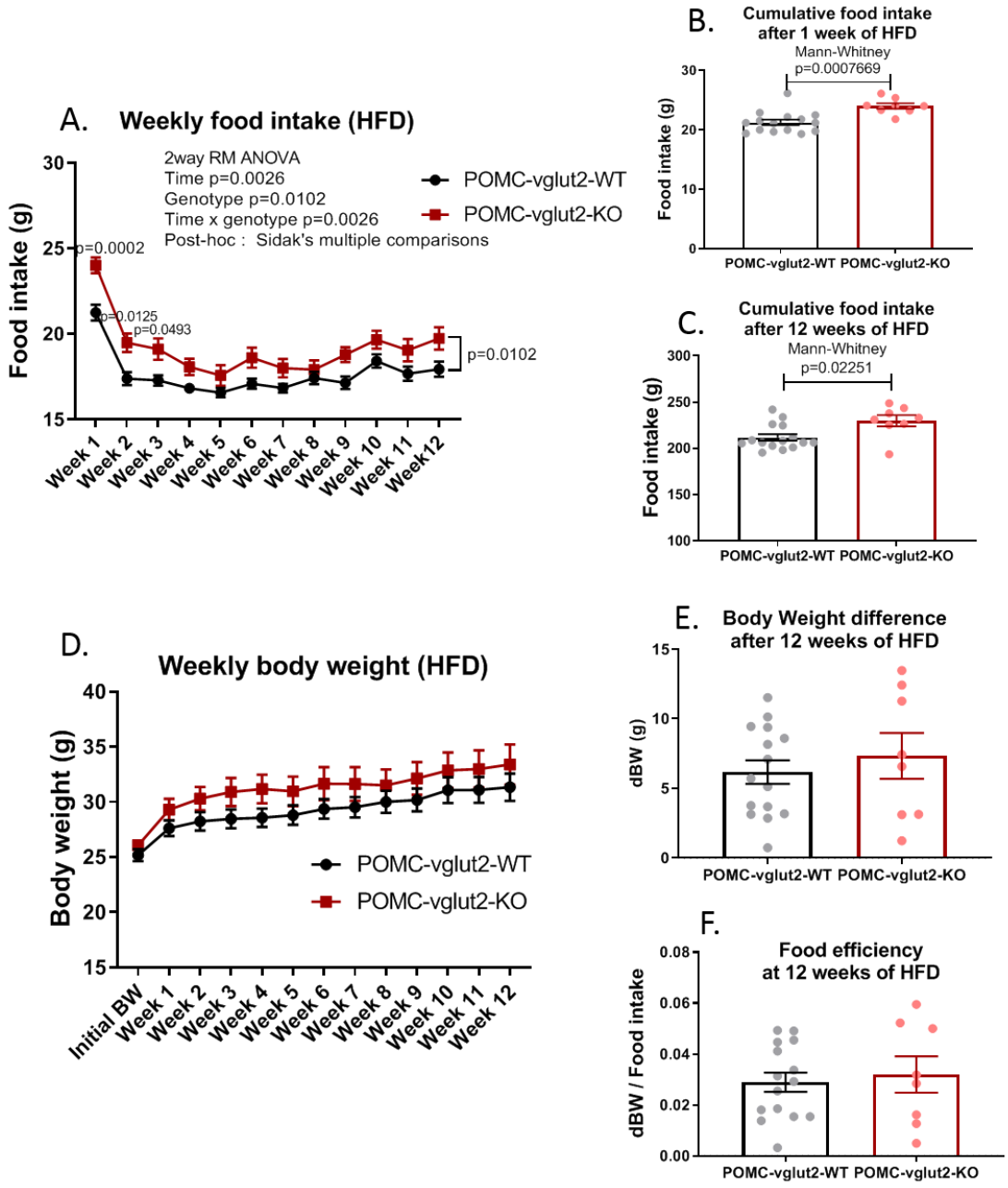

Figure 32: **POMC-vglut2-KO mice are slightly hyperphagic under chronic exposure to HFD**
15 POMC-vglut2-WT and 8 POMC-vglut2-KO chow-fed mice were switched on HFD at the age of 22 weeks and followed for 12 weeks.
A: Weekly food intake over 12 weeks of HFD. **B**: Cumulative food intake of the first week of HFD.
C: Cumulative food intake for the 12 weeks of HFD.
D: Weekly body weight over 12 weeks of HFD. **E**: Body weight difference after 12 weeks of HFD.
F: Food efficiency at 12 weeks of HFD.

Then, by using an EchoMRI system (see Materials and Methods), we evaluated the body composition of the animals before HFD switch and after 9 weeks of HFD exposure. We calculated the difference in fat mass and lean mass between these two time points. There was no genotype difference in either fat mass or lean mass change during these 9 weeks of HFD feeding (Figure 33A and Figure 33B, respectively). However, thanks to these data, we were able to estimate the total energy expenditure (TEE) during this period, using the formula validated in (Ravussin, Gutman *et al.* 2013): TEE=MEI-(ΔFat mass×9.4 + ΔLean mass×1). Here, MEI stands for metabolizable energy intake, and corresponds to the caloric intake over a certain period of time (which must be of at least 30 days to be accurate). ΔFat/Lean mass represents the fat/lean mass changes over the same period and were assigned caloric equivalents (9.4kcal/g for fat mass and 1kcal/g for lean mass). Using this formula, we found that KO mice had a higher energy expenditure over 9 weeks of HFD (857kcal ±25kcal vs 794kcal ±12kcal, p=0.018, Figure 33C), consistent with the fact that they were eating more without gaining body weight.

In summary, these results show that the deletion of vglut2 in POMC neurons is associated with an increase in HFD intake, particularly evident during the first 3 weeks of HFD exposure, which is compensated by a concomitant increase in energy expenditure, so that body weight over time is not affected.

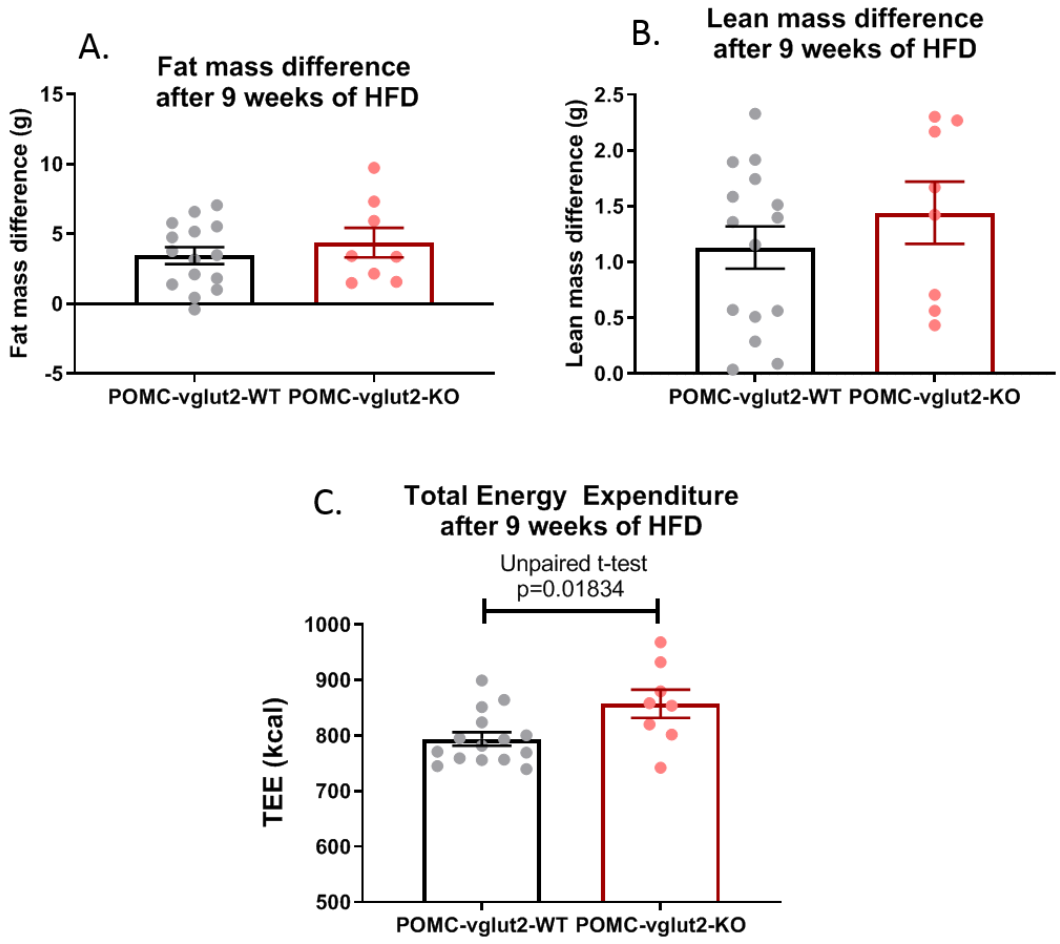

<u>Figure 33</u>: POMC-vglut2-KO mice have an increased total energy expenditure under chronic exposure to HFD

A: Fat mass and **B**: Lean mass difference after 9 weeks of HFD.

C: Total energy expenditure calculated after 9 weeks of HFD

❖ POMC-vglut2-KO mice have an alteration of energy expenditure after thermoneutrality and during HFD feeding

Given the enhanced energy expenditure observed in the previous experiment, we wanted to better characterize daily energy expenditure using indirect calorimetry. To do so, we used another cohort of mice (12 WT vs 12 KO) which were treated as usual: 1 week of habituation in our animal facility, singly housed and handled daily, then treated with tamoxifen, followed by a recovery period of 4 weeks. They were then put into metabolic cages (see Materials and Methods). After a 1-week habituation period, they underwent a thermoneutrality challenge: for 2 days, the temperature was raised up to 33°C, so that the mice do not need to spend energy to maintain their core body temperature and their sympathetic nervous system (SNS) is not engaged. The next day, the temperature returned to 22°C. Food intake, drink intake, respiratory exchange ratio (RER), energy expenditure and locomotor activity were all recorded.

During the thermoneutrality period, we did not observe any significant difference in any of the variables studied (Figure 34), except during the light phase of the first day, in which KO animals had a lower locomotor activity than WT mice ($p=0.012$, Figure 34A). However, when the temperature went back to 22°C, we found an increase in energy expenditure in KO mice during the light phase ($p=0.049$, Figure 34D) possibly suggesting a heightened activity of the SNS.

After a 1 week recovery period at the end of the thermoneutrality challenge, mice were then switched to HFD and all the previous variables were recorded again for 1 week (Figure 35).Surprisingly, we did not find back the hyperphagia observed in the previous cohort of mice under chronic HFD-feeding (Figure 35C). However, an increase in energy expenditure in KO mice was observed during the 6^{th} and 7^{th} day of HFD-feeding (Figure 35D).

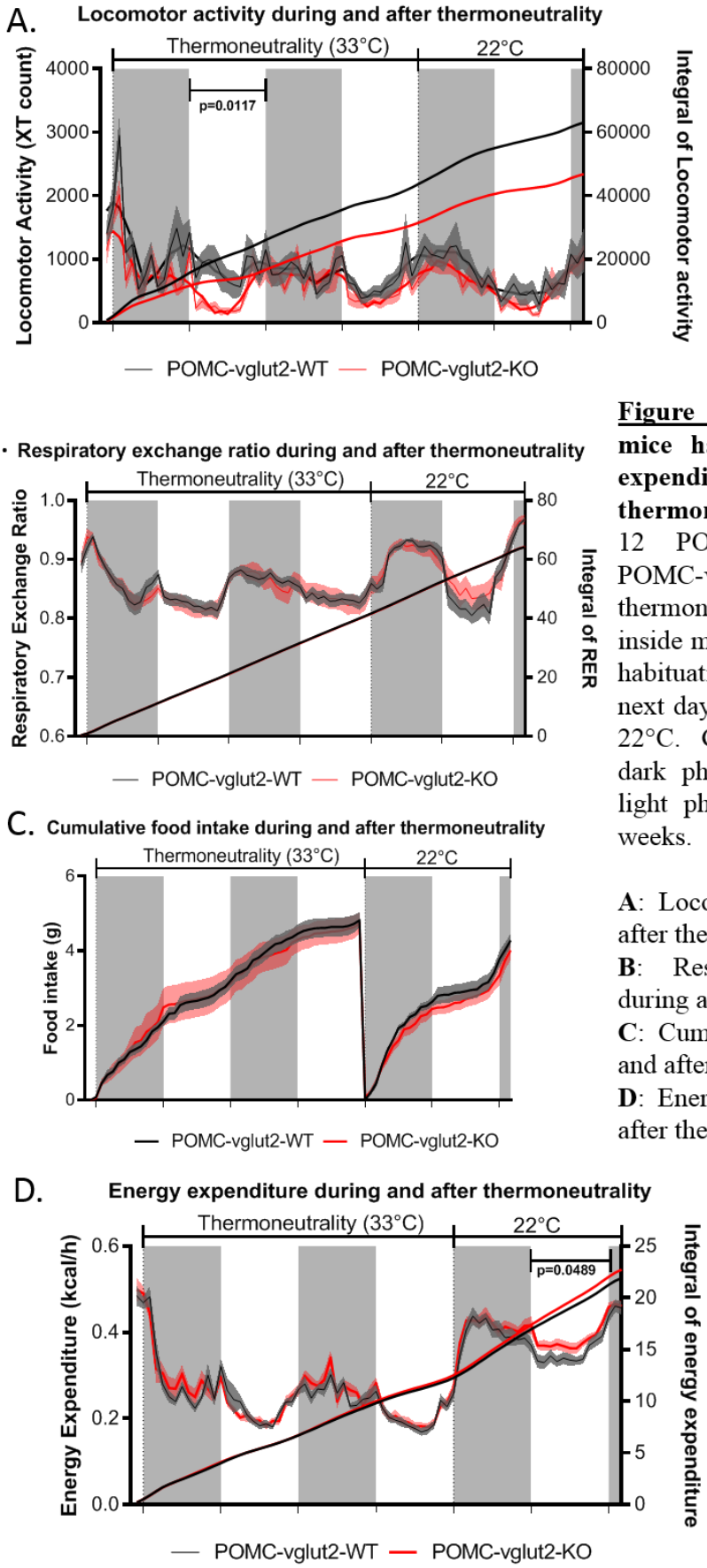

Figure 34: **POMC-vglut2-KO mice have an impaired energy expenditure adaptation from thermoneutrality (33°C) to 22°C.** 12 POMC-vglut2-WT and 12 POMC-vglut-KO mice are put to thermoneutrality (33°C) for 2 days, inside metabolic cages, and after an habituation period of 1 week. The next day, the temperature returns to 22°C. Grey boxes represent the dark phases and white boxes the light phases. Mice were aged 19 weeks.

A: Locomotor activity during and after thermoneutrality.
B: Respiratory exchange ratio during and after thermoneutrality.
C: Cumulative food intake during and after thermoneutrality.
D: Energy expenditure during and after thermoneutrality.

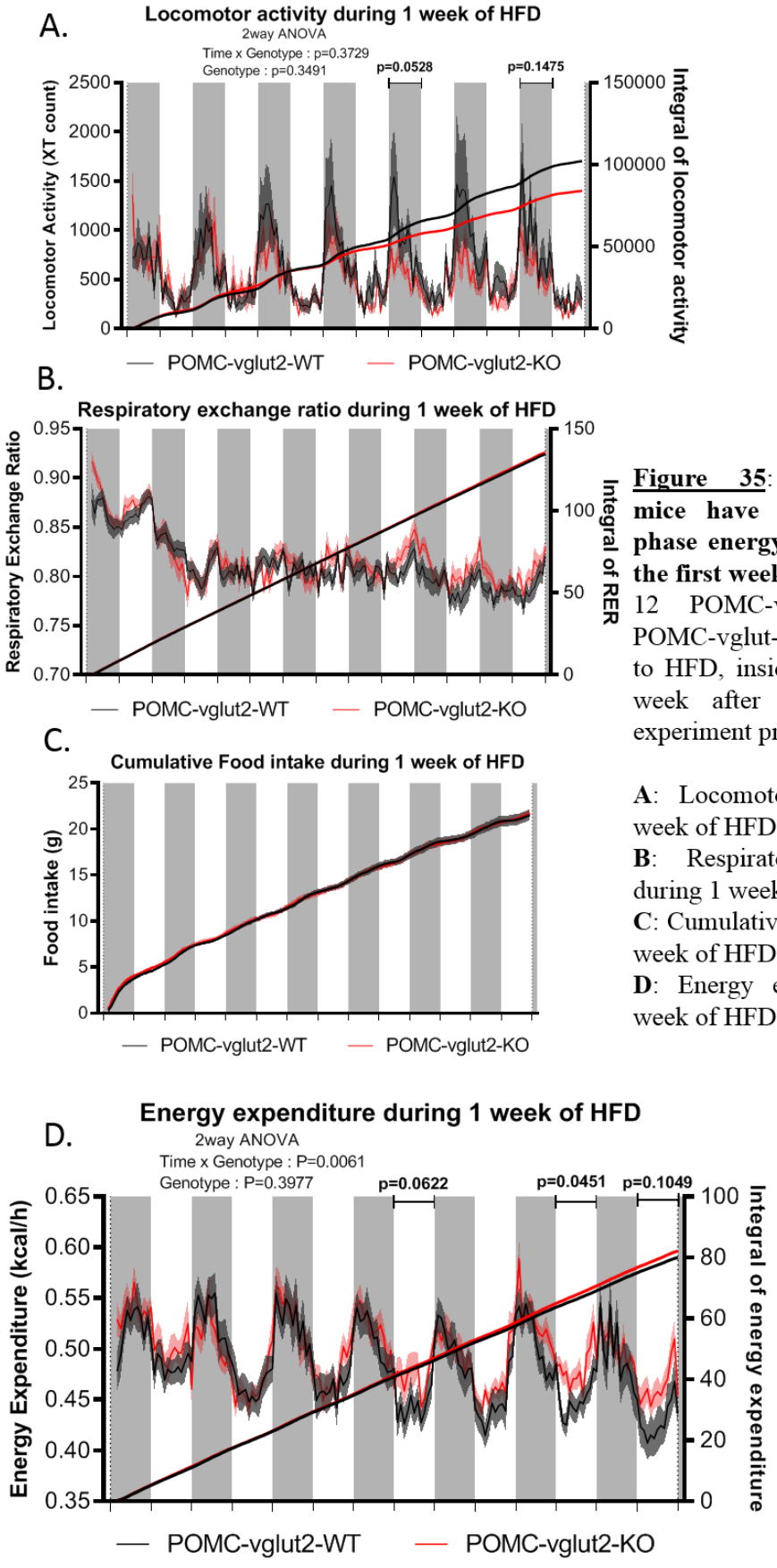

<u>Figure 35</u>: POMC-vglut2-KO mice have an enhanced light-phase energy expenditure during the first week of HFD

12 POMC-vglut2-WT and 12 POMC-vglut-KO mice are switched to HFD, inside metabolic cages, 1 week after the thermoneutrality experiment presented in figure 31.

A: Locomotor activity during 1 week of HFD.
B: Respiratory exchange ratio during 1 week of HFD.
C: Cumulative food intake during 1 week of HFD.
D: Energy expenditure during 1 week of HFD.

❖ Summary

We successfully established a new model to study POMC-Glut neurons by deleting vglut2 from POMC neurons in adult mice, upon tamoxifen-induced cre-mediated recombination. The data that we have gathered so far suggest that the deletion of vglut2 from POMC neurons (which likely prevents any glutamatergic neurotransmission from these neurons) is associated with an exaggerated response to fasting/refeeding and an initial hyperphagia under HFD-feeding that is compensated by an increase in energy expenditure which seems to occur specifically during the light phase.

Discussion

This last part will summarize the main technical and scientific results and put them in perspective with the current literature. We will also propose relevant research perspectives in this context.

❖ FISH and IHC combination: a versatile technique with unpredictable outcomes (at times)

In Chapter 1 of the results, we described the development of a protocol for combining 3 FISH and 1 IHC staining, on free-floating brain slices. Several technical challenges had to be addressed during the 2.5 years leading up to the final version of the protocol and its use in the context of actual experiments detailed here and also part of other studies currently ongoing in the laboratory.

***A gentle touch for optimal tissue quality*:** we started from an optimized protocol for FISH on slides. The first difficulty was to prevent the free-floating slices from being completely degraded due to the high temperature incubations that weakened it. Indeed, during our first tests, the slices were so fragile that we only had fragments left at the end of the experiment. This weakening process is likely due to the destruction of cross-linking methylene bridges between proteins and nucleic acids (formed during formaldehyde fixation) due to high temperature incubations (which is also the basis of antigen retrieval). Indeed, when a tissue is well fixed, it is rather insensitive to external conditions, such as the tonicity of incubating solutions, since the cross-linking chemical bridges keep membrane proteins together and thus prevent any gross morphological alteration. Consequently, the tissue can be handled without major damage risks. However, when such links are removed, the tissue tears more easily and morphological changes are possible, as assessed by the shrinkage of brain slices happening during 0.2M HCl incubations, only after hybridization is done.

Taken into consideration this issue, we tried to remove from the protocol all the steps that could aggravate the destruction of cross-links. We first removed the proteinase K incubation, whose aim is to digest proteins and cross-links in order to facilitate the access of nucleic acids to exogenous probes. Removal of this step did not affect the quality of FISH staining but improved tissue preservation.

We could not reduce much the temperature of hybridization, since it is determined by the sequence of the probe (as explained in the Chapter 1 of the Results). Instead, we tried to shorten the incubation length at 70°C and the subsequent washes at 65°C. However, whatever modification we did in that direction led to a much poorer signal quality (data not shown). As a result, we kept the protocol as it is in this current version and never tried to change temperature settings again.

Finally, we adapted our way of handling slices by keeping them in the same well from the beginning until the end of the experiment: we changed the solutions between steps within each well instead of transferring the slices from well to well, in order to limit unnecessary handling. We also limited the number of slices to 4 per well, maximum. Above this number, slices begin to stick to each other, which increases the risks of damage and makes washes less efficient. These slices must also be evenly distributed in the wells and must be floating all the time, especially within the viscous hybmix, otherwise they will end up being stuck at the bottom of the wells, making them nearly impossible to detach without any damage. Although they might seem anecdotal, these multiple technical tips progressively improved tissue quality at the end of the FISH from "torn pieces of tissue" to "fragile-but-entire slices".

FISH and IHC, a matter of order: in an attempt to combine cFos immunostaining with other FISH staining, we tested several protocols, where IHC is done either after or before FISH. For a successful cFos staining, IHC had to be done before FISH, using a sophisticated TSA-based amplification technique. However, we also used this FISH/IHC combination in other projects outside of this thesis, with different markers. As a result, rather than having one ready-to-use protocol in which probes and antibodies are exchangeable, we ended up with several "template protocols" that can be used in different situations, depending on the compatibility between IHC and FISH staining, i.e. how one affects another (Figure 36). Indeed, we found that for some immunostaining such as GFP (green fluorescent protein), IHC can be performed after FISH without any loss in signal quality (Figure 36A). Others have to be done before in order to succeed,

such as mCherry, in a protocol similar as for cFos (Figure 36B). Finally, for most antigens that we tested in combination with FISH, an "intermediate protocol" works the best, where the FISH and IHC steps are intermingled (Figure 36C): here, the primary antibodies are incubated after probes hybridization but revealed by secondary antibodies only after probes revelation.

The type and number of antigens to detect in combination with FISH dictate the choice of one or the other protocol. Template in Figure 36A is ideal when IHC is not affected by FISH and/or if primary antibodies affect FISH revelation. Of course, this protocol is suitable for multiple IHC staining. Template in Figure 36B is necessary when FISH completely disrupts the antigen of interest, making IHC impossible to do after FISH. However, this protocol only allows one IHC staining before FISH. Finally, template in Figure 36C is, in our hands, the most useful, as the incubation of primary antibody before FISH revelation generally yields to a better signal/noise ratio without affecting FISH staining. In this protocol, secondary antibodies incubation is done after FISH revelation since in our experience, they often seriously decrease FISH signal if incubated before. This last protocol also allows multiple IHC staining. So far, using these different templates, we were able to set up different FISH/IHC combination such as POMC/GAD65-67/vglut2/cFos, POMC/AgRP/ZsGreen1/NeuN or POMC/AgRP/ZsGreen1/Tbx3 among others. We have not presented these results since they are out of the scope of this thesis.

Remaining issues and future development: however advanced our understanding of FISH/IHC combination is by now, some issues remain. For instance, as explained in the Chapter 2 of the Results, we had a technical issue doing the FISH/IHC staining in the "chow (dark phase)" vs "HFD-to-chow" experiment, with a suboptimal GAD65/67 and vglut2 staining (POMC and cFos were perfectly fine). This is likely due to a difference in fixation quality that in return affects the binding of probes and secondary antibodies for probe detection.

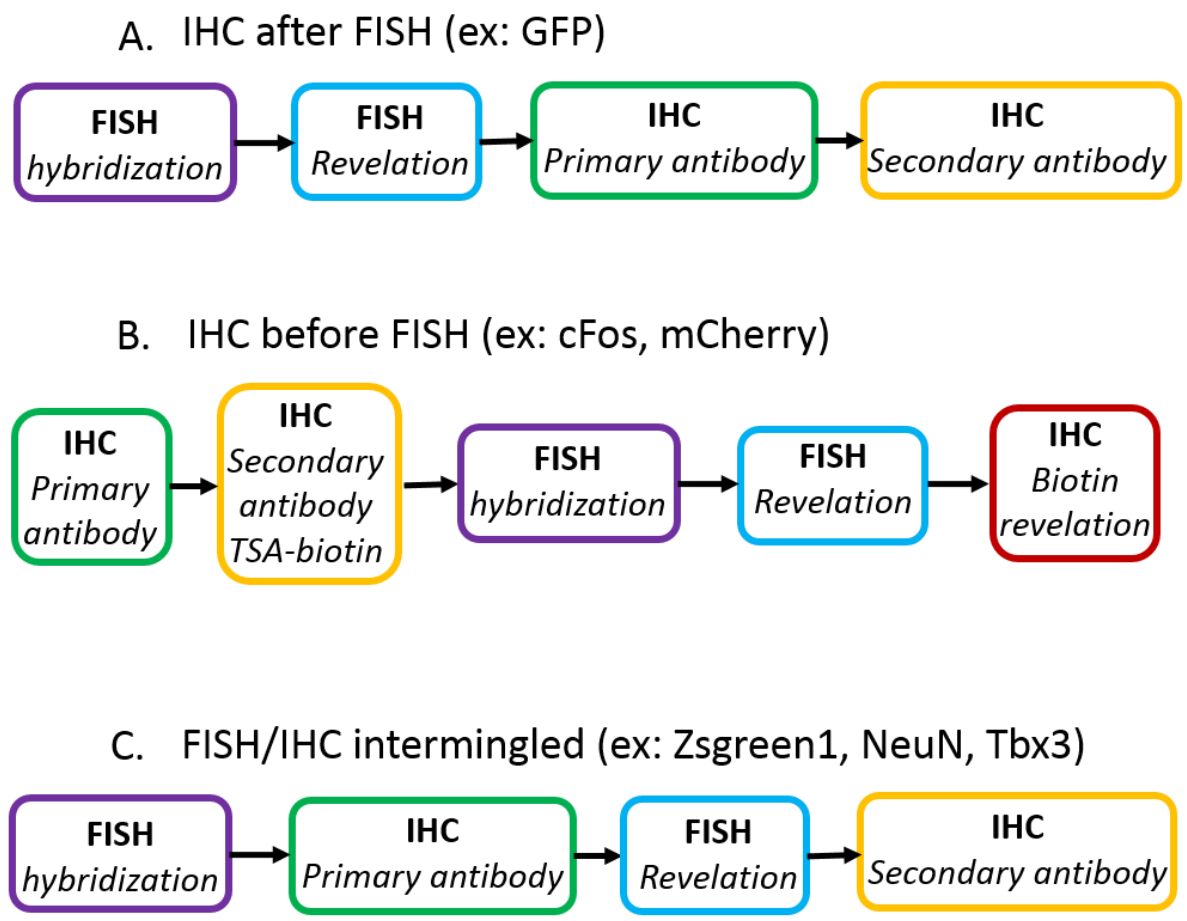

Figure 36: **Different protocol templates for FISH/IHC combination**
A: Template for IHC after FISH. Easiest to do, but acceptable only when FISH doesn't affect IHC signal. Multiple IHC staining can be done at once.
B: Template for IHC before FISH. Same as described in Results, Chapter 1. IHC is done using biotin-TSA revelation before FISH. FISH is performed entirely and biotin revelation is completed at the end of the protocol. It gives the best IHC staining (if the primary antibody is specific). Only one IHC staining can be performed like this.
C: Template for IHC intermingled with FISH. Here, IHC primary antibodies are incubated after probes hybridization but before probes revelation. Revelation of primary antibodies is done at the end. Usually gives better IHC signal, but may cause FISH problems if primary antibodies interfere with probes revelation. Multiple IHC staining can be done at once.

When we faced this issue in the development process, we found that the best way to cope for these inter-experimental variations was to titrate the secondary antibodies (anti-DIG and anti-FITC) for each new experiment, in order to find the best dilution (usually between 1/500 and 1/2000). Here we used a 1/1500 dilution for both anti-DIG and anti-FITC, which is the best-working dilution we found at the end of the FISH/IHC development. However, if the FISH signal is not strong enough, this dilution must be too low for some experiments. Of note, concentrating too much these secondary antibodies usually leads to a lot of non-specific staining, so a balance must be found between sensitivity and specificity. Therefore, even if our protocols are working and reproducible, ideal anti-DIG and anti-FITC antibody dilution must be found empirically for each new experiment in order to achieve the best signal/noise ratio.

So far, we are able to combine 4 different markers (5 in total if we consider the POMC/GAD65-67/vglut2/cFos co-staining, but GAD65 and GAD67 were revealed in the same colour). Would it be possible to go further than that? Probably, yes. For FISH staining, the main limit is the number of "Tags" available to label the probes. Only 4 non-radioactive tags are widely used: DIG, FITC, DNP and biotin. In our experiments, we only used DIG, FITC and DNP probes, because biotin was already used for the IHC before the FISH (Figure 36B). Yet, in theory, it should be possible to add another probe labelled with biotins and use HRP-labelled streptavidins with TSA amplification do detect the signal. However, another limiting step is the number of different fluorophores/colours we can use at once and still be able to discriminate from one another using a confocal microscope. Here, we used blue/green/red/far red fluorophores whose excitation/emission spectra were separated enough to allow proper image acquisition. To optimize this, PerkinElmer has developed a new line of 6 fluorophores for TSA amplification, specifically designed for the simultaneous detection of antigens (Opal 520/540/570/620/650/690). If we consider these Opal

fluorophores together with a blue fluorophore, we could theoretically combine up to 7 markers simultaneously (with a maximum of 4 different FISH staining due to the probe labelling limitation discussed above). Although such a high combination would be probably difficult to set up, it is not impossible and such effort could be initiated, should we need it in the near future.

❖ Identification of activated POMC-Glut and POMC-GABA neurons in brain slices

The FISH/IHC combination developed in the context of this thesis is a necessary tool that allowed us to detect activated (i.e. cFos+) POMC-Glut and POMC-GABA neurons in brain slices, after for instance an acute HFD exposure.

***Phenotype of POMC neurons*:** it should be first noted that the numbers we obtained when defining the different POMC populations (POMC only, POMC-Glut, POMC-GABA and POMC-Glut/GABA, Figure 27B) are overall consistent with what is found in a recent single-cell RNA sequencing study. Indeed, Lam and colleagues reported 46% of POMC-GABA, around 30% of POMC-Glut and 24% of POMC-Glut/GABA (Lam, Cimino *et al.* 2017), while we found 37% of POMC-GABA, 14% of POMC-Glut and 29% of POMC-Glut/GABA. These numbers are quite similar, except for POMC-Glut neurons, which seemed underestimated in our quantification.

However, we found as well 19% of POMC-only neurons, in which neither vglut2 nor GAD65/67 could be detected. It is then very likely that these POMC-only neurons do express vglut2 and/or GAD65/67, but at a very low level, below the detection threshold in our FISH experiment. We could then speculate that most of these neurons are actually glutamatergic since we observed that the POMC-only subpopulation had the same response to HFD as the POMC-Glut one (Figure 27C and Figure 27D). This would be consistent with the fact that Wittmann *et al.* reported the difficulty of detecting vglut2 by radioactive FISH in formaldehyde-fixed brains, compared with fresh-frozen tissue (Wittmann, Hrabovszky *et al.* 2013). Finally, if we add the numbers

of POMC-Glut and POMC-only subpopulations, we get 33%, which is close to the 30% reported by Lam (Lam, Cimino *et al.* 2017).

In summary, our quadruple FISH staining is a reliable way to detect different subpopulations of POMC neurons in mouse brain slices. The results are similar to those obtained by a much more sensitive technique of single cell RNA sequencing. The most difficult marker to detect is vglut2, since a large number of glutamatergic neurons may express it at low levels, making them difficult to identify by FISH and leading to a fourth subpopulation of "POMC only" neurons which might in reality be POMC-Glut ones for the most part.

***Detection of activated POMC neurons*:** another important verification is that our FISH/IHC staining does not alter the quantity of POMC-cFos+ observed. Since we first performed a POMC/cFos immunostaining, we could compare the numbers of total POMC-cFos+ neurons after a classical IHC or FISH/IHC staining. By double-IHC, we found that 36% ±5% of POMC neurons were cFos+ after an acute HFD exposure (Figure 25D). By doing now the FISH/IHC on the same samples, we found 31% ±2% of POMC-cFos+ neurons (data not shown), confirming once more that our FISH/IHC protocol is perfectly reliable to study the activation of glutamatergic vs GABAergic POMC neurons.

***An improved quantification for a deeper understanding*:** the quantification performed in this study only focused on the number of cells in each category. If we want to fully extract the knowledge we can acquire from our images, a more detailed analysis will have to be done. First, a spatial distribution of activated POMC-Glut vs POMC-GABA neurons would be interesting, to see whether the distribution pattern of activated cells follows the distribution pattern of known POMC subpopulations (such as leptin-, insulin- or serotonin- responsive neurons, discussed in the Chapter 5 of the Introduction). To do so, we will need to differentiate the different rostro-caudal levels and laterality (by means of the distance from the third ventricle) in our future analysis. This type of spatial distribution analysis was done by our collaborators in Cambridge for the Saucisse *et al.* manuscript that we have recently submitted (see also annexe).

In addition, quantifying the signal intensity for each marker would be of great relevance. Indeed, Dicken *et al.* found that GAD67 mRNA was a reliable predictor of GABA release from AgRP neurons, so we could speculate that a similar result would be observed in POMC neurons (Dicken, Hughes *et al.* 2015). As such, GAD65/67 mRNA intensities could then be correlated with cFos intensity in order to see whether the activated POMC-GABA neurons are the ones with the highest expression of GAD (and perhaps the highest release of GABA). It should also be noted that although we never quantified intensities, we visually observed a huge variation of POMC signal intensity during the quantification process. Some POMC cells were barely visible while some others were almost at saturation levels. In this context, very preliminary data from our lab seem to indicate that POMC neurons react differently to long-term HFD exposure, depending on their level of POMC expression: after 3 month of HFD feeding, the low-expressing POMC neurons are not anymore detected, although at this stage we still do not know if they are undergoing cell death or simply stop to produce POMC. Thus, it would be very interesting to link the POMC intensity data with their neurotransmitter phenotype. Finally, the quantification of intensities would also bring a more detailed description of the POMC-Glut/GABA population, since we clearly observed differences in vglut2 and GAD expression: some POMC-Glut/GABA expressed much more GAD than vglut2 and *vice versa*. Thus, heterogeneity can be found even among these subpopulations, and a better definition of their phenotype (in favour of Glut or GABA) might help to clarify their physiological role.

❖ POMC-Glut and POMC-GABA respond differently to HFD

***POMC-GABA as potential orexigenic neurons*:** We have found that an acute exposure to HFD during the light phase, which leads to hyperphagia, was associated to an activation of around one third of POMC neurons, among which the majority were POMC-GABA and POMC-Glut/GABA neurons. Interestingly, almost 40% of all POMC-GABA were activated, versus only 20% of all POMC-Glut, suggesting that the GABAergic transmission from POMC neurons might be involved in the hyperphagic behaviour. This is in line with our own data regarding the effect of rapamycin on POMC-GABA neurons: rapamycin, an appetite-stimulant and inhibitor of the mTORC1 kinase, is able to stimulate POMC-GABA activity and enhance POMC GABAergic neurotransmission into the PVH (see annexed article, Figure 2 and Figure 3), suggesting once more an association between POMC-GABA and hyperphagia.

Of note, Lam and colleagues found that 27% of adult POMC neurons also co-expressed AgRP, reflecting the developmental origin of AgRP neurons, with up to 25% of them deriving from the same progenitors as POMC neurons (Padilla, Carmody *et al.* 2010, Lam, Cimino *et al.* 2017). Since these POMC/AgRP neurons were all GABAergic (Lam, Cimino *et al.* 2017), we could speculate that they share a similar physiological function in the regulation of food intake, i.e. stimulating food intake, and could then be part of the activated POMC-GABA neurons under acute HFD exposure (Jarvie, King *et al.* 2017). However, although we did not perform AgRP staining in the same slices, the location of cFos+ nuclei indicate that AgRP cells are not likely to be activated by HFD in our experimental condition, since AgRP is located very close to the third ventricle (see Figure 25C and Figure 27A). Moreover, AgRP neurons physiologically respond strongly to caloric deficit rather than overload, so if POMC/AgRP neurons behave in a similar fashion, they should not be activated in this specific context.

In addition, Jarvie *et al.* found that overnight fasting reduced the number of POMC neurons co-expressing GAD67 (but not GAD65) in male and female mice (Jarvie, King *et al.* 2017), contrary to what is found in AgRP neurons, in which caloric restriction increases GAD67 expression and subsequent GABA release (Dicken, Hughes *et al.* 2015). These results are in contradiction with the fact that POMC-GABA would all behave as AgRP neurons and rather suggest an opposite regulation. However, we cannot exclude the possibility that different subpopulations exist within the POMC-GABA population, some of which may have opposite role. For instance, the 40% POMC-GABA cells activated after acute HFD exposure might not be the same as the ones affected by caloric restriction or co-expressing AgRP. Similarly, the 20% of activated POMC-Glut in this condition might have the same physiological role as the 40% activated POMC-GABA, by acting on different targets, suggesting that subsets of POMC-Glut and POMC-GABA cells could share similar functions.

In summary, our data highlight the fact that POMC-GABA are the main subpopulation that respond to an acute HFD exposure, although 60% of them do not respond to the diet, indicating that the POMC-GABA population might not be functionally homogenous or might express/cover different function in relation to where they project to. Moreover, the causal link between the hyperphagia caused by HFD exposure and the activation of POMC-GABA has yet to be clearly demonstrated. Finally, it should be noted that when mice were sacrificed after 2h HFD exposure, they had already been exposed to HFD four times before, during 24h each time. Consequently, they were not naive to the diet, and we may wonder if the same neurons would be activated after the very first exposition to the diet or not.

***How could POMC-GABA neurons stimulate HFD intake (if they do)*:** it could be far-stretched to hypothesize putative POMC-GABA orexigenic circuits, given that neither our data, nor the current literature have clearly established a causal link between POMC-GABA neurons and hyperphagia. However, if such circuits exist, they might involve brain regions implicated in the exostatic regulation of feeding behaviour, such as the ventral tegmental area (VTA) and the nucleus accumbens (NAc) (discussed in the Chapter 4 of the Introduction). Indeed, the hyperphagia elicited by HFD exposure in the light phase occurred without prior caloric restriction, so that mice were not in a physiological state of negative energy balance. And yet, a subset of POMC-GABA neurons was activated under these circumstances. If their activation is causally linked with the intake of HFD, we could speculate that it involves an enhancement in motivation and/or pleasure to eat. For instance, it is known that POMC to VTA projections increase motivation for food reward through MC3R signaling (Pandit, Omrani *et al.* 2016). In addition, is has been proposed that the orexigenic effect of tetrahydrocannabinol (THC), the principal psychoactive component of marijuana, relies on β-endorphin release from POMC neurons (Koch, Varela *et al.* 2015). These results highlight the relevance of studying neuropeptide production in POMC-Glut vs POMC-GABA, and especially in POMC cells that respond to HFD. Indeed, if POMC neurons are generally known to produce the anorectic neuropeptide α-MSH, a MC4R agonist, POMC processing can also lead to the release of γ-MSH, a MC3R agonist and the orexigenic β-endorphin, an opioid receptor agonist.

In this context, it is possible that different subpopulations of POMC neurons express different neuropeptides, with for instance a preferential β-endorphin release from POMC-GABA neurons into hedonic hotspots within the NAc in response to HFD that could increase the pleasure to eat palatable food. A preferential γ-MSH release from POMC-GABA in the VTA in order to stimulate the motivation for food reward might be another possibility. In any case, these hypotheses remain very speculative, as we have not specifically addressed the motivation and hedonic responses in our experiments.

Moreover, studying neuropeptides production represents a huge challenge in our conditions, since they are produced after POMC cleavage and accumulate mainly in axonal projections. As such, FISH is not an option for their detection (since there are no specific mRNAs for these molecules). A treatment with colchicine, a microtubule polymerization inhibitor that blocks axon trafficking has long been used to induce the accumulation of neuropeptides within cell bodies, allowing their detection by immunostaining. However, this technique is completely incompatible with a functional approach such as cFos co-staining, since colchicine is very toxic and makes mice very sick (beyond the ethical issue of using such a violent treatment in alive animals). An alternative would be to dissect several brain regions (NAc, VTA, hypothalamus) after acute HFD exposure and measure by ELISA the concentration of different neuropeptides (α-MSH, γ-MSH, β-endorphin…) and/or evaluate signal densities in POMC neuronal projections onto these brain areas by using antibodies against these molecules.

In summary, even though it is tempting to imagine that POMC-GABA neurons that respond to HFD might stimulate exostatic circuits to increase HFD consumption, further studies are required to confirm the causal link between POMC-GABA activation and hyperphagia, as well as the circuits and signals by which they may exert such effect.

***The enigmatic POMC-Glut/GABA population*:** so far, we have mainly talked about POMC-GABA, POMC-Glut and POMC-only populations, the latter being probably POMC-Glut in which vglut2 could not be detected by FISH. However, the role of POMC-Glut/GABA neurons remains uncertain. We have found that after acute HFD exposure, the POMC-Glut/GABA population behaved in a similar way as the POMC-GABA population, with 35% of mixed neurons activated by HFD (Figure 27D). As discussed earlier, the quantification of GAD and vglut2 signal intensities would allow us to better define these neurons, as they might have had a predominant GABAergic phenotype, despite expressing both markers. On the other hand, when we studied the effect of rapamycin on POMC neurons, beyond the RAPA-activated POMC-

GABA and RAPA-inhibited POMC-Glut neurons, we also found a third subpopulation that was neither activated nor inhibited by RAPA (see annexed article, Figure2), which was likely to be the POMC-Glut/GABA population. It is yet unclear whether we should consider this mixed subpopulation as distinct from POMC-GABA and POMC-Glut or if it can behave as one or the other depending on the situation.

It is also unknown if POMC-Glut/GABA cells can release either GABA or glutamate onto distinct synapses or if they co-release the two neurotransmitters onto the same targets. Indeed, a co-accumulation of GABA and glutamate has already been described in an artificial model of exogenous expression of vglut3 in GABAergic neurons (Zimmermann, Herman *et al.* 2015). In addition, somatostatin interneurons in the striatum can co-release GABA and glutamate onto different targets (Cattaneo, Zaghi *et al.* 2019). Whether this applies to POMC-Glut/GABA neurons remains to be elucidated.

Another possibility is that these mixed neurons could serve as a reserve pool of POMC neurons whose neurotransmitter identity could adapt to different physiological situations, by switching from a predominant GABAergic to a predominant glutamatergic phenotype (or *vice versa*), on demand. This is supported by the observation that GAD65/67 and vglut2 expression are highly plastic during development (Dennison, King *et al.* 2016) and that GAD67 mRNA respond to energy status (Dicken, Hughes *et al.* 2015, Jarvie, King *et al.* 2017).

Here as well, future studies will need to clarify the role and functioning of this enigmatic mixed neuronal subpopulation.

❖ What about the rebound effect after HFD to chow switch?

We have observed that, after 24h of HFD exposure, the switch back to chow diet induces a hypophagia, likely reflecting the action of endostatic mechanisms trying to compensate the previous caloric overload. This was associated with the activation of 37% of POMC neurons. However, we were unable to identify the different subpopulations among these activated POMC neurons due to a technical issue in the FISH staining, as discussed previously. Therefore, we can only speculate about the results of this experiment. If we consider that the POMC-GABA population is involved in HFD hyperphagic responses, we can on the contrary suggest that the POMC-Glut population would be recruited in an opposite situation. As such, we can expect a higher proportion of POMC-Glut that are cFos+ in the "HFD to chow" group. This hypothesis would also agree with the observed recruitment of the POM-Glut population in relation to cellular energy availability (see annexed article). Of course, as suggested before, we cannot exclude the possibility that other subsets of POMC-GABA neurons might be involved in different responses, so a certain number of activated POMC-GABA neurons are likely to be activated as well.

Another observation based on the double POMC/cFos immunostaining is that the intensity of cFos staining is much more variable from cell to cell in the "HFD to chow" group than for the "HFD" group. This finding can be explained by the fact that mice have been sacrificed 2h after the onset of the dark phase for the "HFD to chow" group, a period in which the animals are active and are likely to respond to many external stimuli. Consequently, different POMC-cFos+ neurons whose cFos intensities are different might have not responded to the same stimulus. It is therefore difficult to link cFos staining with actual neuronal response to the switch of diet, in this particular situation. Again, the quantification of cFos signal intensity might help in overcoming this issue.

To go further, in such situation, neuronal activation markers that could be detected earlier than the classical immediate-early-genes (IEG) would be particularly useful. In this context, proteins that are phosphorylated upon cellular activation are of great interest, since they can be detected early after the stimulus, contrary to IEGs, for which mRNA or protein synthesis has to be completed (≈30min to 2h). Some authors have used phosphoS6, a downstream effector of the mTORC1 pathway as a marker of cellular activation (Knight, Tan *et al.* 2012). Our own data show that pS6 is co-expressed with cFos in neurons, after pharmacogenetic activation (see annexed article, Figure S5). However, due to the opposite response of POMC-GABA and POMC-Glut to rapamycin treatment (see annexed article), an activation marker that is in direct connection with the mTORC1 pathway might not be the best candidate. Another possibility is to use phosphoERK (pERK), a downstream effector of the MAPK (mitogen-activated protein kinases) pathway, as a proxy for neuronal activation (Gao and Ji 2009). The time course of pERK accumulation after a stimulus is much faster than for cFos. For instance, pERK levels reach a peak in the spinal cord between 2 to 5 minutes only after a nociceptive stimulus (Ji, Baba *et al.* 1999). Whether the same time course applies to HFD (or other diets) exposure, fasting/refeeding, food-related cues and other relevant stimuli in the study of feeding behaviour in POMC neurons is unknown. However, given the timing advantage that such an early activation marker could provide, it would be of great interest to test if it could be applied to the study of POMC neurons activation after various physiological stimuli and try to combine pERK immunostaining with our quadruple FISH staining. Replacing cFos with pERK would then bring more accurate information about the very first neurons that respond to different types of stimuli.

❖ POMC-vglut2-KO: a model of mild HFD hyperphagia

Control of vglut2 deletion: The third chapter of the results focused on a new model that we have generated by crossing inducible POMC-CreER^{T2} mice with vglut2-flox mice, in order to delete exon 2 of vglut2 gene (*Slc17a6*) in POMC neurons, after tamoxifen administration in adult male mice. We confirmed the deletion of vglut2 in hypothalami by PCR and verified the specificity of the recombination in POMC-Ai6-CreER^{T2}+ mice. However complementary these approaches were, they are still indirect, and the best way to prove that vglut2 recombination occurred in POMC neurons is to do a FISH, using a probe directed against the exon 2 of vglut2 (that is deleted in KO animal), as in (Tong, Ye *et al.* 2007). Once this will be done, it would also be important to confirm that this mutation prevents any glutamatergic transmission from POMC neurons, as it did in SF1 (steroidogenic factor 1) neurons (Tong, Ye *et al.* 2007).

Phenotype of POMC-vglut2-KO mice: the data that we have gathered so far concerning the metabolic characterization of POMC-vglut2-WT/KO animals show that KO mice have an exaggerated 1h food intake after a 24h fast. Importantly, rapamycin has the exact same effect, by stimulating food intake after 24h fasting and is able to inhibit POMC-Glut neurons (see annexed article, Figure 2). Thus, we can draw a parallel between the results obtained in POMC-vglut2-KO mice and the rapamycin experiments: in both scenario, POMC glutamatergic transmission is suppressed or reduced (either by genetic deletion or pharmacologic inhibition), and short-term food intake enhanced after a 24h fast, suggesting a consistent anorectic action of POMC-Glut in a context of negative energy balance.

In addition, when fed a HFD, POMC-vglut2-KO mice exhibited a mild hyperphagia that was present throughout 12 weeks of HFD feeding. This effect was however compensated by an increase in energy expenditure (EE), so that body weights remained comparable between WT and KO animals. These results suggest once more that POMC-Glut neurons exert an anorexigenic action, this time in a context of chronic positive energy balance. These results are rather consistent with what Dennison and colleagues

observed using a constitutive model of vglut2 deletion in POMC neurons, in which male mice (but not females) were hyperphagic under HFD (Dennison, King *et al.* 2016). In their model, however, the increase in food intake was accompanied by an increase in body weight. Finally, consistent with our data, they found no food intake or body weight difference under chow diet.

Moreover, data obtained from another cohort of mice and placed in calorimetric chambers revealed an increase in energy expenditure of KO animals at the end of the first week of HFD exposure, only in the light phase. Surprisingly, this effect occurred without any increase in food intake contrary to what was observed in the previous cohort, indicating that the effect on EE is independent of food intake. This increase in EE might come from an enhanced sympathetic tone in KO animals, as suggested by their inability to quickly adapt their EE after thermoneutrality. Evaluating markers of SNS activity in the periphery of this KO model may therefore shed light on the possible mechanisms implicated in the observed increase in EE. Besides, repeating indirect calorimetry in chemically sympathectomised animals (after 6-hydroxydopamine injections for instance) might prevent EE increase and induce body weight gain in KO animals.

Taken together, these results suggest a predominant role of POMC-Glut as anorectic neurons in the endostatic regulation of feeding behaviour. This is confirmed by a recent study where a selective restoration of POMC expression in vglut2+ cells was sufficient to normalize body weight and body composition in male and female mice with a hypothalamic POMC *null* background (Jones, Wittmann *et al.* 2019). However, the increase in EE observed in our study in the calorimetric cages, independently from food intake, suggests that POMC-Glut may physiologically favour a reduction in EE, under certain circumstances. Finally, similarly to POMC-GABA, we cannot exclude that different subsets of POMC-Glut exert different actions, so that a global disruption of glutamatergic transmission may provoke concomitant opposite effects. It should also be noted that in this model, vglut2 deletion also affects POMC-Glut/GABA neurons, which are likely to have a different role than POMC-Glut, given their diverse response to HFD observed previously.

Limitations: several limitations in our POMC-vglut2-KO metabolic characterization have to be accounted for. First, we only used male mice in our experiments, even though constitutive vglut2 deletion in POMC neurons differently affects males and females (Dennison, King *et al.* 2016). We should try to replicate our data in female POMC-vglut2-WT/KO mice.

Then, all the mice were individually housed in order to assess individual food intake and avoid confounding effects of feeding behaviour due to the social status. However, such long-term social isolation has various metabolic effects, from increased fat mass to decreased food intake (Sun, Choi *et al.* 2014).

It should also be noted that short-term tamoxifen treatment (such as the one we did in our model) has long-term metabolic effects in mice. Indeed, a 5-days tamoxifen treatment is sufficient to protect mice against diet-induced-obesity and improve glucose metabolism, up to 20 weeks after the end of the treatment (Liu, Cheng *et al.* 2018). For this reason, WT control mice received a similar tamoxifen treatment as KO mice. This protective effect of tamoxifen is probably the reason why, despite 12 weeks of HFD exposure, WT and KO mice had only gained between 5g and 10g of body weight.

Finally, the participation of POMC neurons within the nucleus of the tractus solitarii (NTS) has never been explored in our model. We currently do not know if these neurons have the same neurotransmitter variety than hypothalamic POMC neurons. A GAD/vglut2/POMC co-staining in FISH would then be of interest in WT/KO mice in order to explore the neurotransmitter phenotype of NTS POMC neurons and determine if the consequences of vglut2 deletion are also mediated by glutamatergic NTS POMC transmission.

Perspectives: Future experiments will need to confirm and deepen the characterization of inducible POMC-vglut2-KO mice. First, we will need to reproduce the hyperphagia observed in the first cohort under HFD, since we did not find this phenotype back in the second cohort. One explanation is that mice from the second cohort were placed into calorimetric cages, a more stressful environment, since they are in complete isolation. Another difference is that mice of the first cohort were older that mice of the second cohort, when HFD exposure started (22 weeks vs 17 weeks). Given that mTORC1 pathway is a critical component of POMC neurons physiology (see annexed article) and aging increases mTOR signaling in POMC neurons (Yang, Tien *et al.* 2012), it is therefore possible that an interaction exists between age, HFD exposure and vglut2 deletion in POMC neurons. Thus, we could divide a cohort of mice into different groups that would be exposed to HFD at different ages, to determine if older KO mice are more sensitive to HFD than younger ones.

In addition, we have never looked at glucose metabolism in this model. Since a subset of POMC neurons are glucose-sensitive and control glucose metabolism (Parton, Ye *et al.* 2007), it would be interesting to test the involvement of POMC-Glut in this context. To do so, we could do a series of glucose-, insulin- and pyruvate tolerance tests in chow-fed and HFD-fed WT/KO mice, at different time points throughout their lives.

Moreover, we should perform a preference test between chow and HFD in WT/KO mice. Indeed, if POMC glutamatergic transmission is primarily associated with endostatic regulation of food intake, its suppression in KO animals might lead to an enhanced preference for HFD, by leaving only a functional GABAergic transmission. Of note, such a choice between chow and HFD should be maintained for a long period, to see whether it can influence long-term body weight regulation.

Finally, in order to compare the effects of POMC glutamatergic vs GABAergic transmission, a similar mouse model should be created for the suppression of POMC GABAergic transmission. Since vGat is not expressed in POMC neurons, we could cross $Gad1^{loxP}/Gad2^{loxP}$ mice (in which both Gad1 and Gad2 genes are floxed, The Jackson Laboratory, #031800) with our POMC-$CreER^{T2}$ mice. After tamoxifen treatment, GABA production in POMC neurons would be suppressed in $CreER^{T2}$+ animals. The metabolic characterization of such mice would then give complementary information about the functional relevance of POMC GABAergic transmission in the regulation of energy balance.

❖ General conclusion and long-term research perspectives

***A functional dichotomy between POMC-Glut and POMC-GABA*:** The general aim of this thesis was to characterize different POMC subpopulations based on their neurotransmitter phenotypes and determine if they were functionally equivalent or different. We started with the hypothesis that POMC-Glut and POMC-GABA have opposite roles based on our previous data demonstrating that they were oppositely regulated by rapamycin (see annexed article, Figure 2 and Figure 3). In addition, single-cell transcriptome profiling of adult POMC neurons revealed that POMC-Glut, POMC-GABA and POMC-Glut/GABA neurons have distinct molecular profiles (see annexed article, Figure 1B), reinforcing the idea of a functional segregation. Consistent with this, our data show that POMC-GABA and POMC-Glut/GABA are much more recruited than POMC-Glut by acute HFD exposure and are associated with a hyperphagic behaviour (although a causal link has yet to be demonstrated), suggesting an involvement of POMC-GABA neurons in exostatic regulation of feeding behaviour. On the contrary, POMC-Glut might rather play the classic role of anorectic POMC neurons, based on our POMC-vglut2 inducible deletion data and the effect of the selective POMC re-expression in vglut2 neurons (Jones, Wittmann *et al.* 2019).

Are all POMC-Glut and POMC-GABA the same? Despite the evidence of a functional dichotomy between POMC-Glut and POMC-GABA discussed above, it would be unwise to consider them as homogenous populations. Indeed, even though we observed that 40% of POMC-GABA cells were activated after acute HFD exposure, this also means that 60% of them were not. Similarly, 80% of POMC-Glut neurons did not respond to HFD, but 20% did. This suggests not only that these groups are not homogeneous, but that some POMC-Glut and POMC-GABA might share a similar function. In line with this, when hypothalamic POMC neurons are analysed by single-cell RNA sequencing in an unbiased way, POMC-Glut and POMC-GABA do not fall into distinct clusters (Lam, Cimino *et al.* 2017). Therefore, further studies are needed to fully elucidate the role of different subpopulations of POMC neurons, and perhaps find more relevant markers to better define such functionally distinct subgroups.

***Towards a more precise targeting of POMC-Glut and POMC-GABA*:** in order to expand our understanding of POMC-Glut and POMC-GABA neurons, we could try to acutely manipulate these subpopulations, using pharmaco- and/or optogenetic approaches. An indirect way to do so would be to pharmacogenetically activate all POMC neurons (using a Cre-dependant DREADD in POMC-Cre mice) and inject at the same time either picrotoxin ($GABA_A$ antagonist) or NBQX/APV (glutamate receptor – AMPAR/NMDAR antagonists) in the lateral ventricle or directly in a target region of POMC cells, such has the PVH, in order to block GABAergic or glutamatergic transmission, respectively, under a specific behavioural paradigm. A titration of these drugs should be made, in order to determine a dose for which no effect in food intake is elicited *per se*. Of course, this approach is not the most elegant one, given the off-target effects of GABA/glutamate receptor antagonists.

The biggest challenge is then to express a transgene (e.g. DREADD, channelrhodopsin, fluorescent reporter…) only in POMC-Glut or POMC-GABA neurons. One way to do so would be to use the INTERSECT vectors developed by Karl Deisseroth's lab (Fenno, Mattis *et al.* 2014). Indeed, they have produced viral vectors in which the transgene requires both Cre-recombinase and Flippase (Flip) to be

expressed. Thus, by crossing POMC-Cre mice with vglut2-Flip mice (The Jackson Laboratory, #030212), POMC-Glut neurons in the offspring would co-express Cre and Flip. Using an INTERSECT vector from Deisseroth's lab (Flip- and Cre-dependent), we would then be able to express a transgene only in POMC-Glut neurons. Of note, only few transgenes are available so far (mainly eYFP and channelrhosopsin2). A similar approach could be done in theory by crossing POMC-CreER^{T2} with Gad1-Flip (or Gad2-Flip) mice, but none of them are available so far. The biggest downfall of this technique is that in any case, the POMC-Glut/GABA subpopulation would also be affected by the transgene, in either POMC-Cre-vglut2-Flip or POMC-Cre-Gad-Flip animals.

Then, is there a way to specifically target POMC-GABA, POMC-Glut and POMC-Glut/GABA separately? No, not with the tools that are available to date. However, we can imagine a system in which this could be possible. Indeed, Deisseroth has also developed viruses in which the transgene expression is dependent on Cre-recombinase (**Cre-on**), but also excluded from Flip-expressing cells (**Flip-off**) (or *vice versa* for a **Cre-off/Flip-on** vector) (Fenno, Mattis *et al.* 2014). By crossing vglut2-Flip mice with Gad2-Cre mice (The Jackson Laboratory, #010802), the new mouse line would express Flip in vglut2+ neurons and Cre in GAD65+ neurons. We would finally need to replace the promoter of Deisseroth viral vectors by a POMC promoter and inject the viruses in vglut2-Flip-Gad2-Cre mice to specifically target POMC-GABA, POMC-Glut and POMC-Glut/GABA neurons without overlapping expression, as follows:

- POMC-GABA: injection of a Cre-on/Flip-off vector under a POMC promoter
- POMC-Glut: injection of a Cre-off/Flip-on vector under a POMC promoter
- POMC-Glut/GABA: injection of a Cre-on/Flip-on vector under a POMC promoter

Such approach would open tremendous possibilities in the study of POMC subpopulations, such as specific mapping of neuron projections, pharmaco- or optogenetic modulation, targeted neuronal cell death (with caspase 3 overexpression or diphteric toxin receptor expression followed by diphteric toxin injection), etc. However, setting up these new tools would certainly require a full new PhD project.

References

A.

Abdel-Malek, Z. A. (2001). "Melanocortin receptors: their functions and regulation by physiological agonists and antagonists." Cell Mol Life Sci **58**(3): 434-441.
Albrecht, U. (2012). "Timing to perfection: the biology of central and peripheral circadian clocks." Neuron **74**(2): 246-260.

Andre, C., O. Guzman-Quevedo, C. Rey, J. Remus-Borel, S. Clark, A. Castellanos-Jankiewicz, E. Ladeveze, T. Leste-Lasserre, A. Nadjar, D. N. Abrous, S. Laye and D. Cota (2017). "Inhibiting Microglia Expansion Prevents Diet-Induced Hypothalamic and Peripheral Inflammation." Diabetes **66**(4): 908-919.

Aponte, Y., D. Atasoy and S. M. Sternson (2011). "AGRP neurons are sufficient to orchestrate feeding behaviour rapidly and without training." Nat Neurosci **14**(3): 351-355.

B.

Bagdade, J. D., E. L. Bierman and D. Porte, Jr. (1967). "The significance of basal insulin levels in the evaluation of the insulin response to glucose in diabetic and nondiabetic subjects." J Clin Invest **46**(10): 1549-1557.

Baker, R. A. and M. Herkenham (1995). "Arcuate nucleus neurons that project to the hypothalamic paraventricular nucleus: neuropeptidergic identity and consequences of adrenalectomy on mRNA levels in the rat." J Comp Neurol **358**(4): 518-530.

Balthasar, N., L. T. Dalgaard, C. E. Lee, J. Yu, H. Funahashi, T. Williams, M. Ferreira, V. Tang, R. A. McGovern, C. D. Kenny, L. M. Christiansen, E. Edelstein, B. Choi, O. Boss, C. Aschkenasi, C. Y. Zhang, K. Mountjoy, T. Kishi, J. K. Elmquist and B. B. Lowell (2005). "Divergence of melanocortin pathways in the control of food intake and energy expenditure." Cell **123**(3): 493-505.

Barros, V. N., M. Mundim, L. T. Galindo, S. Bittencourt, M. Porcionatto and L. E. Mello (2015). "The pattern of cFos expression and its refractory period in the brain of rats and monkeys." Frontiers in Cellular Neuroscience **9**(72).

Bell, B., S. Harlan, D. Morgan and K. Rahmouni (2014). "Leptin receptor deletion from POMC neurons increases susceptibility to high fat diet-induced obesity (1126.9)." The FASEB Journal **28**(1_supplement): 1126.1129.

Bellocchio, L., E. Soria-Gomez, C. Quarta, M. Metna-Laurent, P. Cardinal, E. Binder, A. Cannich, A. Delamarre, M. Haring, M. Martin-Fontecha, D. Vega, T. Leste-Lasserre, D. Bartsch, K. Monory, B. Lutz, F. Chaouloff, U. Pagotto, M. Guzman, D. Cota and G. Marsicano (2013). "Activation of the sympathetic nervous system mediates hypophagic and anxiety-like effects of CB(1) receptor blockade." Proc Natl Acad Sci U S A **110**(12): 4786-4791.

Berglund, E. D., C. Liu, J. W. Sohn, T. Liu, M. H. Kim, C. E. Lee, C. R. Vianna, K. W. Williams, Y. Xu and J. K. Elmquist (2013). "Serotonin 2C receptors in pro-opiomelanocortin neurons regulate energy and glucose homeostasis." J Clin Invest **123**(12): 5061-5070.

Berridge, K. C. (2009). "'Liking' and 'wanting' food rewards: brain substrates and roles in eating disorders." Physiology & behaviour **97**(5): 537-550.

Berridge, K. C. and M. L. Kringelbach (2015). "Pleasure systems in the brain." Neuron **86**(3): 646-664.
Bhupathiraju, S. N. and F. B. Hu (2016). "Epidemiology of Obesity and Diabetes and Their Cardiovascular Complications." Circulation research **118**(11): 1723-1735.

Bi, S., Y. J. Kim and F. Zheng (2012). "Dorsomedial hypothalamic NPY and energy balance control." Neuropeptides **46**(6): 309-314.

Blagojevic, M., C. Jinks, A. Jeffery and K. P. Jordan (2010). "Risk factors for onset of osteoarthritis of the knee in older adults: a systematic review and meta-analysis." Osteoarthritis Cartilage **18**(1): 24-33.

Bohula, E. A., S. D. Wiviott, D. K. McGuire, S. E. Inzucchi, J. Kuder, K. Im, C. L. Fanola, A. Qamar, C. Brown, A. Budaj, A. Garcia-Castillo, M. Gupta, L. A. Leiter, N. J. Weissman, H. D. White, T. Patel, B. Francis, W. Miao, C. Perdomo, S. Dhadda, M. P. Bonaca, C. T. Ruff, A. C. Keech, S. R. Smith, M. S. Sabatine and B. M. Scirica (2018). "Cardiovascular Safety of Lorcaserin in Overweight or Obese Patients." New England Journal of Medicine **379**(12): 1107-1117.

Brandt, C., H. Nolte, S. Henschke, L. Engstrom Ruud, M. Awazawa, D. A. Morgan, P. Gabel, H. G. Sprenger, M. E. Hess, S. Gunther, T. Langer, K. Rahmouni, H. Fenselau, M. Kruger and J. C. Bruning (2018). "Food Perception Primes Hepatic ER Homeostasis via Melanocortin-Dependent Control of mTOR Activation." Cell **175**(5): 1321-1335.e1320.

Bray, G. A. (2003). "Low-carbohydrate diets and realities of weight loss." Jama **289**(14): 1853-1855.

Buchwald, H., R. Estok, K. Fahrbach, D. Banel, M. D. Jensen, W. J. Pories, J. P. Bantle and I. Sledge (2009). "Weight and type 2 diabetes after bariatric surgery: systematic review and meta-analysis." Am J Med **122**(3): 248-256.e245.

Bullitt, E. (1990). "Expression of cFos-like protein as a marker for neuronal activity following noxious stimulation in the rat." J Comp Neurol **296**(4): 517-530.

Burnett, C. J., C. Li, E. Webber, E. Tsaousidou, S. Y. Xue, J. C. Bruning and M. J. Krashes (2016). "Hunger-Driven Motivational State Competition." Neuron **92**(1): 187-201.

Butler, A. A. and R. D. Cone (2002). "The melanocortin receptors: Lessons from knockout models." Neuropeptides **36**(2): 77-84.

Butler, A. A., R. A. Kesterson, K. Khong, M. J. Cullen, M. A. Pelleymounter, J. Dekoning, M. Baetscher and R. D. Cone (2000). "A unique metabolic syndrome causes obesity in the melanocortin-3 receptor-deficient mouse." Endocrinology **141**(9): 3518-3521.

C.

Campbell, J. N., E. Z. Macosko, H. Fenselau, T. H. Pers, A. Lyubetskaya, D. Tenen, M. Goldman, A. M. Verstegen, J. M. Resch, S. A. McCarroll, E. D. Rosen, B. B. Lowell and L. T. Tsai (2017). "A molecular census of arcuate hypothalamus and median eminence cell types." Nat Neurosci **20**(3): 484-496.

Cappuccio, F. P., F. M. Taggart, N.-B. Kandala, A. Currie, E. Peile, S. Stranges and M. A. Miller (2008). "Meta-analysis of short sleep duration and obesity in children and adults." Sleep **31**(5): 619-626.

Cardinal, P., C. Andre, C. Quarta, L. Bellocchio, S. Clark, M. Elie, T. Leste-Lasserre, M. Maitre, D. Gonzales, A. Cannich, U. Pagotto, G. Marsicano and D. Cota (2014). "CB1 cannabinoid receptor in SF1-expressing neurons of the ventromedial hypothalamus determines metabolic responses to diet and leptin." Mol Metab **3**(7): 705-716.

Cardinal, P., C. André, C. Quarta, L. Bellocchio, S. Clark, M. Elie, T. Leste-Lasserre, M. Maitre, D. Gonzales, A. Cannich, U. Pagotto, G. Marsicano and D. Cota (2014). "CB1 cannabinoid receptor in SF1-expressing neurons of the ventromedial hypothalamus determines metabolic responses to diet and leptin." Molecular metabolism **3**(7): 705-716.

Cassidy, R. M. and Q. Tong (2017). "Hunger and Satiety Gauge Reward Sensitivity." Frontiers in endocrinology **8**: 104-104.

Cattaneo, S., M. Zaghi, R. Maddalena, F. Bedogni, A. Sessa and S. Taverna (2019). "Somatostatin-Expressing Interneurons Co-Release GABA and Glutamate onto Different Postsynaptic Targets in the Striatum." bioRxiv: 566984.

Cavadas, C., C. A. Aveleira, G. F. Souza and L. A. Velloso (2016). "The pathophysiology of defective proteostasis in the hypothalamus - from obesity to ageing." Nat Rev Endocrinol **12**(12): 723-733.

Chang, S. H., C. R. Stoll, J. Song, J. E. Varela, C. J. Eagon and G. A. Colditz (2014). "The effectiveness and risks of bariatric surgery: an updated systematic review and meta-analysis, 2003-2012." JAMA Surg **149**(3): 275-287.

Chen, Y., Y. C. Lin, T. W. Kuo and Z. A. Knight (2015). "Sensory detection of food rapidly modulates arcuate feeding circuits." Cell **160**(5): 829-841.

Chooi, Y. C., C. Ding and F. Magkos (2019). "The epidemiology of obesity." Metabolism **92**: 6-10.

Ciofi, P., M. Garret, O. Lapirot, P. Lafon, A. Loyens, V. Prevot and J. E. Levine (2009). "Brain-endocrine interactions: a microvascular route in the mediobasal hypothalamus." Endocrinology **150**(12): 5509-5519.

Clement, K., C. Vaisse, N. Lahlou, S. Cabrol, V. Pelloux, D. Cassuto, M. Gourmelen, C. Dina, J. Chambaz, J. M. Lacorte, A. Basdevant, P. Bougneres, Y. Lebouc, P. Froguel and B. Guy-Grand (1998). "A mutation in the human leptin receptor gene causes obesity and pituitary dysfunction." Nature **392**(6674): 398-401.

Colquitt, J. L., K. Pickett, E. Loveman and G. K. Frampton (2014). "Surgery for weight loss in adults." Cochrane Database Syst Rev(8): Cd003641.

Cone, R. D., D. Lu, S. Koppula, D. I. Vage, H. Klungland, B. Boston, W. Chen, D. N. Orth, C. Pouton and R. A. Kesterson (1996). "The melanocortin receptors: agonists, antagonists, and the hormonal control of pigmentation." Recent Prog Horm Res **51**: 287-317; discussion 318.

Considine, R. V., M. K. Sinha, M. L. Heiman, A. Kriauciunas, T. W. Stephens, M. R. Nyce, J. P. Ohannesian, C. C. Marco, L. J. McKee, T. L. Bauer and *et al.* (1996). "Serum immunoreactive-leptin concentrations in normal-weight and obese humans." N Engl J Med **334**(5): 292-295.

Cota, D., K. Proulx and R. J. Seeley (2007). "The Role of CNS Fuel Sensing in Energy and Glucose Regulation." Gastroenterology **132**(6): 2158-2168.

Cota, D., K. Proulx, K. A. Smith, S. C. Kozma, G. Thomas, S. C. Woods and R. J. Seeley (2006). "Hypothalamic mTOR signaling regulates food intake." Science **312**(5775): 927-930.

Coupe, B. and S. G. Bouret (2013). "Development of the hypothalamic melanocortin system." Frontiers in endocrinology **4**: 38-38.

Coupe, B., Y. Ishii, M. O. Dietrich, M. Komatsu, T. L. Horvath and S. G. Bouret (2012). "Loss of autophagy in pro-opiomelanocortin neurons perturbs axon growth and causes metabolic dysregulation." Cell Metab **15**(2): 247-255.

Cummings, D. E., J. Q. Purnell, R. S. Frayo, K. Schmidova, B. E. Wisse and D. S. Weigle (2001). "A preprandial rise in plasma ghrelin levels suggests a role in meal initiation in humans." Diabetes **50**(8): 1714-1719.

D.

Davies, M. J., R. Bergenstal, B. Bode, R. F. Kushner, A. Lewin, T. V. Skjoth, A. H. Andreasen, C. B. Jensen and R. A. DeFronzo (2015). "Efficacy of Liraglutide for Weight Loss Among Patients With Type 2 Diabetes: The SCALE Diabetes Randomized Clinical Trial." Jama **314**(7): 687-699.

Dennison, C. S., C. M. King, M. S. Dicken and S. T. Hentges (2016). "Age-dependent changes in amino acid phenotype and the role of glutamate release from hypothalamic proopiomelanocortin neurons." J Comp Neurol **524**(6): 1222-1235.

Dicken, M. S., A. R. Hughes and S. T. Hentges (2015). "Gad1 mRNA as a reliable indicator of altered GABA release from orexigenic neurons in the hypothalamus." The European journal of neuroscience **42**(9): 2644-2653.

Dicken, M. S., R. E. Tooker and S. T. Hentges (2012). "Regulation of GABA and glutamate release from proopiomelanocortin neuron terminals in intact hypothalamic networks." J Neurosci **32**(12): 4042-4048.

Dietrich, M. O., J. Bober, J. G. Ferreira, L. A. Tellez, Y. S. Mineur, D. O. Souza, X. B. Gao, M. R. Picciotto, I. Araujo, Z. W. Liu and T. L. Horvath (2012). "AgRP neurons regulate development of dopamine neuronal plasticity and nonfood-associated behaviours." Nat Neurosci **15**(8): 1108-1110.

Dikic, I. (2017). "Proteasomal and Autophagic Degradation Systems." Annu Rev Biochem **86**: 193-224.

Djalalinia, S., M. Qorbani, N. Peykari and R. Kelishadi (2015). "Health impacts of Obesity." Pakistan journal of medical sciences **31**(1): 239-242.

Dodd, G. T., S. Decherf, K. Loh, S. E. Simonds, F. Wiede, E. Balland, T. L. Merry, H. Munzberg, Z. Y. Zhang, B. B. Kahn, B. G. Neel, K. K. Bence, Z. B. Andrews, M. A. Cowley and T. Tiganis (2015). "Leptin and insulin act on POMC neurons to promote the browning of white fat." Cell **160**(1-2): 88-104.

E.

Elias, C. F., C. Lee, J. Kelly, C. Aschkenasi, R. S. Ahima, P. R. Couceyro, M. J. Kuhar, C. B. Saper and J. K. Elmquist (1998). "Leptin activates hypothalamic CART neurons projecting to the spinal cord." Neuron **21**(6): 1375-1385.

Elmquist, J. K., C. Bjorbaek, R. S. Ahima, J. S. Flier and C. B. Saper (1998). "Distributions of leptin receptor mRNA isoforms in the rat brain." J Comp Neurol **395**(4): 535-547.

Esclapez, M., N. J. Tillakaratne, D. L. Kaufman, A. J. Tobin and C. R. Houser (1994). "Comparative localization of two forms of glutamic acid decarboxylase and their mRNAs in rat brain supports the concept of functional differences between the forms." J Neurosci **14**(3 Pt 2): 1834-1855.

F.

Faget, L. and T. S. Hnasko (2015). "Tyramide Signal Amplification for Immunofluorescent Enhancement." Methods Mol Biol **1318**: 161-172.

Farooqi, I. S. and S. O'Rahilly (2005). "Monogenic obesity in humans." Annu Rev Med **56**: 443-458.

Farooqi, I. S. and S. O'Rahilly (2008). "Mutations in ligands and receptors of the leptin-melanocortin pathway that lead to obesity." Nat Clin Pract Endocrinol Metab **4**(10): 569-577.

Farrell, R. E. (2010). Chapter 8 - Stringency: Conditions that Influence Nucleic Acid Structure. RNA Methodologies (Fourth Edition). R. E. Farrell. San Diego, Academic Press**:** 173-178.

Feil, S., N. Valtcheva and R. Feil (2009). "Inducible Cre mice." Methods Mol Biol **530**: 343-363.

Felker, A., S. Nieuwenhuize, A. Dolbois, K. Blazkova, C. Hess, L. W. L. Low, S. Burger, N. Samson, T. J. Carney, P. Bartunek, C. Nevado and C. Mosimann (2016). "In Vivo Performance and Properties of Tamoxifen Metabolites for CreERT2 Control." PloS one **11**(4): e0152989-e0152989.

Fenno, L. E., J. Mattis, C. Ramakrishnan, M. Hyun, S. Y. Lee, M. He, J. Tucciarone, A. Selimbeyoglu, A. Berndt, L. Grosenick, K. A. Zalocusky, H. Bernstein, H. Swanson, C. Perry, I. Diester, F. M. Boyce, C. E. Bass, R. Neve, Z. J. Huang and K. Deisseroth (2014). "Targeting cells with single vectors using multiple-feature Boolean logic." Nature methods **11**(7): 763-772.

Fioramonti, X., Z. Song, R. P. Vazirani, A. Beuve and V. H. Routh (2011). "Hypothalamic nitric oxide in hypoglycemia detection and counterregulation: a two-edged sword." Antioxid Redox Signal **14**(3): 505-517.

Fox, K. R. and M. Hillsdon (2007). "Physical activity and obesity." Obes Rev **8 Suppl 1**: 115-121.

Frayling, T. M. (2012). "Are the causes of obesity primarily environmental? No." BMJ : British Medical Journal **345**: e5844.

Fremeau, R. T., Jr., S. Voglmaier, R. P. Seal and R. H. Edwards (2004). "VGLUTs define subsets of excitatory neurons and suggest novel roles for glutamate." Trends Neurosci **27**(2): 98-103.

Fulton, S., P. Pissios, Ramon P. Manchon, L. Stiles, L. Frank, E. N. Pothos, E. Maratos-Flier and J. S. Flier (2006). "Leptin Regulation of the Mesoaccumbens Dopamine Pathway." Neuron **51**(6): 811-822.

G.

Gallagher, D., S. B. Heymsfield, M. Heo, S. A. Jebb, P. R. Murgatroyd and Y. Sakamoto (2000). "Healthy percentage body fat ranges: an approach for developing guidelines based on body mass index." Am J Clin Nutr **72**(3): 694-701.

Gallagher, D., M. Visser, D. Sepulveda, R. N. Pierson, T. Harris and S. B. Heymsfield (1996). "How useful is body mass index for comparison of body fatness across age, sex, and ethnic groups?" Am J Epidemiol **143**(3): 228-239.

Gao, Y.-J. and R.-R. Ji (2009). "cFos and pERK, which is a better marker for neuronal activation and central sensitization after noxious stimulation and tissue injury?" The open pain journal **2**: 11-17.

Garcia-Caceres, C., E. Balland, V. Prevot, S. Luquet, S. C. Woods, M. Koch, T. L. Horvath, C. X. Yi, J. A. Chowen, A. Verkhratsky, A. Araque, I. Bechmann and M. H. Tschop (2019). "Role of astrocytes, microglia, and tanycytes in brain control of systemic metabolism." Nat Neurosci **22**(1): 7-14.

Greenman, Y., Y. Kuperman, Y. Drori, S. L. Asa, I. Navon, O. Forkosh, S. Gil, N. Stern and A. Chen (2013). "Postnatal ablation of POMC neurons induces an obese phenotype characterized by decreased food intake and enhanced anxiety-like behaviour." Mol Endocrinol **27**(7): 1091-1102.

Greenway, F. L., K. Fujioka, R. A. Plodkowski, S. Mudaliar, M. Guttadauria, J. Erickson, D. D. Kim and E. Dunayevich (2010). "Effect of naltrexone plus bupropion on weight loss in overweight and obese adults (COR-I): a multicentre, randomised, double-blind, placebo-controlled, phase 3 trial." Lancet **376**(9741): 595-605.

H.

Haissaguerre, M., N. Saucisse and D. Cota (2014). "Influence of mTOR in energy and metabolic homeostasis." Mol Cell Endocrinol **397**(1-2): 67-77.

Hall, K. D. and J. Guo (2017). "Obesity Energetics: Body Weight Regulation and the Effects of Diet Composition." Gastroenterology **152**(7): 1718-1727.e1713.

Hebert, J. R., D. B. Allison, E. Archer, C. J. Lavie and S. N. Blair (2013). "Scientific Decision Making, Policy Decisions, and the Obesity Pandemic." Mayo Clinic Proceedings **88**(6): 593-604.

Heeley, N. and C. Blouet (2016). "Central Amino Acid Sensing in the Control of Feeding Behaviour." Frontiers in endocrinology **7**: 148-148.

Hentges, S. T., M. Nishiyama, L. S. Overstreet, M. Stenzel-Poore, J. T. Williams and M. J. Low (2004). "GABA release from proopiomelanocortin neurons." J Neurosci **24**(7): 1578-1583.

Hentges, S. T., V. Otero-Corchon, R. L. Pennock, C. M. King and M. J. Low (2009). "Proopiomelanocortin expression in both GABA and glutamate neurons." J Neurosci **29**(43): 13684-13690.

Higginson, A. D., J. M. McNamara and A. I. Houston (2016). "Fatness and fitness: exposing the logic of evolutionary explanations for obesity." Proceedings. Biological sciences **283**(1822): 20152443.
Hommel, J. D., R. Trinko, R. M. Sears, D. Georgescu, Z.-W. Liu, X.-B. Gao, J. J. Thurmon, M. Marinelli and R. J. DiLeone (2006). "Leptin Receptor Signaling in Midbrain Dopamine Neurons Regulates Feeding." Neuron **51**(6): 801-810.

Hopman, A. H., F. C. Ramaekers and E. J. Speel (1998). "Rapid synthesis of biotin-, digoxigenin-, trinitrophenyl-, and fluorochrome-labeled tyramides and their application for *In situ* hybridization using CARD amplification." J Histochem Cytochem **46**(6): 771-777.

Horvath, T. L., S. Diano, P. Sotonyi, M. Heiman and M. Tschop (2001). "Minireview: ghrelin and the regulation of energy balance--a hypothalamic perspective." Endocrinology **142**(10): 4163-4169.

Hrabovszky, E. and S. L. Petersen (2002). "Increased concentrations of radioisotopically-labeled complementary ribonucleic acid probe, dextran sulfate, and dithiothreitol in the hybridization buffer can improve results of *in situ* hybridization histochemistry." J Histochem Cytochem **50**(10): 1389-1400.

Hruby, A., J. E. Manson, L. Qi, V. S. Malik, E. B. Rimm, Q. Sun, W. C. Willett and F. B. Hu (2016). "Determinants and Consequences of Obesity." American journal of public health **106**(9): 1656-1662.

Hu, F. B. (2003). "Sedentary lifestyle and risk of obesity and type 2 diabetes." Lipids **38**(2): 103-108.

Hu, J., L. Jiang, M. J. Low and L. Rui (2014). "Glucose rapidly induces different forms of excitatory synaptic plasticity in hypothalamic POMC neurons." PLoS One **9**(8): e105080.

Huo, R., T. Du, Y. Xu, W. Xu, X. Chen, K. Sun and X. Yu (2015). "Effects of Mediterranean-style diet on glycemic control, weight loss and cardiovascular risk factors among type 2 diabetes individuals: a meta-analysis." Eur J Clin Nutr **69**(11): 1200-1208.

Hurst, J. L. and R. S. West (2010). "Taming anxiety in laboratory mice." Nat Methods **7**(10): 825-826.

J.

J.F, S. and D. Russell (2001). Molecular Cloning: A Laboratory Manual (3-Volume Set).

Jais, A. and J. C. Bruning (2017). "Hypothalamic inflammation in obesity and metabolic disease." J Clin Invest **127**(1): 24-32.

Jansson, J.-O., V. Palsdottir, D. A. Hägg, E. Schéle, S. L. Dickson, F. Anesten, T. Bake, M. Montelius, J. Bellman, M. E. Johansson, R. D. Cone, D. J. Drucker, J. Wu, B. Aleksic, A. E. Törnqvist, K. Sjögren, J.-Å. Gustafsson, S. H. Windahl and C. Ohlsson (2018). "Body weight homeostat that regulates fat mass independently of leptin in rats and mice." Proceedings of the National Academy of Sciences **115**(2): 427.

Jarvie, B. C. and S. T. Hentges (2012). "Expression of GABAergic and glutamatergic phenotypic markers in hypothalamic proopiomelanocortin neurons." J Comp Neurol **520**(17): 3863-3876.

Jarvie, B. C., C. M. King, A. R. Hughes, M. S. Dicken, C. S. Dennison and S. T. Hentges (2017). "Caloric restriction selectively reduces the GABAergic phenotype of mouse hypothalamic proopiomelanocortin neurons." The Journal of physiology **595**(2): 571-582.

Jensen, E. V. and V. C. Jordan (2003). "The Estrogen Receptor." Clinical Cancer Research **9**(6): 1980.

Ji, R. R., H. Baba, G. J. Brenner and C. J. Woolf (1999). "Nociceptive-specific activation of ERK in spinal neurons contributes to pain hypersensitivity." Nat Neurosci **2**(12): 1114-1119.

Jones, G. L., G. Wittmann, E. B. Yokosawa, H. Yu, A. J. Mercer, R. M. Lechan and M. J. Low (2019). "Selective Restoration of Pomc Expression in Glutamatergic POMC Neurons: Evidence for a Dynamic Hypothalamic Neurotransmitter Network." eneuro **6**(2): ENEURO.0400-0418.2019.

K.

Kadouh, H. C. and A. Acosta (2017). "Current paradigms in the etiology of obesity." Techniques in Gastrointestinal Endoscopy **19**(1): 2-11.

Kelly, T., W. Yang, C. S. Chen, K. Reynolds and J. He (2008). "Global burden of obesity in 2005 and projections to 2030." Int J Obes (Lond) **32**(9): 1431-1437.

Kennedy, G. C. (1953). "The role of depot fat in the hypothalamic control of food intake in the rat." Proc R Soc Lond B Biol Sci **140**(901): 578-596.

Knight, Z. A., K. Tan, K. Birsoy, S. Schmidt, J. L. Garrison, R. W. Wysocki, A. Emiliano, M. I. Ekstrand and J. M. Friedman (2012). "Molecular profiling of activated neurons by phosphorylated ribosome capture." Cell **151**(5): 1126-1137.

Koch, M., L. Varela, J. G. Kim, J. D. Kim, F. Hernandez-Nuno, S. E. Simonds, C. M. Castorena, C. R. Vianna, J. K. Elmquist, Y. M. Morozov, P. Rakic, I. Bechmann, M. A. Cowley, K. Szigeti-Buck, M. O. Dietrich, X. B. Gao, S. Diano and T. L. Horvath (2015). "Hypothalamic POMC neurons promote cannabinoid-induced feeding." Nature **519**(7541): 45-50.

Kovner, I., G. Z. Taicher and A. D. Mitchell (2010). "Calibration and validation of EchoMRI™ whole body composition analysis based on chemical analysis of piglets, in comparison with the same for DXA." International journal of body composition research **8**(1): 17-29.

Kraemer, W. J., J. C. Torine, R. Silvestre, D. N. French, N. A. Ratamess, B. A. Spiering, D. L. Hatfield, J. L. Vingren and J. S. Volek (2005). "Body size and composition of National Football League players." J Strength Cond Res **19**(3): 485-489.

Kyle, T. K., E. J. Dhurandhar and D. B. Allison (2016). "Regarding Obesity as a Disease: Evolving Policies and Their Implications." Endocrinology and metabolism clinics of North America **45**(3): 511-520.

L.

Lam, B. Y. H., I. Cimino, J. Polex-Wolf, S. Nicole Kohnke, D. Rimmington, V. Iyemere, N. Heeley, C. Cossetti, R. Schulte, L. R. Saraiva, D. W. Logan, C. Blouet, S. O'Rahilly, A. P. Coll and G. S. H. Yeo (2017). "Heterogeneity of hypothalamic pro-opiomelanocortin-expressing neurons revealed by single-cell RNA sequencing." Mol Metab **6**(5): 383-392.

Laplante, M. and D. M. Sabatini (2012). "mTOR signaling in growth control and disease." Cell **149**(2): 274-293.

Lauter, G., I. Söll and G. Hauptmann (2011). "Multicolor fluorescent *in situ* hybridization to define abutting and overlapping gene expression in the embryonic zebrafish brain." Neural development **6**: 10-10.

Le Foll, C. (2019). "Hypothalamic Fatty Acids and Ketone Bodies Sensing and Role of FAT/CD36 in the Regulation of Food Intake." Frontiers in Physiology **10**(1036).

Le Thuc, O., K. Stobbe, C. Cansell, J.-L. Nahon, N. Blondeau and C. Rovère (2017). "Hypothalamic Inflammation and Energy Balance Disruptions: Spotlight on Chemokines." Frontiers in endocrinology **8**: 197-197.

Liu, G., S. Amin, N. N. Okuhama, G. Liao and L. A. Mingle (2006). "A quantitative evaluation of peroxidase inhibitors for tyramide signal amplification mediated cytochemistry and histochemistry." Histochemistry and cell biology **126**(2): 283-291.

Liu, S. and S. L. Borgland (2019). "Insulin actions in the mesolimbic dopamine system." Exp Neurol **320**: 113006.

Liu, Z., Y. Cheng, Y. Luan, W. Zhong, H. Lai, H. Wang, H. Yu, Y. Yang, N. Feng, F. Yuan, R. Huang, Z. He, F. Zhang, M. Yan, H. Yin, F. Guo and Q. Zhai (2018). "Short-term tamoxifen treatment has long-term effects on metabolism in high-fat diet-fed mice with involvement of Nmnat2 in POMC neurons." FEBS Lett **592**(19): 3305-3316.

Locke, A. E., B. Kahali, S. I. Berndt, A. E. Justice, T. H. Pers, F. R. Day, C. Powell, S. Vedantam, M. L. Buchkovich, J. Yang, D. C. Croteau-Chonka, T. Esko, T. Fall, T. Ferreira, S. Gustafsson, Z. Kutalik, J. Luan, R. Magi, J. C. Randall, T. W. Winkler, A. R. Wood, T. Workalemahu, J. D. Faul, J. A. Smith, J. H. Zhao, W. Zhao, J. Chen, R. Fehrmann, A. K. Hedman, J. Karjalainen, E. M. Schmidt, D. Absher, N. Amin, D. Anderson, M. Beekman, J. L. Bolton, J. L. Bragg-Gresham, S. Buyske, A. Demirkan, G. Deng, G. B. Ehret, B. Feenstra, M. F. Feitosa, K. Fischer, A. Goel, J. Gong, A. U. Jackson, S. Kanoni, M. E. Kleber, K. Kristiansson, U. Lim, V. Lotay, M. Mangino, I. M. Leach, C. Medina-Gomez, S. E. Medland, M. A. Nalls, C. D. Palmer, D. Pasko, S. Pechlivanis, M. J. Peters, I. Prokopenko, D. Shungin, A. Stancakova, R. J.

Strawbridge, Y. J. Sung, T. Tanaka, A. Teumer, S. Trompet, S. W. van der Laan, J. van Setten, J. V. Van Vliet-Ostaptchouk, Z. Wang, L. Yengo, W. Zhang, A. Isaacs, E. Albrecht, J. Arnlov, G. M. Arscott, A. P. Attwood, S. Bandinelli, A. Barrett, I. N. Bas, C. Bellis, A. J. Bennett, C. Berne, R. Blagieva, M. Bluher, S. Bohringer, L. L. Bonnycastle, Y. Bottcher, H. A. Boyd, M. Bruinenberg, I. H. Caspersen, Y. I. Chen, R. Clarke, E. W. Daw, A. J. M. de Craen, G. Delgado, M. Dimitriou, A. S. F. Doney, N. Eklund, K. Estrada, E. Eury, L. Folkersen, R. M. Fraser, M. E. Garcia, F. Geller, V. Giedraitis, B. Gigante, A. S. Go, A. Golay, A. H. Goodall, S. D. Gordon, M. Gorski, H. J. Grabe, H. Grallert, T. B. Grammer, J. Grassler, H. Gronberg, C. J. Groves, G. Gusto, J. Haessler, P. Hall, T. Haller, G. Hallmans, C. A. Hartman, M. Hassinen, C. Hayward, N. L. Heard-Costa, Q. Helmer, C. Hengstenberg, O. Holmen, J. J. Hottenga, A. L. James, J. M. Jeff, A. Johansson, J. Jolley, T. Juliusdottir, L. Kinnunen, W. Koenig, M. Koskenvuo, W. Kratzer, J. Laitinen, C. Lamina, K. Leander, N. R. Lee, P. Lichtner, L. Lind, J. Lindstrom, K. S. Lo, S. Lobbens, R. Lorbeer, Y. Lu, F. Mach, P. K. E. Magnusson, A. Mahajan, W. L. McArdle, S. McLachlan, C. Menni, S. Merger, E. Mihailov, L. Milani, A. Moayyeri, K. L. Monda, M. A. Morken, A. Mulas, G. Muller, M. Muller-Nurasyid, A. W. Musk, R. Nagaraja, M. M. Nothen, I. M. Nolte, S. Pilz, N. W. Rayner, F. Renstrom, R. Rettig, J. S. Ried, S. Ripke, N. R. Robertson, L. M. Rose, S. Sanna, H. Scharnagl, S. Scholtens, F. R. Schumacher, W. R. Scott, T. Seufferlein, J. Shi, A. V. Smith, J. Smolonska, A. V. Stanton, V. Steinthorsdottir, K. Stirrups, H. M. Stringham, J. Sundstrom, M. A. Swertz, A. J. Swift, A. C. Syvanen, S. T. Tan, B. O. Tayo, B. Thorand, G. Thorleifsson, J. P. Tyrer, H. W. Uh, L. Vandenput, F. C. Verhulst, S. H. Vermeulen, N. Verweij, J. M. Vonk, L. L. Waite, H. R. Warren, D. Waterworth, M. N. Weedon, L. R. Wilkens, C. Willenborg, T. Wilsgaard, M. K. Wojczynski, A. Wong, A. F. Wright, Q. Zhang, E. P. Brennan, M. Choi, Z. Dastani, A. W. Drong, P. Eriksson, A. Franco-Cereceda, J. R. Gadin, A. G. Gharavi, M. E. Goddard, R. E. Handsaker, J. Huang, F. Karpe, S. Kathiresan, S. Keildson, K. Kiryluk, M. Kubo, J. Y. Lee, L. Liang, R. P. Lifton, B. Ma, S. A. McCarroll, A. J. McKnight, J. L. Min, M. F. Moffatt, G. W. Montgomery, J. M. Murabito, G. Nicholson, D. R. Nyholt, Y. Okada, J. R. B. Perry, R. Dorajoo, E. Reinmaa, R. M. Salem, N. Sandholm, R. A. Scott, L. Stolk, A. Takahashi, T. Tanaka, F. M. van 't Hooft, A. A. E. Vinkhuyzen, H. J. Westra, W. Zheng, K. T. Zondervan, A. C. Heath, D. Arveiler, S. J. L. Bakker, J. Beilby, R. N. Bergman, J. Blangero, P. Bovet, H. Campbell, M. J. Caulfield, G. Cesana, A. Chakravarti, D. I. Chasman, P. S. Chines, F. S. Collins, D. C. Crawford, L. A. Cupples, D. Cusi, J. Danesh, U. de Faire, H. M. den Ruijter, A. F. Dominiczak, R. Erbel, J. Erdmann, J. G. Eriksson, M. Farrall, S. B. Felix, E. Ferrannini, J. Ferrieres, I. Ford, N. G. Forouhi, T. Forrester, O. H. Franco, R. T. Gansevoort, P. V. Gejman, C. Gieger, O. Gottesman, V. Gudnason, U. Gyllensten, A. S. Hall, T. B. Harris, A. T. Hattersley, A. A. Hicks, L. A. Hindorff, A. D. Hingorani, A. Hofman, G. Homuth, G. K. Hovingh, S. E. Humphries, S. C. Hunt, E. Hypponen, T. Illig, K. B. Jacobs, M. R. Jarvelin, K. H. Jockel, B. Johansen, P. Jousilahti, J. W. Jukema, A. M. Jula, J. Kaprio, J. J. P. Kastelein, S. M. Keinanen-Kiukaanniemi, L. A. Kiemeney, P. Knekt, J. S. Kooner, C. Kooperberg, P. Kovacs, A. T. Kraja, M. Kumari, J. Kuusisto, T. A. Lakka, C. Langenberg, L. L. Marchand, T. Lehtimaki, V. Lyssenko, S. Mannisto, A. Marette, T. C. Matise, C. A. McKenzie, B. McKnight, F. L. Moll, A. D. Morris, A. P. Morris, J. C. Murray, M. Nelis, C. Ohlsson, A. J. Oldehinkel, K. K. Ong, P. A. F. Madden, G. Pasterkamp, J. F. Peden, A. Peters, D. S. Postma, P. P. Pramstaller, J. F. Price, L. Qi, O. T. Raitakari, T. Rankinen, D. C. Rao, T. K. Rice, P. M. Ridker, J. D. Rioux, M. D. Ritchie, I. Rudan, V. Salomaa, N. J. Samani, J. Saramies, M. A. Sarzynski, H. Schunkert, P. E. H. Schwarz, P. Sever, A. R. Shuldiner, J. Sinisalo, R. P. Stolk, K. Strauch, A. Tonjes, D. A. Tregouet, A. Tremblay, E. Tremoli, J. Virtamo, M. C. Vohl, U. Volker, G. Waeber, G. Willemsen, J. C. Witteman, M. C. Zillikens, L. S. Adair, P. Amouyel, F. W. Asselbergs, T. L. Assimes, M. Bochud, B. O. Boehm, E. Boerwinkle, S. R. Bornstein, E. P. Bottinger, C. Bouchard, S. Cauchi, J. C. Chambers, S. J. Chanock, R. S. Cooper, P. I. W. de Bakker, G. Dedoussis, L. Ferrucci, P. W. Franks, P. Froguel, L. C. Groop, C. A. Haiman, A. Hamsten, J. Hui, D. J. Hunter, K. Hveem, R. C. Kaplan, M. Kivimaki, D. Kuh, M. Laakso, Y. Liu, N. G. Martin, W. Marz, M. Melbye, A. Metspalu, S. Moebus, P. B. Munroe, I. Njolstad, B. A. Oostra, C. N. A. Palmer, N. L. Pedersen, M. Perola, L. Perusse, U. Peters, C. Power, T. Quertermous, R. Rauramaa, F. Rivadeneira, T. E. Saaristo, D. Saleheen, N. Sattar, E. E. Schadt, D. Schlessinger, P. E. Slagboom, H. Snieder, T. D. Spector, U. Thorsteinsdottir, M. Stumvoll, J. Tuomilehto, A. G. Uitterlinden, M. Uusitupa, P. van der Harst, M. Walker, H. Wallaschofski, N. J. Wareham, H. Watkins, D. R. Weir, H. E. Wichmann, J. F.

Wilson, P. Zanen, I. B. Borecki, P. Deloukas, C. S. Fox, I. M. Heid, J. R. O'Connell, D. P. Strachan, K. Stefansson, C. M. van Duijn, G. R. Abecasis, L. Franke, T. M. Frayling, M. I. McCarthy, P. M. Visscher, A. Scherag, C. J. Willer, M. Boehnke, K. L. Mohlke, C. M. Lindgren, J. S. Beckmann, I. Barroso, K. E. North, E. Ingelsson, J. N. Hirschhorn, R. J. F. Loos and E. K. Speliotes (2015). "Genetic studies of body mass index yield new insights for obesity biology." Nature **518**(7538): 197-206.

Lopez-Gambero, A. J., F. Martinez, K. Salazar, M. Cifuentes and F. Nualart (2019). "Brain Glucose-Sensing Mechanism and Energy Homeostasis." Mol Neurobiol **56**(2): 769-796.

Lopomo, A., E. Burgio and L. Migliore (2016). "Epigenetics of Obesity." Prog Mol Biol Transl Sci **140**: 151-184.

M.

Madisen, L., T. A. Zwingman, S. M. Sunkin, S. W. Oh, H. A. Zariwala, H. Gu, L. L. Ng, R. D. Palmiter, M. J. Hawrylycz, A. R. Jones, E. S. Lein and H. Zeng (2010). "A robust and high-throughput Cre reporting and characterization system for the whole mouse brain." Nat Neurosci **13**(1): 133-140.

Meldrum, D. R., M. A. Morris and J. C. Gambone (2017). "Obesity pandemic: causes, consequences, and solutions-but do we have the will?" Fertil Steril **107**(4): 833-839.

Mitchel, J. S. and R. E. Keesey (1977). "Defense of a lowered weight maintenance level by lateral hypothamically lesioned rats: evidence from a restriction-refeeding regimen." Physiol Behav **18**(6): 1121-1125.

Moechars, D., M. C. Weston, S. Leo, Z. Callaerts-Vegh, I. Goris, G. Daneels, A. Buist, M. Cik, P. van der Spek, S. Kass, T. Meert, R. D'Hooge, C. Rosenmund and R. M. Hampson (2006). "Vesicular Glutamate Transporter VGLUT2 Expression Levels Control Quantal Size and Neuropathic Pain." The Journal of Neuroscience **26**(46): 12055-12066.

Montague, C. T., I. S. Farooqi, J. P. Whitehead, M. A. Soos, H. Rau, N. J. Wareham, C. P. Sewter, J. E. Digby, S. N. Mohammed, J. A. Hurst, C. H. Cheetham, A. R. Earley, A. H. Barnett, J. B. Prins and S. O'Rahilly (1997). "Congenital leptin deficiency is associated with severe early-onset obesity in humans." Nature **387**(6636): 903-908.

Munzberg, H., J. S. Flier and C. Bjorbaek (2004). "Region-specific leptin resistance within the hypothalamus of diet-induced obese mice." Endocrinology **145**(11): 4880-4889.

Myers, Martin G., Jr. (2015). "Leptin Keeps Working, Even in Obesity." Cell Metabolism **21**(6): 791-792.

O.

Ohlsson, C., D. A. Hagg, F. Hammarhjelm, A. Dalmau Gasull, J. Bellman, S. H. Windahl, V. Palsdottir and J. O. Jansson (2018). "The Gravitostat Regulates Fat Mass in Obese Male Mice While Leptin Regulates Fat Mass in Lean Male Mice." Endocrinology **159**(7): 2676-2682.

Olofsson, L. E., E. K. Unger, C. C. Cheung and A. W. Xu (2013). "Modulation of AgRP-neuronal function by SOCS3 as an initiating event in diet-induced hypothalamic leptin resistance." Proc Natl Acad Sci U S A **110**(8): E697-706.

Ottaway, N., P. Mahbod, B. Rivero, Lee A. Norman, A. Gertler, David A. D'Alessio and D. Perez-Tilve (2015). "Diet-Induced Obese Mice Retain Endogenous Leptin Action." Cell Metabolism **21**(6): 877-882.

P.

Padilla, S. L., J. S. Carmody and L. M. Zeltser (2010). "Pomc-expressing progenitors give rise to antagonistic neuronal populations in hypothalamic feeding circuits." Nat Med **16**(4): 403-405.

Padilla, S. L., D. Reef and L. M. Zeltser (2012). "Defining POMC neurons using transgenic reagents: impact of transient Pomc expression in diverse immature neuronal populations." Endocrinology **153**(3): 1219-1231.

Pandit, R., A. Omrani, M. C. M. Luijendijk, V. A. J. de Vrind, A. J. Van Rozen, R. J. A. O. Ophuis, K. Garner, I. Kallo, A. Ghanem, Z. Liposits, K.-K. Conzelmann, L. J. M. J. Vanderschuren, S. E. la Fleur and R. A. H. Adan (2016). "Melanocortin 3 Receptor Signaling in Midbrain Dopamine Neurons Increases the Motivation for Food Reward." Neuropsychopharmacology **41**(9): 2241-2251.

Parton, L. E., C. P. Ye, R. Coppari, P. J. Enriori, B. Choi, C. Y. Zhang, C. Xu, C. R. Vianna, N. Balthasar, C. E. Lee, J. K. Elmquist, M. A. Cowley and B. B. Lowell (2007). "Glucose sensing by POMC neurons regulates glucose homeostasis and is impaired in obesity." Nature **449**(7159): 228-232.

Piazza, P. V., D. Cota and G. Marsicano (2017). "The CB1 Receptor as the Cornerstone of Exostasis." Neuron **93**(6): 1252-1274.

Plourde, B., J.-F. Sarrazin, I. Nault and P. Poirier (2014). "Sudden cardiac death and obesity." Expert review of cardiovascular therapy **12**: 1099-1110.

Plum, L., M. Schubert and J. C. Brüning (2005). "The role of insulin receptor signaling in the brain." Trends in Endocrinology & Metabolism **16**(2): 59-65.

Purnell, J. (2018). Definitions, Classification, and Epidemiology of Obesity. Endotext.org.

Q.

Quarta, C., X. Fioramonti and D. Cota (2019). "POMC Neurons Dysfunction in Diet-induced Metabolic Disease: Hallmark or Mechanism of Disease?" Neuroscience.

R.

Rahman, M. and A. B. Berenson (2010). "Accuracy of current body mass index obesity classification for white, black, and Hispanic reproductive-age women." Obstet Gynecol **115**(5): 982-988.

Ramírez, S., A. G. Gómez-Valadés, M. Schneeberger, L. Varela, R. Haddad-Tóvolli, J. Altirriba, E. Noguera, A. Drougard, Á. Flores-Martínez, M. Imbernón, I. Chivite, M. Pozo, A. Vidal-Itriago, A. Garcia, S. Cervantes, R. Gasa, R. Nogueiras, P. Gama-Pérez, P. M. Garcia-Roves, D. A. Cano, C. Knauf, J.-M. Servitja, T. L. Horvath, R. Gomis, A. Zorzano and M. Claret (2017). "Mitochondrial Dynamics Mediated by Mitofusin 1 Is Required for POMC Neuron Glucose-Sensing and Insulin Release Control." Cell Metabolism **25**(6): 1390-1399.e1396.

Ravussin, Y., R. Gutman, C. A. LeDuc and R. L. Leibel (2013). "Estimating energy expenditure in mice using an energy balance technique." International journal of obesity (2005) **37**(3): 399-403.

Rexrode, K. M., C. H. Hennekens, W. C. Willett, G. A. Colditz, M. J. Stampfer, J. W. Rich-Edwards, F. E. Speizer and J. E. Manson (1997). "A prospective study of body mass index, weight change, and risk of stroke in women." Jama **277**(19): 1539-1545.

Roberto, C. A., B. Swinburn, C. Hawkes, T. T. K. Huang, S. A. Costa, M. Ashe, L. Zwicker, J. H. Cawley and K. D. Brownell (2015). "Patchy progress on obesity prevention: emerging examples, entrenched barriers, and new thinking." The Lancet **385**(9985): 2400-2409.

Rosen, H. (2014). "Is Obesity A Disease or A Behaviour Abnormality? Did the AMA Get It Right?" Missouri medicine **111**(2): 104-108.

Rothwell, N. J. and M. J. Stock (1979). "Regulation of energy balance in two models of reversible obesity in the rat." J Comp Physiol Psychol **93**(6): 1024-1034.

Ruban, A., K. Stoenchev, H. Ashrafian and J. Teare (2019). "Current treatments for obesity." Clinical medicine (London, England) **19**(3): 205-212.

Runge, C. F. (2007). "Economic Consequences of the Obese." Diabetes **56**(11): 2668.

S.

Salmon, A. B. (2016). "Beyond Diabetes: Does Obesity-Induced Oxidative Stress Drive the Aging Process?" Antioxidants (Basel, Switzerland) **5**(3): 24.

Santesso, N., E. A. Akl, M. Bianchi, A. Mente, R. Mustafa, D. Heels-Ansdell and H. J. Schunemann (2012). "Effects of higher- versus lower-protein diets on health outcomes: a systematic review and meta-analysis." Eur J Clin Nutr **66**(7): 780-788.

Santoro, A., M. Campolo, C. Liu, H. Sesaki, R. Meli, Z.-W. Liu, J. D. Kim and S. Diano (2017). "DRP1 Suppresses Leptin and Glucose Sensing of POMC Neurons." Cell Metabolism **25**(3): 647-660.

Schneeberger, M., M. O. Dietrich, D. Sebastián, M. Imbernón, C. Castaño, A. Garcia, Y. Esteban, A. Gonzalez-Franquesa, I. C. Rodríguez, A. Bortolozzi, P. M. Garcia-Roves, R. Gomis, R. Nogueiras, T. L. Horvath, A. Zorzano and M. Claret (2013). "Mitofusin 2 in POMC neurons connects ER stress with leptin resistance and energy imbalance." Cell **155**(1): 172-187.

Schneeberger, M., R. Gomis and M. Claret (2014). "Hypothalamic and brainstem neuronal circuits controlling homeostatic energy balance." J Endocrinol **220**(2): T25-46.

Schrepfer, E. and L. Scorrano (2016). "Mitofusins, from Mitochondria to Metabolism." Molecular Cell **61**(5): 683-694.

Schwartz, G. J. and L. M. Zeltser (2013). "Functional organization of neuronal and humoral signals regulating feeding behaviour." Annu Rev Nutr **33**: 1-21.

Serra-Juhé, C., G. Á. Martos-Moreno, F. Bou de Pieri, R. Flores, J. A. Chowen, L. A. Pérez-Jurado and J. Argente (2019). "Heterozygous rare genetic variants in non-syndromic early-onset obesity." International Journal of Obesity.

Sinigaglia, C., D. Thiel, A. Hejnol, E. Houliston and L. Leclère (2017). "A safer, urea-based *in situ* hybridization method improves detection of gene expression in diverse animal species." bioRxiv: 133470.

Sohn, J. W., Y. Xu, J. E. Jones, K. Wickman, K. W. Williams and J. K. Elmquist (2011). "Serotonin 2C receptor activates a distinct population of arcuate pro-opiomelanocortin neurons via TRPC channels." Neuron **71**(3): 488-497.

Speakman, J. R. (2007). "A nonadaptive scenario explaining the genetic predisposition to obesity: the "predation release" hypothesis." Cell Metab **6**(1): 5-12.

Speakman, J. R. (2018). "The evolution of body fatness: trading off disease and predation risk." The Journal of Experimental Biology **221**(Suppl 1): jeb167254.

Speakman, J. R., D. A. Levitsky, D. B. Allison, M. S. Bray, J. M. de Castro, D. J. Clegg, J. C. Clapham, A. G. Dulloo, L. Gruer, S. Haw, J. Hebebrand, M. M. Hetherington, S. Higgs, S. A. Jebb, R. J. F. Loos, S. Luckman, A. Luke, V. Mohammed-Ali, S. O'Rahilly, M. Pereira, L. Perusse, T. N. Robinson, B. Rolls, M. E. Symonds and M. S. Westerterp-Plantenga (2011). "Set points, settling points and some alternative models: theoretical options to understand how genes and environments combine to regulate body adiposity." Disease models & mechanisms **4**(6): 733-745.

Sun, M., E. Y. Choi, D. J. Magee, C. W. Stets, M. J. During and E.-J. D. Lin (2014). "Metabolic Effects of Social Isolation in Adult C57BL/6 Mice." International scholarly research notices **2014**: 690950-690950.

Swinburn, B. A., G. Sacks, K. D. Hall, K. McPherson, D. T. Finegood, M. L. Moodie and S. L. Gortmaker (2011). "The global obesity pandemic: shaped by global drivers and local environments." Lancet **378**(9793): 804-814.

T.

Thaler, J. P., C. X. Yi, E. A. Schur, S. J. Guyenet, B. H. Hwang, M. O. Dietrich, X. Zhao, D. A. Sarruf, V. Izgur, K. R. Maravilla, H. T. Nguyen, J. D. Fischer, M. E. Matsen, B. E. Wisse, G. J. Morton, T. L. Horvath, D. G. Baskin, M. H. Tschop and M. W. Schwartz (2012). "Obesity is associated with hypothalamic injury in rodents and humans." J Clin Invest **122**(1): 153-162.

Timper, K. and J. C. Brüning (2017). "Hypothalamic circuits regulating appetite and energy homeostasis: pathways to obesity." Disease Models & Mechanisms **10**(6): 679.

Toda, C., A. Santoro, J. D. Kim and S. Diano (2017). "POMC Neurons: From Birth to Death." Annual review of physiology **79**: 209-236.

Tong, Q., C. Ye, R. J. McCrimmon, H. Dhillon, B. Choi, M. D. Kramer, J. Yu, Z. Yang, L. M. Christiansen, C. E. Lee, C. S. Choi, J. M. Zigman, G. I. Shulman, R. S. Sherwin, J. K. Elmquist and B. B. Lowell (2007). "Synaptic glutamate release by ventromedial hypothalamic neurons is part of the neurocircuitry that prevents hypoglycemia." Cell Metab **5**(5): 383-393.

Torgerson, J. S., J. Hauptman, M. N. Boldrin and L. Sjostrom (2004). "XENical in the prevention of diabetes in obese subjects (XENDOS) study: a randomized study of orlistat as an adjunct to lifestyle changes for the prevention of type 2 diabetes in obese patients." Diabetes Care **27**(1): 155-161.

Tremmel, M., U.-G. Gerdtham, P. M. Nilsson and S. Saha (2017). "Economic Burden of Obesity: A Systematic Literature Review." International journal of environmental research and public health **14**(4): 435.

V.

Varela, L. and T. L. Horvath (2012). "Leptin and insulin pathways in POMC and AgRP neurons that modulate energy balance and glucose homeostasis." EMBO reports **13**(12): 1079-1086.

Vong, L., C. Ye, Z. Yang, B. Choi, S. Chua, Jr. and B. B. Lowell (2011). "Leptin action on GABAergic neurons prevents obesity and reduces inhibitory tone to POMC neurons." Neuron **71**(1): 142-154.

Vong, L., C. Ye, Z. Yang, B. Choi, S. Chua, Jr. and Bradford B. Lowell (2011). "Leptin Action on GABAergic Neurons Prevents Obesity and Reduces Inhibitory Tone to POMC Neurons." Neuron **71**(1): 142-154.

W.

Wang, D., X. He, Z. Zhao, Q. Feng, R. Lin, Y. Sun, T. Ding, F. Xu, M. Luo and C. Zhan (2015). "Whole-brain mapping of the direct inputs and axonal projections of POMC and AgRP neurons." Frontiers in Neuroanatomy **9**(40).

Waterson, Michael J. and Tamas L. Horvath (2015). "Neuronal Regulation of Energy Homeostasis: Beyond the Hypothalamus and Feeding." Cell Metabolism **22**(6): 962-970.

Whitlock, G., S. Lewington, P. Sherliker, R. Clarke, J. Emberson, J. Halsey, N. Qizilbash, R. Collins and R. Peto (2009). "Body-mass index and cause-specific mortality in 900 000 adults: collaborative analyses of 57 prospective studies." Lancet **373**(9669): 1083-1096.

Wilding, J. (2012). "Are the causes of obesity primarily environmental? Yes." BMJ : British Medical Journal **345**: e5843.

Williams, G., C. Bing, X. J. Cai, J. A. Harrold, P. J. King and X. H. Liu (2001). "The hypothalamus and the control of energy homeostasis: different circuits, different purposes." Physiol Behav **74**(4-5): 683-701.

Williams, K. W., L. O. Margatho, C. E. Lee, M. Choi, S. Lee, M. M. Scott, C. F. Elias and J. K. Elmquist (2010). "Segregation of acute leptin and insulin effects in distinct populations of arcuate proopiomelanocortin neurons." J Neurosci **30**(7): 2472-2479.

Wittmann, G., E. Hrabovszky and R. M. Lechan (2013). "Distinct glutamatergic and GABAergic subsets of hypothalamic pro-opiomelanocortin neurons revealed by *in situ* hybridization in male rats and mice." J Comp Neurol **521**(14): 3287-3302.

Woods, S. C. (2005). "Signals that influence food intake and body weight." Physiol Behav **86**(5): 709-716.

Wu, Q., M. B. Lemus, R. Stark, J. A. Bayliss, A. Reichenbach, S. H. Lockie and Z. B. Andrews (2014). "The Temporal Pattern of cFos Activation in Hypothalamic, Cortical, and Brainstem Nuclei in Response to Fasting and Refeeding in Male Mice." Endocrinology **155**(3): 840-853.

Y.

Yang, S. B., A. C. Tien, G. Boddupalli, A. W. Xu, Y. N. Jan and L. Y. Jan (2012). "Rapamycin ameliorates age-dependent obesity associated with increased mTOR signaling in hypothalamic POMC neurons." Neuron **75**(3): 425-436.

Yang, X. and H.-B. Ruan (2015). "Neuronal Control of Adaptive Thermogenesis." Frontiers in Endocrinology **6**(149).

Yanovski, S. Z. and J. A. Yanovski (2014). "Long-term drug treatment for obesity: a systematic and clinical review." Jama **311**(1): 74-86.

Yi, C.-X., M. Walter, Y. Gao, S. Pitra, B. Legutko, S. Kälin, C. Layritz, C. García-Cáceres, M. Bielohuby, M. Bidlingmaier, S. C. Woods, A. Ghanem, K.-K. Conzelmann, J. E. Stern, M. Jastroch and M. H. Tschöp (2017). "TNFα drives mitochondrial stress in POMC neurons in obesity." Nature Communications **8**(1): 15143.

Yoshihara, F., M. Kojima, H. Hosoda, M. Nakazato and K. Kangawa (2002). "Ghrelin: a novel peptide for growth hormone release and feeding regulation." Curr Opin Clin Nutr Metab Care **5**(4): 391-395.

Z.

Zhan, C., J. Zhou, Q. Feng, J. E. Zhang, S. Lin, J. Bao, P. Wu and M. Luo (2013). "Acute and long-term suppression of feeding behaviour by POMC neurons in the brainstem and hypothalamus, respectively." J Neurosci **33**(8): 3624-3632.

Zhang, Y., R. Proenca, M. Maffei, M. Barone, L. Leopold and J. M. Friedman (1994). "Positional cloning of the mouse obese gene and its human homologue." Nature **372**(6505): 425-432.

Zhou, B. F. (2002). "Predictive values of body mass index and waist circumference for risk factors of certain related diseases in Chinese adults--study on optimal cut-off points of body mass index and waist circumference in Chinese adults." Biomed Environ Sci **15**(1): 83-96.

Zhu, G., J. Yan, W. W. Smith, T. H. Moran and S. Bi (2012). "Roles of dorsomedial hypothalamic cholecystokinin signaling in the controls of meal patterns and glucose homeostasis." Physiol Behav **105**(2): 234-241.

Zimmermann, J., M. A. Herman and C. Rosenmund (2015). "Co-release of glutamate and GABA from single vesicles in GABAergic neurons exogenously expressing VGLUT3." Frontiers in synaptic neuroscience **7**: 16-16.

Annexe

mTORC1 signaling orchestrates bidirectional control of food intake by hypothalamic POMC neurons

Nicolas Saucisse[1,2#], Wilfrid Mazier[1,2#], Vincent Simon[1,2#], Elke Binder[1,2], Caterina Catania[1,2], Luigi Bellocchio[1,2], Roman A. Romanov[3], Isabelle Matias[1,2], Philippe Zizzari[1,2], Stephane Leon[1,2], Carmelo Quarta[1,2],Astrid Cannich[1,2], Kana Meece[4], Delphine Gonzales[1,2], Samantha Clark[1,2], Julia Becker[5], Giles S.H. Yeo[5], Florian Merkle[5], Sharon L. Wardlaw[4], Tibor Harkany[3,6], Federico Massa[1,2], Giovanni Marsicano[1,2], Daniela Cota[1,2*]

[1]INSERM, Neurocentre Magendie, Physiophatologie de la Plasticité Neuronale, U1215, F-33000 Bordeaux, France; [2]University of Bordeaux, Neurocentre Magendie, Physiopathologie de la Plasticité Neuronale, U1215, F-33000 Bordeaux, France; [3]Department of Molecular Neurosciences, Center for Brain Research, Medical University of Vienna, A-1090 Vienna, Austria; [4]Department of Medicine, Columbia University College of Physicians and Surgeons, 10032NY New York, United States; [5]Medical Research Council (MRC) Metabolic Diseases Unit, University of Cambridge Metabolic Research Laboratories, Wellcome Trust-MRC Institute of Metabolic Science, Addenbrooke's Hospital, Cambridge CB2 0QQ, UK; [6]Department of Neuroscience, Karolinska Institutet, SE-17177 Stockholm, Sweden.

***Correspondence:** e-mail: daniela.cota@inserm.fr

[#] These authors contributed equally

Summary

Hypothalamic Pro-opiomelanocortin (POMC) neurons classically trigger satiety. However, POMC neurons encompass heterogeneous subpopulations possibly using GABA and/or glutamate as neurotransmitter(s), whose specific functions are unknown.

Here we show that POMC neurons expressing GABA, glutamate or both neurotransmitters possess specific spatial distribution and molecular signatures. Pharmacological blockade of the key energy sensor mechanistic Target of Rapamycin Complex 1 (mTORC1) simultaneously inhibited glutamatergic and activated GABAergic POMC neurons and it oppositely regulated optogenetically-stimulated POMC glutamatergic and GABAergic neurotransmission. Chemogenetics and conditional deletion of mTORC1 then demonstrated that mTORC1 blockade in POMC neurons caused hyperphagia. This was due to decreased POMC-derived anorexigenic α-melanocyte-stimulating hormone and recruitment of endocannabinoid-CB_1 receptor signaling, which restrained feeding by inhibiting POMC GABAergic neurotransmission. Genetic inhibition of glutamate release from POMC neurons also caused hyperphagia, recapitulating the phenotype observed with mTORC1 blockade.

Altogether, these findings pinpoint the molecular mechanisms engaged by POMC neurons to oppositely control feeding, thereby challenging conventional views about their functions.

Keywords: Food intake, hypothalamus, mTORC1, mTORC2, Endocannabinoid, CB_1 receptor, POMC, α-MSH, Glutamate, GABA

Introduction

Food intake is a highly complex behavior controlled by the coordinated action of different neural circuits containing specialized cell types. Within the arcuate nucleus (ARC) of the hypothalamus, two neuronal populations respectively expressing Pro-opiomelanocortin (POMC) and Agouti-related peptide (AgRP) are known to oppositely control food intake and body weight. This is due to the opposed effects of the neuropeptides that they produce on melanocortin receptors type 4 (MC4R) (Koch and Horvath, 2014; Krashes et al., 2016).

Both POMC and AgRP neurons respond to nutrient and hormonal signals reflecting short- and long-term energy availability in the organism (Cota et al., 2007; Krashes et al., 2016). Energy deficit activates AgRP neurons, which drive food seeking and intake through the release of the MC4R antagonist AgRP, the Neuropeptide Y (NPY), and the inhibitory neurotransmitter γ-aminobutyric acid (GABA) (Fan et al., 1997; Ollmann et al., 1997; Tong et al., 2008). Whilst, energy surfeit activates POMC neurons, which typically promote satiety by releasing the MC4R agonist α-melanocyte-stimulating hormone (α-MSH) (Krashes et al., 2016). Re-exposure to food after a prolonged fast (refeeding) increases POMC neurons' activity, regulating meal size through α-MSH dependent MC4R activation in the hypothalamic paraventricular nucleus (PVN), among other brain areas (Balthasar et al., 2005; Fekete et al., 2012; Singru et al., 2007). However, recent studies have also shown that AgRP and POMC neurons match the organism's energy needs to contextual information. In particular, sensory detection of food occurring before food intake simultaneously inhibits AgRP neurons and activates POMC neurons, which in turn prepare the organism to the imminent ingestion of food (Brandt et al., 2018; Chen et al., 2015). Thus, the classic view of AgRP and POMC neurons as "Yin and Yang" partners regulating food intake through their opposite action on melanocortin signaling may be an over-simplistic and incomplete depiction of the relevant circuit. Indeed, AgRP neurons seem physiologically relevant for the search of

food rather than food intake, while POMC neurons may actually be the ones in charge of controlling not only the termination, but also the start of the feeding response (Brandt et al., 2018; Chen et al., 2015). In support of this hypothesis, POMC cleavage does not only produce α-MSH, but also the opioid β-endorphin (β-EP), which stimulates food intake (Koch et al., 2015; Wardlaw, 2011). Besides, and differently from AgRP neurons, which are exclusively GABAergic (Tong et al., 2008), POMC neurons include GABAergic and glutamatergic neurons, as well as cells containing both these neurotransmitters (Dicken et al., 2012; Hentges et al., 2004; Hentges et al., 2009; Jarvie and Hentges, 2012; Mazier et al., 2019; Wittmann et al., 2013). Finally, recent single cell transcriptomic studies have shown that POMC neurons are molecularly heterogeneous (Campbell et al., 2017; Henry et al., 2015; Lam et al., 2017). Nevertheless, the functional specificities of molecularly identified POMC neurons subpopulations in the context of the regulation of food intake remain unexplored.

The mechanistic target of rapamycin (mTOR) kinase is a critical energy sensor, whose increased activity is a readout of increased intracellular energy availability (Haissaguerre et al., 2014; Saxton and Sabatini, 2017). By forming two distinct complexes (mTOR complex 1 - mTORC1, and mTOR complex 2 - mTORC2), mTOR controls cellular metabolism in response to nutrients, growth factors, hormones and cellular stress (Haissaguerre et al., 2014; Saxton and Sabatini, 2017). In neurons, the mTOR pathway regulates soma size, dendrite and axon growth (Bockaert and Marin, 2015), and it affects both glutamatergic and GABAergic neurotransmission (Weston et al., 2012). Others and we have shown that mTORC1 signaling participates in the regulation of energy balance by modulating the function of AgRP and POMC neurons (Burke et al., 2017; Cota et al., 2006; Dagon et al., 2012; Smith et al., 2015). mTORC1 also regulates oxidative metabolism in POMC neurons (Haissaguerre et al., 2018) and glutamatergic transmission in the PVN (Mazier et al., 2019). Yet it remains unknown whether mTORC1 signaling plays a role in matching energy availability to POMC neuronal

function depending on POMC neurotransmitter subtypes, and how this in turn impacts food intake.

GABAergic and glutamatergic neurotransmission, including in areas targeted by POMC neurons, is regulated by specific mechanisms (Dietrich and Horvath, 2013). Among these, the retrograde suppression of neurotransmitter release through endocannabinoids acting at the presynaptic cannabinoid type 1 receptor (CB_1R) is well described (Busquets-Garcia et al., 2018; Castillo et al., 2012). Brain CB_1R activation generally stimulates food intake (Mazier et al., 2015) and it opposes α-MSH-dependent effects in the PVN (Mazier et al., 2019; Monge-Roffarello et al., 2014; Verty et al., 2004). However, the impact of brain CB_1R signaling on food consumption is also cell-type specific (Piazza et al., 2017). For instance, CB_1R-dependent inhibition of glutamatergic neurotransmission induces hyperphagia, while CB_1R-depedent inhibition of GABAergic neurons is hypophagic (Bellocchio et al., 2010; Soria-Gomez et al., 2014b). Whether CB_1R on POMC neurons might affect feeding by participating to the modulation of neurotransmitter release is not known.

Here we have used neuroanatomical, transcriptomic, pharmacological, genetic, chemogenetic, electrophysiological, optogenetic and behavioral approaches to address the physiological role of POMC neurons in the control of food intake. These experiments have revealed the existence of functionally distinct POMC neuronal subclasses, whose activity is under the control of mTORC1 and CB1R signaling. These findings pinpoint the molecular mechanisms engaged by different POMC neurons subpopulations to oppositely regulate feeding, showing how mTORC1 is used to coordinate both neuropeptidergic- and neurotransmitter-dependent responses in relation to food consumption.

Altogether, this evidence challenges classic notions about the role of POMC neurons as exclusive drivers of satiety.

Results

POMC neurons with specific neurotransmitter profiles have distinct spatial distribution and molecular fingerprints

POMC neurons are molecularly heterogeneous (Campbell et al., 2017; Henry et al., 2015; Lam et al., 2017) and may include different subtypes, based on the neurotransmitter they produce (Dicken et al., 2012; Hentges et al., 2004; Hentges et al., 2009; Jarvie and Hentges, 2012; Wittmann et al., 2013). Accordingly, triple FISH analysis carried out in brains of C57BL/6J mice allowed identifying different hypothalamic POMC subpopulations depending on whether or not POMC cells expressed mRNA for the GABA synthesizing enzyme GAD67 and/or the glutamatergic marker vesicular glutamate transporter 2 (vGlut2, Figure 1A). Different POMC subpopulations had specific distance from the ventricle and rostro-caudal distribution (Figure S1A-C). In particular, POMC glutamatergic neurons were furthest from the ventricle and showed a rostro-caudal decrease in number, whereas POMC GABAergic neurons were closest to the ventricle and showed a rostro-caudal increase (Figure S1A-C). POMC GABA/glutamatergic cells and POMC cells negative for the 2 neurotransmitters were somewhat in between these two populations (Figure S1A-C). To then align POMC neurons to GABA, glutamate or mixed neurotransmitters expression, we analyzed publicly available single-cell RNA sequencing data of POMC neurons from the hypothalamus of C57BL/6N mice [GEO accession number: GSE74672, (Romanov et al., 2017)] by means of differential expression profiling (Figure 1B and Figure S2). Of the 28 POMC cells examined, 7 exclusively expressed *Slc17a6*, coding for vGlut2; 11 exclusively contained *Gad1* and *Gad2*, coding for the GABAergic markers GAD67 and GAD65, respectively, and 10 were positive for both glutamatergic and GABAergic markers (Figure 1B). Two out of 11 POMC GABAergic neurons were also positive for *Npy*, and *Npy* and *Agrp*, implying that approximately 18% of POMC GABAergic neurons co-express these orexigenic

neuropeptides. FISH analysis further confirmed that some co-localization between POMC and AgRP exists in the adult mouse hypothalamus (Figure S1D). POMC GABAergic and glutamatergic subpopulations had non-overlapping gene expression profiles (Figure 1B and Figure S2). Conversely, the GABAergic/glutamatergic population expressed a combination of molecular markers typical for both POMC GABAergic and glutamatergic cells (Figure 1B and Figure S2). Further differential gene expression analysis performed on POMC GABAergic *vs.* glutamatergic subpopulations demonstrated that these two groups of neurons are substantially different. POMC GABAergic neurons were enriched in the expression of genes regulating glucose and lipid metabolism as well as protein transcription and catabolism (Table 1). In contrast, POMC glutamatergic neurons had increased expression of genes involved in synaptic vesicular function, purine metabolism and GTP signaling (Table 1). Hence, hypothalamic POMC neurons include different neurotransmitter-type subpopulations, which have specific spatial distribution and distinct molecular signatures. mTOR and associated proteins such as rptor and rictor (Saxton and Sabatini, 2017), as well as CB_1R were detected in all POMC subpopulations (see GEO: GSE74672).

mTORC1 activity oppositely impacts activity of POMC neurons depending on their neurotransmitter profile

Based on these neuroanatomical and transcriptomic data, we asked whether modulation mTORC1 activity, which is a cellular readout of changes in energy availability (Haissaguerre et al., 2014; Saxton and Sabatini, 2017) might differentially regulate distinct POMC neuronal subpopulations. Thus, we monitored POMC neuronal firing in hypothalamic slices from POMC-YFP mice under basal conditions and after bath application of the mTORC1 inhibitor rapamycin (RAPA, 200 nM).

Taken all cell responses together, RAPA had no effect on firing frequency (Figure S3A, n=117). However, individual firing analysis allowed identifying distinct POMC neuronal populations that responded differently to RAPA: (i) POMC neurons inhibited by RAPA ($RAPA^{inh}$, Figures 2A and 2B, n=41/117, 35.1%), (ii) POMC neurons activated by RAPA ($RAPA^{act}$, Figures 2A and 2C, n=37/117, 31.6%), and (iii) POMC neurons with RAPA having no effect on firing frequency ($RAPA^{ns}$, Figures 2A and 2D, n=39/117, 33.3%).

These subpopulations had specific electrophysiological properties, allowing prediction of their functional properties. In particular, $RAPA^{act}$ POMC neurons had higher membrane resting potential (Em) and resistance (Figures 2E and 2F), and lower membrane capacitance (Cm, Figure 2G) than $RAPA^{inh}$ POMC cells. $RAPA^{ns}$ cells had characteristics that were in-between $RAPA^{act}$ and $RAPA^{inh}$ POMC neurons (data not shown). RAPA depolarized $RAPA^{act}$ POMC cells while hyperpolarizing $RAPA^{inh}$ POMC cells (Figure S3B). An inverse correlation was found between the recorded cells' Cm and the firing changes induced by RAPA (Figure 2H).

Cm is an indicator of cell size (Hentges et al., 2009) and relatively smaller size seems the most reliable marker to distinguish POMC GABAergic neurons *vs.* glutamatergic ones (Hentges et al., 2004; Hentges et al., 2009). Based on the Cm, we hypothesized that $RAPA^{inh}$ POMC cells were likely glutamatergic, while $RAPA^{act}$ POMC neurons were GABAergic. To confirm this, recorded neurons were filled with biocytin and subsequently labelled with an antiserum directed against the GABAergic markers GAD65/67. $RAPA^{act}$ POMC neurons had significant GAD65/67 staining, whereas $RAPA^{inh}$ POMC neurons did not overcome background staining levels (Figures 2I, 2J, S3C and S3D). Importantly, GAD65/67 staining inside the cell positively correlated with the firing changes induced by RAPA (Figure 2K) and was inversely associated with the Cm of the analyzed cells (Figure S3E). A negative

correlation was also found between the firing changes induced by RAPA and the Cm (Figure S3F), overall implying that small POMC cells activated by RAPA are very likely GABAergic. Then, by using an optogenetic approach, we evaluated whether the pharmacological inhibition of mTORC1 activity could actually alter POMC-driven neurotransmission. We evaluated this effect onto parvocellular neurons of the PVN, which are known target of the action of POMC neurons for the control of food intake (Mazier et al., 2019; Singru et al., 2012).

Using the FLEX system (Atasoy et al., 2008) in POMC-Cre neurons (Balthasar et al., 2004), we specifically expressed the photoactivable channelrhodopsin-2 (ChR2) (Atasoy et al., 2008) and recorded light-evoked ARC POMC synaptic inputs onto PVN parvocellular neurons (Figure 3A), which were recognized based on their electrophysiological properties (Luther and Tasker, 2000). About 1 in 10 parvocellular neurons were synaptically connected to terminals arising from infected POMC neurons (31/321 cells; 9.66%). Pharmacological assays on light-evoked synaptic transmission were performed in 17 parvocellular cells (Figure 3B, S4 and Table S1). The majority of the POMC terminals connecting onto parvocellular neurons released pure glutamatergic inputs (58.82%; 10/17); a proportion of the recorded cells received pure GABAergic (17.65%; 3/17) or mixed GABA/glutamate inputs (23.53%; 4/17) (Figure 3B). To test the involvement of mTORC1 in the control of neurotransmitter release from POMC terminals onto parvocellular neurons, we challenged light-evoked neurotransmission by adding RAPA to the perfusate. Acute inhibition of mTORC1 activity reduced light-evoked excitatory post-synaptic currents (eEPSCs) amplitude (Figures 3C and 3D), while increasing light-evoked inhibitory post-synaptic currents (eIPSCs) amplitude (Figures 3C and 3E). Thus, mTORC1 activity oppositely regulates POMC GABAergic and glutamatergic neurotransmission.

mTORC1 signaling in POMC neurons regulates fasting-induced food intake

Hypothalamic POMC neurons are typically recruited in response to fasting-induced food intake (or refeeding), a condition engaging α-MSH dependent MC4R signaling in the PVN, which then helps terminating the meal (Balthasar et al., 2005; Fekete et al., 2012; Singru et al., 2007).

To test the relevance of the mTORC1 pathway in modulating POMC neurons-associated feeding responses, we first evaluated the impact of RAPA on the refeeding of C57BL/6J mice. Intracerebroventricular (icv) administration of RAPA just before allowing 24-h fasted mice access to food strongly increased food intake (Figure 4A).

To then assess whether mTORC1 in POMC neurons was necessary for RAPA-induced hyperphagia, we tested the effect of the drug in POMC-*Rptor*-KO, which carry a specific deletion of the gene *rptor*, necessary for functional mTORC1 (Hara et al., 2002), in POMC neurons (Haissaguerre et al., 2018). RAPA icv induced hyperphagia in POMC-*Rptor*-controls, but not in POMC-*Rptor*-KO littermates (Figure 4B). In contrast, RAPA administered icv to conditional mutant mice lacking the gene *rictor* [required for mTORC2 formation (Sarbassov et al., 2004)] in POMC neurons (POMC-*Rictor*-KO mice; Figures S5A and B) still increased food intake (Figure 4C). Thus, acute pharmacological inhibition of mTORC1 activity causes hyperphagia by specifically targeting mTORC1 in POMC neurons.

To then evaluate whether activation of POMC neurons, could counteract RAPA-induced hyperphagia, we used the designer-receptors-exclusively-activated-by-designer-drugs (DREADD) method (Alexander et al., 2009). The gene encoding the evolved human M3-muscarinic receptor fused to the fluorescent protein mCherry (hM3Dq-mCherry) was selectively expressed in POMC neurons by injecting a Cre-inducible adeno-associated viral vector (AAV-DIO-hM3Dq-mCherry) into the ARC of POMC-Cre mutants to obtain POMC-ARC^{hM3Dq} mice [Figure S5C and (Zhan et al., 2013)]. As expected, systemic administration of the hM3Dq ligand clozapine-N-oxide (CNO, 1mg/kg) in these mice increased the

expression of the neuronal activity marker c-Fos in mCherry-positive POMC neurons (Figure S5D and S5E). Cells that expressed c-Fos were also largely co-labeled by an antiserum detecting the phosphorylated form of the S6 ribosomal protein (Figure S5D and S5F), a downstream target of mTORC1 (Saxton and Sabatini, 2017). Systemic CNO administration did not alter the refeeding response of POMC-ARC^{hM3Dq} mice (Figure S5G). However, when it was combined with icv RAPA administration, CNO treatment fully prevented the hyperphagic effect of RAPA (Figure 4D). CNO was unable to block RAPA-induced hyperphagia in POMC-ARC^{hM3Dq}-control mice, obtained by injecting AAV-DIO-hM3Dq-mCherry into the ARC of mice not expressing Cre in POMC neurons (Figure S5H).

Hence, inhibition mTORC1 signaling increases food intake by altering the function of POMC neurons. Consequently, we went on to assess which changes in POMC-derived neuropeptides and/or POMC-associated neurotransmitters could be involved in this phenomenon.

Acute inhibition of mTORC1 activity causes fasting-like changes in hypothalamic α-MSH and endocannabinoids levels

POMC is a precursor protein that must be cleaved to generate active peptides that modulate food intake [Figure 5A and (Wardlaw, 2011)]. We therefore measured hypothalamic content of POMC protein, its processing intermediates and its cleavage products in 24-h fasted and 2-h refed mice treated icv with RAPA or its vehicle. Neither POMC itself nor its initial cleavage product adrenocorticotrophic hormone (ACTH) was altered by RAPA or refeeding (Table S2). However, hypothalamic levels of α-MSH were increased after 2-h refeeding relative to fasting, and RAPA administration just before access to food completely prevented this increase (Figure 5B). As mentioned earlier, α-MSH is implicated in determining satiety (Balthasar et al., 2005; Singru et al., 2007; Singru et al., 2012), while β-EP stimulates feeding (Koch et al., 2015). Also β-EP showed changes, albeit non-significant, similar to α-MSH in

response to refeeding and to RAPA (Table S2). When we calculated ratios of α-MSH/POMC, α-MSH/ACTH and α-MSH/β-EP, a significant relative reduction in hypothalamic α-MSH was found in refed, RAPA-treated mice as compared to vehicle (Figure 5C-E). Thus, acute inhibition of mTORC1 activity prevents the increase in hypothalamic α-MSH levels classically observed with food consumption (Krashes et al., 2016).

Opposite to α-MSH, hypothalamic endocannabinoids levels are high in fasting and low in refeeding (Kirkham et al., 2002) and CB_1R activation counteracts α-MSH effects (Mazier et al., 2019; Monge-Roffarello et al., 2014; Verty et al., 2004). We therefore reasoned that changes in hypothalamic α-MSH levels induced by the acute blockade of mTORC1 activity could be accompanied by opposite changes in hypothalamic endocannabinoid levels. As compared to fasting, refeeding dampened hypothalamic levels of the endocannabinoid anandamide (AEA) (Figure 5F). However, icv administration of RAPA just before access to food maintained hypothalamic AEA levels high, like in fasting (Figure 5F). RAPA had no effect on the hypothalamic (Figure 5G) or extra-hypothalamic (Table S2) content of the other main endocannabinoid 2-arachidonoyl glycerol (2-AG) or on extra-hypothalamic levels of AEA (Table S2), independently of the feeding state. To then determine whether RAPA-induced changes in hypothalamic α-MSH and AEA levels were causally linked, we co-administered RAPA icv together with the stable α-MSH analog MTII, used at a dose that did not have any effect on food intake or on hypothalamic AEA levels *per se* (0.02 μg icv, Figure S6A and S6B). In refed mice, MTII blocked the effect of RAPA on hypothalamic AEA levels (Figure 5H). Similarly, chemogenetic activation of POMC neurons prevented the effect of RAPA on hypothalamic AEA levels (Figure 5I). Hence, re-establishment of melanocortin signaling precludes the hypothalamic increase of AEA caused by mTORC1 inhibition.

mTORC1-dependent recruitment of CB_1R signaling restrains GABA release from POMC neurons

To then verify whether the hyperphagia induced by RAPA was due to increased endocannabinoid-CB_1R signaling at the level of POMC neurons, we evaluated the effect of the mTORC1 inhibitor in POMC-*CB_1*-KO mice (Mazier et al., 2019). Deletion of *CB_1* from POMC neurons had no effect *per se* on the refeeding response (Figure 6A). As expected, icv RAPA administration just before access to food caused hyperphagia in POMC-*CB_1*-control mice (Figure 6A). Surprisingly, however, POMC-*CB_1*-KO mice displayed greater hyperphagia than their controls in response to RAPA, implying that CB_1R on POMC neurons might actually inhibit food intake (Figure 6A). Past work from our laboratory has demonstrated that while activation of CB_1R on glutamatergic neurons increases fasting-induced food intake, its activation on GABAergic terminals decreases it (Bellocchio et al., 2010). As RAPA stimulates the firing of POMC GABAergic cells (Figure 2) and POMC GABAergic transmission onto the PVN (Figure 3), we hypothesized that deletion of CB_1R in POMC neurons would not restrain anymore GABA release from POMC synaptic terminals, thereby further increasing food intake under acute mTORC1 blockade. Confirming this idea, co-administration of a sub-effective dose [i.e. unable to affect food intake when administered alone (0.03 μg/μl icv, see Figures S7A and S7B)] of the $GABA_A$ receptor antagonist picrotoxin (Ptx), blocked the excessive RAPA-induced hyperphagia observed in POMC-*CB_1*-KO mice, reducing their hyperphagic response to similar levels as RAPA-treated, POMC-*CB_1*-control littermates (Figure 6A). Then, to test whether lack of CB_1Rs on POMC neurons indeed alters POMC GABAergic transmission, we evaluated miniature inhibitory post-synaptic currents (mIPSCs) frequency onto parvocellular neurons of the PVN. Bath application of the CB_1R agonist WIN 55,212-2 inhibited mIPSCs frequency in control littermates, but not in POMC-*CB_1*-KO mice (Figure S7 C-E).

Altogether, these data indicate that acute mTORC1 inhibition activates POMC GABAergic transmission, which in turn drives feeding and is under the negative control of CB_1R.

Inhibition of glutamate release from POMC neurons causes hyperphagia

Our electrophysiology studies also indicated that acute blockade of mTORC1 activity inhibited POMC glutamatergic transmission. To evaluate *in vivo* the relevance of this effect for feeding behavior, we generated tamoxifen-inducible POMC-$CreER^{T2}$/$vglut2^{fl/fl}$ mice (thereafter called POMC-*vGlut2*-KO). We used POMC-$CreER^{T2}$-Ai6 reporter mice to confirm that tamoxifen induced recombination in POMC neurons (Figure S7F) and verified deletion of vGlut2 in hypothalamic samples of POMC-*vGlut2*-KO and control littermates by PCR (Figure S7G). As compared to their controls, POMC-*vGlut2*-KO mice showed hyperphagia in refeeding (Figure 6B), which was likely the result of the POMC GABAergic component being still functional in this mouse model. Besides, POMC-*vGlut2*-KO mice did not respond to the icv administration of RAPA (Figure 6C). Thus, the genetic inhibition of glutamate signaling from POMC neurons recapitulates the hyperphagic phenotype obtained with the pharmacological blockade of mTORC1.

Overall, the data indicate that POMC GABAergic and glutamatergic neurons counterbalance each other in an mTORC1-dependent manner to modulate feeding.

Discussion

Over the past 20 years, several studies have outlined the functions of AgRP and POMC neurons in the context of energy balance, leading to the widespread notion that AgRP neurons increase food intake, while POMC neurons unvaryingly control feeding cessation. The present data reveal that the functional meaning of two distinct POMC neuronal subtypes, one GABAergic, the other glutamatergic, is to oppositely regulate food intake under the control of the mTORC1 pathway.

When energy levels are low, like in fasting, mTORC1 activity in POMC neurons is low, causing concomitant activation of POMC GABAergic neurons and inhibition of POMC glutamatergic cells and melanocortin signaling. This leads to the recruitment of endocannabinoid-CB_1R signaling, which acts as a break on feeding behavior by inhibiting excessive GABA release from POMC neurons. In contrast, during food intake, increased mTORC1 activity in POMC neurons simultaneously increases glutamatergic and decreases GABAergic neurotransmission, stimulates α-MSH secretion and decreases AEA levels, ceasing food intake. Accordingly, deletion of glutamatergic signaling from POMC neurons of adult mice behaviorally recapitulates the effects observed by blocking mTORC1 with rapamycin, which intracellularly mimics a negative energy state (Saxton and Sabatini, 2017).

Collectively, these findings uncover a more complex and dynamic role for POMC neurons in the control of food intake than has been appreciated so far and substantially suggest that the dichotomic view of AgRP *vs.* POMC neurons in the control of food intake is one piece of a far more complex picture. Recent fiber photometry studies have shown that the sensory detection of food is sufficient to immediately switch off AgRP neurons and activate POMC neurons (Chen et al., 2015). This happens before any food is consumed (Chen et al., 2015) and it helps preparing the organism to the imminent ingestion of food (Brandt et al., 2018). However, these studies did not address the neurotransmitter nature of the POMC cells

involved. Our data provide explanation of how POMC neurons, thanks to their heterogeneity, can both favor ingestion of food and lead to the termination of the meal. Future studies will address the interesting question of the nature of POMC neurons activated in pre- and post-prandial conditions.

Previous investigations have proposed that at least 3 subpopulations of POMC neurons can be distinguished based on the neurotransmitter expressed (Dicken et al., 2012; Jarvie and Hentges, 2012; Jones et al., 2019; Wittmann et al., 2013). Our findings now offer functional significance to this long overlooked information, presenting evidence for an mTORC1-dependent opposite regulation of POMC glutamatergic and GABAergic neuronal subpopulations in the context of feeding behavior.

Our neuroanatomical analysis shows that distinct POMC neurotransmitter cells subtypes have specific spatial location within the ARC. This is in agreement with other recent studies describing specific spatial distribution of POMC neurons based on the expression of GABAergic and glutamatergic markers (Jones et al., 2019). Spatial location could be eventually associated with specific projections targets, as it has been already demonstrated for AgRP neurons (Betley et al., 2013). Transcriptomic profiling also demonstrates that POMC glutamatergic and GABAergic subpopulations have specific neurochemical features. POMC GABAergic cells are endowed with higher glycolytic capacity and expression of transcription factors and lower expression of synaptic proteins than POMC glutamatergic neurons. Notably, a small % of GABAergic POMC neurons in the hypothalamus of C57BL/6 mice also co-expressed *NPY* and/or *AgRP*. This implies that there is an additional subpopulation of GABAergic cells in the adult mouse hypothalamus that contains both POMC and AgRP, as we have further confirmed by FISH analysis. This observation agrees with previous transcriptomic data obtained by using reporter mice to trace and identify POMC and AgRP

neurons (Henry et al., 2015; Lam et al., 2017), likely reflecting the shared developmental origins of POMC and AgRP cells (Padilla et al., 2010).

It has been proposed that the proportion of glutamatergic and GABAergic POMC neurons varies with age (Dennison et al., 2016). In this context, future longitudinal studies will address the interesting possibility that the dual GABA/glutamatergic population that we have also identified might be indicative of a switch in neurotransmitter phenotype over time and/or it might represent another way for POMC neurons to fine-tune their actions on target circuits. Noteworthy, the heterogeneity in neurotransmitter type likely explains the inability to observe acute, rapid changes in food intake reported in several studies using optogenetic or chemogenetic approaches to modulate POMC neurons activity [present findings and (Aponte et al., 2011; Koch et al., 2015; Zhan et al., 2013)]. Accordingly, the fact that POMC-*Rptor*-KO, POMC-*Rictor*-KO and POMC-CB_1-KO mice did not have *per se* a phenotype during the fasting-induced food intake paradigm could be possibly due to the similar expression of the deleted genes across the different POMC neuronal subpopulations and their counterbalancing physiological functions.

Our optogenetic electrophysiology studies also demonstrate that POMC glutamatergic and GABAergic neurons functionally project to parvocellular neurons of the PVN, contributing to the activity of this brain region. This evidence agrees with previous studies illustrating both synaptic GABA and glutamate release from POMC neurons (Atasoy et al., 2008; Dicken et al., 2012; Hentges et al., 2004; Mazier et al., 2019). However, another study in which optogenetics was used to assess glutamatergic POMC transmission onto the PVN was unable to find any, rather showing that such transmission depends upon ARC vGlut2-positive neurons, 44% of which were nevertheless POMC neurons (Fenselau et al., 2017). These differences could be due to the genetic models used, the interval between the intra-ARC virally-mediated delivery of the opsin and actual electrophysiological recordings, and the

number and type of PVN cells analyzed. For instance, Fenselau et al. did not evaluate transmission onto parvocellular neurons, but studied all neurons expressing MC4R (Fenselau et al., 2017). Besides, our study demonstrates that POMC glutamatergic activity is particularly relevant to inhibit food intake. Accordingly, others have shown that mice with constitutive deletion of vGlut2 in POMC neurons are prone to develop diet-induced obesity (Dennison et al., 2016).

After the discovery of the involvement of the mTORC1 pathway in the hypothalamic regulation of energy balance (Cota et al., 2006), several studies have investigated the role of the mTOR kinase or of components of its pathway in AgRP and POMC neurons (Burke et al., 2017; Caron et al., 2016; Smith et al., 2015). Some of these investigations have shown that sustained mTORC1 activity, induced by genetic manipulation or aging, causes functional and morphological alterations in POMC neurons, leading to hyperphagia and obesity (Mori et al., 2009; Yang et al., 2012).

The current findings now demonstrate that mTORC1 is critically implicated in the recruitment of POMC neurons in response to energy availability and that, depending on the neurotransmitter type, mTORC1 activity leads to opposite effects on the regulation of neurotransmission and food intake. Previous studies have shown that the mTOR pathway has a key role in neurotransmission, particularly in the hippocampus, by modulating dendrite length and spine density, and by modifying the function and coding properties of individual synapses (Weston et al., 2012). Accordingly, we have found that rapamycin rapidly alters action potentials of POMC neurons and modulates POMC neurotransmission onto PVN parvocellular neurons in opposite ways depending upon the POMC neurotransmitter type. While further studies will have to investigate the molecular mechanisms underlying the effects of rapamycin on POMC neuronal activity, it is worth mentioning that mTOR activity

differentially regulate glutamatergic and GABAergic neurotransmission in other brain areas as well (Weston et al., 2012).

Changes in POMC neuronal activity induced by mTORC1 are then associated with changes in hypothalamic levels of α-MSH and the endocannabinoid AEA, which eventually modulate neurotransmitter release and the feeding response. Thus, mTORC1 activity coordinates neuropeptidergic- (i.e. levels of α-MSH) and neurotransmitter-dependent responses in POMC neurons in relation to food intake. In agreement with previous evidence (Mazier et al., 2019; Monge-Roffarello et al., 2014; Verty et al., 2004), the recruitment of melanocortin signaling is upstream endocannabinoid-dependent CB_1R activation. The latter not only inhibits POMC glutamatergic transmission (Mazier et al., 2019), but it exerts an important inhibitory action on the POMC GABAergic neuronal subpopulation, whose mTORC1-dependent activation stimulates food intake. The phenomena described are part of the classic effects attributed to presynaptic CB_1R and are consistent with our past work demonstrating opposite roles of CB_1R signaling on food intake depending on the neurotransmitter cell type (Bellocchio et al., 2010; Soria-Gomez et al., 2014a). Besides, although not investigated in the current study, it is likely that the potential endocannabinoid-dependent retrograde suppression of GABA release and consequent modulation of food intake may involve POMC GABAergic projections onto the PVN, as our previous findings have shown that blockade of CB_1R signaling in the PVN further increases food intake during refeeding (Soria-Gomez et al., 2014b). Recent work has also shown that POMC neurons drive the hyperphagia induced by exogenous cannabinoids in sated mice through a mechanism that relies on CB_1R modulation of presynaptic inputs onto POMC cells and on CB_1R-dependent mitochondrial adaptations in POMC neurons, causing a switch in the release from α-MSH to β-EP (Koch et al., 2015). In view of our current findings, it is possible that mTORC1 regulates POMC processing in response to different

endogenous or exogenous stimuli, and that such processing might differ depending on the specific neurotransmitter cell subtype engaged in different moments of the feeding process.

The present study provides compelling evidence for a sophisticated role of POMC neurons in the regulation of feeding, indicating that specific subpopulations of POMC neurons differentially impact this behavior. These findings reveal an unforeseen neuronal mechanism, which modifies our notion of hypothalamic circuits regulating food intake, energy balance and associated pathological states.

Acknowledgements

We thank the animal facility, the genotyping and bioinformatics platforms of the INSERM U1215, funded by INSERM and Labex Brain, for animal care, mouse lines management and genotyping. We thank the analytical chemistry facility of the INSERM U1215, funded by INSERM, for endocannabinoids quantification. The microscopy was done in the Bordeaux Imaging Center, a service unit of the CNRS-INSERM and Bordeaux University, member of the national infrastructure France BioImaging supported by the Labex Brain. The help of F. Cordelières, C. Poujol, S. Marais and P. Mascalchi (University of Bordeaux) is acknowledged. We thank the biochemistry and biophysics Platform of Bordeaux NeuroCampus, supported by the Labex Brain, and Dr. A. Zeisel and Dr. S. Linnarsson (Karolinska Institutet, Stockholm, Sweden) for help with single-cell RNA sequencing studies. We thank Drs. S.C. Woods (University of Cincinnati), F. Chaouloff, and P. Ciofi (INSERM U1215) for useful suggestions, and C. Padgett for the artwork. Supported by INSERM, Aquitaine Region, EFSD-Sanofi, ANR-13-BSV4-0006, ANR-17-CE14-0029 and Labex BRAIN ANR-10-LABX-43 (D.C. and G.M.); ANR-2010-1414-01, ANR-10-EQX-008-1 OPTOPATH and FFRD, which is sponsored by Fédération Française des Diabétiques,

AstraZeneca, Eli Lilly, Merck Sharp & Dohme, Novo Nordisk and Sanofi (D.C.); ANR-16-CE37-0010 (G.M.); INSERM/Aquitaine Region PhD fellowship and FRM PhD fellowship FDT20150532545 (N.S.); PhD fellowship from the French Ministry of Higher Education and FRM PhD fellowship FDT201805005371 (V.S.); PhD fellowship from the French Ministry of Higher Education (S.L.); European Community's Seventh Framework Programme (Marie Curie IRG n°224757 to D.C., HEALTH-F2-2008-223713 and HEALTH-603191 to G.M., FP7-People2009-IEF-251494 to D.C. and E.B., ERC-2010-StG-260515 and ERC-2014-PoC-640923 to G.M.), FRM (to C.C., F.M., L.B. and G.M.); NIH DK080003 (S.L.W.); Swedish Research Council, Hjärnfonden, the Novo Nordisk Foundation, ERC SECRET-CELLS, and intramural funds of the Medical University of Vienna (T.H.); EMBO long-term research fellowship ALTF 596-2014 and Marie Curie Actions EMBOCOFUND2012 GA-2012-600394 (R.A.R.).

Author Contributions

N.S., W.M., V.S., E.B., C.C., L.B., R.A.R., I.M., P.Z., S.L., C.Q., A.C., K.M. D.G., S.C. and J.B. performed the experiments and collected the data; N.S., W.M., V.S., G.S.H.Y., F.Me., S.L.W., T.H., F.M. and D.C. analyzed the data; T.H., F.M. and G.M. critically contributed to discussion; D.C. conceptualized all studies and supervised the work; N.S., W.M., V.S., and D.C. wrote the manuscript; all authors edited the manuscript. All authors have read and approved the final version of the manuscript.

Declaration of interest

The authors have nothing to disclose.

Figure Legends

Figure 1. POMC neurons include GABAergic and glutamaterigic subtypes with distinct molecular fingerprints.

(**A**) Representative images from triple FISH, illustrating the presence of different POMC subpopulations expressing or not GABAergic (Gad67) and glutamatergic (vGlut2) markers. A total of 3914 POMC neurons from 4 C57BL/6J mice were analyzed. Scale bars: 15µm. (**B**) Neurotransmitter type-specific single-cell transcriptome profiling of hypothalamic *Pomc*$^{+}$ neurons. The heat map illustrates the differential expression of several genes depending on whether *Pomc*$^{+}$ cells are GABAergic (11 cells studied, column 1 to 11 from the left), glutamatergic (7 cells studied, columns 12 to 18 from the left) or GABA/glutamatergic (10 cells studied, columns 19 to 28 from the left). The color scale bar shows the color coding of the single-cell expression level. Data are normalized to maximum single-cell level in the dataset for every gene. On the right: gene names. See also Table 1 and Figures S1 and S2.

Figure 2. mTORC1 blockade oppositely regulates POMC neurons activity depending on neurotransmitter cell type.

(**A**) Repartition of the tested POMC neurons as a function of their response to rapamycin (RAPA) and time course of the POMC neurons response after RAPA perfusion (200nM). (**B-D**) Representative traces of POMC neurons firing during RAPA perfusion recorded in whole cell current clamp configuration from POMC-YFP mice and corresponding firing changes in response to RAPA (right side). RAPA decreases (B, n=41/117 cells), increases (C, n=37/117 cells) or has no effect (D, n=39/117 cells) on POMC firing (46 mice analyzed in total). (**E-G**) RAPA^{act} POMC neurons (n=37) have increased membrane resting potential (Em; E), and membrane resistance (Rm; F), and decreased cell capacitance (Cm; G) as compared to RAPA^{inh} POMC neurons (n=41). (**H**) Change in cell firing in response to RAPA is correlated

with Cm (n=78 cells). (**I**) Representative 3D-reconstruction from Z-stack confocal images of $RAPA^{inh}$ and $RAPA^{act}$ POMC neurons used for electrophysiological recordings. Reconstruction of cell body (biocytin: blue surface) and GAD staining (GAD65/67: red spots, left panel), and corresponding images showing only the GAD spots present inside the cell body surface (yellow, right panel). (**J**) Number of GAD65/67 spots over membrane capacitance is higher in $RAPA^{act}$ POMC neurons as compared to $RAPA^{inh}$ POMC neurons (n=7-11 cells). (**K**) Change in action potential firing under RAPA correlates with the number of GAD spots present inside the cell body (n=18 cells). Data are mean ± SEM. **p<0.01; ***p<0.001. Scale bar in I: 3 μm. For statistical analysis, see Table S3. See also Figure S3.

Figure 3. mTORC1 activity modulates POMC neurons neurotransmission onto PVN parvocellular cells.

(**A**) Representative image of mCherry-positive, ChR2-expressing projections from ARC POMC neurons onto the hypothalamic paraventricular nucleus (PVN). (**B**) Distribution of the neurotransmission type recorded in PVN parvocellular neurons after photostimulation (n=17 cells) and representative traces of light-evoked post-synaptic currents recorded from parvocellular neurons of the PVN for each neurotransmission type. POMC neurons mainly release glutamate (58.82%, 10/17 cells) onto parvocellular neurons; however pure GABAergic (17.65%; 3/17 cells) and mixed GABA/Glutamate (23.53%, 4/17 cells) connections were also observed. (**C**) Amplitude time course of light-evoked EPSC (red; n=6 cells) and IPSC (green; n=5 cells) normalized to baseline. RAPA decreases eEPSCs amplitude (**D**), and increases eIPSCs amplitude (**E**). Representative traces of eEPSC (D; top) and eIPSC (E; top) before (bef, in C) and after (aft, in C) RAPA application. Data are mean ± SEM.*p<0.05, ***p<0.001. V: 3^{rd} ventricle. Scale bar in A: 50 μm. Blue square: light. For statistical analysis, see Table S3. See also Figure S4.

Figure 4. mTORC1 in POMC neurons controls food intake.

Fasting-induced food intake (refeeding) in C57BL/6J mice (**A**, n=5 mice per group), POMC-*Rptor*-Control and KO littermates (**B**, n=6-9 mice per group), and POMC-*Rictor*-Control and KO littermates (**C**, n=5 mice per group) treated icv with RAPA or its vehicle. (**D**) Acute ip CNO injection inhibits icv RAPA-induced hyperphagia in POMC-ARC^{hM3Dq} mice (n=5 mice per group). Data are mean ± SEM. *p<0.05; **p<0.01; ***p<0.001. $^{\#}$p<0.05, treatment effect. For statistical analysis, see Table S3. See also Figure S5.

Figure 5. mTORC1 blockade induces fasting-like α-MSH and AEA changes in hypothalamus.

(**A**) Schematic diagram illustrating hypothalamic POMC processing. (**B**) α-MSH content in the hypothalami of 24-h fasted or 2-h refed C57BL/6J mice treated icv with RAPA or its vehicle (n=8 mice per group). (**C**-**E**) Hypothalamic α-MSH/POMC (C), α-MSH/ACTH (D) and α-MSH/β-EP (E) ratios in 2-h refed C57BL/6J mice treated icv with RAPA or its vehicle (n=8 mice per group). (**F**, **G**) Effect of icv administration of RAPA or its vehicle on hypothalamic AEA (F) and 2-AG (G) content in fasted or refed C57BL/6J mice (n=3-5 mice per group). (**H**) Effect of the combined icv administration of the α-MSH analog MTII (0.02 µg) and RAPA on hypothalamic AEA content in refed C57BL/6J mice (n=6 mice per group). (**I**) Effect of the combined administration of CNO and RAPA on hypothalamic AEA content in refed POMC-ARC^{hM3Dq} mice (n=8-10 mice per group). Data are mean ± SEM. *p<0.05; **p<0.01; ***p<0.001. For statistical analysis, see Table S3. See also Figure S6.

Figure 6. POMC GABAergic and glutamatergic neurons oppositely regulate food intake.

(**A**) Refeeding in POMC-*CB_1*-WT and KO littermates treated icv with RAPA, its vehicle or a combination of RAPA and the $GABA_A$ receptor antagonist picrotoxin (Ptx) (n=8-18 mice per group, 2 experiments pooled together). (**B**) Refeeding response in POMC-*vGlut2*-Control and KO littermates (n=8-14 mice per group) and (**C**) effect of an icv administration of RAPA or its vehicle on refeeding in POMC-*vGlut2*-KO mice (n=8 mice per group). Data are mean ± SEM. *p<0.05; **p<0.01; ***p<0.001. For statistical analysis, see Table S3. See also Figure S7.

Table 1. Gene annotation enrichment analysis of differentially expressed genes in POMC GABAergic and glutamatergic neurons.

	Database	Term	Fold Enrichment	Count	p-value
Enriched in POMC GABA Neurons	Gene Ontology	Glutamate decarboxylase activity	67.11	2	2,94E-02
	Gene Ontology	Glucose-6-phosphate/hexose phosphate transport	45.07	2	4,35E-02
	Gene Ontology	Transcriptional repressor complex	11.75	5	7,79E-04
	Gene Ontology	Proteasomal ubiquitin-dependent protein catabolic process	9.01	4	9,52E-03
	Gene Ontology	Neutral lipid metabolic process	6.01	4	2,84E-02
	Gene Ontology	Glycerol ether metabolic process	6.01	4	2,84E-02
	Gene Ontology	Triglyceride metabolic process	5.63	3	9,81E-02
	Gene Ontology	Chromatin binding	4.33	10	5,03E-04
	Gene Ontology	Regulation of gene-specific transcription	4.04	4	7,59E-02
	Gene Ontology	Transcription coactivator activity	4.03	6	1,65E-02
	Gene Ontology	Transcription cofactor activity	3.82	12	3,10E-04
	Gene Ontology	Transcription repressor activity	3.73	10	1,45E-03
	Gene Ontology	Transcription corepressor activity	3.73	4	9,12E-02
	Gene Ontology	Glycerolipid metabolic process	3.14	6	4,19E-02
	Gene Ontology	Ubiquitin-dependent protein catabolic process	2.88	6	5,74E-02
	Gene Ontology	Transcription factor binding	2.80	12	3,82E-03
	Gene Ontology	Negative regulation of transcription	2.54	14	3,56E-03
	Gene Ontology	Negative regulation of gene expression	2.47	15	3,04E-03
	Gene Ontology	Transcription factor complex	2.25	8	6,50E-02
Enriched in POMC Glutamate Neurons	Gene Ontology	Synaptic vesicle membrane	34.64	2	5,48E-02
	Gene Ontology	Synaptic vesicle membrane	34.64	2	5,48E-02
	Gene Ontology	Clathrin coated vesicle membrane	27.42	3	5,04E-03
	Gene Ontology	Cytoplasmic vesicle membrane	11.35	3	2,72E-02
	Kegg pathway	Purine metabolism	7.31	3	5,46E-02
	Gene Ontology	GTP binding	4.42	4	5,68E-02
	Gene Ontology	Vesicle	3.17	5	6,59E-02

Experimental Procedures

Animals

All experiments were conducted in strict compliance with the European Union recommendations (2013/63/EU) and were approved by the French Ministry of Agriculture and Fisheries (animal experimentation authorization n°3309004) and the local ethical committee of the University of Bordeaux (DIR1354; APAFIS13232). For the triple FISH studies, no regulated procedures under the Animals (Scientific Procedures) Act 1986 were carried out on the animals used and the studies was reviewed by the University of Cambridge Animal Welfare and Ethical Review Body (AWERB) processes. Maximal efforts were made to reduce any suffering and the number of animals used. Number of animals for each experiment is detailed in the figure legends.

Male mice, aged 7 to 16 weeks, were housed individually in standard plastic rodent cages, maintained on a 12-h light-dark cycle (lights off at 1300 h) with *ad libitum* access to pelleted chow (A03, SAFE, France) and water, unless otherwise specified. C57BL/6J mice (Janvier, France), POMC-Cre mice [Tg(Pomc1-cre)16Lowl/J, JAX Stock #005965, The Jackson Laboratory, USA; (Balthasar et al., 2004)], POMC-YFP mice, POMC-*Rptor*-KO, POMC-*Rictor*-KO, POMC-CB_1-KO, as well as POMC-CreER^{T2}/vGlut2-flox (thereafter called POMC-*vGlut2*-KO after tamoxifen administration), POMC-CreER^{T2}-Ai6 and their control littermates were used for the studies.

POMC-YFP mice were obtained by crossing POMC-Cre mice with Rosy mice [B6.129X1-Gt(ROSA)26Sortm1(EYFP)Cos/J, JAX Stock #006148, The Jackson Laboratory]. POMC-*Rptor*-KO and control littermates were generated by crossing POMC-Cre mice with Rptor-Flox mice (B6.Cg-Rptortm1.1Dmsa/J, JAX Stock #013188, The Jackson Laboratory). POMC-*Rictor*-KO and control littermates were obtained by crossing POMC-Cre mice with Rictor-Flox mice (Rictortm1.1Klg/SjmJ, JAX Stock #020649, The Jackson Laboratory).

POMC-*CB_1*-KO and control littermates were generated by crossing POMC-Cre mice with CB_1-Flox mice (Marsicano et al., 2003). Tamoxifen inducible POMC-*vGlut2*-KO and control littermates were generated by crossing POMC-CreER^{T2} mice [C57BL/6J-Tg(Pomc-creERT2), kind gift of Dr. Joel Elmquist at UT Southwestern, (Berglund et al., 2013)] with vGlut2-flox mice [Slc17a6tm1Lowl/J, JAX stock #012898, (Tong et al., 2007)]. Inducible POMC-CreER^{T2}-Ai6 mice were generated by crossing POMC-CreER^{T2} mice with Ai6 mice [B6.Cg-Gt(ROSA)26Sortm6(CAG-ZsGreen1)Hze/J, JAX stock #007906, (Madisen et al., 2010)]. New conditional KO lines were generated following a three step backcrossing method (Bellocchio et al., 2013). All lines were in a mixed genetic background. All animals used in experiments involving mutant mice were littermates. We have previously characterized POMC-*Rptor*-KO mice and POMC-*CB_1*-KO mice (Haissaguerre et al., 2018; Mazier et al., 2019). Effective Cre-mediated deletion of rictor in POMC neurons was assessed by immunohistochemistry; while appropriate recombination after tamoxifen administration was evaluated by immunohistochemistry using the reporter POMC-CreER^{T2}-Ai6 mouse and by assessing vGlut2 deletion in POMC neurons by PCR (see further below).

PCR for mouse genotyping

Mice were genotyped from genomic DNA purified from tail biopsies by PCR using specific primers. For analysis of induced vGlut2 excision in POMC-*vGlut2*-KO mice and their control littermates, fresh hypothalami were dissected on ice and snap frozen after cervical dislocation. Tails or hypothalamic samples were incubated overnight at 56°C in Proteinase K buffer (100mM Tris-HCl pH8, 5mM EDTA, 0.2 % SDS, 200mM NaCl, 0,2mg/mL PK). After 10 min at 13200 rpm, the supernatants were purified on silica columns, according to the manufacturer protocol (Macherey nagel kit), on a zephyr automatic station. PCR assay was carried out using a Biorad C1000 thermal cycler, with GoTaq G2 Hot Start Green Master Mix

(Promega), and 0.3 to 0.6µM of each primer in a 25µL volume. PCR conditions were as follows: 1 cycle, 5 min at 95°C; 37 cycles, 30 sec at 95°C, 30 sec at 55°C for, 1 min at 72°C; 1 cycle, 5 min at 72°C. PCR products was analyzed on a Labchip GX microfluidic electrophoresis system (Caliper) using the DNA5k kit.

Primers for genotype analysis.

Mouse line	Primer	sequence 5'3'	expected fragment & length	
POMC-Cre	Cre-F	GCGGTCTGGCAGTAAAAACTATC	Cre	100 pb
	Cre-R	GTGAAACAGCATTGCTGTCACTT		
POMC-CreER^{T2}	Cre-F	GCGGTCTGGCAGTAAAAACTATC	CreER^{T2}	100 bp
	Cre-R	GTGAAACAGCATTGCTGTCACTT		
CB_1-Flox	CB1-F	GCTGTCTCTGGTCCTCTTAAA	wt	450 bp
	CB1-R	GGTGTCACCTCTGAAAACAGA	Flox	555 bp
	CB1-ex	CTCCTGTATGCCATAGCTCTT	excision	680 bp
Rictor-Flox	Rictor-F	CAAGCATCATGCAGCTCTTC	Flox	560 bp
	Rptor-R	TCCCAGAATTTCCAGGCTTA	wt	410 bp
Rptor-Flox	Rptor-F	CTCAGTAGTGGTATGTGCTCAG	Flox	200 bp
	Rptor-R	GGGTACAGTATGTCAGCACAG	wt	160 bp
vGlut2-flox	vglut2-F	CTGAGCGAAGGTGAGCTGAA	Flox	400 bp
	vglut2-R	TGGGCCAGAACACAGGATATG	wt	270 bp
	vglut2-ex	TCACTGCCTTGTTCCTAGTGC	excision	700 bp
POMC-YFP	WT-F	AAAGTCGCTCTGAGTTGTTAT	wt	620 bp
	Ki-F	GCGAAGAGTTTGTCCTCAACC	Ki	330 bp
	Common-R	GGAGCGGGAGAAATGGATATG		
Ai6	Ai6-WT-F	AAGGGAGCTGCAGTGGAGTA	wt	300 bp
	Ai6-WT-R	CCGAAAATCTGTGGGAAGTC		
	Ai6-mut-F	AACCAGAAGTGGCACCTGAC	Ai6	210 bp
	Ai6-mut-R	GGCATTAAAGCAGCGTATCC		

AAV vectors for hM3Dq and channelrhodopsin-2 (ChR2) expression

Gq-coupled human M3 muscarinic DREADD (hM3Dq) fused to mCherry (Alexander et al., 2009), provided by Brian L. Roth (University of North Carolina, Chapel Hill, NC, USA) was subcloned in a CAG-DIO rAAV vector for Cre-dependent expression (Atasoy et al., 2008) by using standard molecular biology techniques. AAV-DIO-hChR2-mCherry was generated using pAAV-Ef1a-DO-hChR2(H134R)-mCherry-WPRE-pA plasmid as backbone

(ADDGENE #37082). Vectors used were of an AAV1/AAV2 mixed serotype, and were generated by calcium phosphate transfection of HEK-293T cells and subsequent purification as described (Monory et al., 2006).

Tamoxifen treatment for the induction of Cre-mediated recombination

First, a 1g/mL suspension of tamoxifen (T5648, Sigma-Aldrich, Saint-Quentin Fallavier, France) in 100% ethanol (20821.330, VWR, Briare, France) was prepared. Then, corn oil (C8267, Sigma-Aldrich, Saint-Quentin Fallavier, France) pre-heated to 55°C was added to obtain a 50mg/mL stock solution. Enough solution was prepared for a 5-day treatment. After vortexing to ensure complete dissolution of tamoxifen, 1-day treatment aliquots were kept at -20°C. Mice were administered with 150mg/kg of tamoxifen, daily, for 5 consecutive days by oral gavage. Each day, one aliquot was warmed up to 37°C before the drug administration. Any leftover was discarded. We used polypropylene flexible gavage needles (FTP-20, Instechlabs, Plymouth Meeting, PA, USA) to reduce trauma and decrease the risk of esophagus perforation. Gavage volume was of 3mL/kg (i.e. 90µL for a 30g mouse).

Stereotaxic surgery

Mice were anesthetized with a mixture of ketamine (100 mg/kg, ip) and xylazine (10 mg/kg, ip), placed in a stereotaxic holder (David Kopf Instruments, USA) and implanted with a cannula in the lateral cerebral ventricle (coordinate AP/DV/ML = −0.5/−2.1/-1.2 mm). Cannula placement was verified by administering 5 µg of neuropeptide Y (NPY) (Phoenix Pharmaceuticals Inc., France) in 0.1 M PBS (pH 7.4) and by assessing subsequent food intake, as in (Brown et al., 2006).

Stereotaxic virus injection. POMC-Cre$^{+/+}$ and POMC-Cre$^{-/-}$ mice were anesthetized and placed in a stereotaxic holder. Hamilton syringe with NanoFil needle (85 µm tip diameter)

were filled with AAV and inserted into the ARC. AAV vectors (500 nL) were infused with pressure (coordinate AP/DV/ML = −1.5/−5.5/±0.2 mm; infusion speed = 100 nL/min; UltraMicroPump UMP3 (one) with SYS-Micro4 Controller, WPI, USA). To activate neurons, AAV-DIO-hM3Dq-mCherry vectors were injected into the ARC of POMC-Cre$^{+/+}$ mice (thereafter named POMC-ARC^{hM3Dq} mice). For control, AAV-DIO-hM3Dq-mCherry virus was also injected into the ARC of POMC-Cre$^{-/-}$ mice (thereafter named POMC-ARC^{hM3Dq}-control mice). Mice were then implanted with cannulae into the lateral cerebral ventricle as detailed above. Mice were used for the behavioral studies after at least 4 weeks from the intra-ARC AAV administration. For optogenetic electrophysiology studies, 5-weeks old POMC-Cre$^{+/+}$ mice were stereotaxically and bilaterally injected with an AAV-DIO-hChR2-mCherry virus at same coordinates as before (injection volume: 500 nL and injection speed: 100 nL/min). Animals were used for electrophysiology studies after 4 to 5 weeks from the intra-ARC AAV administration.

Drugs preparations and food intake studies

Rapamycin (RAPA, EMD Millipore, USA), and picrotoxin (Ptx, Sigma-Aldrich, USA), were dissolved in DMSO, the α-MSH analog melanotan II (MTII, Phoenix Pharmaceuticals, USA) was dissolved in phosphate-buffered saline (PBS), and clozapine-N-oxide (CNO, Sigma-Aldrich, USA) was dissolved in saline.

Fasting-induced food intake studies. Mice were singly housed for at least 7 days before the fasting-induced food intake experiments. The day before the experiment, food was removed from the cages for 24 hours. Fasted mice received an icv injection of RAPA (25 µg in 1 µl DMSO) or its vehicle, which were administered 4 h before dark onset. The same protocol was followed when Ptx (0.03 µg in 1 µl DMSO), MTII (0.02 µg in 1 µl PBS) or CNO (1 mg/kg in saline, ip) were combined with RAPA. Ptx or MTII were simultaneously administered icv

with RAPA; CNO or its vehicle were administered 15 min before the icv administration of RAPA or its vehicle. Food was returned immediately after the drugs injections and intake was recorded after 1h, 2h and, in some cases, after 24h. Body weight was measured immediately before and 24 h after the treatments.

MTII and Ptx dose-responses. The MTII and the Ptx dose-response were carried out in 24-h fasted C57BL/6J mice that received MTII (0.5, 0.25, 0.125, 0.0625, 0.03, 0.02 or 0.01 µg/µL in saline, icv) or Ptx (0.03, 0.06 or 0.09 µg/µL in DMSO, icv) respectively 1 h and 4 h before dark onset. Food intake was recorded at 1h, 2h and 24h. Body weight was measured immediately before and 24h after the treatments.

In order to reduce the number of animals to employ, whenever possible a latin square design was used in which the same animals belonging to the same genotype underwent the different treatments. Animals showing sign of stress or malaise during the behavioral experiments were removed from further analysis.

Immunohistochemistry

Mice were deeply anesthetized using pentobarbital given ip and then perfused transcardially with ice-cold PBS, pH 7.4, followed by 4% paraformaldehyde (PFA, Sigma-Aldrich, France) in PBS with 0.2% picric acid. Brains were extracted and postfixed in 4% PFA overnight at 4°C, then cryoprotected with 30% sucrose in PBS at 4°C. Coronal sections (30 µm) were cut with a cryostat (CM1950, Leica, Germany), collected in PBS and stored in antifreeze solution (30% ethylene glycol, 30% glycerol in KPBS) at -20°C until further used.

Single-labeling immunohistochemistry. Brain sections from 90 min refed POMC-ARC^{hM3Dq} mice were processed for the co-localization of mCherry and POMC. Sections were first incubated with 10% normal goat serum (Dako, Denmark) and then with rabbit anti-POMC antibody (1:2000; Phoenix Pharmaceuticals, USA) overnight at 4°C. The next day, sections

were washed in PBS and incubated for 1h with A488-conjugated secondary goat anti-rabbit antibody (1:500, Cell Signaling, USA). Similar procedures were followed for POMC labelling in brain sections from POMC-CreER^{T2}-Ai6 mice. Because of the endogenous green fluorescence of Zsgreen1expressed in this mouse line after tamoxifen administration, an A647-conjugated secondary donkey anti-rabbit antibody (1:500, Cell Signaling) was used to reveal the POMC staining.

Double-labeling immunohistochemistry. Brain sections from POMC-*Rictor*-KO and their control littermates were processed for the co-localization of rictor and POMC. Sections were first incubated with 10% normal goat serum (Dako) and then with rabbit anti-rictor antibody (1:1000, Bethyl Laboratories, Inc., USA) overnight at 4°C. The next day sections were washed in PBS and incubated for 1h with A647-conjugated secondary goat anti-rabbit antibody (1:500, Cell Signaling). Sections were washed in PBS and incubated with Goat Fab Fragment Anti-Rabbit IgG (1:100, Jackson ImmunoResearch Laboratories, USA) to avoid cross-reactivity. Sections were then washed in PBS and blocked with 10% normal goat serum (Dako) and then incubated with rabbit anti-POMC antibody (1:2000; Phoenix Pharmaceuticals) overnight at 4°C. The next day sections were washed in PBS and incubated for 1h with A488-conjugated secondary goat anti-rabbit antibody (1:500, Cell Signaling).

Evaluation of chemogenetic activation of POMC neurons. Free-fed POMC-ARC^{hM3Dq} mice received a single injection of CNO (1 mg/kg, ip) or its vehicle 90 minutes before sacrifice and expression of c-Fos and phosphorylated S6 ribosomal protein (p-S6) in mCherry-expressing POMC neurons was evaluated. Collected sections were first incubated with 10% normal donkey serum (Jackson ImmunoResearch Laboratories) and then with goat anti-c-Fos antibody (1:250; Santa Cruz Biotechnology, USA) overnight at 4°C. The next day sections were washed in PBS and incubated for 1h with A488-conjugated secondary donkey anti-goat antibody (1:500, EMD Millipore, USA). Sections were then washed in PBS and

blocked with 10% normal goat serum (Dako) and subsequently incubated with rabbit anti-p-S6 ser240/244 antibody (1:200; Cell Signalling) overnight at 4°C. The next day sections were washed in PBS and incubated for 1h with A647-conjugated secondary goat anti-rabbit antibody (1:500, Cell Signaling).

Quantification of the immunohistochemical signal. All sections processed for immunohistochemistry were mounted and cover-slipped. Fluorescent images were acquired with a confocal microscope (SP8-STED, Leica, Germany), corrected for brightness and contrast, and sections containing the ARC were rostro-caudally analyzed using ImageJ.

Fluorescent in situ hybridization (FISH)

Double FISH. Brain sections from perfused POMC-CreER^{T2}-Ai6 mice were also used to assess possible co-expression of AgRP and POMC mRNA. Digoxigenin-labeled riboprobe against mouse AgRP (AgRP-DIG, Allen Brain Atlas, #RP_050419_04_D06) and fluorescein-labeled probe against mouse POMC (POMC-FITC, Allen Brain Atlas, RP_Baylor_102974) were prepared as previously described (Marsicano et al., 2002). Free-floating sections from perfused mouse brains containing the ARC were treated with 0.2M HCl then acetylated with 0.25% acetic anhydride in 0.1 M triethanolamine, pH=8.0 for 10 min. Between all steps, sections were rinsed in PBS-DEPC (PBS with 0.01% diethylpyrocarbonate). Hybmix solution was prepared by dissolving AgRP-DIG and POMC-FITC probes 1/1000 and heated at 90°C for 5min. After hybridization overnight at 70°C, sections were washed at 65°C with increased stringency buffers (5X SSC for 5min, 2X SSC+50%Formamide Amide, 1X SSC+50%Formamide Amide and 0.1X SSC for 30min each, with 0.1% Tween20 added to each buffer). After blocking 1h in TNB buffer (AkoyaBiosciences, prepared as per manufacturer's instructions), sections were incubated overnight at 4°C in HRP-anti-DIG antibody (1/1500, Sigma) in TNB. The revelation was made using TSA-Cy3 kit (1/100,

30min, AkoyaBiosciences). After quenching the peroxidase with 3% H_2O_2 in PBS (30min) and 0.2M HCl treatment (20min), sections were incubated in HRP-anti-FITC antibody (1/1500, Sigma) in TNB for 2h. The revelation was made using TSA-FITC kit (1/100, 30min, AkoyaBiosciences).

Triple FISH. Seven-week-old male C57BL/6J mice with ad libitum access to food and water, were killed by an overdose of pentobarbital. The brains were removed, instantly embedded in OCT Embedding Medium (Thermo Scientific) and stored at -80°C. 10 µm thick coronal sections of the entire ARC were prepared on a Leica CM1950 Cryostat. One section every 100 µm was stained and analyzed from each animal. The following primers were used for FISH antisense probe production: Pomc forward GCAGTGACTAAGAGAGGCCACT, Pomc reverse ATTTAGGTGACACTATAGAAGAGGACTGCCATCTCCCCACAC; Gad67 forward GAAAGGGCCAATTCAGTCAC, Gad67 reverse ATTTAGGTGACACTATAGAGCTGCCTTCAGTGAGATGGCCTAG; vGlut2 forward TCATTGCTGCACTCGTCCACTA, vGlut2 reverse ATTTAGGTGACACTATAGAAGAGCCCTGGGATAGTTTGCAGTCCA. Reverse primers included a SP6 recognition sequence. A hypothalamic mouse RNA library was reverse transcribed into a cDNA library and DNA templates for the relevant transcripts were obtained via PCR using the above primers. Subsequently, these templates were in vitro transcribed into antisense RNA probes using MAXIscript SP6 In Vitro Transcription Kit (Thermo Scientific). 35% of the UTP in each reaction was replaced with either Fluorescein-12-UTP (Roche), Digoxigenin-11-UTP (Roche) or DNP-11-UTP (PerkinElmer) for Pomc, VGlut2 and Gad67 probe production, respectively. For FISH, the following antibodies and tyramide solutions were used: Anti-Fluorescein-POD Fab fragments (Roche), Anti-Digoxigenin-POD Fab fragments (Roche) and Anti-DNP HRP Conjugate (PerkinElmer) as well as Cyanine 3 Tyramide Reagent and Cyanine 5 Tyramide Reagent and Fluorescein Tyramide Reagent (all

PerkinElmer), respectively. Briefly, cryosections were fixed in 4% PFA, washed in PBST and 0.1 M TEA and acetylated, washed again in PBST, and in 5x SSC/50% formamide at 65°C. They were pre-hybridised in prehybridization buffer for 30 min at 65°C and incubated with hybridisation buffer containing all three antisense RNA probes overnight at 65°C. Following washes in 5x SSC, 1x SSC/50% formamide, 2x SSC and 0.2x SSC at 65°C, slides were rinsed with MABT, incubated with one of the above antibodies for 1h, washed with MABT again and developed with one of the above tyramide solutions for 20 min in the dark. Slides were washed with PBST and the remaining enzyme activity of the antibody quenched with 3% H2O2 in PBS for 30 min and subsequent citrate buffer at 95°C for 10 min. The antibody and tyramide incubation steps and the quenching procedure were repeated twice with the remaining antibodies and tyramide solutions. Finally, slides were washed several times in MABT, counterstained with DAPI in PBST and mounted with Aqua-Poly/Mount (Polysciences). All steps were carried out at room temperature unless stated otherwise.

Whole-slide images were acquired on a Axio Scan.Z1 (Zeiss). Image analysis and cell counts were obtained manually in the HALO software (Indica Labs Inc.). Analysis thresholds were applied before images were taken. Brightness and contrast were subsequently modified to facilitate signal visibility. A schematic image of each analyzed coronal brain section was created using Adobe Illustrator CS5 (Adobe Systems Software). For each POMC neuron, its distance to the ventricle and the subpopulations it belonged to was extracted from these schematic images by a custom-written Python script (Graham N. Stratton).

Hypothalamic neuropeptides assays

Hypothalami from 24h fasted or 2h refed C57BL/6J mice, treated icv with RAPA or its vehicle, were extracted in 0.1N HCl and assayed for POMC peptides as previously described (Savontaus et al., 2004). α-MSH RIA was performed with antiserum that cross-reacts fully

with des-acetyl-α-MSH, but has no cross-reactivity with ACTH or CLIP, nor with the free acid form of α-MSH that has not been amidated. β-EP RIA was performed with an antiserum directed at β-EP_{18-25}. ACTH RIA was performed with antiserum directed against $ACTH_{7–18}$ (IgG Corp. TN, USA), which cross-reacts with Pro-ACTH but has no cross-reactivity with α-MSH, CLIP or β-EP (Papadopoulos and Wardlaw, 1999). ELISA for POMC protein was performed with reagents provided by Dr. Anne White at the University of Manchester (Tsigos et al., 1993). Data are expressed versus mg protein.

Endocannabinoid measurements

Hypothalamus, hippocampus and cortex of 24h fasted or 1h refed C57BL/6J mice, treated icv with RAPA or its vehicle, were dissected, flash frozen and stored at -80°C until analysis. In other experiments, hypothalami were collected from 1 h refed C57BL/6J mice injected icv with MTII (0.02µg) or PBS, or with RAPA or with RAPA combined to MTII. Hypothalami were also collected from 1h refed POMC-ARC^{hM3Dq} mice sacrificed after ip injection of CNO or its vehicle and icv administration of RAPA. Measurements of AEA and 2-AG were carried out as in (Gatta-Cherifi et al., 2012). Endocannabinoids content was expressed as fmol or pmol of mg of tissue.

Single-cell RNA sequencing analysis

RNA-seq data on *Pomc*-expressing neurons (≥2 mRNA copies per cell) were extracted from our publicly available dataset on hypothalamic neurons obtained from 2-4 weeks old C57BL/6N mice (GEO accession number: GSE74672, (Romanov et al., 2017). We evaluated the distribution of cells expressing *Pomc* transcripts in the hypothalamus through public databases on in situ mRNA hybridization (Allen Brain Atlas, Mouse Brain, experiments 2493 and 2494) and noted highly specific *Pomc* expression in the ARC. This validates that *Pomc*-

expressing neurons in our single-cell RNA-seq dataset originate from the ARC, and can be used for subtype deconvolution. For the validity of our following analysis, we checked cells for outliers using Principal Component Analysis to exclude those neurons coming to the dataset because of the contamination/ectopic *Pomc* gene transcription. Finally, we performed differential gene expression profiling of *Pomc*$^{+}$ neurons by using Genepattern 3.9.8 (Reich et al., 2006); https://genepattern.broadinstitute.org) with the "ComparativeMarkerSelection" and "ExtractComparativeMarkerResults" modules. Data were then rendered into heatmaps (HeatMapImage module) for maximum visual clarity. The Database for Annotation, Visualization and Integrated Discovery (DAVID) Bioinformatics Resources 6.7 was used to identify the genes that had statistically significant differences in expression among the different POMC neuron subpopulations (Huang da et al., 2009). To interpret our data, we used the «Functional annotation chart» tool. This tool associates gene ID with a biological term which belongs to one out of the 40 annotation categories available in DAVID, including Gene Ontology terms and Kyoto Encyclopedia of Genes and Genomes (KEGG) pathways. This extended annotation coverage increases the analytic power by allowing investigators to analyze their genes from many different biological aspects in a single space. Each functional annotation was associated with an enrichment score, which depended on the distribution of the enrichment (p-values) of each gene. A good enrichment score was obtained when most of genes had good p-values. This score is a relative score instead of a statistical probability with a minimum and a maximum value. This means that enrichment scores could be considered only together, by comparing them.

Electrophysiology

Brain slices preparation. Acute coronal brain slices were prepared from 8 to 12 week-old mice expressing YFP or Chr2 coupled to mCherry selectively in POMC neurons or from

POMC-*CB1*-KO and their control littermates. Animals were anesthetized with isoflurane, the brain extracted and immediately placed in an ice-cold oxygenated cutting solution (in mM: 180 Sucrose, 26 $NaHCO_3$, 11 Glucose, 2.5 KCl, 1.25 NaH_2PO_4, 12 $MgSO_4$, 0.2 $CaCl_2$, saturated with 95% O2-5% CO2). Slices were obtained using a vibratome (VT1200S Leica, Germany) and transferred into a 34°C bath of oxygenated aCSF (in mM: 123 NaCl, 26 $NaHCO_3$, 11 Glucose, 2.5 KCl, 1.25 NaH_2PO_4, 1.3 $MgSO_4$, 2.5 $CaCl_2$; osmolarity 310 mOsm/l, pH 7.4) for 30 minutes and then cooled down progressively till room temperature (RT; 23-25°C) in oxygenated aCSF. After a 45 min recovery period at RT, slices were bisected by cutting along the third ventricle axis. The hemi-slice was anchored with platinum wire at the bottom of the recording chamber and continuously bathed in oxygenated aCSF (32-34°C; 2ml/min) during recording.

Evaluation of WIN effect on mIPSC on PVN parvocellular neurons of POMC-*CB1* mice. Patch electrodes were pulled (micropipette puller P-97, Sutter instrument, USA) from borosilicate glass (O.D. 1.5 mm, I.D. 0.86 mm, Sutter Instrument) to a resistance of 2-4 mΩ. Electrophysiological data were recorded using a Multiclamp 700B amplifier (Molecular devices, UK), low-pass filtered at 4 kHz and digitized at 10Hz (current clamp) or 4 Hz (voltage clamp) (Digidata 1440A, Molecular devices, UK). Signals were analyzed offline (Clampfit software, pClamp 10, Molecular devices, UK). The pipette internal solution contained [in mM: 125 potassium gluconate, 5 KCl, 10 Hepes, 0.6 EGTA, 2 $MgCl_2$, 7 Phosphocreatine, 3 adenosine-5'-triphosphate (magnesium salt), 0.3 guanosine-5'-triphosphate (sodium salt) (pH adjusted to 7.25 with KOH; osmolarity 300 mOsm/l adjusted with d-Mannitol; liquid junction potential -14.8mV corrected on the data presented)]. Parvocellular neurons were differentiated from magnocellular neurons immediately after patch rupture by preliminary electrophysiological analysis. Indeed, when submitted to a depolarizing current magnocellular neurons exhibit a large transient outward rectification, not

found in parvocellular neurons (Luther and Tasker, 2000). Then cells were switched in voltage clamp (Vh = -70 mV). Miniature GABAergic transmission was pharmacologically isolated using a mix of NBQX (10 μM), APV (50 μM) and tetrodotoxin (TTX, 1μM). Note that as a control, few cells were perfused with a GABAA selective antagonist (picrotoxin, 100 μM) at the end of the experiment to fully block miniature transmission. To challenge the CB1 receptor, the selective agonist (WIN55-212, 5 μM) was added. For statistical analysis, miniature events frequency and amplitude during the last 4 minutes of baseline were compared to the same parameters after 10 minutes of drug perfusion (4 minutes also).

Evaluation of RAPA effect on POMC neurons firing. Fluorescent POMC-YFP neurons were identified onto 250 μm thick slices obtained from 8-12 weeks old male POMC-YFP mice, using fluorescence/infrared light (pE-2 CoolLED excitation system, UK). Neurons action potential firing was monitored in whole-cell current-clamp recording configuration. For each recorded neuron, membrane potential (Em), membrane capacitance (Cm) and membrane resistance (Rm) were collected right after cell opening. After a 10 min baseline, RAPA (200 nM) was added in the bath for 20 minutes. For the analysis, considering the variability of the POMC neurons basal firing, the significance of RAPA-induced changes in action potential firing was calculated by comparing the firing rate before and during RAPA application (bin size of 10 sec) using a normalization via Z-score transformation of individuals instantaneous frequencies values (Courtin et al., 2014). Z-score values were calculated by subtracting bin average instantaneous frequencies to the average baseline instantaneous frequency established over at least 120 sec preceding RAPA application and by dividing the difference by the baseline standard deviation. Scores under drug application were obtained comparing the firing rate of recorded neurons 120 sec before and after 4 min of drug application. Neurons with at least 5 significant positive or negative z-score bins (z-score > ±1.96, $p < 0.05$) after RAPA application onset were considered as drug-responsive neurons.

Effect of RAPA on light-evoked POMC to parvocellular neurons neurotransmission. Brains from POMC-Cre$^{+/+}$ mice bilaterally injected with an AAV-DIO-hChR2 were obtained after 5 weeks from the AAV intra-ARC administration and 350μm thick brain slices were prepared following the preparation protocol described above. Here the aCSF was modified in order to increase the neurotransmission success rate (3 mM Ca2+, 0.1 mM Mg2+ and 100μM 4 aminopyridine). Parvocellular neurons were switched in voltage clamp configuration (Vh = -70mV) and synaptic transmission was evoked with a 5 milliseconds flash of blue light (470nm, 1-3mW at 0.03 Hz; pE-2 CoolLED excitation system). Light-evoked glutamatergic or GABAergic transmission was pharmacologically isolated using picrotoxin (100μM) or a NBQX/APV mix (10μM/50μM), respectively. RAPA was added for 20 minutes after at least 10 minutes of stable amplitude light-evoked eEPSCs or eIPSCs. At the end of each experiment, responses were fully blocked using TTX (1μM). For statistical analysis, mean eEPSCs or eIPSCs amplitudes during the last 4 minutes of baseline period were compared to the amplitudes obtained in the same cells after 5 minutes of RAPA perfusion.

POMC neuronal type characterization by immunofluorescence after recording. In order to get information about the cell type of the recorded POMC neurons, we ran immunostaining against the GABAergic marker GAD65/67. The presence of this enzyme within the cell body of the recorded cell indicated a GABAergic profile. During recording POMC neurons were filled via passive diffusion of biocytin (0.4% in internal solution, Sigma, France). Afterwards, slices were fixed overnight at 4°C in 4% PFA-containing phosphate buffer (PB). After washing (3x15min in PB), slices were permeabilized and saturated for 3 hours at RT (0.3% triton, 10% bovine serum albumin in PB). Slices were incubated with primary antibody (anti-GAD65/67 made in rabbit, 1/2000, Millipore) for 72 hours at 4°C. Then the fluorophore-coupled secondary antibody (A647-conjugated secondary goat anti-rabbit antibody, 1:500, Cell Signaling, USA) and a fluorescent streptavidin (AMCA, anti-biotin, 1/1000, Vector

laboratories) were applied overnight at 4°C. Slices were mounted with fluoromount and stored at 4°C in the dark. Pictures of POMC cells were captured using a confocal microscope with objective 63X (SP8-STED, Leica) setting fixed acquisition parameters. Sampling rate respected the optic resolution of the system (voxel size: 0.0819x0.0819x0.2985 μm^3) and z-axis stacks were processed (around 20 images per cells). Images were acquired separately for each wavelength (blue=405nm and far red=647nm) and then merged for analysis. Using Imaris 8.1.2 software (Bitplane, Switzerland), POMC cell body volume (default settings for surface reconstruction) and individual GAD65/67 staining spots (0.4 μm diameters dots, threshold of 3500 pixels set taking into account background signal obtained from staining carried out in the absence of the primary antibody) were automatically reconstructed in 3D. A dedicated analysis module allowed making a clear distinction between the GAD65/67 spots located around the cell and the ones present within the cell body of the POMC neuron.

Statistical analyses

Statistical analyses were performed using Prism (Graphpad, USA). All values are reported as means ± SEM. Data were analyzed by unpaired or paired Student's t-tests or by 1-way or 2-way ANOVAs, as appropriate. Repeated measures for matched individuals were used when same animals underwent different treatments. Significant ANOVAs were followed by Fisher LSD post-hoc test. A Kruskal-Wallis test followed by Dunn's post-test was carried out to test for differences in the distance to the ventricle across the different POMC subpopulations. To describe rostro-caudal changes in the distance to the ventricle for each subpopulation, linear regression analysis was performed using R. Single-cell RNA-seq data for the various *Pomc*$^+$ cells subgroups was analyzed using Student's t-test on log-transformed mRNA copy data. $P<0.05$ denote statistical significance.

Supplemental Information

Supplemental Information includes 7 figures, 2 data tables, and 2 tables with detailed statistical analysis description.

References

Alexander, G.M., Rogan, S.C., Abbas, A.I., Armbruster, B.N., Pei, Y., Allen, J.A., Nonneman, R.J., Hartmann, J., Moy, S.S., Nicolelis, M.A., McNamara, J.O., and Roth, B.L. (2009). Remote control of neuronal activity in transgenic mice expressing evolved G protein-coupled receptors. Neuron *63*, 27-39.

Aponte, Y., Atasoy, D., and Sternson, S.M. (2011). AGRP neurons are sufficient to orchestrate feeding behavior rapidly and without training. Nat Neurosci *14*, 351-355.

Atasoy, D., Aponte, Y., Su, H.H., and Sternson, S.M. (2008). A FLEX switch targets Channelrhodopsin-2 to multiple cell types for imaging and long-range circuit mapping. J Neurosci *28*, 7025-7030.

Balthasar, N., Coppari, R., McMinn, J., Liu, S.M., Lee, C.E., Tang, V., Kenny, C.D., McGovern, R.A., Chua, S.C., Jr., Elmquist, J.K., and Lowell, B.B. (2004). Leptin receptor signaling in POMC neurons is required for normal body weight homeostasis. Neuron *42*, 983-991.

Balthasar, N., Dalgaard, L.T., Lee, C.E., Yu, J., Funahashi, H., Williams, T., Ferreira, M., Tang, V., McGovern, R.A., Kenny, C.D., Christiansen, L.M., Edelstein, E., Choi, B., Boss, O., Aschkenasi, C., Zhang, C.Y., Mountjoy, K., Kishi, T., Elmquist, J.K., and Lowell, B.B. (2005). Divergence of melanocortin pathways in the control of food intake and energy expenditure. Cell *123*, 493-505.

Bellocchio, L., Lafenetre, P., Cannich, A., Cota, D., Puente, N., Grandes, P., Chaouloff, F., Piazza, P.V., and Marsicano, G. (2010). Bimodal control of stimulated food intake by the endocannabinoid system. Nat Neurosci *13*, 281-283.

Bellocchio, L., Soria-Gomez, E., Quarta, C., Metna-Laurent, M., Cardinal, P., Binder, E., Cannich, A., Delamarre, A., Haring, M., Martin-Fontecha, M., Vega, D., Leste-Lasserre, T., Bartsch, D., Monory, K., Lutz, B., Chaouloff, F., Pagotto, U., Guzman, M., Cota, D., and Marsicano, G. (2013). Activation of the sympathetic nervous system mediates hypophagic and anxiety-like effects of CB(1) receptor blockade. Proc Natl Acad Sci U S A *110*, 4786-4791.

Berglund, E.D., Liu, C., Sohn, J.W., Liu, T., Kim, M.H., Lee, C.E., Vianna, C.R., Williams, K.W., Xu, Y., and Elmquist, J.K. (2013). Serotonin 2C receptors in pro-opiomelanocortin neurons regulate energy and glucose homeostasis. J Clin Invest *123*, 5061-5070.

Betley, J.N., Cao, Z.F., Ritola, K.D., and Sternson, S.M. (2013). Parallel, redundant circuit organization for homeostatic control of feeding behavior. Cell *155*, 1337-1350.

Bockaert, J., and Marin, P. (2015). mTOR in Brain Physiology and Pathologies. Physiol Rev *95*, 1157-1187.

Brandt, C., Nolte, H., Henschke, S., Engstrom Ruud, L., Awazawa, M., Morgan, D.A., Gabel, P., Sprenger, H.G., Hess, M.E., Gunther, S., Langer, T., Rahmouni, K., Fenselau, H., Kruger, M., and Bruning, J.C. (2018). Food Perception Primes Hepatic ER Homeostasis via Melanocortin-Dependent Control of mTOR Activation. Cell *175*, 1321-1335 e1320.

Brown, L.M., Clegg, D.J., Benoit, S.C., and Woods, S.C. (2006). Intraventricular insulin and leptin reduce food intake and body weight in C57BL/6J mice. Physiol Behav *89*, 687-691.

Burke, L.K., Darwish, T., Cavanaugh, A.R., Virtue, S., Roth, E., Morro, J., Liu, S.M., Xia, J., Dalley, J.W., Burling, K., Chua, S., Vidal-Puig, T., Schwartz, G.J., and Blouet, C. (2017).

mTORC1 in AGRP neurons integrates exteroceptive and interoceptive food-related cues in the modulation of adaptive energy expenditure in mice. Elife *6*.

Busquets-Garcia, A., Bains, J., and Marsicano, G. (2018). CB1 Receptor Signaling in the Brain: Extracting Specificity from Ubiquity. Neuropsychopharmacology *43*, 4-20.

Campbell, J.N., Macosko, E.Z., Fenselau, H., Pers, T.H., Lyubetskaya, A., Tenen, D., Goldman, M., Verstegen, A.M., Resch, J.M., McCarroll, S.A., Rosen, E.D., Lowell, B.B., and Tsai, L.T. (2017). A molecular census of arcuate hypothalamus and median eminence cell types. Nat Neurosci *20*, 484-496.

Caron, A., Labbe, S.M., Mouchiroud, M., Huard, R., Richard, D., and Laplante, M. (2016). DEPTOR in POMC neurons affects liver metabolism but is dispensable for the regulation of energy balance. Am J Physiol Regul Integr Comp Physiol *310*, R1322-1331.

Castillo, P.E., Younts, T.J., Chavez, A.E., and Hashimotodani, Y. (2012). Endocannabinoid signaling and synaptic function. Neuron *76*, 70-81.

Chen, Y., Lin, Y.C., Kuo, T.W., and Knight, Z.A. (2015). Sensory detection of food rapidly modulates arcuate feeding circuits. Cell *160*, 829-841.

Cota, D., Proulx, K., and Seeley, R.J. (2007). The role of CNS fuel sensing in energy and glucose regulation. Gastroenterology *132*, 2158-2168.

Cota, D., Proulx, K., Smith, K.A., Kozma, S.C., Thomas, G., Woods, S.C., and Seeley, R.J. (2006). Hypothalamic mTOR signaling regulates food intake. Science *312*, 927-930.

Courtin, J., Chaudun, F., Rozeske, R.R., Karalis, N., Gonzalez-Campo, C., Wurtz, H., Abdi, A., Baufreton, J., Bienvenu, T.C., and Herry, C. (2014). Prefrontal parvalbumin interneurons shape neuronal activity to drive fear expression. Nature *505*, 92-96.

Dagon, Y., Hur, E., Zheng, B., Wellenstein, K., Cantley, L.C., and Kahn, B.B. (2012). p70S6 kinase phosphorylates AMPK on serine 491 to mediate leptin's effect on food intake. Cell Metab *16*, 104-112.

Dennison, C.S., King, C.M., Dicken, M.S., and Hentges, S.T. (2016). Age-dependent changes in amino acid phenotype and the role of glutamate release from hypothalamic proopiomelanocortin neurons. J Comp Neurol *524*, 1222-1235.

Dicken, M.S., Tooker, R.E., and Hentges, S.T. (2012). Regulation of GABA and glutamate release from proopiomelanocortin neuron terminals in intact hypothalamic networks. J Neurosci *32*, 4042-4048.

Dietrich, M.O., and Horvath, T.L. (2013). Hypothalamic control of energy balance: insights into the role of synaptic plasticity. Trends Neurosci *36*, 65-73.

Fan, W., Boston, B.A., Kesterson, R.A., Hruby, V.J., and Cone, R.D. (1997). Role of melanocortinergic neurons in feeding and the agouti obesity syndrome. Nature *385*, 165-168.

Fekete, C., Zseli, G., Singru, P.S., Kadar, A., Wittmann, G., Fuzesi, T., El-Bermani, W., and Lechan, R.M. (2012). Activation of Anorexigenic Pro-Opiomelanocortin Neurones during Refeeding is Independent of Vagal and Brainstem Inputs. J Neuroendocrinol *24*, 1423-1431.

Fenselau, H., Campbell, J.N., Verstegen, A.M., Madara, J.C., Xu, J., Shah, B.P., Resch, J.M., Yang, Z., Mandelblat-Cerf, Y., Livneh, Y., and Lowell, B.B. (2017). A rapidly acting glutamatergic ARC-->PVH satiety circuit postsynaptically regulated by alpha-MSH. Nat Neurosci *20*, 42-51.

Gatta-Cherifi, B., Matias, I., Vallee, M., Tabarin, A., Marsicano, G., Piazza, P.V., and Cota, D. (2012). Simultaneous postprandial deregulation of the orexigenic endocannabinoid anandamide and the anorexigenic peptide YY in obesity. Int J Obes (Lond) *36*, 880-885.

Haissaguerre, M., Ferriere, A., Simon, V., Saucisse, N., Dupuy, N., Andre, C., Clark, S., Guzman-Quevedo, O., Tabarin, A., and Cota, D. (2018). mTORC1-dependent increase in oxidative metabolism in POMC neurons regulates food intake and action of leptin. Mol Metab *12*, 98-106.

Haissaguerre, M., Saucisse, N., and Cota, D. (2014). Influence of mTOR in energy and metabolic homeostasis. Mol Cell Endocrinol *397*, 67-77.

Hara, K., Maruki, Y., Long, X., Yoshino, K., Oshiro, N., Hidayat, S., Tokunaga, C., Avruch, J., and Yonezawa, K. (2002). Raptor, a binding partner of target of rapamycin (TOR), mediates TOR action. Cell *110*, 177-189.

Henry, F.E., Sugino, K., Tozer, A., Branco, T., and Sternson, S.M. (2015). Cell type-specific transcriptomics of hypothalamic energy-sensing neuron responses to weight-loss. Elife *4*.

Hentges, S.T., Nishiyama, M., Overstreet, L.S., Stenzel-Poore, M., Williams, J.T., and Low, M.J. (2004). GABA release from proopiomelanocortin neurons. J Neurosci 24, 1578-1583.

Hentges, S.T., Otero-Corchon, V., Pennock, R.L., King, C.M., and Low, M.J. (2009). Proopiomelanocortin expression in both GABA and glutamate neurons. J Neurosci *29*, 13684-13690.

Huang da, W., Sherman, B.T., and Lempicki, R.A. (2009). Systematic and integrative analysis of large gene lists using DAVID bioinformatics resources. Nat Protoc *4*, 44-57.

Jarvie, B.C., and Hentges, S.T. (2012). Expression of GABAergic and glutamatergic phenotypic markers in hypothalamic proopiomelanocortin neurons. J Comp Neurol *520*, 3863-3876.

Jones, G.L., Wittmann, G., Yokosawa, E.B., Yu, H., Mercer, A.J., Lechan, R.M., and Low, M.J. (2019). Selective Restoration of Pomc Expression in Glutamatergic POMC Neurons: Evidence for a Dynamic Hypothalamic Neurotransmitter Network. eNeuro *6*.

Kirkham, T.C., Williams, C.M., Fezza, F., and Di Marzo, V. (2002). Endocannabinoid levels in rat limbic forebrain and hypothalamus in relation to fasting, feeding and satiation: stimulation of eating by 2-arachidonoyl glycerol. Br J Pharmacol *136*, 550-557.

Koch, M., and Horvath, T.L. (2014). Molecular and cellular regulation of hypothalamic melanocortin neurons controlling food intake and energy metabolism. Mol Psychiatry *19*, 752-761.

Koch, M., Varela, L., Kim, J.G., Kim, J.D., Hernandez-Nuno, F., Simonds, S.E., Castorena, C.M., Vianna, C.R., Elmquist, J.K., Morozov, Y.M., Rakic, P., Bechmann, I., Cowley, M.A., Szigeti-Buck, K., Dietrich, M.O., Gao, X.B., Diano, S., and Horvath, T.L. (2015). Hypothalamic POMC neurons promote cannabinoid-induced feeding. Nature *519*, 45-50.

Krashes, M.J., Lowell, B.B., and Garfield, A.S. (2016). Melanocortin-4 receptor-regulated energy homeostasis. Nat Neurosci *19*, 206-219.

Lam, B.Y.H., Cimino, I., Polex-Wolf, J., Nicole Kohnke, S., Rimmington, D., Iyemere, V., Heeley, N., Cossetti, C., Schulte, R., Saraiva, L.R., Logan, D.W., Blouet, C., O'Rahilly, S., Coll, A.P., and Yeo, G.S.H. (2017). Heterogeneity of hypothalamic pro-opiomelanocortin-expressing neurons revealed by single-cell RNA sequencing. Mol Metab *6*, 383-392.

Luther, J.A., and Tasker, J.G. (2000). Voltage-gated currents distinguish parvocellular from magnocellular neurones in the rat hypothalamic paraventricular nucleus. J Physiol *523 Pt 1*, 193-209.

Madisen, L., Zwingman, T.A., Sunkin, S.M., Oh, S.W., Zariwala, H.A., Gu, H., Ng, L.L., Palmiter, R.D., Hawrylycz, M.J., Jones, A.R., Lein, E.S., and Zeng, H. (2010). A robust and high-throughput Cre reporting and characterization system for the whole mouse brain. Nat Neurosci *13*, 133-140.

Marsicano, G., Wotjak, C. T., Azad, S. C., Bisogno, T., Rammes, G., Cascio, M. G., Hermann, H., Tang, J., Hofmann, C., Zieglgänsberger, W., Di Marzo V., and Lutz, B. (2002). The endogenous cannabinoid system controls extinction of aversive memories. Nature *418*, 530-534.

Marsicano, G., Goodenough, S., Monory, K., Hermann, H., Eder, M., Cannich, A., Azad,

S.C., Cascio, M.G., Gutierrez, S.O., van der Stelt, M., Lopez-Rodriguez, M.L., Casanova, E., Schutz, G., Zieglgansberger, W., Di Marzo, V., Behl, C., and Lutz, B. (2003). CB1 cannabinoid receptors and on-demand defense against excitotoxicity. Science *302*, 84-88.

Mazier, W., Saucisse, N., Gatta-Cherifi, B., and Cota, D. (2015). The Endocannabinoid System: Pivotal Orchestrator of Obesity and Metabolic Disease. Trends Endocrinol Metab *26*, 524-537.

Mazier, W., Saucisse, N., Simon, V., Cannich, A., Marsicano, G., Massa, F., and Cota, D. (2019). mTORC1 and CB1 receptor signaling regulate excitatory glutamatergic inputs onto the hypothalamic paraventricular nucleus in response to energy availability. Mol Metab *28*, 151-159.

Monge-Roffarello, B., Labbe, S.M., Roy, M.C., Lemay, M.L., Coneggo, E., Samson, P., Lanfray, D., and Richard, D. (2014). The PVH as a site of CB1-mediated stimulation of thermogenesis by MC4R agonism in male rats. Endocrinology *155*, 3448-3458.

Monory, K., Massa, F., Egertova, M., Eder, M., Blaudzun, H., Westenbroek, R., Kelsch, W., Jacob, W., Marsch, R., Ekker, M., Long, J., Rubenstein, J.L., Goebbels, S., Nave, K.A., During, M., Klugmann, M., Wolfel, B., Dodt, H.U., Zieglgansberger, W., Wotjak, C.T., Mackie, K., Elphick, M.R., Marsicano, G., and Lutz, B. (2006). The endocannabinoid system controls key epileptogenic circuits in the hippocampus. Neuron *51*, 455-466.

Mori, H., Inoki, K., Munzberg, H., Opland, D., Faouzi, M., Villanueva, E.C., Ikenoue, T., Kwiatkowski, D., MacDougald, O.A., Myers, M.G., Jr., and Guan, K.L. (2009). Critical role for hypothalamic mTOR activity in energy balance. Cell Metab *9*, 362-374.

Ollmann, M.M., Wilson, B.D., Yang, Y.K., Kerns, J.A., Chen, Y., Gantz, I., and Barsh, G.S. (1997). Antagonism of central melanocortin receptors in vitro and in vivo by agouti-related protein. Science *278*, 135-138.

Padilla, S.L., Carmody, J.S., and Zeltser, L.M. (2010). Pomc-expressing progenitors give rise to antagonistic neuronal populations in hypothalamic feeding circuits. Nat Med *16*, 403-405.

Papadopoulos, A.D., and Wardlaw, S.L. (1999). Endogenous alpha-MSH modulates the hypothalamic-pituitary-adrenal response to the cytokine interleukin-1beta. J Neuroendocrinol *11*, 315-319.

Piazza, P.V., Cota, D., and Marsicano, G. (2017). The CB1 Receptor as the Cornerstone of Exostasis. Neuron *93*, 1252-1274.

Reich, M., Liefeld, T., Gould, J., Lerner, J., Tamayo, P., and Mesirov, J.P. (2006). GenePattern 2.0. Nat Genet *38*, 500-501.

Romanov, R.A., Zeisel, A., Bakker, J., Girach, F., Hellysaz, A., Tomer, R., Alpar, A., Mulder, J., Clotman, F., Keimpema, E., Hsueh, B., Crow, A.K., Martens, H., Schwindling, C., Calvigioni, D., Bains, J.S., Mate, Z., Szabo, G., Yanagawa, Y., Zhang, M.D., Rendeiro, A., Farlik, M., Uhlen, M., Wulff, P., Bock, C., Broberger, C., Deisseroth, K., Hokfelt, T., Linnarsson, S., Horvath, T.L., and Harkany, T. (2017). Molecular interrogation of hypothalamic organization reveals distinct dopamine neuronal subtypes. Nat Neurosci *20*, 176-188.

Sarbassov, D.D., Ali, S.M., Kim, D.H., Guertin, D.A., Latek, R.R., Erdjument-Bromage, H., Tempst, P., and Sabatini, D.M. (2004). Rictor, a novel binding partner of mTOR, defines a rapamycin-insensitive and raptor-independent pathway that regulates the cytoskeleton. Curr Biol *14*, 1296-1302.

Savontaus, E., Breen, T.L., Kim, A., Yang, L.M., Chua, S.C., Jr., and Wardlaw, S.L. (2004). Metabolic effects of transgenic melanocyte-stimulating hormone overexpression in lean and obese mice. Endocrinology *145*, 3881-3891.

Saxton, R.A., and Sabatini, D.M. (2017). mTOR Signaling in Growth, Metabolism, and Disease. Cell *168*, 960-976.

Singru, P.S., Sanchez, E., Fekete, C., and Lechan, R.M. (2007). Importance of melanocortin signaling in refeeding-induced neuronal activation and satiety. Endocrinology *148*, 638-646.

Singru, P.S., Wittmann, G., Farkas, E., Zseli, G., Fekete, C., and Lechan, R.M. (2012). Refeeding-activated glutamatergic neurons in the hypothalamic paraventricular nucleus (PVN) mediate effects of melanocortin signaling in the nucleus tractus solitarius (NTS). Endocrinology *153*, 3804-3814.

Smith, M.A., Katsouri, L., Irvine, E.E., Hankir, M.K., Pedroni, S.M., Voshol, P.J., Gordon, M.W., Choudhury, A.I., Woods, A., Vidal-Puig, A., Carling, D., and Withers, D.J. (2015). Ribosomal S6K1 in POMC and AgRP Neurons Regulates Glucose Homeostasis but Not Feeding Behavior in Mice. Cell Rep *11*, 335-343.

Soria-Gomez, E., Bellocchio, L., Reguero, L., Lepousez, G., Martin, C., Bendahmane, M., Ruehle, S., Remmers, F., Desprez, T., Matias, I., Wiesner, T., Cannich, A., Nissant, A., Wadleigh, A., Pape, H.C., Chiarlone, A.P., Quarta, C., Verrier, D., Vincent, P., Massa, F., Lutz, B., Guzman, M., Gurden, H., Ferreira, G., Lledo, P.M., Grandes, P., and Marsicano, G. (2014a). The endocannabinoid system controls food intake via olfactory processes. Nat Neurosci *17*, 407-415.

Soria-Gomez, E., Massa, F., Bellocchio, L., Rueda-Orozco, P.E., Ciofi, P., Cota, D., Oliet, S.H., Prospero-Garcia, O., and Marsicano, G. (2014b). Cannabinoid type-1 receptors in the paraventricular nucleus of the hypothalamus inhibit stimulated food intake. Neuroscience *263*, 46-53.

Tong, Q., Ye, C., McCrimmon, R.J., Dhillon, H., Choi, B., Kramer, M.D., Yu, J., Yang, Z., Christiansen, L.M., Lee, C.E., Choi, C.S., Zigman, J.M., Shulman, G.I., Sherwin, R.S., Elmquist, J.K., and Lowell, B.B. (2007). Synaptic glutamate release by ventromedial hypothalamic neurons is part of the neurocircuitry that prevents hypoglycemia. Cell Metab *5*, 383-393.

Tong, Q., Ye, C.P., Jones, J.E., Elmquist, J.K., and Lowell, B.B. (2008). Synaptic release of GABA by AgRP neurons is required for normal regulation of energy balance. Nat Neurosci *11*, 998-1000.

Tsigos, C., Crosby, S.R., Gibson, S., Young, R.J., and White, A. (1993). Proopiomelanocortin is the predominant adrenocorticotropin-related peptide in human cerebrospinal fluid. J Clin Endocrinol Metab *76*, 620-624.

Verty, A.N., McFarlane, J.R., McGregor, I.S., and Mallet, P.E. (2004). Evidence for an interaction between CB1 cannabinoid and melanocortin MCR-4 receptors in regulating food intake. Endocrinology *145*, 3224-3231.

Wardlaw, S.L. (2011). Hypothalamic proopiomelanocortin processing and the regulation of energy balance. Eur J Pharmacol *660*, 213-219.

Weston, M.C., Chen, H., and Swann, J.W. (2012). Multiple roles for mammalian target of rapamycin signaling in both glutamatergic and GABAergic synaptic transmission. J Neurosci *32*, 11441-11452.

Wittmann, G., Hrabovszky, E., and Lechan, R.M. (2013). Distinct glutamatergic and GABAergic subsets of hypothalamic pro-opiomelanocortin neurons revealed by in situ hybridization in male rats and mice. J Comp Neurol *521*, 3287-3302.

Yang, S.B., Tien, A.C., Boddupalli, G., Xu, A.W., Jan, Y.N., and Jan, L.Y. (2012). Rapamycin ameliorates age-dependent obesity associated with increased mTOR signaling in hypothalamic POMC neurons. Neuron *75*, 425-436.

Zhan, C., Zhou, J., Feng, Q., Zhang, J.E., Lin, S., Bao, J., Wu, P., and Luo, M. (2013). Acute and long-term suppression of feeding behavior by POMC neurons in the brainstem and hypothalamus, respectively. J Neurosci *33*, 3624-3632.

Figure 1

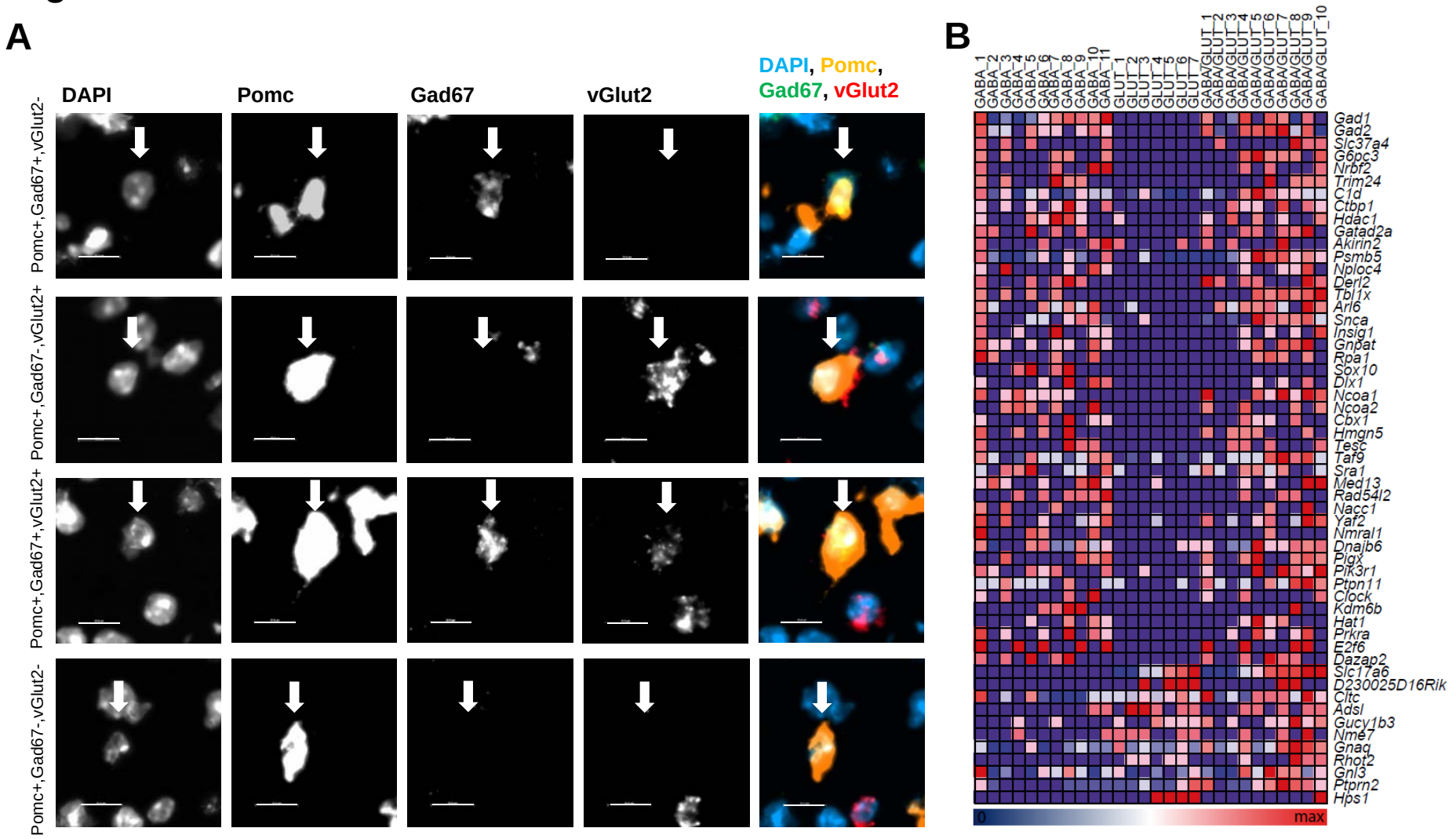
A
DAPI
Pomc
Gad67
vGlut2
DAPI, Pomc, Gad67, vGlut2
Pomc+,Gad67+,vGlut2-
Pomc+,Gad67-,vGlut2+
Pomc+,Gad67+,vGlut2+
Pomc+,Gad67-,vGlut2-
B
GABA_1
GABA_2
GABA_3
GABA_4
GABA_5
GABA_6
GABA_7
GABA_8
GABA_9
GABA_10
GABA_11
GLUT_1
GLUT_2
GLUT_3
GLUT_4
GLUT_5
GLUT_6
GLUT_7
GABA/GLUT_1
GABA/GLUT_2
GABA/GLUT_3
GABA/GLUT_4
GABA/GLUT_5
GABA/GLUT_6
GABA/GLUT_7
GABA/GLUT_8
GABA/GLUT_9
GABA/GLUT_10
Gad1
Gad2
Slc37a4
G6pc3
Nrbf2
Trim24
C1d
Ctbp1
Hdac1
Gatad2a
Akirin2
Psmb5
Nploc4
Derl2
Tbl1x
Arl6
Snca
Insig1
Gnpat
Rpa1
Sox10
Dlx1
Ncoa1
Ncoa2
Cbx1
Hmgn5
Tesc
Taf9
Sra1
Med13
Rad54l2
Nacc1
Yaf2
Nmral1
Dnajb6
Pigx
Pik3r1
Ptpn11
Clock
Kdm6b
Hat1
Prkra
E2f6
Dazap2
Slc17a6
D230025D16Rik
Cltc
Adsl
Gucy1b3
Nme7
Gnaq
Rhot2
Gnl3
Ptprn2
Hps1
0
max

Figure 2

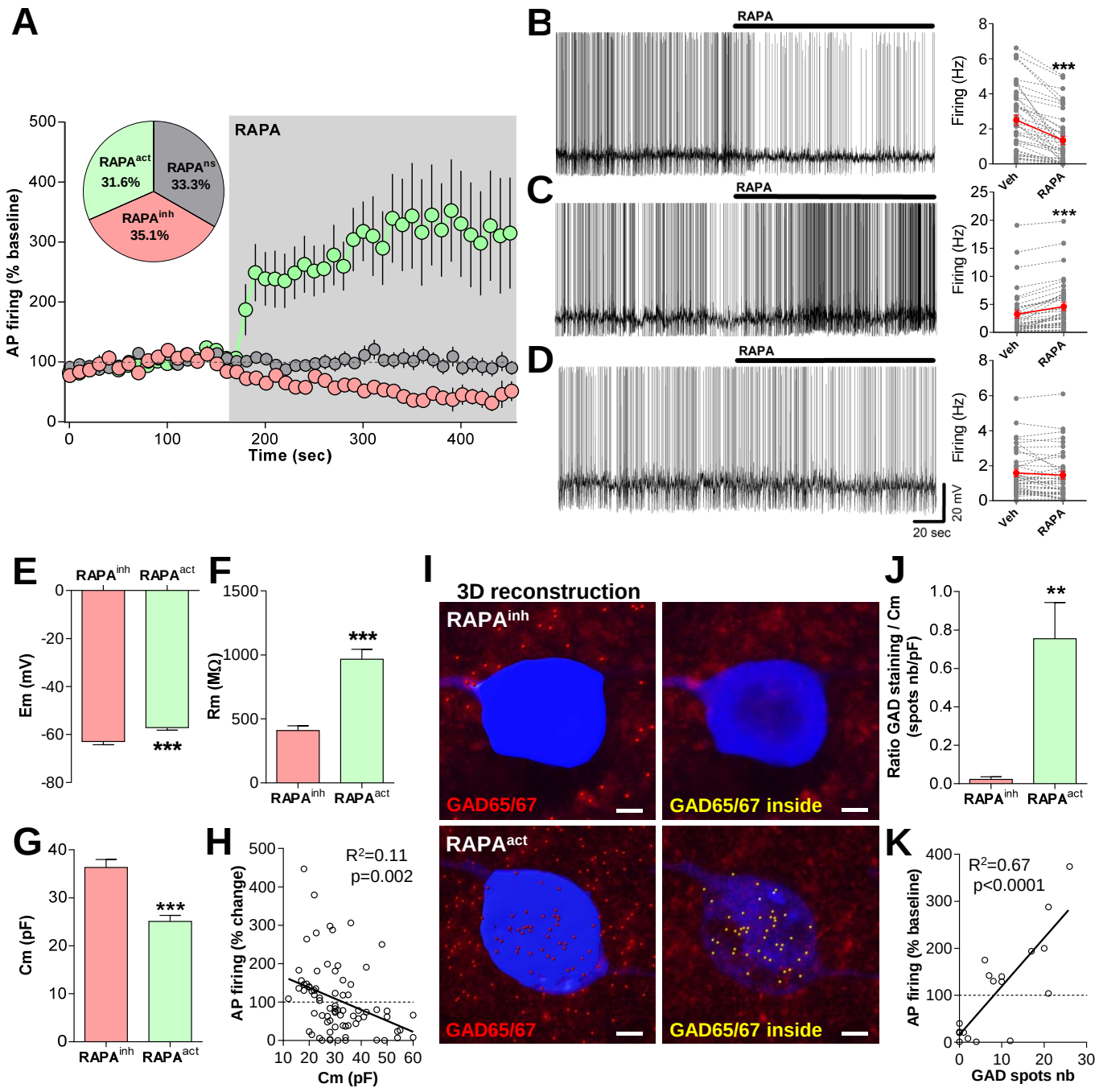
A
RAPA
RAPA^act 31.6%
RAPA^ns 33.3%
RAPA^inh 35.1%
AP firing (% baseline)
Time (sec)
B
C
D
RAPA
Firing (Hz)
Veh
RAPA
***
20 mV
20 sec
E
RAPA^inh
RAPA^act
Em (mV)
***
F
Rm (MΩ)
***
G
Cm (pF)
***
H
R²=0.11
p=0.002
AP firing (% change)
Cm (pF)
I
3D reconstruction
RAPA^inh
RAPA^act
GAD65/67
GAD65/67 inside
J
Ratio GAD staining / Cm (spots nb/pF)
**
K
R²=0.67
p<0.0001
AP firing (% baseline)
GAD spots nb

Figure 3

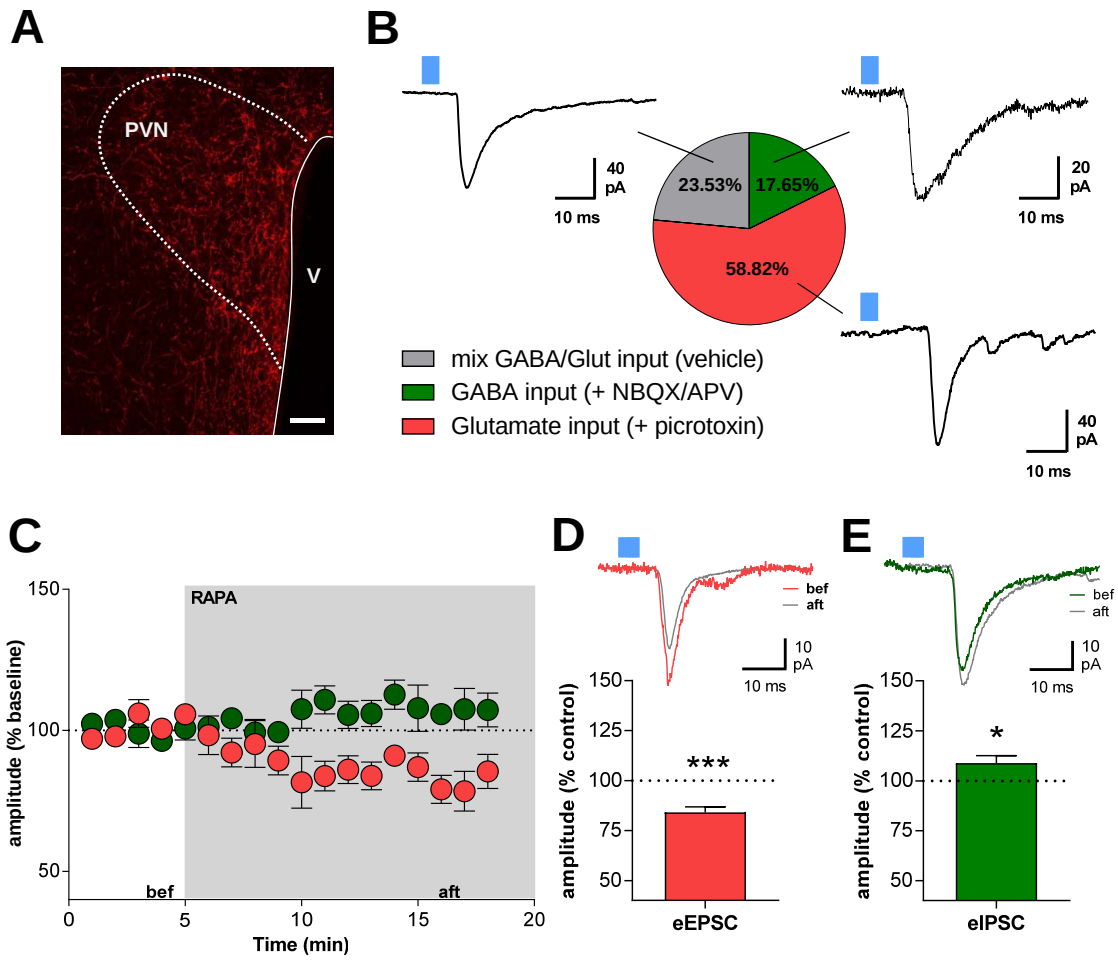
A
PVN
V
B
40
pA
10 ms
23.53%
17.65%
58.82%
20
pA
10 ms
40
pA
10 ms
mix GABA/Glut input (vehicle)
GABA input (+ NBQX/APV)
Glutamate input (+ picrotoxin)
C
RAPA
amplitude (% baseline)
150
100
50
bef
aft
0
5
10
15
20
Time (min)
D
bef
aft
10
pA
10 ms
amplitude (% control)
150
125
100
75
50
***
eEPSC
E
bef
aft
10
pA
10 ms
amplitude (% control)
150
125
100
75
50
*
eIPSC

Figure 4

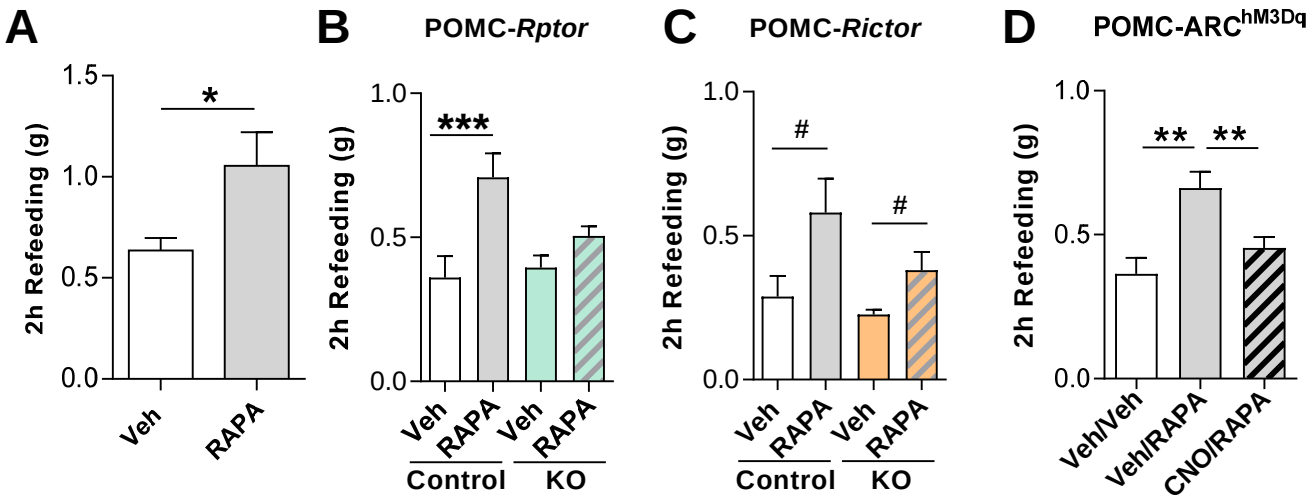
A
B
POMC-*Rptor*
C
POMC-*Rictor*
D
POMC-ARC^{hM3Dq}
2h Refeeding (g)
1.5
1.0
0.5
0.0
*
Veh
RAPA
***
Control
KO
#
Veh/Veh
Veh/RAPA
CNO/RAPA
**

Figure 5

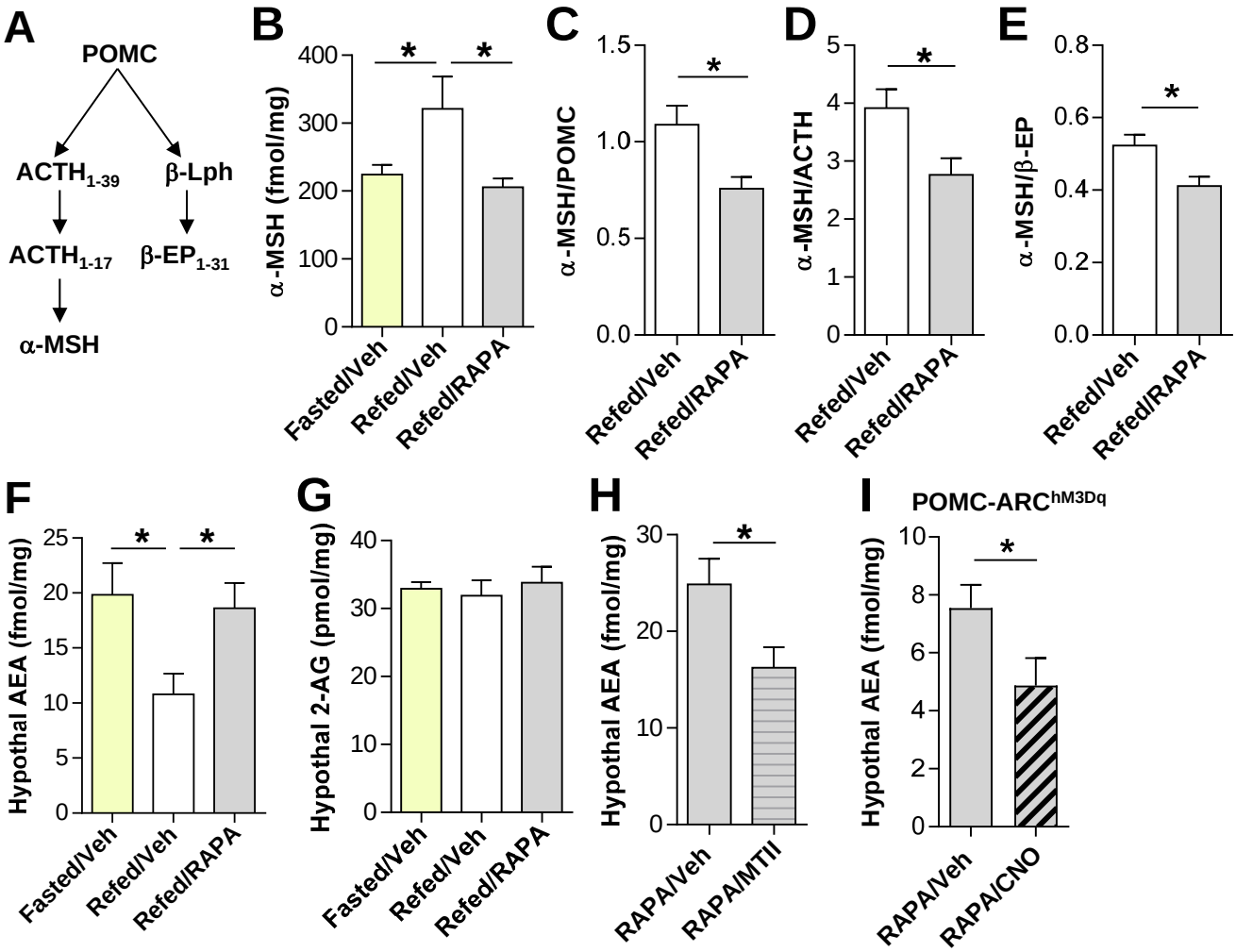
A
POMC
ACTH1-39
β-Lph
ACTH1-17
β-EP1-31
α-MSH
B
α-MSH (fmol/mg)
Fasted/Veh
Refed/Veh
Refed/RAPA
C
α-MSH/POMC
Refed/Veh
Refed/RAPA
D
α-MSH/ACTH
Refed/Veh
Refed/RAPA
E
α-MSH/β-EP
Refed/Veh
Refed/RAPA
F
Hypothal AEA (fmol/mg)
Fasted/Veh
Refed/Veh
Refed/RAPA
G
Hypothal 2-AG (pmol/mg)
Fasted/Veh
Refed/Veh
Refed/RAPA
H
Hypothal AEA (fmol/mg)
RAPA/Veh
RAPA/MTII
I
POMC-ARChM3Dq
Hypothal AEA (fmol/mg)
RAPA/Veh
RAPA/CNO

Figure 6

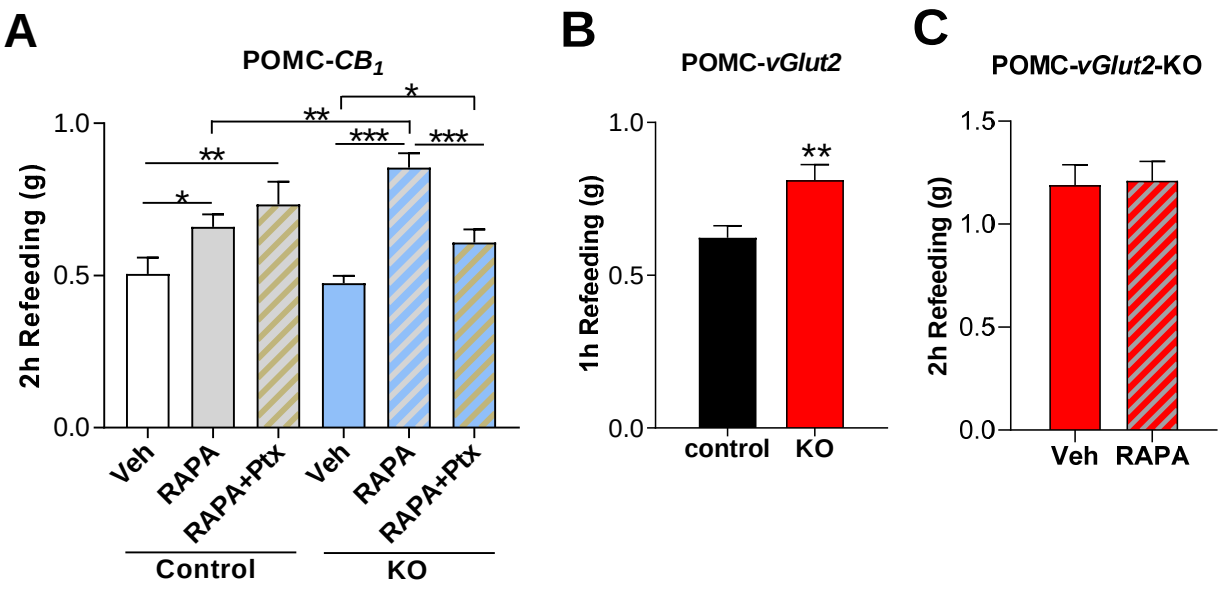
A
POMC-CB1
2h Refeeding (g)
1.0
0.5
0.0
*
**
***
***
**
*
Veh
RAPA
RAPA+Ptx
Veh
RAPA
RAPA+Ptx
Control
KO
B
POMC-vGlut2
1h Refeeding (g)
1.0
0.5
0.0
**
control
KO
C
POMC-vGlut2-KO
2h Refeeding (g)
1.5
1.0
0.5
0.0
Veh
RAPA

Table S1. Detailed data about the different light-evoked POMC inputs recorded in 17 connected parvocellular neurons (Related to Figure 3). Recorded cell features (Em, Cm and Rm) were collected right after patch establishment. Parameters on light-evoked transmission (Peak amplitude, Time of peak and Decay time constant) are indicated as the mean of 4 minutes (± sem) after at least 10 minutes of treatment.

Recorded cell	Treatment	Peak Amplitude (pA)	Time of peak (msec)	Decay (msec)
Pure Glut (no effect of picrotoxin)				
Cell# 1	Veh	-32.3 ± 3.41	15.1 ± 0.16	2.7 ± 0.23
-44mV 22pF MΩ	Picrotoxin	-33.1 ± 0.47	14.9 ± 0.05	2.6 ± 0.18
Cell# 2	Veh	-43.8 ± 2.62	19.8 ± 0.1	2.3 ± 0.08
-43mV 19pF 750MΩ	Picrotoxin	-46.3 ± 1.43	21.5 ± 0.53	2.0 ± 0.11
Cell# 3	Veh	-24.5 ± 1.32	14.8 ± 0.08	2.6 ± 0.17
-44mV 22pF 750MΩ	Picrotoxin	-27.9 ± 2.02	15.1 ± 0.15	2.4 ± 0.13
Cell# 4	Veh	-138.0 ± 0.97	12.5 ± 0.03	3.5 ± 0.04
-52mV 34pF 750MΩ	Picrotoxin	-144.0 ± 1.70	12.5 ± 0.02	3.2 ± 0.09
Pure Glut (full blockade by NBQX APV)				
Cell# 5	Veh	-22.8 ± 1.09	16.1 ± 0.30	2.7 ± 0.20
-42mV 23pF 800MΩ	NBQX/APV	no peak	no peak	no peak
Cell# 6	Veh	-32.4 ± 1.06	10.9 ± 0.04	1.6 ± 0.01
-48mV 23pF 710MΩ	NBQX/APV	no peak	no peak	no peak
Cell# 7	Veh	-27.5 ± 0.91	13.1 ± 0.07	1.9 ± 0.34
-49mV 26pF 650MΩ	NBQX/APV	no peak	no peak	no peak
Cell# 8	Veh	-26.0 ± 1.52	11.6 ± 0.03	2.2 ± 0.04
-46mV 21pF 850MΩ	NBQX/APV	no peak	no peak	no peak
Cell# 9	Veh	-87.3 ± 2.44	21.5 ± 0.18	3.1 ± 0.05
-49mV 18pF 750MΩ	NBQX/APV	no peak	no peak	no peak
Cell# 10	Veh	-40.2 ± 2.21	12.5 ± 0.23	2.1 ± 0.17
-46mV 23pF 930MΩ	NBQX/APV	no peak	no peak	no peak
Pure GABA (full blockade by picrotoxin)				
Cell# 11	Veh	-79.0 ± 1.44	50.6 ± 0.63	7.6 ± 0.16
-44mV 19pF 1500MΩ	Picrotoxin	no peak	no peak	no peak
Cell# 12	Veh	-56.0 ± 1.78	15.1 ± 0.09	11.7 ± 0.67
-42mV 15pF 2000MΩ	Picrotoxin	no peak	no peak	no peak
Cell# 13	Veh	-25.7 ± 0.82	18.7 ± 0.29	8.1 ± 0.64
-44mV 17pF 2000MΩ	Picrotoxin	no peak	no peak	no peak
GABA/Glut (isolation of Glut)				
Cell# 14	Veh	-220.9 ± 7.31	14.3 ± 0.04	6.3 ± 0.21
-42mV 17pF 900MΩ	Picrotoxin	-26.7 ± 1.09	12.4 ± 0.06	2.9 ± 0.27
Cell# 15	Veh	-20.7 ± 0.25	18.3 ± 0.07	3.5 ± 0.07
-48mV 22pF 820MΩ	Picrotoxin	-24.9 ± 1.21	18.3 ± 0.52	2.9 ± 0.14
GABA/Glut (isolation of GABA)				
Cell# 16	Veh	-72.7 ± 2.14	13.3 ± 0.03	5.4 ± 0.07
-45mV 19pF 750MΩ	NBQX/APV	-44.9 ± 0.96	13.3 ± 0.06	5.9 ± 0.17
Cell# 17	Veh	-63.7 ± 1.20	20.7 ± 0.08	5.1 ± 0.12
-48mV 23pF 1800MΩ	NBQX/APV	-47.4 ± 2.24	21.7 ± 0.16	4.9 ± 0.04

Table S2. POMC and POMC-derived peptides ACTH and β-EP levels in the hypothalamus and endocannabinoid levels in the cortex and the hippocampus of mice fasted or refed and treated with an icv injection of RAPA or its vehicle. Data are Mean ± SEM.

Analyte	Fasted/Veh	Refed/Veh	Refed/RAPA	N mice	Analysis	Degree of freedom & F/t/R etc value	p-value
POMC (fmol/mg prot)	254.18 ± 14.85	292.94 ± 29.63	281.99 ± 24.07	8	One-way ANOVA	F (2, 21) = 0.7140	0.5012
ACTH (fmol/mg prot)	71.98 ± 11.06	84.88 ± 12.95	78.91 ± 8.15	8	One-way ANOVA	F (2, 21) = 0.3511	0.7080
β-EP (fmol/mg prot)	462.2 ± 26.11	620.0 ± 88.03	502.4 ± 22.15	8	One-way ANOVA	F (2, 21) = 2.261	0.1291
AEA (fmol/mg tissue)							
Hippocampus	38.99 ± 4.99	43.14 ± 4.45	38.16 ± 4.03	3-5	One-way ANOVA	F (2, 10) = 0.3972	0.6823
Cortex	35.22 ± 4.52	38.72 ± 4.38	38.25 ± 6.72	3-5	One-way ANOVA	F (2, 10) = 0.08910	0.9155
2-AG (pmol/mg tissue)							
Hippocampus	12.55 ± 2.94	14.89 ± 1.14	13.85 ± 1.66	3-5	One-way ANOVA	F (2, 10) = 0.3893	0.6873
Cortex	16.84 ± 0.50	15.38 ± 0.68	16.53 ± 2.15	3-5	One-way ANOVA	F (2, 10) = 0.2237	0.8035

Table S3. Statistical analyses for main figures.

Figure	Dependent variable(s)	Factor Analyzed	Analysis	n	Degree of freedom & F/t/R etc value	P value
2B	POMC AP firing	Treatment	Paired t-test	41 cells	t=7.175 df=40	p<0.0001
2C	POMC AP firing	Treatment	Paired t-test	37 cells	t=6.707 df=36	p<0.0001
2D	POMC AP firing	Treatment	Paired t-test	39 cells	t=1.692 df=38	p=0.0989
2E	POMC cell Em	Group	Unpaired t-test	41-37 cells	t=3.425 df=76	p=0.0010
2F	POMC cell Rm	Group	Unpaired t-test	41-37 cells	t=6.653 df=76	p<0.0001
2G	POMC cell Cm	Group	Unpaired t-test	41-37 cells	t=5.282 df=76	p<0.0001
2H	RAPA effect vs POMC cell Cm	Correlation	Linear Regression	78 cells	R^2=0.1191	p=0.0020
2J	Ratio GAD spots number / Cm	Group	Unpaired t-test	7-11 cells	t=3.063 df=16	p=0.0074
2K	AP firing change (%) vs GAD spots number	Correlation	Linear Regression	18 cells	R^2=0.6683	p<0.0001
3D	% Change in eEPSC amplitude	Treatment	Paired t-test, one-tailed	6 cells	t=6.802, df=5	p=0.0005
3E	% Change in eIPSC amplitude	Treatment	Paired t-test, one-tailed	5 cells	t=2.290, df=4	p=0.041
4A	2h food intake	Treatment	Unpaired t-test	5	t=2.359 df=8	p=0.0460
4B	2h food intake	Genotype	RM Two-way ANOVA	6-9	F (1, 13) = 1.828	p=0.1994
4B	2h food intake	Treatment	RM Two-way ANOVA	6-9	F (1, 13) = 21.71	p=0.0004
4B	2h food intake	Interaction	RM Two-way ANOVA	6-9	F (1, 13) = 5.870	p=0.0307
4B	2h food intake	Matched individuals	RM Two-way ANOVA	6-9	F (13, 13) = 1,623	p=0.1970
4C	2h food intake	Genotype	RM Two-way ANOVA	5	F (1, 8) = 4.325	p=0.0711
4C	2h food intake	Treatment	RM Two-way ANOVA	5	F (1, 8) = 6,337	p=0.0360
4C	2h food intake	Interaction	RM Two-way ANOVA	5	F (1, 8) = 0.6067	p=0.4585
4C	2h food intake	Matched individuals	RM Two-way ANOVA	5	F (8, 8) = 0.5056	p=0.8229
4D	2h food intake	Treatment	RM one-way ANOVA	5	F (1.938, 7.751) = 30,42	p=0.0002
4D	2h food intake	Matched individuals	RM one-way ANOVA	5	F (4, 8) = 7.995	p=0.0067
5B	α-MSH levels	Treatment	One-way ANOVA	8	F (2, 21) = 4.440	p=0.0246
5C	α-MSH/POMC	Treatment	Unpaired t-test	8	t=2.873 df=14	p=0.0123
5D	α-MSH/ACTH	Treatment	Unpaired t-test	8	t=2.646 df=14	p=0.0192
5E	α-MSH/β-EP	Treatment	Unpaired t-test	8	t=2.807 df=14	p=0.0140
5F	AEA levels	Treatment	One-way	3-5	F (2, 10) = 4.737	p=0.0357

			ANOVA			
5G	2-AG levels	Treatment	One-way ANOVA	3-5	F (2, 10) = 0,2019	p=0.8204
5H	AEA levels	Treatment	Unpaired t-test	6	t=2.556 df=10	p=0.0286
5I	AEA levels	Treatment	Unpaired t-test	8-10	t=2.171 df=16	p=0.0453
6A	2h food intake	Genotype	Two-way ANOVA	8-18	F (1, 78) = 0.111	p=0.739
6A	2h food intake	Treatment	Two-way ANOVA	8-18	F (2, 78) = 20.37	p<0.0001
6A	2h food intake	Interaction	Two-way ANOVA	8-18	F (2, 78) = 6.288	p=0.0029
6B	1h food intake	Genotype	Unpaired t-test	8-14	t=2.902 df=20	p=0.0088
6C	2h food intake	Treatment	Paired t-test	8	t=0.1839 df=7	p=0.859

Table S4. Statistical analyses for supplemental figures.

Figure	Dependent variable(s)	Factor Analyzed	Analysis	n	Degree of freedom & F/t/R etc value	P value
S1B	Distance from ventricle	Group	Kruskal-Wallis test	3914 cells		p<0.0001
S1C	Slope of the lines	Group	Linear regression	3914 cells	F=1.185e+014 dfn=3	p<0.0001
S3A	POMC AP firing	Treatment	Paired t-test	117 cells	t=0.0793 df=116	p=0.9369
S3B	Change in Em under RAPA	Group	Unpaired t-test	41-37 cells	t=5.244 df=76	p<0.0001
S3E	GAD staining vs POMC size	Correlation	Linear Regression	18 cells	R^2=0.4008	p=0.0048
S3F	AP firing change (%) vs POMC size	Correlation	Linear Regression	18 cells	R^2=0.5256	p=0.0007
S5B	% of Rictor expression in POMC neurons	Genotype	Unpaired t-test	4	t=61.38 df=6	p<0.0001
S5E	% c-Fos in mCherry-POMC positive neurons	Treatment	Unpaired t-test	2-4	t=3.774 df=4	p=0.019
S5F	% of p-S6 in mCherry and c-Fos positive POMC neurons	Treatment	Unpaired t-test	2-4	t=46.60 df=4	p<0.0001
S5G	2h food intake	Treatment	Paired t-test	6	t=0.03704 df=5	p=0.9719
S5H	2h food intake	Treatment	Paired t-test	7	t=3.090 df=6	p=0.0214
S6A	2h food intake	Treatment	One-way ANOVA	6-23	F (7, 67) = 7.475	p<0.0001
S6B	AEA levels	Treatment	Unpaired t-test	6	t=0.183 df=10	p=0.8584
S7A	2h food intake	Treatment	One-way ANOVA	6-8	F (3, 25) = 0.770	p=0.5217
S7B	24h food intake	Treatment	One-way ANOVA	6-8	F (3, 25) = 5.000	p=0.0075
S7C	mIPSC frequency	Treatment	Paired t-test	10 cells	t=2.609 df=9	P=0.0283
S7D	mIPSC frequency	Treatment	Paired t-test	12 cells	t=1.511 df=11	P=0.159
S7E	Change mIPSC	Genotype	Unpaired t-test	10-12 cells	t=2.272 df=20	P=0.0343

Supplemental Figure Legends

Figure S1. Analysis of the distribution of the different POMC subpopulations in the hypothalamic ARC, Related to Figure 1. (**A**) Rostro-caudal distribution of different POMC subpopulations in C57BL/6J mice, expressing or not GABAergic and glutamatergic markers. (**B**) All subpopulations differ significantly concerning distance from the ventricle irrespective of rostro-caudal position, as determined by a Kruskal-Wallis test. (**C**) Linear regression was applied to each individual subpopulation. Slope parameters for all POMC neurons (black, R^2=0.01, p=1.44*10^{-13}), for glutamatergic POMC neurons (red, R^2=0.09, p=2.06*10^{-10}) and for GABA/GLUT POMC neurons (orange, R^2=0.007, p=3.21*10^{-7}) differ significantly from 0. For data in A-C, brains from 4 C57BL/6J mice were analyzed. (**D**) Representative FISH images illustrating AgRP and POMC mRNA colocalization in the ARC of adult POMC-CreER^{T2}-Ai6 mice (n=2 mice). Scale bar in A is 100μm, scale bar in D is 50μm and 25μm for smaller inset. *p<0.05; ***p<0.001.V: 3rd ventricle. For statistical analysis see Table S4.

Figure S2. POMC GABAergic, glutamatergic and GABA/glutamatergic neurons have specific gene expression profile, Related to Figure 1. Neurotransmitter type-specific single cell transcriptome profiling of hypothalamic *Pomc*$^+$ neurons. The heat map illustrates top rank 100 genes differently expressed in each *Pomc*$^+$ neurotransmitter-determined group (GABA, GLUT and GABA/GLUT, indicated by green rectangle). Left to heatmaps – p values for log transformed data, group of interest vs other 2 groups; right – gene names.

Figure S3. Differential response of POMC neurons to mTORC1 blockade depending on their neurotransmitter type, Related to Figure 2. (**A**) Taking all analyzed POMC neurons

together (n=117 cells), RAPA perfusion has no significant effect on cell firing. (**B**) Effect of RAPA treatment on cell membrane potential in POMC RAPA^{act} neurons (+2.13 ± 0.43 mV, n=37 cells) and in POMC RAPA^{inh} neurons (-1.23 ± 0.46 mV, n=41 cells). (**C**,**D**) Representative images (Z-stack 3D-reconstruction) of a recorded POMC neuron (C) and a hippocampal CA1 pyramidal cell (D). When running the immunofluorescence protocol in absence of the primary antibody anti-GAD65/67, POMC cells do not exhibit GAD signal within the cell surface (C), some background signal can still be observed; CA1 pyramidal cells (glutamatergic cells), which were used as negative control, do not have GAD staining (D). (**E**,**F**) POMC neurons capacitance negatively correlates with GAD spots quantity (E) and with the change in action potential firing induced by RAPA perfusion (F) (n= 18 cells). Scale bar in C and D is 3μm. Data are mean ± SEM. ***p<0.001. For statistical analysis see Table S4.

Figure S4. Pharmacological strategies used to characterize the nature of light-evoked POMC inputs on parvocellular neurons, Related to Figure 3. Neurotransmission classification (mixed GABA/Glut, pure GABA and pure Glut) was made after perfusion of picrotoxin to block $GABA_A$ related currents (**A**) or of NBQX/APV to block AMPA/NMDA receptors mediated currents (**B**).

Figure S5. Expression of rictor protein in hypothalamic POMC neurons and characterization of DREADD strategy to activate hypothalamic POMC neurons, Related to Figure 4. (**A, B**) Representative images illustrating rictor (red) protein staining in POMC-expressing neurons (green) in the ARC of POMC-*Rictor*-KO and control littermates (A) and related quantification (B) (n=4 mice per group). Scale bar in A 50 μm; 5 μm for smaller inset.

(**C**) POMC neurons in the ARC (green) express mCherry-labelled DREADD (red, arrowheads). Scale bar in C: 25 μm. (**D-F**) Representative images (D) from the ARC of POMC-ARC^{hM3Dq} mice treated with CNO or its vehicle and related quantification of c-Fos expression (green, E) and phosphorylation of S6 (p-S6, purple, F) in POMC mCherry-positive neurons (red) (n=2-4 mice per group). Scale bar in D: 50 μm; 10 μm for smaller inset. (**G**) Acute ip injection of CNO does not alter refeeding response in POMC-ARC^{hM3Dq} mice having received an icv administration of DMSO (vehicle used for RAPA) (n=6 mice per group). (**H**) Acute ip CNO injection does not alter RAPA-induced hyperphagia in POMC-ARC^{hM3Dq}-control littermates that do not express the Cre recombinase (n=7 mice per group). Data are mean ± SEM. *p<0.05 and ***p<0.001. V: 3rd ventricle. For statistical analysis see Table S4.

Figure S6. Effect of the α-MSH analog MTII on food intake and hypothalamic AEA levels, Related to Figure 5. (**A**) Dose-response effect of an icv administration of MTII on 2h refed C57BL/6J mice (n=6-23 mice per group; 3 experiments pooled together). (**B**) Hypothalamic AEA content in refed C57BL/6J mice treated with MTII (0.02 μg, icv) or its vehicle (n=6 mice per group). Data are mean ± SEM. *p<0.05; **p<0.01; ***p<0.001. For statistical analysis see Table S4.

Figure S7. Evaluation of GABAergic transmission in POMC-*CB$_1$*-KO and of genetic deletion of vGlut2 in POMC neurons, Related to Figure 6. (**A**, **B**) Dose-response effect of an icv administration of the $GABA_A$ receptor antagonist picrotoxin (Ptx) in 2h refed C57BL/6J mice (n=6-8 mice per group). (**C**-**E**) Effect of the CB_1R agonist WIN55-212 on miniatures inhibitory post-synaptic currents (mIPSC) frequency of parvocellular neurons of the PVN of POMC-*CB$_1$*-

Control (C, n=10 cells) and -KO littermates (D, n=12 cells); (E) Change in mIPC frequency under WIN (n=10-12 cells). (**F**) Representative images of the co-expression of Zsgreen1 (green) and POMC (red) in POMC-CreER^{T2}-Ai6 mice to demonstrate appropriate recombination in the ARC after tamoxifen (TAM) administration (4 mice per group). (**G**) Representative PCR showing deletion of vGlut2 in hypothalami of POMC-*vGlut2*-KO mice. Note the excision fragment obtained at 700bp in the KO after tamoxifen administration. Data are mean ± SEM. *p<0.05, **p<0.01. Scale bar in F: 100µm; V= 3rd ventricle. For statistical analysis see Table S4.

Figure S1, related to Figure 1

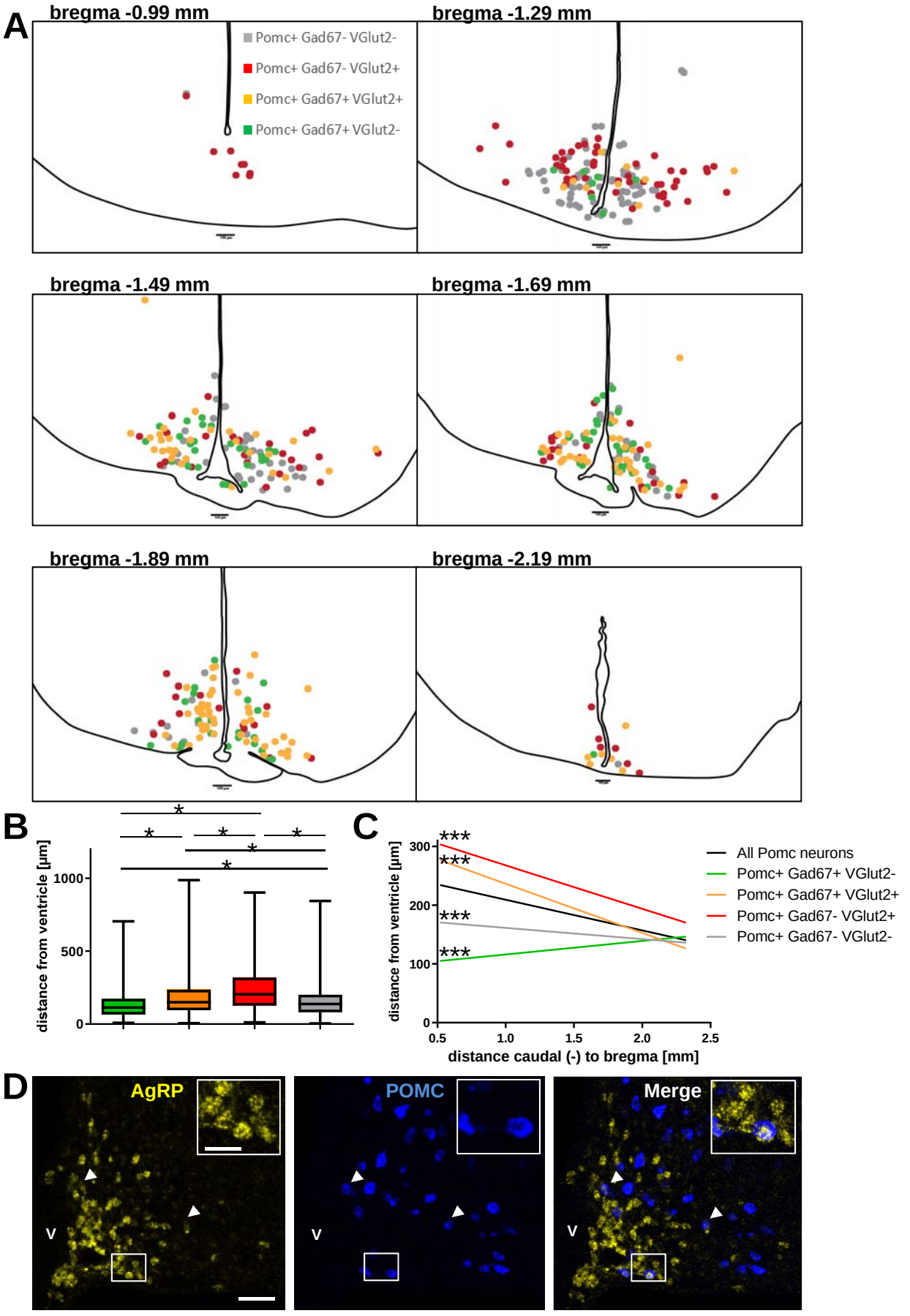

Figure S2, related to Figure 1

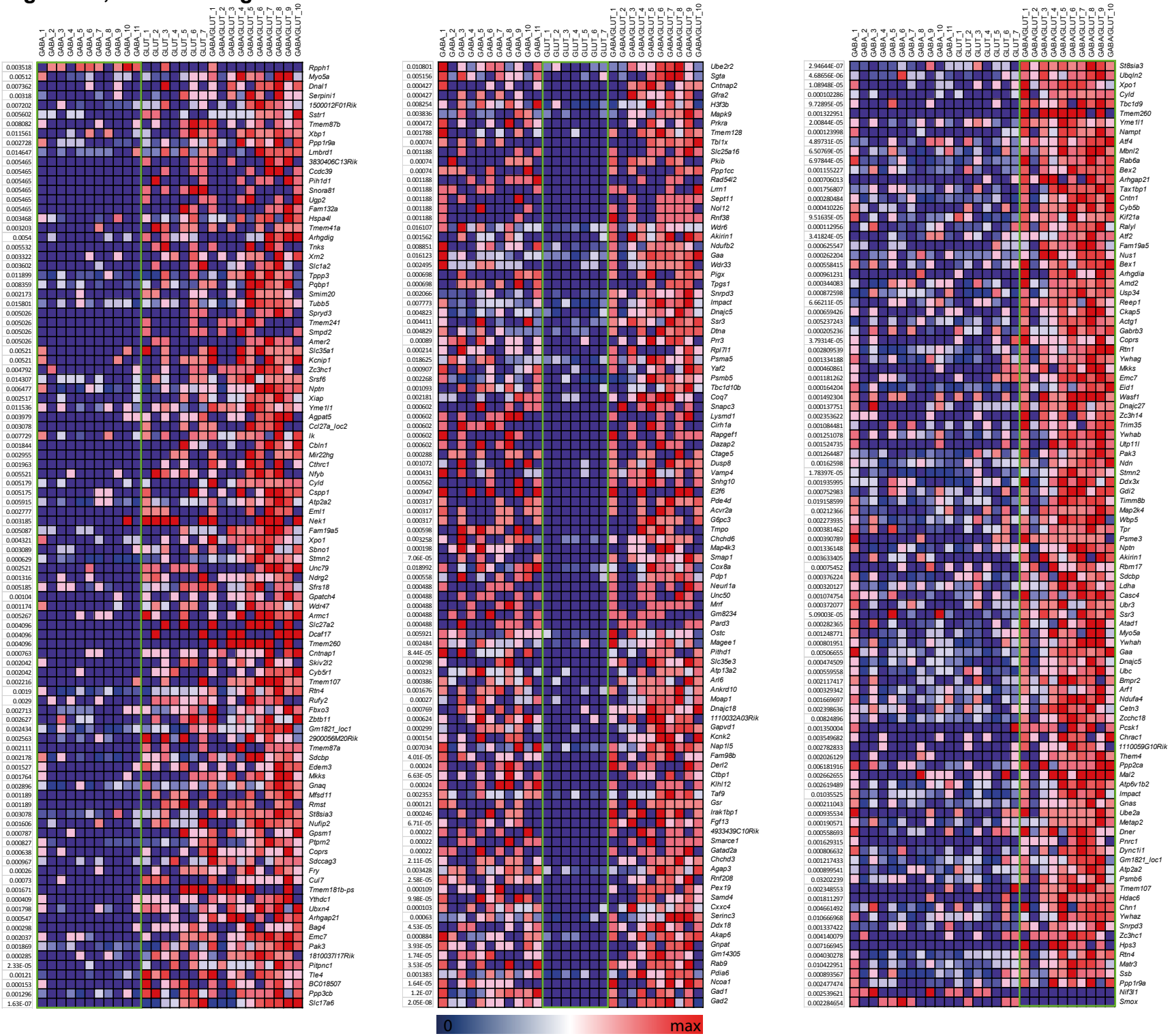

Figure S3, related to Figure 2

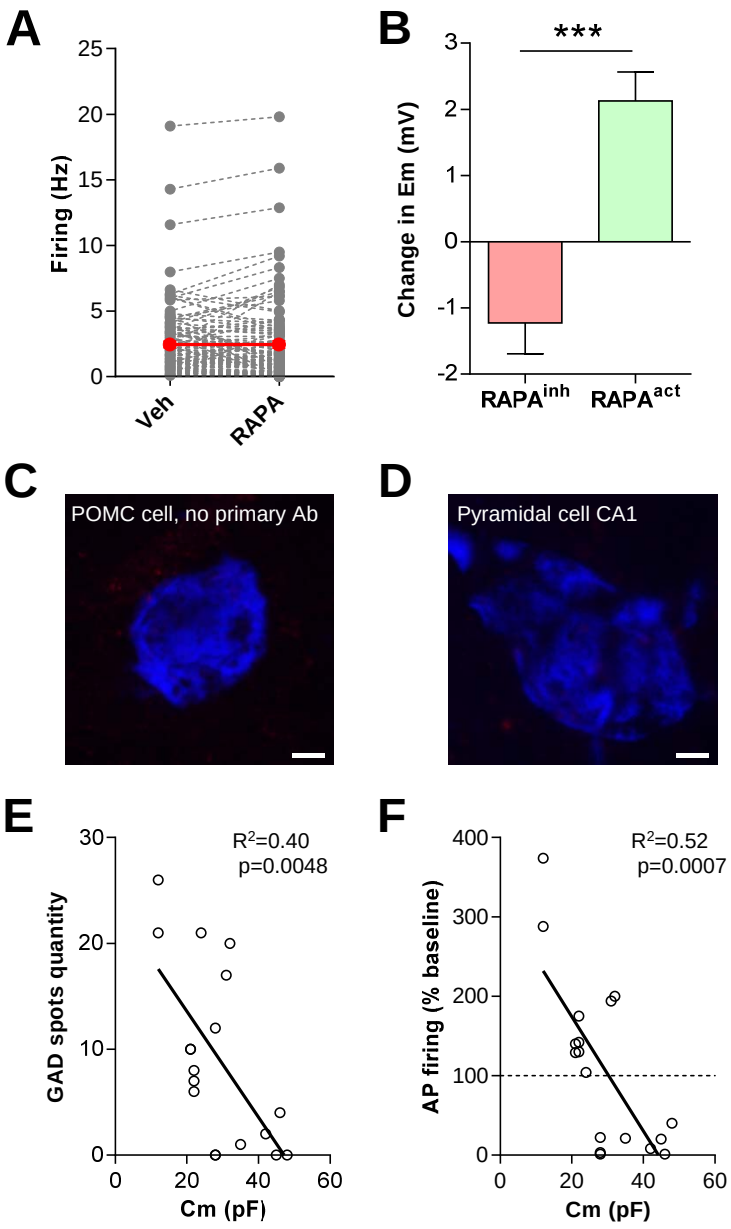

Figure S4, related to Figure 3

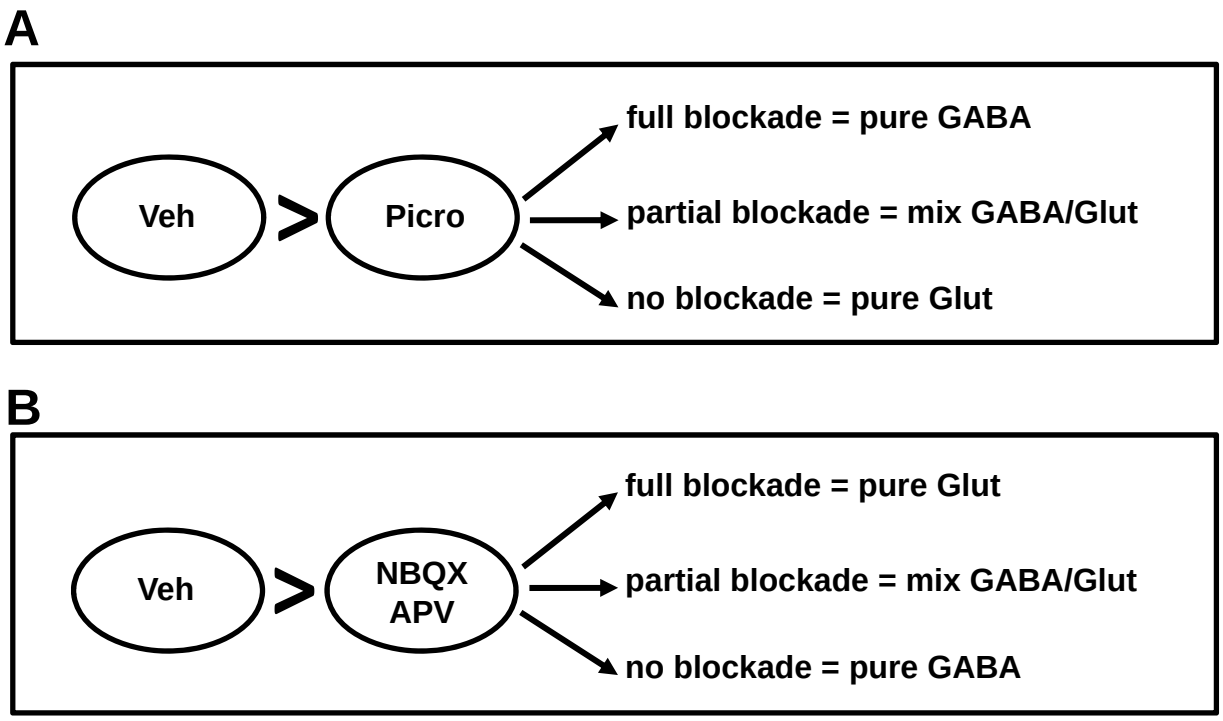

Figure S5, related to Figure 4

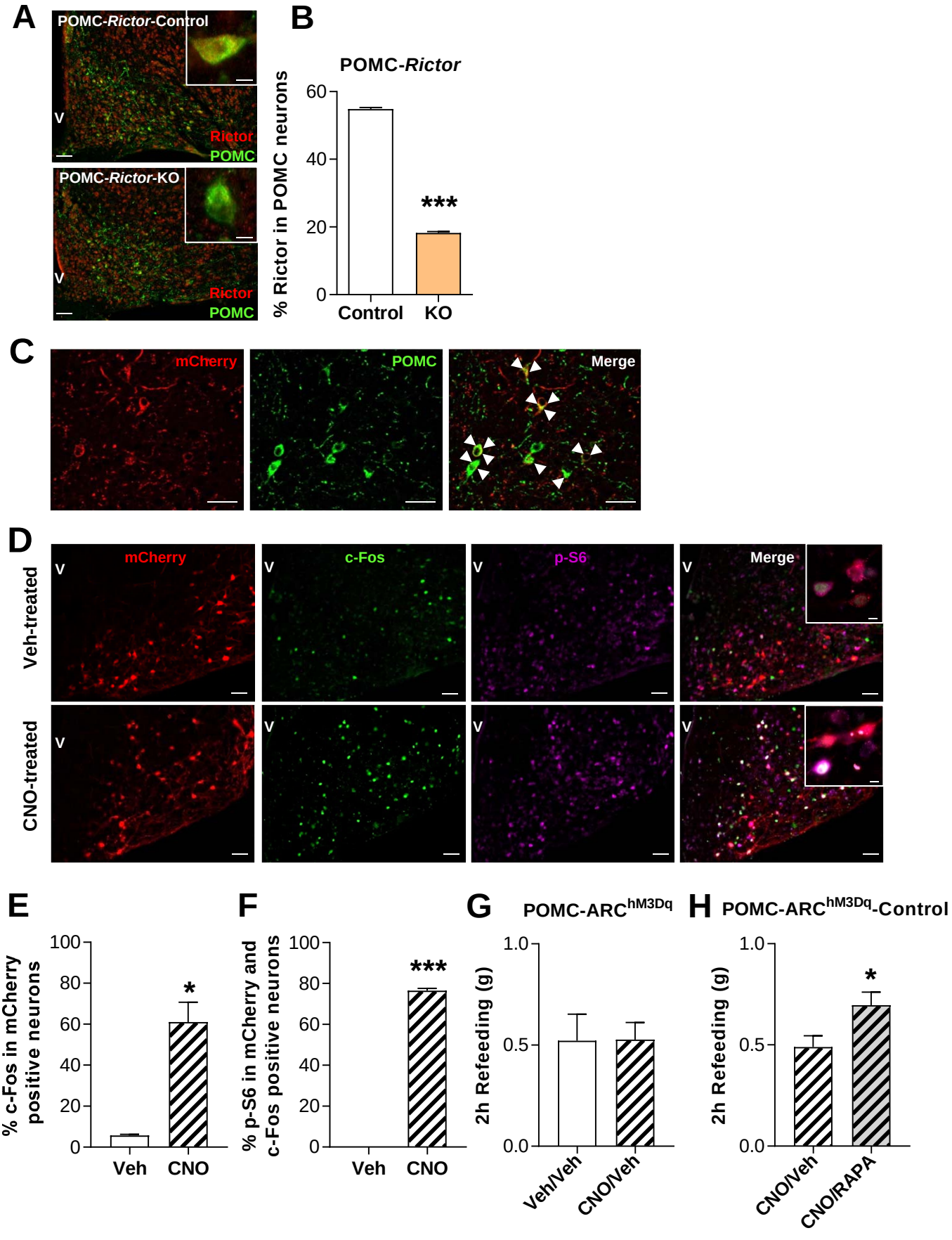

Figure S6, related to Figure 5

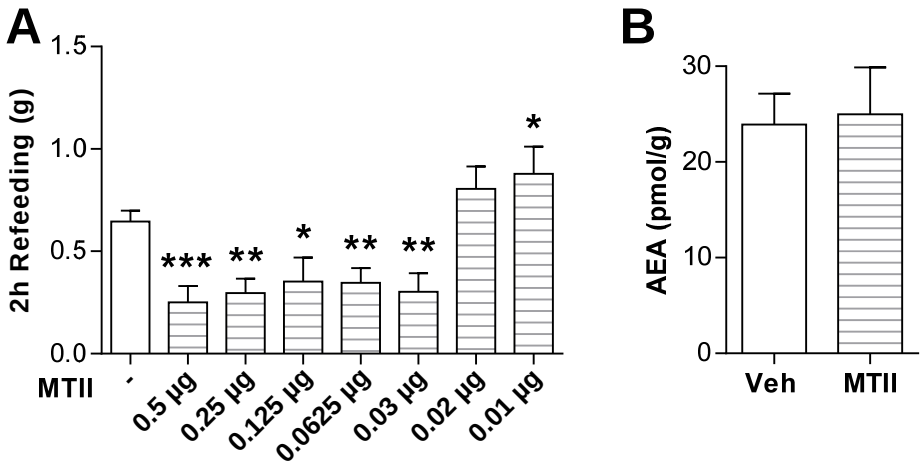

Figure S7, related to Figure 6